Discovery of mechanisms of herbicide resistance using the liverwort *Marchantia polymorpha*

Chloe Anne Lara Casey

Balliol College

Department of Plant Sciences

University of Oxford

Thesis submitted for the degree of Doctor of Philosophy

Hilary 2022

Discovery of mechanisms of herbicide resistance using the liverwort *Marchantia polymorpha*

Chloe Casey

Balliol College, Department of Plant Sciences, University of Oxford

Thesis submitted for the degree of Doctor of Philosophy

Hilary 2022

Abstract

Non-target site resistance (NTSR) to herbicides in weeds is a threat to global crop yields. Few specific alleles conferring NTSR have been identified, only two of which involve loss of gene function. Here, I show that the mechanism of NTSR to the herbicide thaxtomin A (TXTA) conferred by loss-of-function of the gene *PAM16* is conserved in *Marchantia polymorpha*, validating its use as a species with which to study NTSR. To identify novel NTSR mechanisms, I used forward genetics in *M. polymorpha* to generate 13 TXTA-resistant mutants and identified candidate NTSR-conferring SNPs in these mutants via mapping-by-sequencing. I identified a novel mechanism of NTSR to TXTA conferred by loss-of-function of the gene *RAD8*. To functionally characterise this mechanism, I generated *rad8* loss-of-function mutants and found that they are cross-resistant to isoxaben, overproduce reactive oxygen species, and produce less of a putative TXTA metabolite than wild-type. I also found 4 candidate resistance-conferring SNPs in *M. polymorpha* homologues of genes associated with NTSR in the weed *Amaranthus tuberculatus.* These results demonstrate that forward genetics in *M. polymorpha* can identify novel NTSR alleles and corroborate existing candidate NTSR alleles, and that reverse genetics in *M. polymorpha* can be used to functionally characterise these resistance mechanisms.

Table of Contents

Acknowledgements

First, I would like to thank my supervisor Prof. Liam Dolan, for your continual support and advice. I am very grateful for the opportunities you have opened to me in and beyond the lab. To my assessors throughout my DPhil Prof. Gail Preston, Prof. Lee Sweetlove, Prof. Phil Poole, and Prof. Nick Harberd, thank you for your advice and guidance. Thank you to the BBSRC and the Gregor Mendel Institute for funding me.

A big thank you to everyone in the Dolan lab past and present, I couldn't have wished for a better lab in which to do my DPhil. Thank you to Dr. Clement Champion for helping me to get started in the lab, and for your advice from career choices to bioinformatics. To Dr. Alex Casey, thank you for always brightening my day, even while extracting RNA at midnight, I am so happy we got to do our DPhils together. To Sam Caygill, thanks for making the lab so fun, and for always cheering me up. Thanks also to Alex and Sam for your help with all things herbicide, and for proofreading this thesis. Thanks to Dr. Radka Slovak for your help with bioinformatics and data analysis, and for all our long Friday lunches. Thanks to Dr. Sandy Hetherington, Dr. Anna Thamm, Dr. Susanna Streubel, Hugh Mulvey, and Sarah Attrill for your input and ideas in lab meetings and at the pub. Thank you to Dr. Magda Mosiolek and Kathi Jandrasits for your huge support and for welcoming me to Vienna. Thanks also to Helen Prescott and Lida Chen for all your help in Oxford. Thank you to the VBCF NGS facility for carrying out the whole genome sequencing and thank you to Dr. Thomas Köcher from the VBCF metabolomics facility for carrying out the metabolomics analyses.

Finally, I would like to thank my friends and family. To Alex and Sam, thank you for making my time in Vienna so fun - I am glad that such nice people decided to study

herbicides. To Emily, thank you for your constant cheerfulness and support whether from across the bench, across the pub, or across the sea, and for your refreshing perspective on everything from science to life outside the lab. To Stefi, Lois, and Chels, thank you for all your moral support from the beginning and for the good times we had in Oxford – even during lockdown! To Suze and Devo, thank you for always having my back and being there on the other end of the phone. To Stefan, thank you for keeping me sane and making me laugh through the hardest part of my DPhil, I feel very lucky to have met you (in Billa). And finally, merci and thank you to Maman and Dad for always being there for and believing in me, and for the constant supply of English sweets and tea, without which I would be a few pounds lighter but a great deal more homesick.

Abbreviations

2,4-D	2,4-dichlorophenoxyacetic acid
ABC transporter	ATP-binding cassette transporter
ACCase	Acetyl-CoA Carboxylase
AHAS	Acetohydroxyacid Synthase
BLAST	Basic Local Alignment Search Tool
bp	Base Pair
CEQORH	Chloroplast Envelope Quinone Oxidoreductase Homologue
CoQ	Coenzyme Q
CRISPR	Clustered Regularly Interspaced Short Palindromic Repeats
CSR	Chlorsulfuron Resistant mutant
DAB	3,3'-diaminobenzidine
DCB	Dichlobenil
DMSO	Dimethyl Sulfoxide
DNA	Deoxyribonucleic Acid
EMS	Ethyl Methanesulfonate
EPSPS	5-enolpyruvylshikimate-3-phosphate synthase
FOX	Ferric-xylenol Orange
gDNA	Genomic DNA
GO	Gene Ontology
GR	Glyphosate Resistant
GST	Glutathione-S-transferase
GT	Glycosyltransferase
GWAS	Genome Wide Association Study

H_2O_2	Hydrogen Peroxide
HPPD	4-hydroxyphenylpyruvate dioxygenase
IC_{50}	Median Inhibitory Concentration
LC-MS/MS	Liquid Chromatography-tandem Mass Spectrometry
LD_{100}	Lethal Dose
MHR	Multiple Herbicide Resistance
MNU	Methyl-nitrosourea
morpho	Morphologically defective mutant
Mp*chlr*	*Marchantia polymorpha* chlorsulfuron resistant mutant
Mp*pam16*	*Marchantia polymorpha pam16* mutant
Mp*rad8*	*Marchantia polymorpha rad8* mutant
Mp*tar*	*Marchantia polymorpha* thaxtomin-A resistant mutant
NADCC	Sodium Dichloroisocyanurate
NCBI	National Center for Biotechnology Information
NGS	Next Generation Sequencing
NTSR	Non-target site resistance
P450	Cytochrome P450
PAM16	Presequence Translocase Associated Motor Protein 16
PCR	Polymerase Chain Reaction
PSI	Photosystem I
PSII	Photosystem II
RAD8	Radiation sensitive 8
RI	Resistance Index
RNA	Ribonucleic Acid
RNA-seq	RNA Sequencing

ROS	Reactive Oxygen Species
RTN4IP1	Reticulon 4 Interacting Protein 1
sgRNA	Single Guide RNA
SNP	Single Nucleotide Polymorphism
Tak-1	Takaragaike-1
Tak-2	Takaragaike-2
TSR	Target Site Resistance
TXTA	Thaxtomin A
UV-B	Ultraviolet B

Chapter 1: Introduction

1.1. Summary

In this literature review I introduce the need for herbicides in agriculture, and the consequent threat to global crop yields posed by herbicide resistance in weeds. Herbicide resistance in weeds has evolved due to the strong selection pressure exerted by the repeated use of the same herbicides in agriculture over many years, and it is becoming a pressing issue due to the lack of novel herbicide modes of action with which to combat resistant weeds. I introduce target site resistance (TSR) and non-target site resistance (NTSR) and explain the differences between the two. NTSR is particularly problematic due to its complex polygenic basis which makes it difficult to identify molecular mechanisms of NTSR, as well as the potential ability of NTSR to confer resistance to multiple herbicides. It is therefore important to identify mechanisms of NTSR to better understand how it evolves and how to manage it in the field.

I then describe how specific molecular mechanisms of NTSR can be identified, namely by gene silencing, heterologous expression, transcriptomics, population genomics, or forward genetics. I describe the benefits and disadvantages of each method, concluding that forward genetics can potentially identify novel mechanisms of NTSR conferred by loss of gene function, of which very few examples have been identified in *Arabidopsis thaliana*, and none yet in weeds. I conclude the literature review by highlighting the characteristics of *Marchantia polymorpha* which make it particularly well suited to forward genetics, informing my choice of a forward genetics approach in *M. polymorpha* to identify novel mechanisms of NTSR conferred by loss of gene function.

1.2. Herbicides are required to control weeds in agriculture

Weeds are currently the greatest biotic threat to global agriculture, causing greater total potential global crop losses than both insect pests and pathogens combined (Pimentel, 2005, Oerke, 2006). Weeds decrease crop yields by competing for resources such as nutrients, light, and water, and can cause allelopathic damage via production of biochemicals which have a detrimental effect on crops (Bridges, 1994).

A weed is defined as “a plant that causes economic losses or ecological damage, creates health problems for humans or animals, or is undesirable where it is growing” (WSSA, 2016). Different weed species dominate in different geographical areas according to environmental conditions and types of crops grown: for example, Palmer amaranth (*Amaranthus palmeri*) is considered one of the most troublesome weed in cotton and corn fields in the southern U.S. (Ward *et al.*, 2013), blackgrass (*Alopecurus myosuroides*) is the most prevalent weed in wheat fields in Europe (Moss *et al.*, 2007), and ryegrass (*Lolium rigidum*) is the primary weed in southern Australia (Goggin *et al.*, 2012).

Traditionally, weeds were controlled using physical control methods such as manual weeding or tillage, or cultural methods such as crop rotation which prevent specific weed species from becoming established in a field (Schreiber, 1992). Since the 1940s however herbicides have been widely employed to manage weed populations (Heap, 2014). Herbicides are chemicals which bind to a target molecule within a plant and inhibit its function, causing detrimental physiological effects resulting in death. Herbicides are cheaper and easier to use than traditional methods of weeding and remain the most effective method of weed control 80 years since their large-scale application to agriculture (Powles *et al.*, 2010, Gaines *et al.*, 2020).

1.3. Herbicides are classified by mode of action

Herbicides are classed by their mode of action which is defined by the cellular process they inhibit: 26 classes of herbicides are currently available on the market (Heap, 2022). The modes of action of herbicides are summarized in Table 1.1. Herbicides with different modes of action have different efficacies when applied to different weeds (Hoss *et al.*, 2003), so a range of modes of action are required to control different weeds.

HRAC group	Target site	Example	Method of toxicity	Reference(s)
1	Acetyl CoA Carboxylase	Diclofop	Inhibition of fatty acid biosynthesis	(Burton *et al.*, 1987)
2	**Acetohydroxyacid synthase**	**Chlorsulfuron**	**Inhibition of branched-chain amino acid synthesis**	**(Chaleff and Ray, 1984, Larossa and Schloss, 1984)**
3	Tubulin	Oryzalin	Inhibition of microtubule assembly	(Morejohn *et al.*, 1987)
4	**Auxin signalling pathway**	**2,4-D**	**Auxin mimics – disrupt plant growth**	**(Grossmann, 2010)**
5	**Photosystem II D1 protein (serine 264)**	**Atrazine**	**Inhibition of photosynthesis; light activation of ROS**	**(Pfister *et al.*, 1981, Steinback *et al.*, 1981, Erickson *et al.*, 1984)**
6	Photosystem II D1 protein (histidine 215)	Bentazon	Inhibition of photosynthesis; light activation of ROS	(Pedroso *et al.*, 2016)
9	Enolpyruvyl-shikimate phosphate synthase	Glyphosate	Inhibition of aromatic amino acid biosynthesis	(Amrhein *et al.*, 1980)
10	Glutamine synthetase	Glufosinate	Inhibition of glutamine biosynthesis; light activation of ROS	(Takano *et al.*, 2020)
12	Phytoene desaturase	Norflurazon	Inhibition of carotenoid biosynthesis; light activation of ROS	(Sandmann and Böger, 1989)
13	Deoxy-D-Xyulose phosphate synthase	Clomazone	Inhibition of steroid biosynthesis; light activation of ROS	(Ferhatoglu and Barrett, 2006)
14	Protoporphyrinogen oxidase	Acifluorfen	Inhibition of chlorophyll biosynthesis; light activation of ROS	(Dayan *et al.*, 2019b)
15	Very long chain fatty acids	Thiobencarb	Inhibition of very long chain fatty acid biosynthesis	(Tanetani *et al.*, 2013)
18	Dihydropteroate synthase	Asulam	Inhibition of folate biosynthesis	(Devine *et al.*, 1993)
19	Auxin transporters	Naptalam	Inhibition of auxin transport	(Subramanian *et al.*, 1997)
22	**Photosystem I**	**Paraquat**	**Diversion of electrons from photosystem I; light activation of ROS**	**(Fukushima *et al.*, 1993, Hawkes, 2014)**

23	Microtubules	Carbetamide	Disruption of microtubule organization	(Gimenez-Abian *et al.*, 1998)
24	Photosynthetic electron transport chain, oxidative phosphorylation	Dinoseb	Uncoupler; inhibition of ATP synthesis due to inhibition of proton gradient formation across thylakoid and inner mitochondrial membranes	(Oettmeier and Masson, 1980)
27	Hydroxyphenyl Pyruvate Dioxygenase	Mesotrione	Inhibition of tyrosine catabolism; light activation of ROS	(Almsick, 2009)
28	Dihydroorotate dehydrogenase	Tetflupyrolimet	Inhibition of nucleotide biosynthesis	(Dayan *et al.*, 2019a)
29	**Cellulose synthesis**	**Isoxaben**	**Inhibition of cellulose biosynthesis**	**(Heim *et al.*, 1990, Scheible *et al.*, 2001)**
30	Fatty acid thioesterase	Cinmethylin	Inhibition of fatty acid release from plastids	(Campe *et al.*, 2018)
31	Serine threonine protein phosphatase	Endothall	Disruption of microtubule cytoskeleton arrangement and mitosis	(Tresch *et al.*, 2011, Bajsa *et al.*, 2012)
32	**Solanesyl diphosphate synthase**	**Aclonifen**	**Inhibition of plastoquinone biosynthesis; light activation of ROS**	**(Kahlau *et al.*, 2020)**
33	Homogentisate solanesyltransferase	Cyclopyrimorate	Inhibition of plastoquinone biosynthesis; light activation of ROS	(Shino *et al.*, 2021)
34	**Inhibition of lycopene cyclase**	**Amitrole**	**Inhibition of carotenoid biosynthesis; light activation of ROS**	**(Clough *et al.*, 2016)**
Ø	**Unknown**	**Thaxtomin A**	**Suspected inhibition of cellulose synthesis: elongation inhibition of dark grown hypocotyls, inhibition of ^{14}C incorporation into the cellulosic cell wall fraction, depletion of cellulose synthase subunits at the plasma membrane**	**(King *et al.*, 2001, Scheible *et al.*, 2003, Dayan *et al.*, 2012, Dayan and Duke, 2014)**

Table 1.1. A comprehensive list of herbicides classified by their mode of action. The method of toxicity and references regarding the mode of action of each herbicide class is included. Herbicide classes highlighted in bold represent those which are relevant to the current study.

1.4. History of herbicide resistance in weeds

The widespread use of herbicides to kill weeds exerts a strong pressure that selects for weeds to evolve resistance (Gaines *et al.*, 2020). Weeds are classed as herbicide resistant when they can survive and reproduce in the presence of a herbicide. The first case of herbicide resistance in weeds was documented in 1957, when a population of *Commelina diffusa* resistant to the herbicide 2,4-D was identified (Hilton, 1957) (Fig. 1.1). Since then, the number of unique species with resistance to herbicides increases every year: to date, 509 unique cases of herbicide resistant weeds have been reported to 21 of the 26 herbicide classes (Heap, 2022) (Fig. 1.1).

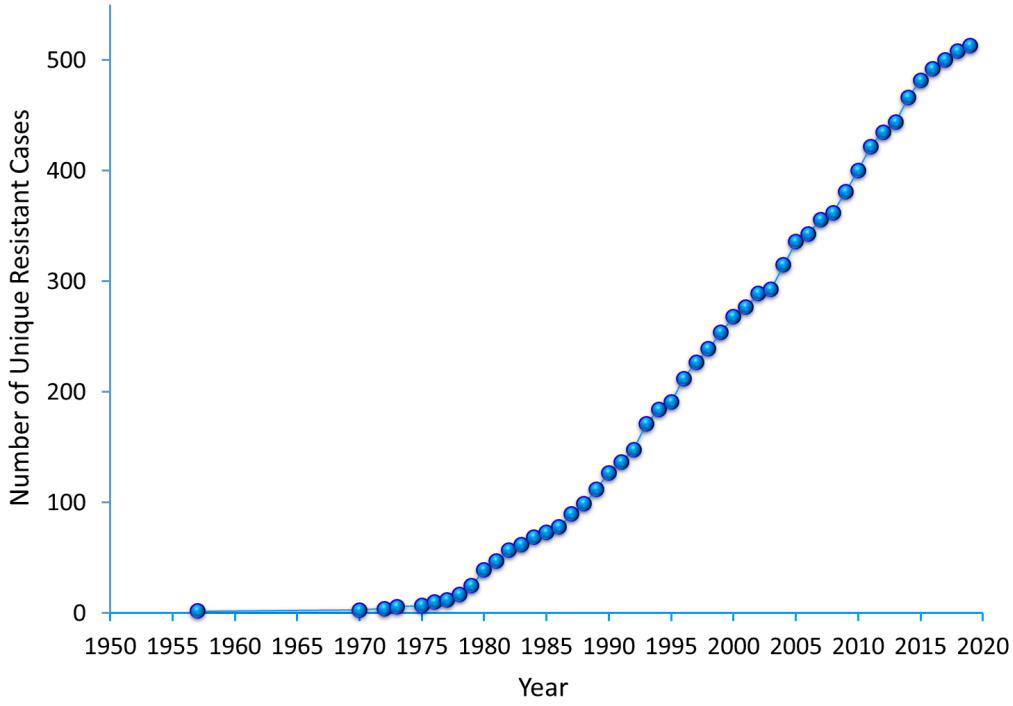

Fig. 1.1. Chronological increase in number of unique cases of herbicide resistance. A unique case of herbicide resistance is defined as a particular species with resistance to a particular herbicide mode of action. Sourced from (Heap, 2022).

Initially, herbicide resistance in weeds was primarily limited to resistance to photosystem II (PSII) inhibitors (Table 1.1): by 1980, 39 cases of herbicide resistance had been recorded, 32 of which were cases of resistance to PSII inhibitors (Heap, 2022) (Fig. 1.1). These weeds carried substantial fitness costs and were easily controlled by using herbicides with different modes of action, so herbicide resistance in weeds was not initially considered a substantial threat to agriculture (Shaner, 2014). However, the extensive use of ACCase inhibitors and AHAS inhibitors (Table 1.1), introduced in the 1980s, resulted in strong selection pressures globally leading to the evolution of resistance to these modes of action. The first cases of resistance to these herbicides were reported within 5 years of their introduction onto the market, and numbers of cases of resistant weeds increased almost five-fold from 39 to 192 between 1980 and 1995, mostly the result of evolution of resistance to these two herbicide classes (Heap, 2022) (Fig. 1.1).

The herbicide glyphosate was introduced onto the market in 1974: it is a broad-spectrum herbicide affecting many plant species, so although it provided good weed control between crop rows and in urban areas, it could not be used on crops for selective control of weeds due to its non-selectivity (Powles, 2008). This changed in 1996, with the introduction of glyphosate-resistant (GR) soybean, maize, canola, and cotton crops: GR crops are genetically transformed with a gene encoding a resistant version of 5-enolpyruvylshikimate-3-phosphate synthase (EPSPS), the glyphosate target (Table 1.1) (Padgette *et al.*, 1995, Barry *et al.*, 1997). GR crops were widely adopted as they are simpler to farm than alternatives requiring complex herbicide tank or sequence mixtures or additional adjuvants, and cheaper than weed management systems using a variety of herbicides especially since the expiration of the glyphosate patent in 2000 (Powles, 2008). GR crops also allowed glyphosate

application in fields throughout the crop life cycle, maximising the number of weeds killed and significantly increasing crop yields (Duke and Powles, 2008, Green, 2012). Glyphosate is now the world's most widely used herbicide, primarily due to the use of GR crops (Duke and Powles, 2008). Although there was no evidence of glyphosate-resistant weeds for the 20 years of its use prior to the introduction of GR crops, and although scientists from the glyphosate manufacturer predicted that evolution of glyphosate resistance in weeds would occur rarely (Bradshaw *et al.*, 1997, Duke and Powles, 2008), the huge selection pressure exerted by the widespread adoption of GR crops led to the evolution of glyphosate resistance in a population of *L. rigidum* less than a year after the introduction of GR crops (Powles *et al.*, 1998). To date, 55 unique cases of glyphosate resistant weeds have been reported (Heap, 2022).

1.5. Reasons behind the current acute herbicide resistance problem

Since the advent of herbicide resistance in weeds, farmers have used herbicides with different modes of action to manage weeds resistant to a particular herbicide. Before the 1990s, a novel herbicide mode of action was introduced approximately every 3 years: however, only 1 herbicide mode of action (inhibition of fatty acid thioesterase, introduced in 2020) has been introduced into the market since 1985 (Campe *et al.*, 2018). There are three main reasons for this.

Firstly, the widespread adoption of GR crops has led to a decrease in the range of herbicide modes of action used in agriculture, decreasing the demand for novel modes of action: the number of herbicides applied to US soybean crops decreased from 11 in 1995 to glyphosate alone in 2002 (USDA, 2004), and a decrease in US herbicide patents and in the rate of active ingredient introductions followed the introduction of GR crops (Fig. 1.2).

Secondly, consolidation of the herbicide industry has resulted in the number of companies conducting research into novel modes of action dropping by over 75 % since 1970, reducing the diversity of scientific approaches to discovering modes of action and adversely affecting the rate of mode of action discovery (Duke, 2012).

Thirdly, the average cost of bringing a herbicide to the market increased from $152 million in 1995 to $256 million in 2008 due to the larger numbers of chemicals which must be screened to find a suitable product and increasingly stringent toxicological requirements which a herbicide must pass (McDougall, 2010).

The combination of reduction in herbicide research diversity and increased cost of bringing a herbicide to market – compounded by decreased market value of novel herbicides owing to overreliance on glyphosate – have caused a lack of introduction of novel herbicide modes of action. As a result, the same herbicide modes of action have been used for almost 40 years, not only generating a strong selective pressure for herbicide resistant weeds to evolve, but also leaving increasingly limited options for the management of herbicide resistant weeds. Herbicide resistance is therefore an important issue for agriculture.

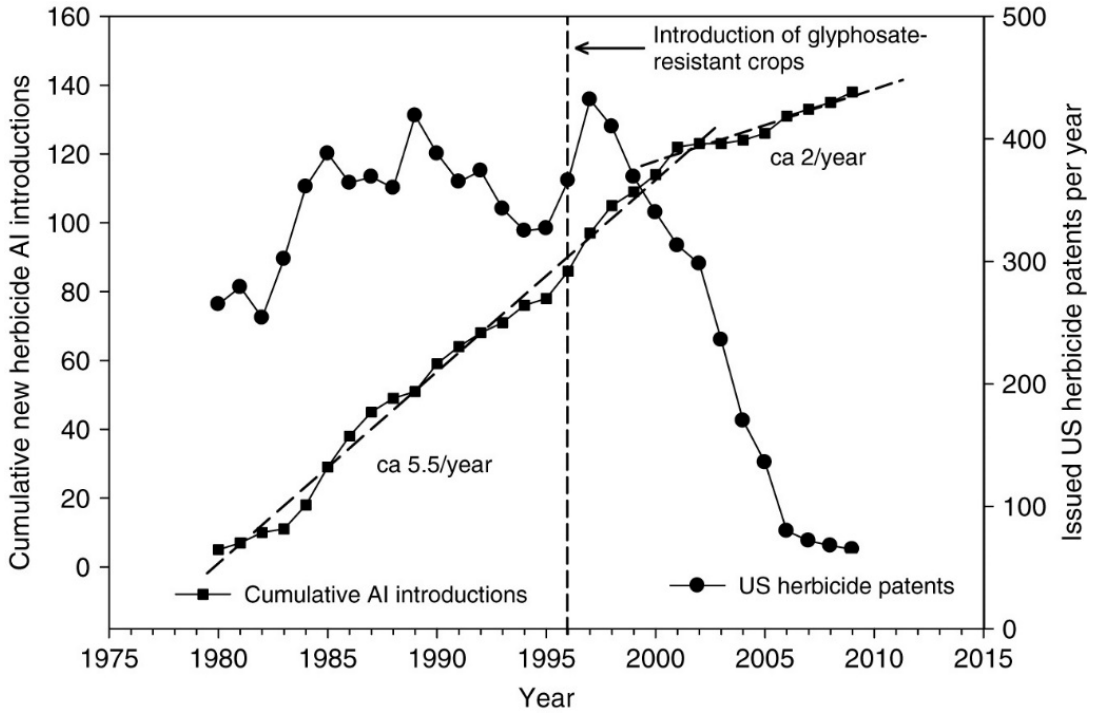

Fig. 1.2. The number of new herbicide active ingredient introductions and US herbicide patents over a thirty-year period spanning the introduction of glyphosate-resistant crops. Sourced from (Duke, 2012).

1.6. Target site (TSR) and non-target site resistance (NTSR)

Resistance to herbicides can occur either through the evolution of target site resistance (TSR) or non-target site resistance (NTSR).

1.6.1 Target site resistance (TSR)

Target site resistance (TSR) refers to resistance arising from changes affecting a herbicide binding site. It can arise because of mutations causing amino acid changes in the herbicide target protein which decrease the affinity of the herbicide for its target. (Delye et al., 2013). TSR can also be caused by overproduction of the herbicide target; in this case the herbicide can still bind the target but there is a higher concentration of unbound functional target molecules (Powles et al., 2010).

The first serious case of herbicide resistance in 1970 (Fig. 1.1) involved a resistant population of the weed *Senecio vulgaris* which was resistant to triazine herbicides (PSII inhibitors – Table 1.1); the basis of the resistance was later identified as a target site mutation in the DI protein of photosystem II leading to amino acid changes hindering binding of triazines (Ryan, 1970, Hirschberg *et al.*, 1987).

1.6.2. Non-target site resistance (NTSR)

Non-target site resistance (NTSR) encompasses mechanisms decreasing the amount of herbicide reaching the target site thereby increasing the tolerance of a plant to the herbicide. NTSR can be conferred by a variety of molecular mechanisms including increased metabolism of the herbicide to non-toxic products (detoxification), decreased translocation, increased sequestration of the herbicide in cellular compartments where it cannot access the target, and alleviation of herbicidal toxic effects (Powles et al., 2010).

i) Herbicide detoxification

The metabolism of herbicides to non-toxic products is known as herbicide detoxification. Herbicide detoxification involves three phases: conversion, conjugation, and compartmentation (Hatzios, 1997). Phase I (conversion) usually involves oxidation or hydrolysis of the herbicide to a less toxic form, catalysed by enzymes such as cytochrome P450 monooxygenases (P450s) or other oxygenases (Yuan *et al.*, 2007). During Phase II, the modified herbicide molecule is conjugated to sugars or thiols, involving enzymes such as glutathione-S-transferases (GSTs) or glycosyl transferases (GTs) (Yuan *et al.*, 2007). Phase III involves sequestration of the modified herbicide into cellular compartments away from its target via transporters such as ABC transporters (Yuan *et al.*, 2007). The modified herbicide

then sometimes undergoes Phase IV detoxification, involving further modification in the vacuole or extracellular space (Yuan *et al.*, 2007).

Mutations which increase the expression or activity of the enzymes and transporters involved in herbicide detoxification can confer NTSR. For example, the P450 gene *CYP81A10v7* is constitutively more highly expressed in herbicide-resistant populations of the weed *L. rigidum* compared to herbicide-sensitive populations, and experimental overexpression of *CYP81A10v7* in transgenic rice conferred resistance to a variety of herbicides with different modes of action including the ACCase inhibitor diclofop, the AHAS inhibitor chlorsulfuron, the HPPD inhibitor mesotrione, the PSII inhibitor atrazine, and the tubulin inhibitor trifluralin (Han *et al.*, 2021). Experimental overexpression of *CYP81A10v7* in transgenic rice caused increased metabolism of diclofop-methyl to polar metabolites, suggesting that the constitutive higher expression of this gene in herbicide-resistant *L. rigidum* confers herbicide resistance via increased detoxification (Han *et al.*, 2021).

ii) Decreased herbicide translocation and increased herbicide sequestration

Foliar applied herbicides usually translocate through the phloem of the plant to reach their molecular target. A decrease in the amount of herbicide reaching its target can result from decreased translocation of the herbicide through the plant. Decreased translocation is often achieved by herbicide sequestration into the vacuole or extracellular space where it cannot access the target (Gaines *et al.*, 2020).

An increase in expression or activity of herbicide transporters – such as ABC transporters – can lead to decreased herbicide translocation via increased herbicide sequestration away from its molecular target. Transcriptomic studies have found several ABC transporter genes which are more highly expressed in herbicide-

resistant weeds than in sensitive weeds, either constitutively or in response to the herbicide glyphosate (Peng *et al.*, 2010, Piasecki *et al.*, 2019). The first specific ABC transporter gene confirmed to confer resistance in weeds was reported recently: Ec*ABCC8*, which is constitutively upregulated in glyphosate-resistant *Echinocloa colona* compared to herbicide-sensitive plants, conferred resistance to glyphosate and increased glyphosate efflux into the apoplast when overexpressed in rice (Pan *et al.*, 2021). This suggests that constitutive upregulation of Ec*ABCC8* leads to glyphosate resistance due to decreased translocation via increased sequestration in glyphosate-resistant *E. colona*.

Decreased translocation of a herbicide can also occur via the “phoenix phenomenon” whereby localised necrosis of plant tissue due to rapid herbicide action prevents a herbicide from spreading to other parts of the plant, and rapid regrowth is observed from non-sprayed portions of the plant (Gaines *et al.*, 2020). Glyphosate is usually a slow-acting herbicide, however glyphosate-resistant *Ambrosia trifida* has evolved to respond more rapidly to glyphosate involving an increase in the reactive oxygen species hydrogen peroxide resulting in rapid cell death of sprayed tissues (Moretti *et al.*, 2018, Van Horn *et al.*, 2018). This prevents glyphosate from translocating to the meristems, and the plant regrows from the unaffected meristems.

iii) Alleviation of herbicide toxicity

NTSR can also result from mutations which alleviate the toxic effects of a herbicide downstream from its molecular target. There are fewer examples of this type of NTSR in the literature, however one example is that of a multiple herbicide-resistant (MHR) population of *A. myosuroides* in which a constitutively overexpressed GST (Am*GSTF1*) is thought to enhance MHR by both enhancing herbicide detoxifying

enzymes and also by causing increased accumulation of antioxidant flavonol metabolites, leading to resistance to herbicides whose toxic action depends on ROS overaccumulation such as paraquat, chlortoluron, and fluorodifen (Cummins *et al.*, 1999, Cummins *et al.*, 2009, Cummins *et al.*, 2013). Increases in antioxidant enzyme activity is also thought to contribute to NTSR in several weed species; for example increased activity of enzymes associated with metabolic turnover of antioxidant polyamines has been suggested to contribute to NTSR to paraquat in the weed *Eleusine indica* (Delye, 2013, An *et al.*, 2014). There have been substantially fewer examples of NTSR due to alleviation of herbicide toxicity reported in the literature, suggesting either that these types of NTSR mechanisms are less prevalent in weeds than those involving increased detoxification or decreased translocation, or that these mechanisms are found in weeds but remain largely undiscovered.

1.6.3 Differences between TSR and NTSR

TSR is generally a monogenic trait, involving mutations affecting only the gene encoding the target site of the herbicide. Molecular mechanisms of TSR are therefore easy to identify if the herbicide target site is known. Plants with a TSR mutation are usually strongly herbicide resistant, surviving concentrations much higher than the lethal dose (LD_{100}). TSR biotypes of the weed *Euphorbia heterophylla* can survive more than 50 times the recommended field dose of the AHAS inhibitor imazamox in (Rojano-Delgado *et al.*, 2019).

Some individual NTSR alleles can also lead to strong herbicide resistance; for example, overexpression of the *E. colona* ABC transporter Ec*ABCC8* in rice confers 22-fold higher glyphosate resistance compared to wild-type rice (Pan *et al.*, 2021). However, individual NTSR alleles usually confer weaker resistance to herbicides in

comparison to TSR (Gressel, 2000). Strong NTSR-based resistance in the field is = therefore usually thought to be the result of a process called “allele stacking”, whereby several NTSR alleles each conferring a low level of herbicide resistance accumulate in a single individual thereby conferring stronger herbicide resistance (Gressel, 2009, Delye, 2013) (Fig. 1.3). For example, four genes (two P450s, a nitronate monooxygenase, and a GT) were more highly expressed in nine separate populations of *Lolium rigidum* with field-evolved metabolic resistance to the herbicide diclofop than in sensitive populations (Gaines *et al.*, 2014). However, transcript quantification of these 4 genes in different *L. rigidum* populations with different diclofop resistance levels showed that high expression of the GT alone, or of one P450 and the GT only, were insufficient to confer resistance, suggesting that metabolic resistance to diclofop requires high expression of all 4 NTSR alleles. It has been reported that separate NTSR alleles – such as different genes involved in herbicide detoxification – can be arranged in genomic co-expression clusters (Giacomini *et al.*, 2020). It is therefore possible that a single mutation affecting the regulation of an NTSR cluster could lead to the overexpression of several genes conferring NTSR, leading to a polygenic NTSR mechanism conferred by a single mutation (Torra *et al.*, 2021).

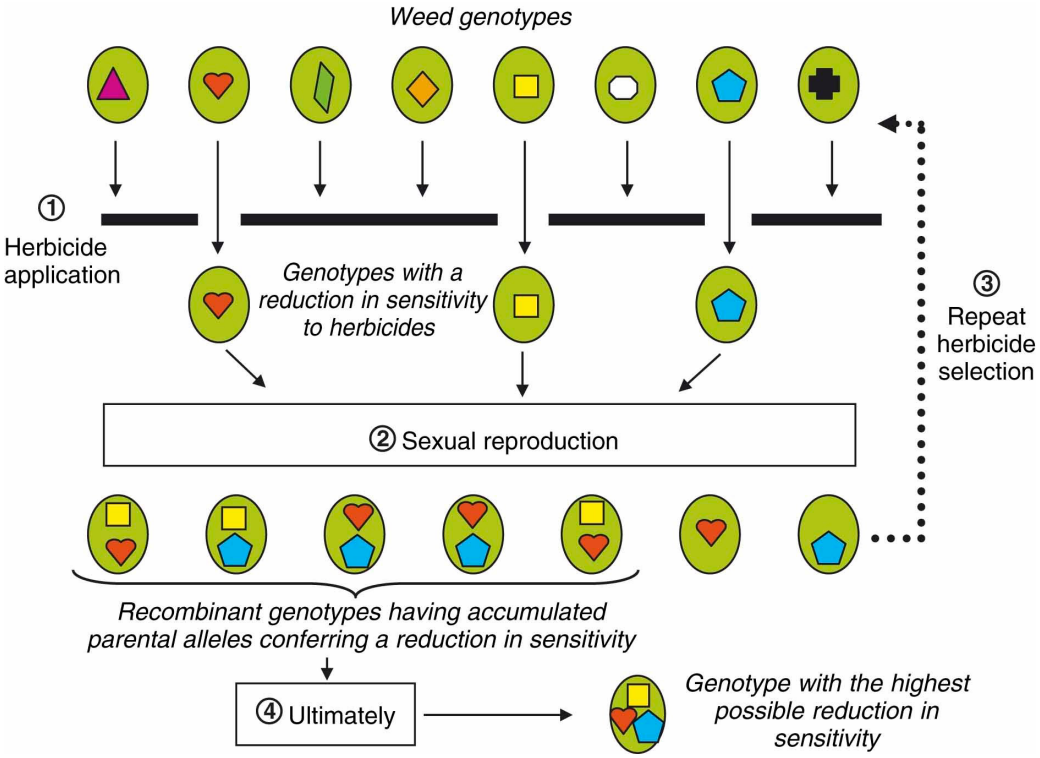

Fig. 1.3. Evolution of NTSR by allele stacking. Herbicide application selects for individuals carrying alleles conferring herbicide resistance (1). These individuals reproduce (2), leading to stacking of resistance genes in the progeny. Recurrent rounds of herbicide application repeat the process (3), resulting in individuals with many alleles conferring herbicide resistance (4). Sourced from (Delye, 2013).

TSR involves a mutation affecting the gene encoding the herbicide target site therefore a single TSR allele can only confer resistance to herbicides with that specific molecular target. However, single NTSR alleles can confer resistance to herbicides with different modes of action, known as herbicide cross-resistance (Gaines *et al.*, 2020). Various enzymes in the CYP81A family of P450s in particular have been shown to metabolise herbicides with different chemistries (Gaines *et al.*, 2020). For example, the *L. rigidum* CYP81A gene *CYP81A10v7* – which is constitutively more highly expressed in herbicide-resistant populations – conferred resistance to 5 herbicides with 5 different modes of action when overexpressed in rice, and the overexpression in *A. thaliana* of either CYP81A12 or CYP81A21 – which are both constitutively overexpressed in herbicide resistant *Echinochloa phyllopogon* – conferred resistance to 11 herbicides with 4 different modes of action (Iwakami *et al.*, 2014a, Dimaano *et al.*, 2020). Since NTSR is often a polygenic trait, resistance to herbicides with different modes of action can also occur from the stacking of different NTSR alleles conferring resistance to different herbicides, known as multiple herbicide resistance (Gaines *et al.*, 2020). One population of *L. rigidum* which is resistant to glyphosate, ACCase inhibitors, and ALS inhibitors had no TSR mutations in any of the genes encoding the targets of these herbicides; plants from this population showed decreased glyphosate translocation, and the P450 inhibitors amitrole and malathion reversed resistance to ACCase inhibitors and AHAS inhibitors respectively, suggesting that three distinct NTSR-based mechanisms were responsible for the plants' resistance to these three herbicides (Yu *et al.*, 2009). NTSR weeds are therefore more likely to be resistant to several classes of herbicide than TSR weeds, making them harder to manage via herbicide treatment.

Multiple herbicide resistance (MHR) can also involve a mixture of TSR and NTSR: one biotype of *L. rigidum* was resistant to paraquat due to reduced translocation, resistant to ACCase inhibitors due to a TSR mutation in the gene encoding ACCase, and resistant to glyphosate due to both a TSR mutation in the gene encoding EPSPS and reduced glyphosate translocation (Yu *et al.*, 2007). TSR weeds can therefore be resistant to herbicides with different modes of action if their genome also contains other resistance-conferring alleles. However, only NTSR weeds can be resistant to more than one herbicide mode of action due to a single allele, so resistance to multiple herbicides is more commonly associated with NTSR.

1.7. NTSR is more problematic to agriculture than TSR

NTSR in weeds is quickly becoming more problematic for agriculture than TSR for several reasons.

Firstly, unlike TSR which can only confer resistance to a herbicide with a single mode of action, NTSR has the potential to confer herbicide cross-resistance, even to herbicides to which the weed was not exposed, or to novel herbicides which have not yet reached the market (Delye, 2013). For example, resistance to as many as 16 herbicide molecules have been reported in a single population of *L. rigidum*: these herbicide molecules comprise of 9 modes of action, 4 of which the population had never been exposed to (Burnet *et al.*, 1994). NTSR weeds with herbicide cross-resistance therefore cannot be managed as easily as TSR weeds: farmers typically manage TSR by switching to a herbicide with a different mode of action, but NTSR weeds can be resistant to multiple modes of action, so farmers have fewer herbicide options with which to manage NTSR weeds than TSR weeds (Delye *et al.*, 2011a). Herbicides with novel modes of action such as cinmethylin which was introduced

onto the market in 2020 (Campe *et al.*, 2018) offer a solution to treat herbicide cross-resistant weeds which cannot easily be controlled by herbicides on the market: however, since NTSR can confer resistance to herbicides the plant has never been exposed to, it is possible that NTSR weeds are resistant to and cannot be controlled by novel herbicides. Ultimately, this means that NTSR weeds are much harder to control with present and future herbicides than TSR weeds; given that agriculture currently relies heavily on the use of herbicides, NTSR is therefore more problematic to agriculture than TSR.

Secondly, comparatively few mechanisms of NTSR have been elucidated due to its complex often polygenic genetic basis and limited genomic resources in weeds (Yuan *et al.*, 2007). Those that have been discovered predominantly involve only four gene families – P450s, GSTs, GTs, and ABC transporters (Yuan *et al.*, 2007). By contrast, the genetic basis of TSR is well understood, and has led to the development of quick and cheap PCR-based diagnostic tools to identify TSR mutations encoding the target site of an enzyme, some within an hour of field sampling (Delye *et al.*, 2011b, Yu *et al.*, 2015, Edwards and Onkokesung, 2020). Rapid identification of TSR mechanisms – indicating which herbicide a weed is resistant to based on which herbicide target is mutated – allows fast decisions about effective weed management using herbicides with a mode of action the weed is sensitive to. However, due to the lack of information regarding the genetic basis of NTSR, there is only one rapid diagnostic tool for NTSR: an antibody-based test in *A. myosuroides* based on the overexpression of Am*GSTF1* in NTSR plants (Cummins *et al.*, 2013, Edwards and Onkokesung, 2020). The lack of diagnostic tools with which to rapidly identify NTSR in the field means that new weeds may be treated with herbicides without knowledge of if they are NTSR or not, increasing the risk of

selecting for herbicide resistant individuals (Delye, 2013). Furthermore, even if NTSR is suspected in a weed, the inability to identify its genetic basis means that NTSR weeds have unpredictable cross-resistance patterns, and treating an NTSR weed with a herbicide without knowledge of its resistance pattern risks selecting for individuals with resistance to multiple herbicides (Delye, 2013). Therefore, the lack of understanding of the genetic basis of NTSR means that NTSR weeds are harder to rapidly identify and effectively manage than TSR weeds, and the subsequent ineffective management of NTSR weeds risks selecting for NTSR in the field.

Finally, there are increasing numbers of cases of NTSR in the field to glyphosate, the world's most used herbicide, and to ACCase inhibitors and AHAS inhibitors (Delye *et al.*, 2010, Powles *et al.*, 2010, Delye, 2013). Together, these three modes of action make up approximately 50 % of the world's herbicide market (Peters and Strek, 2018). NTSR therefore already presents a threat to the most widely used herbicides globally, and since it is harder to identify and manage than TSR, it is likely that the relative prevalence of NTSR compared to TSR worldwide will continue to increase.

It is important to broaden our understanding of molecular mechanisms of NTSR to better understand how to manage it and prevent its selection in the field.

1.8. Methods to identify molecular mechanisms of NTSR

NTSR in *A. myoruroides* based on overexpression of Am*GSTF1* can be detected by a rapid antibody test (Cummins *et al.*, 2013, Edwards and Onkokesung, 2020); NTSR in other weed species can be confirmed by biochemical assays measuring differences in the rate of metabolism of herbicides or in the herbicide metabolites produced by resistant and sensitive weeds, and P450 inhibitors can be used to determine whether resistance of a weed relies on P450 activity (Ma *et al.*, 2013).

However – aside from the antibody test to detect Am*GSTF1* overexpression in *A. myosuroides* – unlike rapid PCR-based diagnostic tools available for TSR (Delye *et al.*, 2011b, Yu *et al.*, 2015, Edwards and Onkokesung, 2020), these assays do not identify the genetic basis of NTSR. To identify specific genes involved in NTSR, several experimental approaches can be taken.

1.8.1. Gene silencing of a candidate NTSR allele can confirm that it causes resistance

One approach to determine the genetic basis of NTSR in species which are readily genetically tractable is knockdown or knockout of a candidate NTSR allele (Dimaano *et al.*, 2020). For example, the first specific P450 gene shown to confer NTSR was *CYP81A6* in rice, which was identified by map-based cloning in a rice mutant sensitive to bentazon and sulfonylureas, to which wild type rice (*Oryza sativa ssp. indica*) is resistant via NTSR (Pan *et al.*, 2006). Knockdown of the gene in wild-type rice using its antisense RNA reversed the resistance, proving that *CYP81A6* was responsible for the NTSR (Pan *et al.*, 2006). The silencing of specific cytochrome P450 genes to confirm their role in NTSR has been used in the crop species rice, corn, and cotton (Pan *et al.*, 2006, Li *et al.*, 2013, Thyssen *et al.*, 2018). However, the lack of tools with which to carry out genetic modification of weed species makes it difficult to use this method to identify genes conferring NTSR in weeds.

1.8.2. Heterologous expression of candidate NTSR alleles from weeds in model species can confirm that they confer resistance

Several gene families have already been implicated in NTSR, namely P450s, GSTs, GTs and ABC transporters (Yuan *et al.*, 2007). Heterologous expression of weed genes from these families into model species can demonstrate that specific alleles

can confer NTSR, either via observation of herbicide metabolism (in *S. cerevisiae*) or herbicide resistance (in *A. thaliana* or *N. tabacum*) in the transgenic individuals (Lamb *et al.*, 1998, Cummins *et al.*, 2013, Iwakami *et al.*, 2014a). For example, *A. thaliana* lines transformed with *E. phyllopogon CYP81A12* or *CYP81A21* were resistant to bensulfuron-methyl and penoxulsam, and *S. cerevisiae* transformed with *E. phyllopogon CYP81A12* or *CYP81A21* metabolised bensulfuron-methyl, suggesting that the observed overexpression of these two genes in a resistant population of *E. phyllopogon* is the basis of its NTSR (Iwakami *et al.*, 2014a).

However, the candidate genes in these studies are chosen on the basis that they are from families already implicated in NTSR, such as the *CYP81* family of P450s: the study in *E. phyllopogon* based their choice of candidate genes due to the established ability of *CYP81* genes to metabolise herbicides in rice (Pan *et al.*, 2006, Iwakami *et al.*, 2014a, Dimaano *et al.*, 2020). While heterologous expression can be used to confirm the ability of a candidate gene to confer NTSR, the identification of novel candidate genes which are unrelated to families already implicated in NTSR cannot be achieved using heterologous expression alone.

1.8.3. Transcriptomics can identify candidate NTSR alleles which are more highly expressed in herbicide-resistant than in herbicide-sensitive weeds

The most widely used method to identify genes associated with NTSR in weeds is to compare the transcriptomes of sensitive and resistant weeds and identify genes which are constitutively overexpressed, or differentially expressed in response to a herbicide, in resistant individuals: Table 1.2 references and describes a variety of studies using transcriptomics to identify candidate genes conferring NTSR in a variety of weeds.

Plant species	Conditions for identification of DEG between S and R	Genes associated with NTSR	Reference
Lolium rigidum	In untreated conditions In segregating F_2 population Induced in S by 2,4-D In 9 untreated R populations	2 P450s 1 GT 1 nitronate monooxygenase	(Gaines *et al.*, 2014)
Eleusine indica	In untreated conditions In response to paraquat	4 ABC transporters 14 other transporters 10 polyamine biosynthesis	(An *et al.*, 2014)
Ipomoea purpurea	In response to glyphosate	1 P450 growth and defence genes	(Leslie and Baucom, 2014)
Lolium spp.	In untreated conditions In response to pyroxsulam	6 P450s 6 GSTs 1 GT 17 other (carbonic anhydrase, other)	(Duhoux *et al.*, 2015)
Alopecurus myosuroides	In untreated conditions In response to iodosulfuron + mesosulfuron	3 P450s 1 peroxidase 1 disease resistance protein	(Gardin *et al.*, 2015)
Brachypodium hybridum	In untreated conditions In response to pinoxaden Searched for genes from families already implicated in NTSR	P450s GSTs GTs other (oxidation, glucose conjugation)	(Matzrafi *et al.*, 2017)
Alopecurus aequalis	In untreated conditions In response to mesosulfuron-methyl	4 P450s 2 GSTs 2 GTs 2 ABC transporters 7 other (oxidation, hydrolysis, stress)	(Zhao *et al.*, 2017)
Helianthus annuus	In untreated conditions	P450s GSTs GTs ABC transporters	(Gil *et al.*, 2018)
Conyza bonariensis	In response to glyphosate Searched for genes from families already implicated in NTSR	10 P450s 1 GST 5 GTs 19 ABC transporters 8 ROS metabolism	(Piasecki *et al.*, 2019)
Lolium multiflorum	In response to glyphosate	3 GTs 1 ABC transporters 9 cell membrane related genes 6 other (oxidoreductase, cell wall, other)	(Cechin *et al.*, 2020)
Beckmannia syzigachne	In untreated conditions In response to mesosulfuron-methyl	1 P450 3 GSTs 3 disease resistance proteins 4 other	(Wang *et al.*, 2021)
Lolium rigidum	In untreated conditions Heterologous expression in rice	1 P450	(Han *et al.*, 2021)
Leptochloa chinensis	In response to cyhalofop-butyl	3 P450s 3 ABC transporters	(Chen *et al.*, 2021a)

Table 1.2. A selection of transcriptomic studies identifying genes associated with NTSR in resistant weeds. The conditions for identification of NTSR associated genes is listed: in all cases genes were selected based on differential expression (DE) between sensitive (S) and resistant (R) weed populations in different conditions. The types of genes associated with NTSR identified in each study are also listed.

Transcriptomics can identify NTSR mechanisms conferred by large changes in gene expression: however, transcriptomics cannot identify NTSR mechanisms conferred by small changes in expression of multiple genes or by loss of gene function. In addition, our lack of knowledge concerning the genetic bases of NTSR other than from gene families already implicated in NTSR (P450s, GSTs, GT, ABC transporters) means that transcriptomics studies tend to focus exclusively on candidates from these families (Table 1.2) (Yuan *et al.*, 2007, Matzrafi *et al.*, 2017, Gil *et al.*, 2018, Piasecki *et al.*, 2019, Chen *et al.*, 2021a).

Furthermore, constitutively increased expression of a gene in resistant weed populations does not necessarily equate to a role in NTSR. For example, two P450s (*CYP71AK2* and *CYP72A254*) were expressed more highly in bispyribac resistant *E. phyllopogon* in comparison to sensitive populations; however, heterologous expression of these genes in *A. thaliana* did not confer bispyribac resistance (Iwakami *et al.*, 2014b, Dimaano *et al.*, 2020). Functional characterisation is therefore required to confirm that a candidate gene identified by transcriptomics is responsible for NTSR. It is difficult to undertake functional characterisation in weed species, so in many cases genes identified by transcriptomics are classed as candidates for conferring NTSR without follow up experiments to confirm their involvement in resistance (An *et al.*, 2014, Leslie and Baucom, 2014, Duhoux *et al.*, 2015, Gardin *et al.*, 2015, Matzrafi *et al.*, 2017, Zhao *et al.*, 2017, Gil *et al.*, 2018, Piasecki *et al.*, 2019, Cechin *et al.*, 2020, Chen *et al.*, 2021a, Wang *et al.*, 2021) (Table 1.2). Gaines et al. used several criteria to support the role of four candidate genes in conferring NTSR to diclofop in *L. rigidum*, namely confirming their segregation with resistance in individuals from a cross between sensitive and resistant plants, as well as confirming their induction upon pretreatment with 2,4-D

(which has been shown to confer resistance to diclofop) and their overexpression in 9 separate diclofop resistant populations (Gaines *et al.*, 2014) (Table 1.2). Although these methods of validation strongly support the role of these four genes in conferring NTSR to diclofop, they still do not definitely prove that overexpression of these genes is responsible for diclofop resistance in *L. rigidum*. Transcriptomics alone therefore cannot prove that a candidate gene is definitively involved in NTSR.

To complement transcriptomics studies, heterologous expression in other organisms can be used to prove that a candidate gene identified by transcriptomics confers NTSR. Overexpression of *CYP81A10v7*, which was constitutively more highly expressed in herbicide resistant than in sensitive *L. rigidum*, conferred herbicide cross-resistance and increased diclofop metabolism in rice (Han *et al.*, 2021). However, since NTSR is more often a polygenic trait (Delye, 2013), it is possible that overexpression of several genes is required to confer resistance. For example studies of the expression levels of the four genes identified by Gaines et al. in *L. rigidum* populations with different levels of resistance to diclofop showed that high expression of one or two of the genes alone was insufficient to confer resistance (Gaines *et al.*, 2014), so a multiple order mutant would be required to confirm that overexpression of these genes confers NTSR. Furthermore, in most transcriptomics studies, a large number of candidate genes responsible for NTSR are identified, making it difficult to prioritise which genes should be functionally characterised (An *et al.*, 2014, Duhoux *et al.*, 2015, Zhao *et al.*, 2017, Piasecki *et al.*, 2019, Cechin *et al.*, 2020, Wang *et al.*, 2021) (Table 1.2).

1.8.4. Population genomics can identify candidate NTSR alleles in regions of the genome associated with NTSR

Recent advances in the ease of generating draft genomes for weed species has led to the ability to conduct population genomics studies to identify genes associated with resistance in resistant weed populations (Martin *et al.*, 2019). Only a handful of studies have so far employed population genomics approaches to identifying mechanisms of NTSR.

Kreiner et al. identified genes associated with NTSR in glyphosate resistant populations of *A. tuberculatus* via a GWAS (Kreiner *et al.*, 2019, Kreiner *et al.*, 2021). The genomes of 163 *A. tuberculatus* individuals from 19 glyphosate-resistant or sensitive populations across the US and Canada were sequenced, and a GWA (statistically controlling for the presence of two target-site mutations in EPSPS) identified SNPs in 274 *A. tuberculatus* genes associated with NTSR to glyphosate (Kreiner *et al.*, 2019, Kreiner *et al.*, 2021). The majority of these 274 genes are not in the families previously associated with NTSR, so represent candidates for novel mechanisms of NTSR which have not yet been studied (Yuan *et al.*, 2007, Kreiner *et al.*, 2021). Van Etten et al. also recently conducted a population genomics analysis to identify the basis of glyphosate resistance in the weed *Ipomea purpurea* (Van Etten *et al.*, 2020). SNPs between 10 *I. purpurea* individuals from each of 4 sensitive and 4 glyphosate resistant populations were identified using nextRAD sequencing and from this data 5 regions of the genome were identified which exhibited signs of selection and were therefore potentially involved in glyphosate resistance (Van Etten *et al.*, 2020). These 5 regions were all enriched in P450, GST, GT, and ABC transporter genes. 1 of these regions containing a tandemly repeated group of 7 GT

genes and 9 P450 genes exhibited particularly high genetic similarity between the 4 resistant populations, so the genes within this region are strong candidates for conferring NTSR to glyphosate (Martin *et al.*, 2019, Van Etten *et al.*, 2020).

An important strength of population genomics approaches is that they have the potential to identify loci containing novel mechanisms of NTSR conferred by genes which have not yet been implicated in NTSR (Kreiner *et al.*, 2021). However, because GWAS is based on a statistical correlation between genetic polymorphisms and phenotypes, it is likely that some of the identified candidate alleles cause NTSR but that some do not. Functional characterisation is therefore required to confirm that a candidate gene is involved in the resistance phenotype (Martin *et al.*, 2019). Functional characterisation is difficult to undertake in weed species, therefore similarly to the candidate genes identified by transcriptomics in weed species, there is no proof that the identified genes cause NTSR.

1.8.5. Forward genetics can identify NTSR alleles conferred by loss of gene function

Forward genetics is a potential method of identifying NTSR mechanisms. Forward genetics involves mutagenizing a wild-type population of individuals, screening the mutagenized population for a phenotype of interest – in this case herbicide resistance – and identifying the genetic basis of the phenotype (Ostergaard and Yanofsky, 2004).

There are a variety of methods available to mutagenize individuals: physical mutagenesis involves the use of radiation such as UV-B or ɣ radiation, and chemical mutagenesis involves the use of chemicals such as ethyl methanesulfonate (EMS), sodium azide, or methyl-nitrosourea (MNU) (Jin *et al.*, 2021). Each method introduces different types of mutation into the genome (Olsen *et al.*, 1993, Jander *et*

al., 2003, Gruszka *et al.*, 2012, Brash, 2015), therefore forward genetics has the potential to identify NTSR conferred by a variety of mutations in the genome.

Traditionally, forward genetics approaches were constrained by the difficulty of classical mapping to identify the gene responsible for a mutant phenotype (Schierenbeck *et al.*, 2015). However, recent advances in genomics technologies have led to the development of fast mapping strategies using next generation sequencing to identify candidate SNPs in mutants responsible for a phenotype, making mapping much more feasible (Schneeberger, 2014). This type of "fast forward genetics" approach was first carried out in the yeast *Pichia stipitis* (Smith et al., 2008), and has since been used for fast genetic mapping in mutants of various model species such as *C. reinhardtii*, *A. thaliana*, and *M. polymorpha*, and crop plants such as barley and sorghum (Mascher *et al.*, 2014, Schneeberger, 2014, Schierenbeck *et al.*, 2015, Addo-Quaye *et al.*, 2017, Champion *et al.*, 2021).

Forward genetics has been extensively used to identify mutations conferring TSR (Jander *et al.*, 2003, Shim *et al.*, 2018, Chen *et al.*, 2021b, Jin *et al.*, 2021), but has been used to a limited extent to identify mechanisms of NTSR. One example of forward genetics identifying a mechanism of NTSR involves the herbicide-sensitive rice mutant in which the first specific P450 gene shown to confer NTSR was identified, which came from a population of γ-radiated rice individuals (Pan *et al.*, 2006). The mutant had a single base deletion in the *CYP81A6* gene leading to a loss of gene function which conferred sensitivity to bentazon and sulfonylureas: introduction of the wild-type gene rescued the sensitivity, and heterologous expression of the wild-type copy of *CYP81A6* in *A. thaliana* and *N. benthamiana* conferred resistance to these two herbicides, confirming that this allele can confer

NTSR (Pan *et al.*, 2006, Liu *et al.*, 2012). In this case, the loss-of-function mutant derived from the forward genetic screen was herbicide-sensitive, so the comparative resistance in the wild-type rice variety is due to a gain in gene function compared to the mutant.

Very few mechanisms of NTSR conferred by loss-of-function have been identified; those that have were identified via forward genetics screens in *A. thaliana*. Scheible et al. conducted a forward genetics screen to identify mutations which could confer resistance to the novel herbicide thaxtomin A (Scheible *et al.*, 2003). A thaxtomin A resistant mutant generated from this screen had an early stop codon in a then unknown gene named *txr-1*; it was therefore suggested that complete loss-of-function of *TXR-1* confers resistance to thaxtomin A (thaxtomin resistant 1) (Scheible *et al.*, 2003). *TXR-1* was later identified as the gene *PAM16*, a component of the mitochondrial inner membrane transport complex (Scheible *et al.*, 2003, Huang *et al.*, 2013). The resistance in At*pam16* loss-of-function mutants is thought to be NTSR rather than TSR as At*pam16* mutants are weakly resistant to thaxtomin A, uptake less thaxtomin A than wild-type, and are cross-resistant to the herbicide isoxaben (Scheible *et al.*, 2003, Tegg *et al.*, 2013). The only other example of NTSR conferred by loss-of-function in the literature is from a PhD thesis by Reavell-Roy, where EMS mutagenised *A. thaliana* seeds were screened for resistance to the herbicide indaziflam (Reavell-Roy, 2019). The screen yielded one indaziflam-resistant line, *izr1*, which had a SNP in *CULLIN1* (*CUL1*), a component of SCF ubiquitin ligase complexes which mediates responses to auxin (Hellmann *et al.*, 2003, Moon *et al.*, 2007, Reavell-Roy, 2019). The phenotypes of other *A. thaliana cul1* loss-of-function mutants are consistent with disruption of auxin signalling and are resistant to auxin-mimicking herbicides (Hobbie *et al.*, 2000, Moon *et al.*, 2007).

izr1 had a SNP in the same region of the CULLIN1 protein as these *cul1* mutants, and displayed similar phenotypes such as small growth, loss of apical dominance, and strong resistance to the auxin mimic 2,4-D, suggesting that *izr1* mutants are loss-of-function mutants of *CUL1* (Moon *et al.*, 2007, Reavell-Roy, 2019). *izr1* mutants were very weakly resistant to indaziflam – with a resistance index of approximately 1.13 – therefore their resistance to indaziflam is likely due to NTSR, suggesting that loss-of-function of *CUL1* confers NTSR to indaziflam (Reavell-Roy, 2019).

Forward genetics has the potential to identify NTSR which arises as a result of loss of gene function, such as that conferred by loss-of-function of *PAM16* or *CUL1* in *A. thaliana* (Scheible *et al.*, 2003, Reavell-Roy, 2019). No mechanisms of NTSR arising from loss of gene function have been reported yet in weed species, yet based on these two studies carried out in the model species *A. thaliana*, loss of gene function can confer NTSR in plants. It is therefore possible that NTSR involving loss of gene function has evolved in weeds but remains undetected and unreported. Forward genetics could therefore be used to identify these potential mechanisms of NTSR conferred by loss-of-function in weeds.

Since genomic resources and mutagenesis techniques are limited in weed species, it is easier to carry out forward genetic screens in model species where mutagenesis, genetic mapping, and subsequent functional characterisation of identified resistance genes by reverse genetics can be carried out more easily. Therefore, rather than directly identifying the resistance mechanisms present in resistant weeds, forward genetics can identify potential mechanisms of NTSR which can occur in model plants and could therefore be responsible for NTSR in weeds. However, mutant screens in

diploid models such as *A. thaliana* are limited in scale due to the considerable effort required to reach the F_2 screening population. Screening of the F_2 generation is required to identify recessive resistance-conferring alleles in diploids, constraining the number of mutants that can be screened for herbicide resistance: a typical *A. thaliana* screen is limited to 2000-3000 individuals (Page and Grossniklaus, 2002). The use of forward genetics to identify mechanisms of NTSR has therefore so far been mostly unsuccessful. However, novel model species such as *Marchantia polymorpha* which are more suited to forward genetic screens present an opportunity to discover novel mechanisms of NTSR by forward genetics.

1.9. *Marchantia polymorpha* is suited to forward genetics

Marchantia polymorpha is emerging as a model system in which is it possible to carry out mutagenesis screens at a significantly larger scale than in diploid angiosperms. One *M. polymorpha* plant can produce millions of spores which can be rapidly mutagenized, and its dominant haploid form means that mutations are observed in the same generation as mutagenesis, enabling larger-scale and faster production and screening of mutants (Ishizaki *et al.*, 2016, Kohchi *et al.*, 2021).

Although forward genetic screens using single-celled haploid model organisms such as *C. reinhardtii* also enable large-scale mutant generation, *M. polymorpha* is more similar physiologically to agricultural weeds than algae (Baker, 1974, Kohchi *et al.*, 2021). It has also been suggested that gene networks underlying bryophyte gametophyte physiology are similar to those in the dominant sporophyte of later diverging land plants, including weeds (Ligrone *et al.*, 2012b, Pires and Dolan, 2012), justifying the use of the *M. polymorpha* gametophyte as a model for dominant sporophytic weeds. In addition, *M. polymorpha* mutant lines can be easily maintained

due to the production of clonal propagules (via asexual propagules called gemmae): thallus excision even allows maintenance of lines with defective reproduction (Shimamura, 2015). Genetic mapping mutations is facilitated both by its dioecy – which allows controlled crossing analyses – and growing bioinformatic resources including an annotated genome (Bowman *et al.*, 2017). Mapping-by-sequencing has already successfully been used to identify mutations responsible for defective rhizoid phenotypes in *M. polymorpha*, demonstrating the potential for "fast forward genetics" approaches in *M. polymorpha* (Champion *et al.*, 2021). Furthermore, targeted mutagenesis via homologous recombination and CRISPR-Cas9 is possible in *M. polymorpha*, which is particularly useful for confirming resistance-conferring mutations via reverse genetics (Sugano *et al.*, 2014, Ishizaki *et al.*, 2016). The ability to generate large numbers of mutants combined with the ease of mutant maintenance, mutation mapping, and reverse genetics for candidate gene functional characterisation makes *M. polymorpha* a model system well suited to forward genetics.

In this DPhil thesis, I use *M. polymorpha* to identify novel mechanisms of NTSR conferred by loss of gene function. I first show that loss-of-function of PAM16, one of the two known mechanisms of NTSR conferred by loss-of-function, is a conserved mechanism of NTSR in *M. polymorpha*, validating its use as a model with which to study NTSR. I then use a forward genetics approach in *M. polymorpha* and identify a novel mechanism of NTSR involving loss-of-function of the gene *RAD8*, and 8 further candidate genes conferring NTSR, 4 of which have been associated with NTSR in the weed *A. tuberculatus* by population genomics. The novel mechanism of NTSR I discovered is only the third reported NTSR mechanism involving loss of gene function, and involves a gene which has never been implicated in NTSR. I also

functionally characterise the mechanism of resistance I identified using loss-of-function mutants, and study the cross-resistance patterns and basis of resistance of this mechanism of NTSR. My approach can therefore not only identify completely novel mechanisms of NTSR, but also characterise the resistance thereby broadening our understanding of how NTSR can arise and how best to manage it in the field.

Chapter 2: A mechanism of non-target site resistance conferred by loss-of-function of *PAM16* is conserved in *Marchantia polymorpha*

2.1. Abstract

Non-target site resistance (NTSR) to herbicides in weeds threatens the efficacy of herbicides and consequently global crop yields. It is important to identify NTSR mechanisms to understand how to manage NTSR and prevent its evolution in the field. However, NTSR mechanisms are difficult to characterise because NTSR is often a polygenic trait involving multiple alleles each conferring relatively low levels of resistance. Most NTSR mechanisms described in the literature are caused by gain-of-function mutations that result in overexpression of genes that modify or compartmentalise the herbicide. There are very few reports of NTSR conferred by loss of gene function (Scheible *et al.*, 2003, Reavell-Roy, 2019). One of the two examples reported is in the model plant *Arabidopsis thaliana*, where a loss-of-function allele in the gene encoding the mitochondrial inner membrane transport complex subunit protein PAM16 in a mutant isolated from a mutagenesis screen confers weak resistance to the herbicide thaxtomin A (TXTA). I propose to use *Marchantia polymorpha* to identify novel NTSR mechanisms. In this chapter I generated loss-of-function lines of the *M. polymorpha* homologue of *PAM16* to demonstrate that this mechanism of NTSR could also be found in *M. polymorpha*. I generated 33 independent Mp*pam16* mutant lines, of which 9 were weakly resistant to TXTA. These data demonstrate that mutations in Mp*PAM16* can confer resistance to TXTA in *M. polymorpha*, validating the use of *M. polymorpha* as a model in which to discover mechanisms of NTSR.

2.2. Introduction

Herbicide resistance in weeds is a growing threat to agriculture; non-target site resistance (NTSR) is becoming a pressing issue due to the difficulty in identifying its genetic basis in weeds as well as its potential to confer resistance to different classes of herbicides, a phenomenon known as herbicide cross-resistance. The mechanisms of NTSR which have been discovered mainly involve increased expression or activity of enzymes from a few gene families such as cytochrome P450 monooxygenases which metabolise the herbicide or ABC transporters involved in herbicide translocation and sequestration away from the target (Yuan *et al.*, 2007, Gaines *et al.*, 2020). NTSR conferring alleles are mostly identified by comparing gene expression between sensitive and resistant weeds and identifying mRNAs whose steady state or herbicide induced levels are higher in resistant than sensitive weeds. Gain-of-function mutations resulting in the overexpression of the gene that confers resistance are responsible for these mechanisms of NTSR. It has been more difficult to identify mechanisms of NTSR conferred by loss of gene function.

While there are no examples of NTSR conferred by loss-of-function mutations in weeds, there are two examples in the model plant *Arabidopsis thaliana* (Scheible *et al.*, 2003, Reavell-Roy, 2019). Loss-of-function mutations in the *PAM16* gene confer weak resistance to the herbicide thaxtomin A (TXTA). A TXTA-resistant mutant was discovered in a screen of an EMS mutagenised *A. thaliana* population: the resistance-conferring mutation was mapped to a then unknown protein named TXR-1, later identified as PAM16 (Scheible *et al.*, 2003, Huang *et al.*, 2013). At*pam16* mutants are approximately 10 times more resistant than the wild-type accession Col-0, and less TXTA accumulates in At*pam16* tissues than in Col-0. Their TXTA

resistance is weak and dose-dependent, suggesting NTSR rather than target site resistance (TSR). The PAM16 protein is part of the PAM complex that transports proteins across the mitochondrial inner membrane. Loss of *PAM16* function leads to disruption of the PAM complex and increased cellular reactive oxygen species. The protein sequence of PAM16 is highly conserved across eukaryotes (Chen *et al.*, 2013). Furthermore, the *A. thaliana* PAM16 protein rescues the phenotype of *Saccharomyces cerevisiae pam16* mutants, and the *S. cerevisiae* PAM16 protein complements *A. thaliana pam16* mutants (Huang et al., 2013), suggesting that PAM16 protein function is also highly conserved.

The aim of my project is to identify novel mechanisms of NTSR, especially conferred by loss-of-function mutations, using forward genetics in *M. polymorpha*. Although *M. polymorpha* is suited to forward genetics, its physiology is different from angiosperm weeds (Baker, 1974, Kohchi *et al.*, 2021). However, many herbicide targets are present in its genome, and the gene networks of bryophyte gametophytes are similar to those of dominant sporophytes (Ligrone *et al.*, 2012a, Pires and Dolan, 2012) therefore *M. polymorpha* may be a good system for herbicide research. To test if *M. polymorpha* is a suitable model with which to identify mechanisms of NTSR, I carried out a phylogenetic analysis of the conservation of Mp*PAM16* across land plants, and generated Mp*pam16* mutant lines and tested their resistance to TXTA. I found that *M. polymorpha* has one copy of *PAM16* which is highly conserved compared to the sequences of *PAM16* orthologues in other land plants. Several Mp*pam16* putative loss-of-function mutant lines were significantly but weakly resistant to TXTA, suggesting that the mechanism of NTSR conferred by loss-of-function of *PAM16* is conserved across land plants. These data provide proof-of-concept support for using *M. polymorpha* as a system with which to discover mechanisms of NTSR.

2.3. Materials and Methods

2.3.1. Phylogenetic analysis of *PAM16* homologues

Homologues of the *A. thaliana* gene At3G59280 were identified by protein BLASTp search against the reference proteomes of various species (Table 2.1). Only homologues with an E value less than 1E-5 were used to construct the tree.

Homologues were aligned via the L-INS-i strategy using MAFFT version 7 (Katoh *et al.*, 2019). The alignment was trimmed using BioEdit7.2. A maximum likelihood tree was constructed with PhyML 3.0 using an estimated gamma distribution parameter and the LG model of amino acid substitution. A non-parametric approximate likelihood ratio test based on a Shimodaira-Hasegawa-like procedure was used to calculate branch support values using PhyML 3.0 (Guindon *et al.*, 2010). The tree was rooted with the *Saccharomyces cerevisiae PAM16* gene.

2.3.2. Plant lines and growth conditions

Wild-type plants were *M. polymorpha* laboratory accessions Takaragaike-1 (Tak-1) and Takaragaike-2 (Tak-2) (Ishizaki *et al.*, 2008). Mp*pam16* lines were generated via CRISPR-Cas9 mutagenesis of wild-type *M. polymorpha* spores (generated from a cross between Tak-1 and Tak-2).

All lines were maintained via asexual propagation of gemmae or thallus excision in the case of mutants which did not produce gemmae. Plants were grown on solid Johnson's or ½ Gamborg medium with 0.8 % agar (Section 2.3.11). All plant material used for experiments was grown in a growth chamber at 23 °C under 24-hour 10-30 µmol m^{-2} s^{-1} white light. Plant material to be stored long-term was kept in a growth chamber at 17 °C under 6 hours 10-30 µmol m^{-2} s^{-1} white light and 18 hours dark. To

produce spores, plants were grown on a mixture of John Innes n. 2 compost and fine vermiculite at a ratio of 2:1. Plants were grown in growth chambers at 23 °C and under 16 hours white light and continuous far-red light to induce transition to the reproductive phase. Once mature, water was pipetted onto the antheridia produced by male plants to collect sperm, then transferred to archegonia produced by female plants. Sporangia were harvested before bursting and stored fresh at 4 °C in sterile dH_2O.

2.3.3. Fresh spore sterilisation

Fresh sporangia were sterilised with 1 % NaDCC (sodium dichloroisocyanurate) for 4 minutes followed by rinsing with sterile dH_2O.

2.3.4. Chemicals and stock solution preparation

Thaxtomin A (TXTA) (SML1456) was obtained from Sigma-Aldrich. Stock solutions were prepared by dissolving in pure dimethyl sulfoxide (DMSO) (D8418) from Sigma-Aldrich.

2.3.5. Gemmaling dose-response assays

Gemmae were grown for 14 days on solid Johnson's or ½ Gamborg medium (Section 2.3.11) supplemented with different concentrations of herbicide dissolved in DMSO. The concentration of DMSO (0.1 %) was determined not to exert a significant detrimental effect on plant growth (Supplementary Fig. S2.1). Gemmalings were imaged using a Berthold Nightowl II LB 983 *In Vivo* Imaging System (Berthold, Bad Wildbad, Germany). Images were taken after exposing gemmalings to 120 s white light. The imaging system detects chlorophyll autofluorescence (560 nm). The lateral area of autofluorescing (living) tissue was

determined using the indiGo™ software package (Berthold, Bad Wildbad, Germany). Dose-response curves were generated using the ggplot2 and drc packages in R (Wickham, 2009, Ritz *et al.*, 2015); the four-parameter log-logistic equation was used to fit a dose-response curve to the data.

2.3.6. Guide RNA design

A single *M. polymorpha* homologue to At*PAM16* (*PAM16*) was identified by protein BLAST of the *M. polymorpha* reference proteome (Tak1v5.1). Guide RNAs which would anneal to different parts of the gene (Mp3g09390.1, referred to as Mp*PAM16*) in order for the Cas9 nuclease to introduce targeted double strand breaks were designed to be 5' of an "NGG" site (PAM sequence) as required by the CRISPR-Cas9 system (Sugano *et al.*, 2014). The guide RNA sequences are as follows:

sgRNA 1	GGCGCAACAATCAGAACCAC
sgRNA 2	CGGCTCGGGTGTGCTTCTTC
sgRNA 3	GAATTTGATCGTCCTCGGCT
sgRNA 4	GATCTAAAGTTCAGCGAGCCA
sgRNA 5	GTTCGAAAGAAATGCGAAGAT

2.3.7. Cloning of CRISPR-Cas9 vectors

Oligos were ordered and annealed using T4 PNK (New England Biolabs) using the following reaction components and conditions:

2 µl each oligo (Fw and Rv)

5 µl T4 ligase buffer (NEB)

1 µl T4 PNK (NEB)

40 µl dH_2O

30 min 37 °C

5 in 97 °C, 5 °C decrease in temperature every 30 s

20 min room temperature

The *M. polymorpha* vectors for single guide RNA (MpEN03) or double guide RNA (HBp453) were digested with BbsI and run on 1 % agarose gel, followed by gel extraction using the GeneJET gel extraction kit as per the Thermo Fisher Scientific protocol and dephosphorylation with Antarctic Phosphatase as per the NEB protocol. Ligation of digested vector and annealed oligos from sgRNA 1 was performed using NEB T4 ligase for one hour at room temperature with the following reaction components:

50 ng digested vector

3 µl annealed oligos

1 µl T4 ligase (NEB)

2 µl T4 DNA ligase buffer (NEB)

One Shot® OmniMAX™ chemically competent cells were transformed with the ligation products by heat-shock at 42 °C and plated on solid LB media supplemented with 100 µg ml^{-1} ampicillin (HBp453) or 50 µg ml^{-1} kanamycin (MpEN03) to grow overnight at 37 °C. Single surviving colonies were grown in liquid LB containing the appropriate antibiotics (ampicillin for HBp453; kanamycin for MpEN03) shaking overnight at 160 rpm at 37 °C, and the desired plasmid extracted using the GeneJET plasmid miniprep kit according to the Thermo Fisher Scientific protocol. For the double guide RNA vector (HBp453) only, the extracted plasmid was re-digested using BsmBI (NEB) and ligated to annealed oligos from sgRNA 2. The process of transformation in competent cells and plasmid extraction via miniprep was repeated to yield a plasmid with two guide RNAs. Gateway Cloning using LR Clonase II

(Thermo Fisher Scientific) was then used to insert either a single guide RNA or two guide RNAs into the final vector containing the Cas9 (pMpGEO010) and a hygromycin resistance gene (Fig. 2.4).

2.3.8. *Agrobacterium tumefaciens*-mediated transformation of *M. polymorpha* spores

Vectors were transformed into *Agrobacterium tumefaciens* strain GV3101 by electroporation (modified from (Ishizaki *et al.*, 2008)). The strain is resistant to rifampicin and gentamycin, and successful transformants are resistant to spectromycin. Transformed *A. tumefaciens* was plated on solid LB media supplemented with 50 μg ml^{-1} spectromycin, 50 μg ml^{-1} gentamycin, and 50 μg ml^{-1} rifampicin, and grown for 2 days at 28 °C to select for bacteria which had successfully taken up the CRISPR-Cas9 vectors. Single colonies were grown in liquid LB medium supplemented with spectromycin, gentamycin and rifampicin and grown for 2 days shaking at 150 rpm at 28 °C. The culture was then centrifuged and the resulting pellet resuspended in 100 μM acetosyringone and grown for 3-6 hours shaking at 150 rpm at 28 °C to induce the *Agrobacterium.* Following induction, 1 ml *Agrobacterium* culture was added to 25 ml wild type *M. polymorpha* spores (resulting from a cross between Tak-1 and Tak-2 strains). Spores for use in *A. tumefaciens* mediated transformation were sterilised and grown for a week in 25 ml M51C media (Section 2.3.11) in a Sanyo growth chamber at 23 °C under 24-hour 10-30 μmol m^{-2} s^{-1} white light prior to co-cultivation with *A. tumefaciens.* Acetosyringone was added to a final concentration of 100 μM. The spores and *A. tumefaciens* were then co-cultivated for 2 days shaking at 120 rpm at 23 °C. The culture was poured through a 50 μm cell strainer to collect the sporelings, which were washed with 150 ml dH_2O.

Sporelings were plated on solid Johnson's media supplemented with 100 µg ml^{-1} cefotaxime (to kill residual *A. tumefaciens*) and 10 µg ml^{-1} hygromycin to select for transformants. The sporelings were grown in a Sanyo growth chamber at 23 °C under 24-hour 10-30 µmol m^{-2} s^{-1} white light for 1-2 weeks. Surviving plants were then transferred to fresh solid Johnson's media supplemented with 100 µg ml^{-1} cefotaxime (to kill residual *A. tumefaciens*) and 10 µg ml^{-1} hygromycin and grown for a week in the same conditions.

2.3.9. Genotyping potential Mp*pam16* mutants generated by CRISPR-Cas9 mutagenesis

Putative Mp*pam16* mutants were genotyped using the Phire Plant Direct PCR kit (Thermo Scientific™) as per the kit protocol. The primers used were designed to anneal to the Mp*PAM16* gene on either side of sgRNA 1 and sgRNA 2 to amplify the gene fragments in which mutations are expected following CRISPR-Cas9 mutagenesis (Section 2.3.10). PCR products were run on a 1 % agarose gel and extracted using the GeneJET gel extraction kit (Thermo Scientific™) as per the protocol. The extracted PCR products were Sanger sequenced and aligned with the consensus Mp*PAM16* sequence (Tak1v5.1) using Geneious Prime® 2019.0.3 or CLC Genomics Workbench 9 to determine the nature of any introduced mutations.

2.3.10. Primers

Primer	Sequence	Use
GCC3Fw	TTCGAAATCAATGACCACGGG	Genotyping Mp*pam16* lines (sgRNA1 and sgRNA 2); sequencing Mp*pam16* lines (sgRNA1)
GCC1Rv	GTGTTCTCAGAAACGCCTAAG	Genotyping Mp*pam16* lines (sgRNA1)
GCC6Rv	TCCTGGATCTGAAGTGACC	Genotyping Mp*pam16* lines (sgRNA 2); sequencing Mp*pam16* lines (sgRNA2)

2.3.11. Media

Johnson's medium

Component	Final concentration
KNO_3	6 mM
$MgSO_4$	1 mM
$Ca(NO_3)_2.4H_2O$	4 mM
KCl	25 µM
H_3BO_4	10 µM
$MnSO_4.4H_2O$	1 µM
$ZnSO_4.7H_2O$	1 µM
$CuSO_4.5H_2O$	250 nM
$(NH_4)_6Mo_7O_{24}.4H_2O$	250 nM
$FeSO_4.7H_2O$	25 µM
Na_2EDTA	25 µM
$NH_4H_2PO_4^{3-}$	0.6 mM
$(NH_4)_2SO_4$	0.4 mM
Inositol	0.55 mM
MES	0.533 g/l (w/v)
Sucrose	1 % (w/v)
Agar (Sigma-Aldrich)	0.8 % (w/v)

pH adjusted to 5.6 using 1M KOH

½ Gamborg medium

Component	Final concentration
Gamborg B5 medium basal salt mixture	1.5 g/l (w/v)
MES	0.5 g/l (w/v)
Sucrose	1 % (w/v)
Agar (Sigma-Aldrich)	0.8 % (w/v)

pH adjusted to 5.5 using 1M KOH

M51C medium

Component	Final concentration
KNO_3 (Sigma)	19.8 µM
NH_4NO_3 (Sigma)	5 µM
$MgSO_4$ (Fisher Scientific)	1.5 µM
$CaCl_2$ (Sigma)	2 µM
KH_2PO_4 (Sigma)	2 µM
EDTA-Fe(III) (Sigma)	110 nM
Na_2MoO_4 (Sigma)	1 µM
$CuSO_4$ (Sigma)	100 nM
$CoCl_2$ (Sigma)	100 nM
$ZnSO_4$ (Sigma)	7 µM
$MnSO_4$ (Fisher Scientific)	40 µM
H_3BO_3 (Fisher Scientific)	49 µM
Myo-inositol (Sigma)	555 µM
Nicotinic acid (Sigma)	8 µM
Pyridoxine hydrochloride (Sigma)	5 µM
Thiamine hydrochloride (Sigma)	30 µM
Sucrose (Sigma)	58 mM
L-glutamine (Sigma)	2 mM
casein hydrolysate (Fluka Analytical)	0.1 % w/v

pH adjusted to 5.8

2.4. Results

2.4.1. There is a single *PAM16* gene in *Marchantia polymorpha*

To identify orthologues of *PAM16* in *M. polymorpha* and test if *PAM16* is conserved across land plants, I undertook a phylogenetic analysis. I identified protein sequences similar to AtPAM16 (At3G59280) from 11 species using the BlastP algorithm to search their proteomes (Table 2.1). The species included were the liverwort *Marchantia polymorpha*, the moss *Physcomitrium patens*, the hornwort *Anthoceros agrestis*, the lycophyte *Selaginella moellendorfii*, the fern *Azolla filiculoides*, the gymnosperm *Picea abies*, and the angiosperms *Amborella trichopoda, Arabidopsis thaliana*, *Zea mays*, and *Oryza sativa*. *PAM16* from the yeast *Saccharomyces cerevisiae* was used as an outgroup. I aligned the sequences via the L-INS-i strategy in MAFFT and trimmed them to remove poorly conserved regions. The PAM16 protein contains an N-terminal mitochondrial targeting sequence which targets the protein to the inner mitochondrial membrane (Mokranjac *et al.*, 2006) and a J-like domain which is essential to its function (D'Silva *et al.*, 2005). These two functional regions are highly conserved across land plants (Fig. 2.1). I constructed a maximum likelihood tree and used a non-parametric approximate likelihood ratio test based on a Shimodaira-Hasegawa-like procedure to calculate node support values using PhyML 3.0 (Guindon *et al.*, 2010) (Fig. 2.2). There were between one and three copies of *PAM16* in each species; there was one copy in *M. polymorpha* (Mp3g09390), and two copies in *A. thaliana* (At*PAM16* and At*PAM16L*). Mp3g09390 is therefore the only *PAM16* gene in the *M. polymorpha* genome and will be referred to as Mp*PAM16*.

Species	Gene ID	E value	Version	BLAST tool
Arabidopsis thaliana	AT3G59280.1 (*PAM16*)	7.00E-81	TAIR10	Phytozome
Arabidopsis thaliana	AT5G61880.1 (*PAM16L*)	9.70E-50	TAIR10	Phytozome
Marchantia polymorpha	Mp3g09390.1	2.00E-43	MpTak1 v5.1	marchantia.info
Physcomitrium patens	Phpat.012G064600.1.p_	2.10E-48	v3.3	Phytozome
Physcomitrium patens	Phpat.021G010400.1.p_	5.50E-48	v3.3	Phytozome
Physcomitrium patens	Phpat.018G069100.1.p_	3.80E-43	v3.3	Phytozome
Selaginella moellendorffii	SmoeALL_402411	1.70E-45	v1.0	Phytozome
Selaginella moellendorffii	SmoeALL_76729	2.80E-41	v1.0	Phytozome
Oryza sativa	Os10g33910.1	2.90E-55	v7_JGI	Phytozome
Zea mays	Mo17_PWZ52230.1/B6UGA4	3.00E-54	taxid:4577 (Mo17)	NCBI
Zea mays	Mo17_NP_001146797.1/B6TGT3	3.00E-53	taxid:4577 (Mo17)	NCBI
Amborella trichopoda	Amtr_evm_27.model.AmTr_v1.0_scaffold00148.51	3.90E-31	v1.0	Phytozome
Picea abies	Pa_MA_203823g0010	2.74 E-39	v1.0	Congenie
Anthoceros agrestis	AagrBONN_evm.model.Sc2ySwM_368.3318.1	4E-34	v1.0	UZH
Anthoceros agrestis	AagrBONN_evm.model.Sc2ySwM_228.728.1	4E-34	v1.0	UZH
Anthoceros agrestis	AagrBONN_evm.model.Sc2ySwM_362.2602.1	2E-27	v1.0	UZH
Azolla filiculoides	Azfi_s0003.g007767	8E-47	v1.2	FernBase
Azolla filiculoides	Azfi_s0409.g068485	2E-44	v1.2	FernBase
Saccharomyces cerevisiae	Sc_YJL104W (*PAM16*)	4.00E-13	S288C	SGD

Table 2.1. Orthologues of the *A. thaliana* gene At3G59280 identified by protein BLAST search (E value < 1E-5). Corresponding E values and details of reference proteome versions and BLAST tools are also shown.

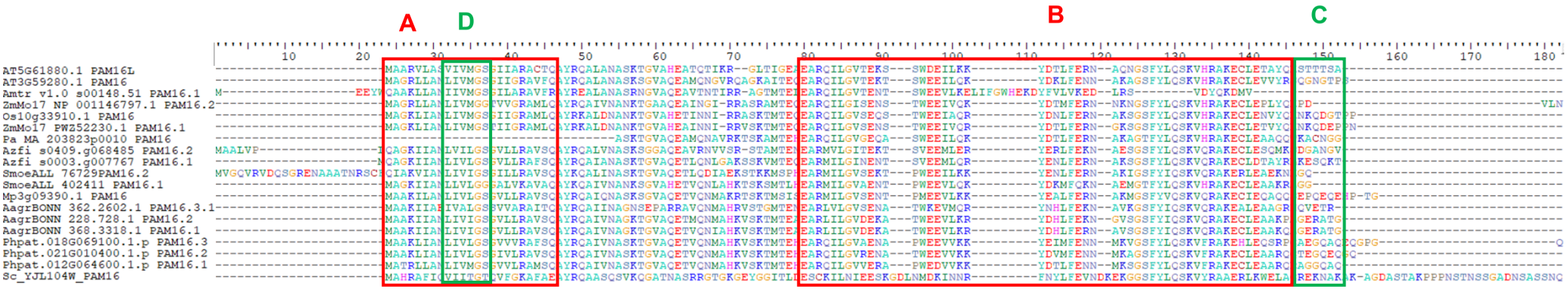

Fig. 2.1 Amino acid alignment of proteins similar to AtPAM16 from a variety of land plants and *Saccharomyces cerevisiae*.
Proteins similar to AtPAM16 were identified by protein BLAST search (E value < 1E-5) against the reference proteomes of various species (Table 2.1). Orthologues were aligned via the L-INS-i strategy using MAFFT version 7. **(A)** Signal peptide **(B)** J-like domain **(C)** region targeted by sgRNA 1 **(D)** region targeted by sgRNA 2.

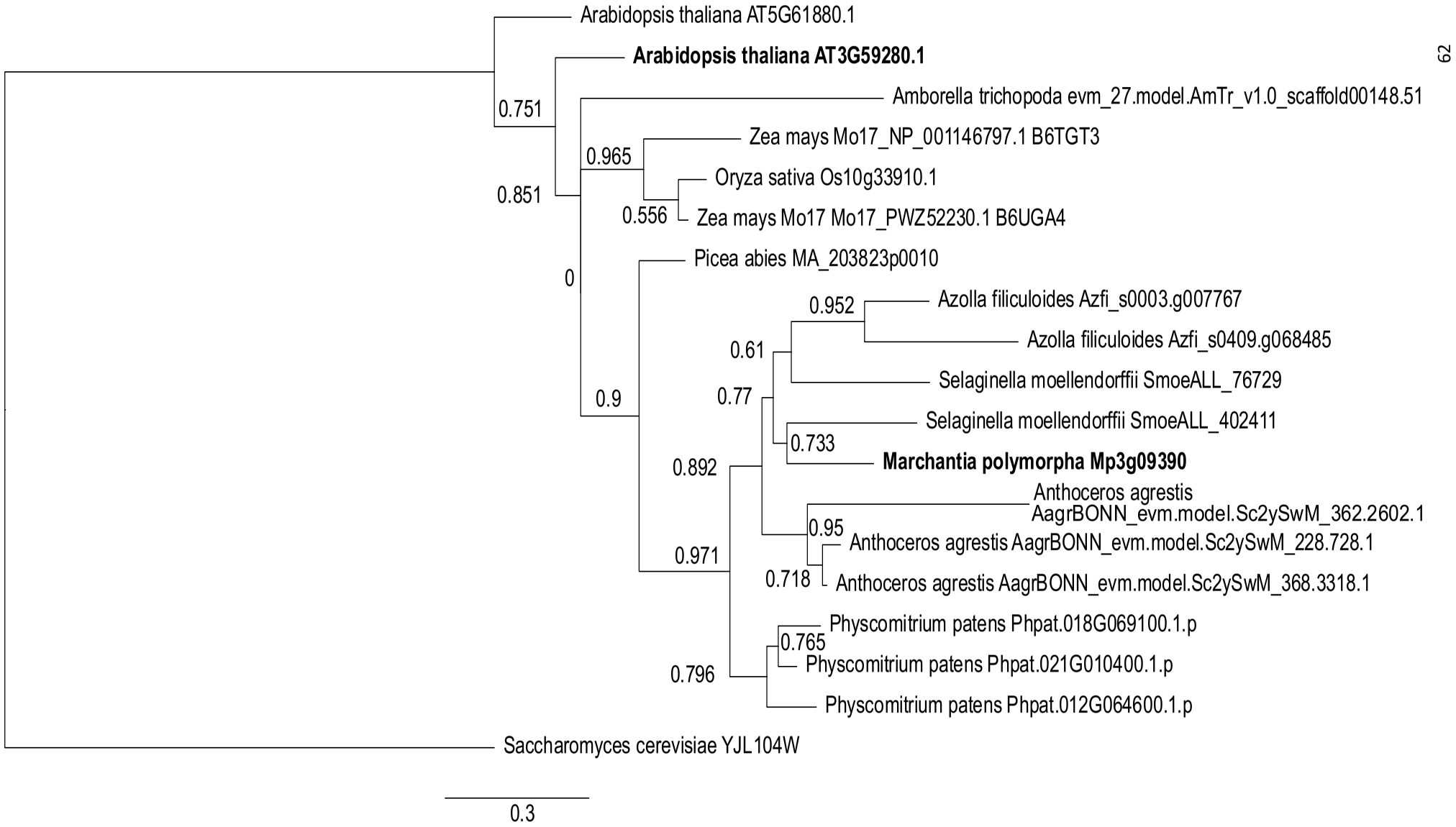

Fig. 2.2. Phylogenetic analysis of *PAM16* in plants. A phylogenetic tree (rooted with *PAM16* sequence from *S. cerevisiae*) of a maximum likelihood analysis conducted by PhyML 3.0 using an estimated gamma distribution parameter, the LG model of amino acid substitution and a non-parametric approximate likelihood ratio test based on a Shimodaira-Hasegawa-like procedure to calculate branch support values (Guindon *et al.*, 2010).

2.4.2. Thirty-three Mp*pam16* mutants were generated using CRISPR-Cas9 mutagenesis

To test if the mechanism of NTSR involving loss of gene function of *PAM16* in *A. thaliana* is conserved in *M. polymorpha*, I generated Mp*pam16* mutants using CRISPR-Cas9 mutagenesis. The *A. thaliana PAM16* loss-of-function mutant line has a mutation leading to the replacement of arginine at position 98 to an early stop codon; this leads to a truncation of the protein in a conserved region and was therefore assumed to confer loss-of-function (Scheible *et al.*, 2003). I designed several guide RNAs with the intent of generating loss-of-function mutations, either by targeting essential parts of the protein or by inducing frameshifts or large indels. I designed five guide RNAs that were complementary to different regions of the *PAM16* coding sequence. Two guide RNAs targeted the putative signal peptide of Mp*PAM16* (sgRNAs 2 and 3), one guide RNA targeted the putative J-like domain of Mp*PAM16* (sgRNA 5), one guide RNA induced mutations near Arg98 which is mutated in *A. thaliana* TXTA-resistant *pam16* mutants to replicate this mutation (sgRNA 4), and one guide RNA targeted a non-conserved region to try and generate weak loss-of-function lines in case strong loss-of-function of Mp*PAM16* is lethal (sgRNA 1) (Fig. 2.1, Fig. 2.3). Since *PAM16* is an essential gene in *S. cerevisiae* and a double knockout of *PAM16* and *PAM16L* in *A. thaliana* is lethal, I also designed a guide RNA to target the less highly conserved C-terminal end of Mp*PAM16* to induce a weak loss-of-function phenotype in case a complete loss-of-function is lethal (sgRNA1) (Fig. 2.1, Fig. 2.3).

The guide RNAs were cloned into vectors containing the Cas9 coding sequence and the final vectors were transformed into *A. tumefaciens* (Fig. 2.4). Wild-type *M.*

polymorpha spores (from a cross between Tak-1 and Tak-2 wild-type lines) were transformed with the *A. tumefaciens* strains carrying the CRISPR-Cas9 constructs, and positive transformants were selected for and genotyped. In total, 33 Mp*pam16* mutants were generated with mutations in the regions complementary to sgRNA 1 and sgRNA 2 (Table 2.2, Fig. 2.5). No mutants were recovered from transformations with the other sgRNAs. I also predicted the protein sequences of the PAM16 protein in each Mp*pam16* mutant line based on their mutations in the Mp*PAM16* gene (Fig. 2.6).

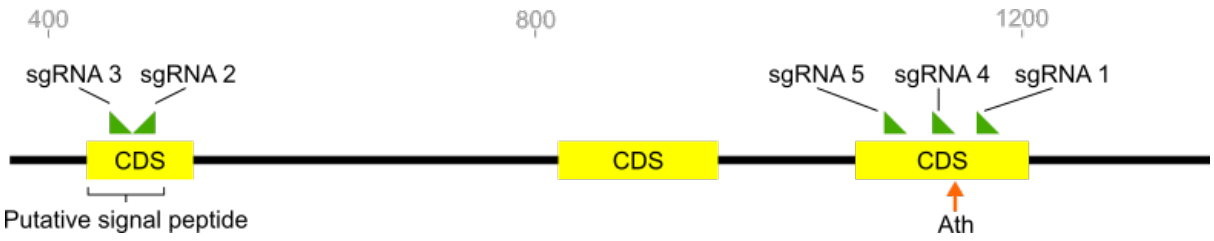

Fig. 2.3. **Region of the Mp*PAM16* gene targeted by sgRNAs.** Coding sequences are annotated in yellow ("CDS"), the position of the putative signal peptide is indicated, sgRNA positions are annotated in green, and the amino acid residue which is mutated in the At*txr1-1* line (Scheible *et al.*, 2003) is annotated with an orange arrow labelled "Ath".

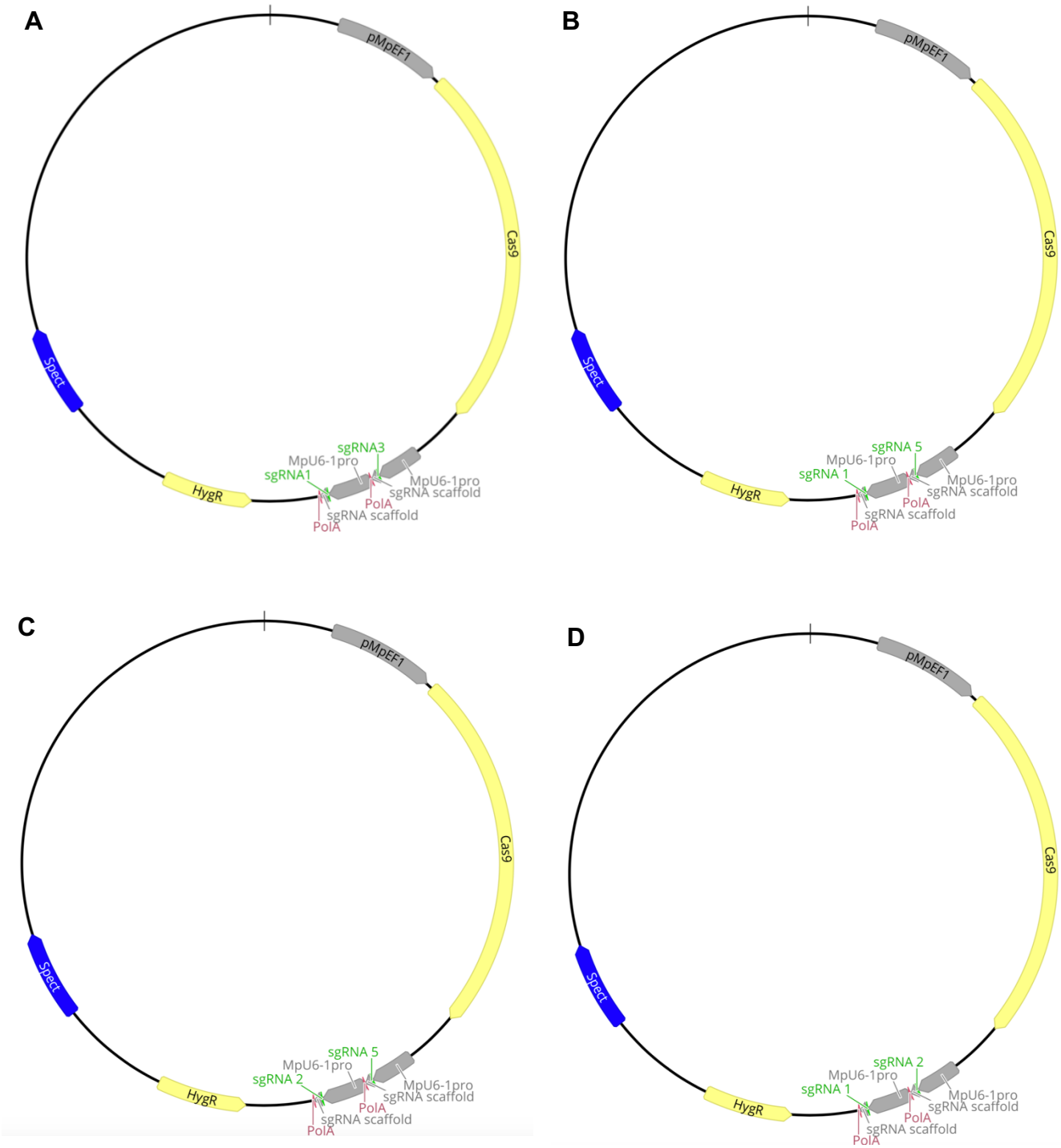

Vector	gRNA targeted	N. plants genotyped	N. mutants identified	CRISPR efficiency
A	1 (and 3)	85	2	2.35 %
B	1 (and 5)	60	3	5.00 %
C	2 (and 5)	90	24	26.67 %
D	1 and 2	19	4	21.05 %

Fig. 2.4. CRISPR-Cas9 vectors used to generate mutations in Mp*PAM16* and their mutation efficiencies. Vectors used to generate **(A)** Mp*pam16*^{GE1} **(B)** Mp*pam16*^{GE2} – Mp*pam16*^{GE6}, Mp*pam16*^{GE12*} **(C)** Mp*pam16*^{GE7} – Mp*pam16*^{GE9} , Mp*pam16*^{GE13*} **(D)** Mp*pam16*^{GE23*}

Line	gRNA	Mutation (del = deletion, sub = substitution, ins = insertion)
Mp*pam16*^{GE01}	1	9 bp del
Mp*pam16*^{GE02}	1	10 bp del, 1 bp sub
Mp*pam16*^{GE03}	1	1 bp ins
Mp*pam16*^{GE06}	1	3 bp del
Mp*pam16*^{GE123}	1	9 bp del
Mp*pam16*^{GE07}	2	21 bp del
Mp*pam16*^{GE08}	2	15 bp del; 2 bp sub
Mp*pam16*^{GE09}	2	4 bp sub; 3 bp ins
Mp*pam16*^{GE1311}	2	9 bp del
Mp*pam16*^{GE1312}	2	15 bp del
Mp*pam16*^{GE1327}	2	12 bp del
Mp*pam16*^{GE133}	2	15bp del
Mp*pam16*^{GE1332}	2	30 bp del, 1 bp sub
Mp*pam16*^{GE1334}	2	12 bp del
Mp*pam16*^{GE1335}	2	3 bp sub
Mp*pam16*^{GE1336}	2	15 bp del
Mp*pam16*^{GE1339}	2	24 bp del
Mp*pam16*^{GE1340}	2	47 bp ins, 8 bp del
Mp*pam16*^{GE1343}	2	15 bp del
Mp*pam16*^{GE1348}	2	6 bp del
Mp*pam16*^{GE1350}	2	6 bp del
Mp*pam16*^{GE1352}	2	12 bp del
Mp*pam16*^{GE1353}	2	9 bp ins
Mp*pam16*^{GE1355}	2	18 bp ins
Mp*pam16*^{GE1356}	2	5 bp del, 23 bp sub
Mp*pam16*^{GE1358}	2	15 bp sub
Mp*pam16*^{GE136}	2	9 bp del
Mp*pam16*^{GE137}	2	2 bp sub
Mp*pam16*^{GE138}	2	57 bp ins
Mp*pam16*^{GE233}	2	3 bp del
Mp*pam16*^{GE2310}	2	9 bp del
Mp*pam16*^{GE2311}	2	5 bp sub, 21 bp del
Mp*pam16*^{GE2313}	2	12 bp ins
Mp*pam16*^{OE1}	N/A	T-DNA insertion in 5’ end of promoter

Table 2.2. List of Mp*pam16* lines and the mutations present in their copy of Mp*PAM16*. Mp*pam16* lines were generated using CRISPR-Cas9 mutagenesis to target the Mp*PAM16* gene. Wild-type spores (from a cross between Tak-1 and Tak-2) were transformed with *Agrobacterium tumefaciens* strains carrying the vector containing the Cas9 gene and guide RNAs to target Mp*PAM16*. Positive transformants were genotyped using Sanger sequencing to determine the mutations induced by the CRISPR-Cas9 complex.

A

```
Mp PAM16          GCGCAACAATCAGAAC-CACAGGAACAAGAGCATCCC-A
Mppam16^GE3       GCGCAACAATCAGAACTCACAGGAACAAGAGCATCCC-A
Mppam16^GE6       GCGCAACAATCAGA----ACAGGAACAAGAGCATCCC-A
Mppam16^GE1       GCGCAACAATCAGA----------ACAAGAGCATCCC-A
Mppam16^GE123     GCGCAACAATCAGA----------ACAAGAGCATCCC-A
Mppam16^GE2       GCGCAACAATCAGA----------ACAAGAGCATTTCCA
```

B

```
Mp PAM16          TAAAATATTAGCGAATTTGATCGTCCTCGG----------CTCGGGTGTGCTTCTTCGCGCTGTATCTCAAGCTTACCGTCAAGCGATTCAA
Mppam16^GE1335    TAAAATATTAGCGAATTTGATCGTCCTCCG----------TCCGGGTGTGCTTCTTCGCGCTGTATCTCAAGCTTACCGTCAAGCGATTCAA
Mppam16^GE1336    TAAAATATTAGCGAATTTGATCGTCCTCCG----------TCCGGGTGTGCTTCTTCGCGCTGTATCTCAAGCTTACCGTCAAGCGATTCAA
Mppam16^GE137     TAAAATATTAGCGAATTTGATCGTCCTCGG----------GGCGGGTGTGCTTCTTCGCGCTGTATCTCAAGCTTACCGTCAAGCGATTCAA
Mppam16^GE233     TAAAATATTAGCGAATTTGATCGTCCTCGG----------GGGTGTGCTTCTTCGCGCTGTATCTCAAGCTTACCGTCAAGCGATTCAA
Mppam16^GE1348    TAAAATATTAGCGAATTTGATCGTCCTC----------GGTGTGCTTCTTCGCGCTGTATCTCAAGCTTACCGTCAAGCGATTCAA
Mppam16^GE1350    TAAAATATTAGCGAATTTGATCGTCCTC----------GGTGTGCTTCTTCGCGCTGTATCTCAAGCTTACCGTCAAGCGATTCAA
Mppam16^GE1311    TAAAATATTAGCGAATTTGATCGTCCTC----------GGGCTTCTTCGCGCTGTATCTCAAGCTTACCGTCAAGCGATTCAA
Mppam16^GE2310    TAAAATATTAGCGAATTTGATCGTCCTC----------GTGCTTCTTCGCGCTGTATCTCAAGCTTACCGTCAAGCGATTCAA
Mppam16^GE1339    TAAAATA----------TTGGGTGTGCTTCTTCGCGCTGTATCTCAAGCTTACCGTCAAGCGATTCAA
Mppam16^GE1340    TAAAATA----------TTGGGTGTGCTTCTTCGCGCTGTATCTCAAGCTTACCGTCAAGCGATTCAA
Mppam16^GE2313    TAAAATATTAGCGAATTTGATCGTCCTCGGGTG----------TGCTAAATCCTCGGGTGTGCTTCTTCGCGCTGTATCTCAAGCTTACCGTCAAGCGATTCAA
Mppam16^GE1353    TAAAATATTAGCGAATTTGATCGTCCTCGGATG----------TGCTTCCTCGGGTGTGCTTCTTCGCGCTGTATCTCAAGCTTACCGTCAAGCGATTCAA
Mppam16^GE8       TAAAATATTAGCGAATTTGATC----------GTATTTCTTCGCGCTGTATCTCAAGCTTACCGTCAAGCGATTCAA
Mppam16^GE1312    TAAAATATTAGCGAATTTGATC----------GTGCTTCTTCGCGCTGTATCTCAAGCTTACCGTCAAGCGATTCAA
Mppam16^GE133     TAAAATATTAGCGAATTTGATC----------GTCCTTCTTCGCGCTGTATCTCAAGCTTACCGTCAAGCGATTCAA
Mppam16^GE1327    TAAAATATTAGCGAATTTG----------CCGGGTGTGCTTCTTCGCGCTGTATCTCAAGCTTACCGTCAAGCGATTCAA
Mppam16^GE1334    TAAAATATTAGCGAATTTG----------ATCGGTGTGCTTCTTCGCGCTGTATCTCAAGCTTACCGTCAAGCGATTCAA
Mppam16^GE1352    TAAAATATTAGCGAATTAT----------TCGGGTGTGCTTCTTCGCGCTGTATCTCAAGCTTACCGTCAAGCGATTCAA
Mppam16^GE1358    TAAAATATTAGCGAATTTTAT----------ATATTTGGGTGTGCTTCTTCGCGCTGTATCTCAAGCTTACCGTCAAGCGATTCAA
Mppam16^GE136     TAAAATATTAGCGAATTTTAT----------ATATTTGGGTGTGCTTCTTCGCGCTGTATCTCAAGCTTACCGTCAAGCGATTCAA
Mppam16^GE7       TAAAATATTAGCGAA----------TGTGCTTCTTCGCGCTGTATCTCAAGCTTACCGTCAAGCGATTCAA
Mppam16^GE1355    TAAAATATTAGCGAATTTGATCGTCCTCGGAGG----------ACGAT--CAAATATTTTAGCGGGTGTGCTTCTTCGCGCTGTATCTCAAGCTTACCGTCAAGCGATTCAA
Mppam16^GE9       TAAAATATTAGCGAATTTGATCG----------AGGTTGCGTCCTCGGGTGTGCTTCTTCGCGCTGTATCTCAAGCTTACCGTCAAGCGATTCAA
Mppam16^GE1332    TAAAATAT----------G----------GCTTCTTCGCGCTGTATCTCAAGCTTACCGTCAAGCGATTCAA
Mppam16^GE1343    TAAAATATTAGCGAATTTGATCAAATTCGCTAA----------TATTTTAGCGAATTTTAGCGAATTTAAGCCCACAGCCTCGGGTGTGCTTCTTCGCGCTGTATCTCAAGCTTACCGTCAAGCGATTCAA
Mppam16^GE138     TAAAATATTAGCGAATTTGATCGTCCTCGGACGGACGATCAAATTCGGGTTTAATTTGATCGTCCTCGGGACGATCAAATCATCGTCCTCGGGTGTGCTTCTTCGCGCTGTATCTCAAGCTTACCGTCAAGCGATTCAA
Mppam16^GE2311    TAAAATATTAGCGAATTTGA----------TACACAGCGCTGTATCTCAAGCTTACCGTCAAGCGATTCAA
Mppam16^GE1356    TAAAATATTAGCGAATTTGATCGTCCTCGGG----------TGGGGTGCGTCTCGTTGCGCTGCATGCTTAGCGTCCCGCGATGCGATTCAT
```

Fig. 2.5. Predicted nucleotide sequences of Mp*PAM16* in Mp*pam16* lines. Mp*pam16* lines were generated using CRISPR-Cas9 mutagenesis to target the Mp*PAM16* gene. Wild-type spores (from a cross between Tak-1 and Tak-2) were transformed with *Agrobacterium tumefaciens* strains carrying the vector containing the Cas9 gene and **(A)** sgRNA 1 **(B)** sgRNA 2 targeting Mp*PAM16*. Positive transformants were genotyped using Sanger sequencing to determine the mutations induced by the CRISPR-Cas9 complex. Predicted protein sequences were determined based on the mutations in each line. Nucleotide sequences were aligned via the L-INS-i strategy using MAFFT version 7. The top row in both **(A)** and **(B)** is the reference Mp*PAM16* nucleotide sequence (MpTak1v6.1). Lines highlighted in green are resistant to TXTA with respect to Tak-1 and Tak-2.

A

```
MpPAM16          EPQEQEHPTG----------
Mppam16GE01      ---EQEHPTG----------
Mppam16GE123     ---EQEHPTG----------
Mppam16GE06      E-QEQEHPTG----------
Mppam16GE02      ---EQEHPHF----HRLRQRF
Mppam16GE03      ------ELTGTRASHRLRQRF
```

B

```
MpPAM16          AAKILANLIVLG------------------SGVLLRAV----------------------------------------
Mppam16GE137     AAKILANLIVLG------------------AGVLLRAV----------------------------------------
Mppam16GE1335    AAKILANLIVLR------------------PGVLLRAV----------------------------------------
Mppam16GE233     AAKILANLIVLG------------------GVLLRAV----------------------------------------
Mppam16GE1353    AAKILANLIVLGCA----------------SSGVLLRAV----------------------------------------
Mppam16GE2313    AAKILANLIVLGCA----------------KSSGVLLRAV----------------------------------------
Mppam16GE1348    AAKILANLIVL-------------------GVLLRAV----------------------------------------
Mppam16GE1350    AAKILANLIVP-------------------GVLLRAV----------------------------------------
Mppam16GE1358    AAKILANFIYL-------------------GVLLRAV----------------------------------------
Mppam16GE1311    AAKILANLIVLG-----------------LLRAV----------------------------------------
Mppam16GE136     AAKILANLIVL-------------------VLLRAV----------------------------------------
Mppam16GE2310    AAKILANLIVL-------------------VLLRAV----------------------------------------
Mppam16GE1355    AAKILANLIVLGGRSN------------ILAGVLLRAV----------------------------------------
Mppam16GE1312    AAKILANLI---------------------VLLRAV----------------------------------------
Mppam16GE133     AAKILANLI---------------------VLLRAV----------------------------------------
Mppam16GE1343    AAKILANLI---------------------VLLRAV----------------------------------------
Mppam16GE08      AAKILANLI---------------------VFLRAV----------------------------------------
Mppam16GE1336    AAKILANL----------------------GVLLRAV----------------------------------------
Mppam16GE1327    AAKILANLP---------------------GVLLRAV----------------------------------------
Mppam16GE1334    AAKILANLI---------------------GVLLRAV----------------------------------------
Mppam16GE1352    AAKILANYS---------------------GVLLRAVSQAYRQAIQSMYCIPSTIRNTISLSRIKQFAHNFRPVKIRS
Mppam16GE138     AAKILANLIVLGRTIKFGFNLIVLGTIKSSSSGVLLRAV----------------------------------------
Mppam16GE09      AAKILANLIEVA------------------SSGVLLRAV----------------------------------------
Mppam16GE07      AAKILAN-----------------------VLLRAV----------------------------------------
Mppam16GE1339    AAKIL-------------------------GVLLRAV----------------------------------------
Mppam16GE2311    AAKILANLIHS-------------------------AV----------------------------------------
Mppam16GE1340    AAKILANLIKFANI------LANFSEFKPTASGVLLRAV----------------------------------------
Mppam16GE1356    AAKILANLIVLGWGAS----RCAASLPSSDSKYVLYS----------------------------------------
Mppam16GE1332    AAKIW-----------------------------LLRAV----------------------------------------
```

Fig. 2.6. Predicted protein sequences of MpPAM16 in Mp*pam16* lines. Mp*pam16* lines were generated using CRISPR-Cas9 mutagenesis to target the Mp*PAM16* gene. Wild-type spores (from a cross between Tak-1 and Tak-2) were transformed with *Agrobacterium tumefaciens* strains carrying the vector containing the Cas9 gene and **(A)** sgRNA 1 or **(B)** sgRNA 2 targeting Mp*PAM16*. Positive transformants were genotyped using Sanger sequencing to determine the mutations induced by the CRISPR-Cas9 complex. Predicted protein sequences were determined based on the mutations in each line. Protein sequences were aligned via the L-INS-i strategy using MAFFT version 7. The top row in both **(A)** and **(B)** is the reference MpPAM16 protein sequence (MpTak1v6.1). Lines highlighted in green are resistant to TXTA.

2.4.3. Twenty-nine out of thirty-three Mp*pam16* mutant lines are putative weak loss-of-function lines

I used the predicted MpPAM16 protein sequence of each of the 33 Mp*pam16* mutant lines to class them as putative weak or strong loss-of-function lines. Mutations which strongly affect the protein structure (frameshifts or early truncations) are more likely to cause strong loss-of-function. I identified 2 lines, Mp*pam16*^{GE1352} and Mp*pam16*^{GE1356}, with predicted frameshifts and alternative stop codons (Fig. 2.6). A further 2 lines, Mp*pam16*^{GE138} and Mp*pam16*^{GE1340}, had mutations affecting more than 15 amino acids in frame (Fig. 2.6). I classed these 4 Mp*pam16* lines as putative strong loss-of-function lines, and I classed the remaining 29 Mp*pam16* lines – which had mutations affecting fewer than 15 amino acids in frame – as putative weak loss-of-function lines. Most of the Mp*pam16* lines that I generated are therefore putative weak loss-of-function lines. However, I did not measure the function of the PAM16 protein in Mp*pam16* lines, so these lines are only predicted loss-of-function lines.

2.4.4. The herbicide thaxtomin A (TXTA) exerts a dose-dependent toxicity on *M. polymorpha* thallus

To measure the inhibition of the lateral growth (area) by TXTA on the gametophyte of wild-type *M. polymorpha*, I grew gemmae from the wild-type lines Tak-1 and Tak-2 on solid ½ Gamborg medium supplemented with different concentrations of TXTA and quantified the area of living gemmaling tissue after two weeks (Fig. 2.7). Since only living tissue was measured, for dead gemmalings the gemmaling area is quantified as zero although the actual area is greater than zero (Fig. 2.8).

TXTA causes dose-dependent growth inhibition of gemmalings from both wild-type lines. I calculated 2 parameters to quantify the dose-dependent effect of TXTA on

the growth of Tak-1 and Tak-2; the IC_{50} (dose at which average area of gemmalings is 50 % relative to untreated control), and the LD_{100} (lethal dose at which no plant tissue is alive). The IC_{50} was 56 ± 6 nM for Tak-1, and 135 ± 24 nM for Tak-2; according to this parameter, Tak-2 is more resistant to TXTA. However, the LD_{100} for Tak-2 was 5 µM, and although most Tak-1 plants also died at 5 µM TXTA a few plants grew very little at this concentration (Fig. 2.7) so when measuring resistance according to this parameter Tak-1 is slightly more resistant than Tak-2.

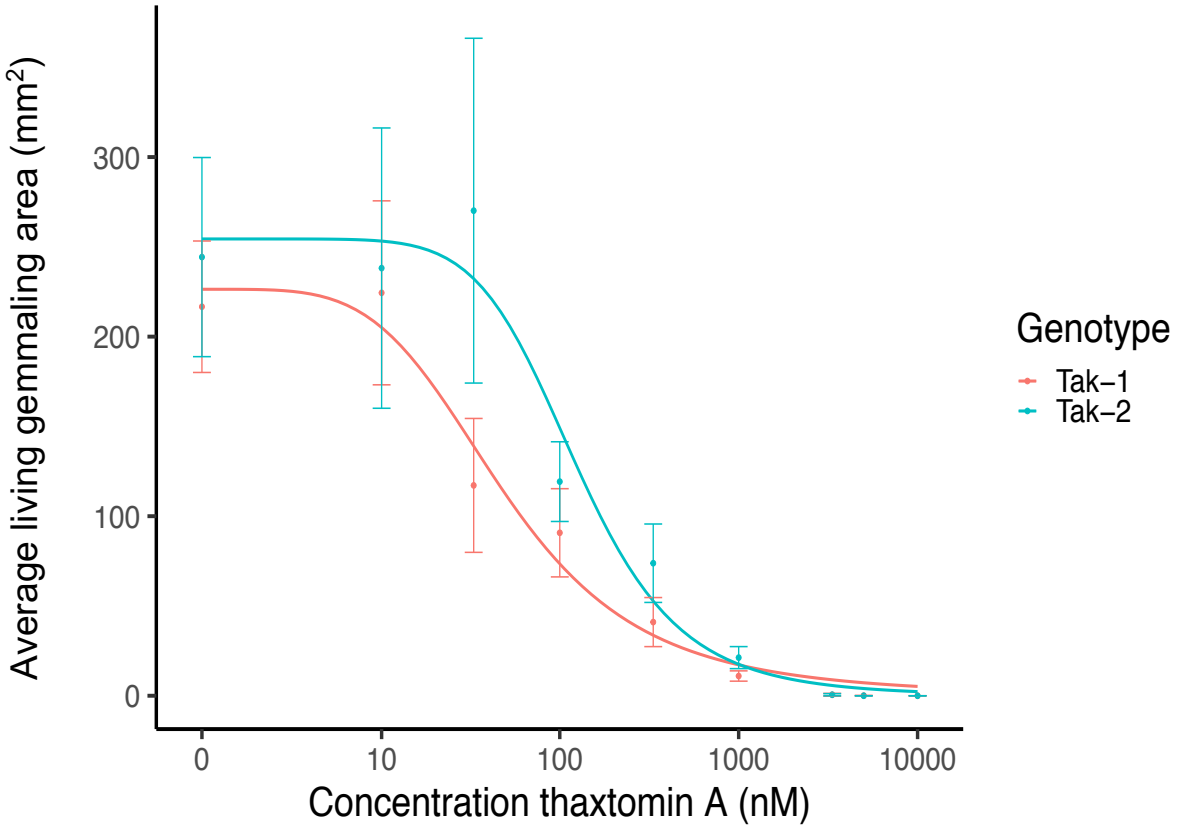

Fig. 2.7. Thaxtomin A (TXTA) exerts a dose-dependent growth inhibition on *M. polymorpha*.
Wild-type gemmae (Tak-1 and Tak-2) were grown for 14 days on solid ½ Gamborg medium supplemented with different concentrations of TXTA**.** Gemmalings were imaged using a Berthold Nightowl II LB 983 *In Vivo* Imaging System which detects chlorophyll autofluorescence (560nm). The lateral area of autofluorescing (living) tissue was determined after 14 days of growth using the indiGo™ software package and plotted using the ggplot2 package in R. The fitted curve was calculated using the four-parameter log-logistic equation included in the drc package in R. Error bars represent ± standard deviation (n = 18).

2.4.5. Nine Mp*pam16* predicted loss-of-function mutants are resistant to TXTA

A mutant line of *Arabidopsis thaliana* with a mutation in At*PAM16* is resistant to thaxtomin A (TXTA). To determine if loss of *PAM16* gene function in *M. polymorpha* results in TXTA resistance, I grew gemmae from the 33 Mp*pam16* predicted loss-of-function mutant lines on solid medium supplemented with 5 µM TXTA (Fig. 2.8). Wild-type lines die or grow very little on 5 µM TXTA (Fig. 2.7), so any mutant lines which survived this dose were considered resistant. I also grew mutant gemmae from a Mp*pam16* putative gain-of-function mutant line, Mp*pam16*^{OE1}, identified in a T-DNA insertion mutagenesis screen previously conducted in the lab.

To test if Mp*pam16* mutant lines were resistant to TXTA, I measured the lateral area of living tissue of gemmalings after 12 days of growth on 5µM TXTA (Fig. 2.9). Since only living tissue was measured, for dead gemmalings the gemmaling area is quantified as zero although the actual area is greater than zero (Fig. 2.8). Nine Mp*pam16* lines were significantly larger than both Tak-1 and Tak-2 on 5 µM of TXTA so were classed as TXTA-resistant; the resistant lines were Mp*pam16*^{GE1358}, Mp*pam16*^{GE1355}, Mp*pam16*^{GE1335}, Mp*pam16*^{GE136}, Mp*pam16*^{GE1350}, Mp*pam16*^{GE2310}, Mp*pam16*^{GE138}, Mp*pam16*^{GE1353}, and Mp*pam16*^{GE1311} ($p<0.05$) (Fig. 2.8, Fig. 2.9).

The putative Mp*PAM16* overexpressor line Mppam16^{OE1} was not significantly resistant to TXTA (Fig. 2.9), suggesting that a perturbation in the amount of PAM16 protein does not confer resistance to TXTA (although it remains to be shown whether this mutant produces more PAM16 protein than wild-type lines).

All 9 TXTA-resistant lines were mutated in the region targeted by sgRNA 2 (Table 2.2). This region is part of the predicted signal peptide targeting the MpPAM16 protein to the mitochondria and is highly conserved (Fig. 2.1). Mutations in a

functional domain or a conserved region of the protein are more likely to cause loss-of-function, therefore the 9 TXTA-resistant lines are predicted loss-of-function lines. Predicted loss-of-function mutations in Mp*pam16* mutants can therefore result in TXTA resistance; if the mutations cause loss of *PAM16* function, the mechanism of NTSR to TXTA conferred by loss-of-function of *PAM16* is conserved in these 9 Mp*pam16* lines.

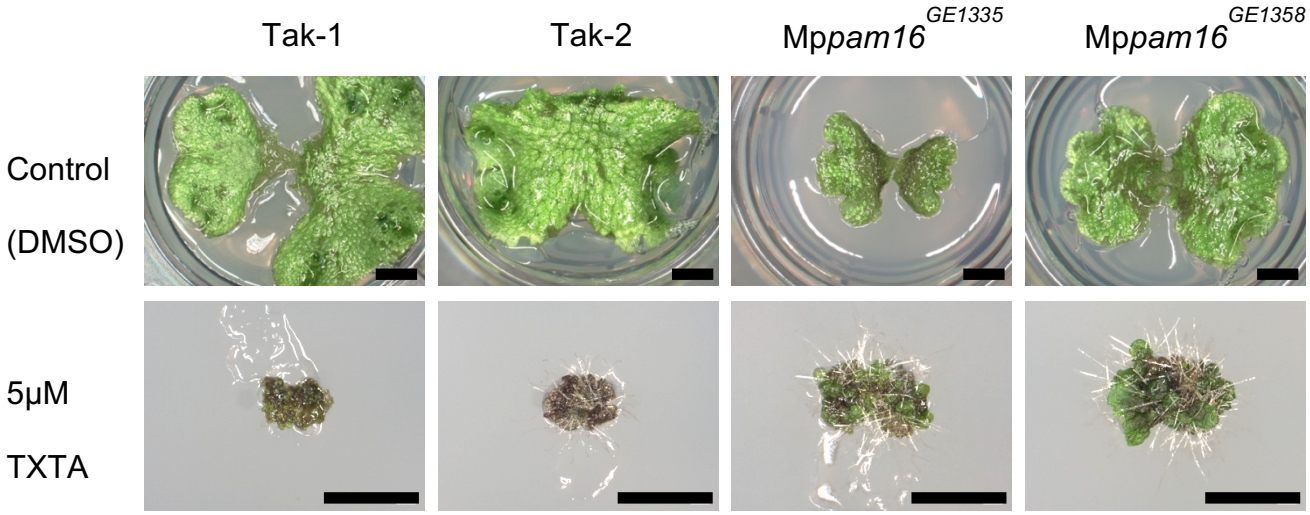

Fig. 2.8. Gemmalings from wild-type and 2 independent Mp*am16* loss-of-function lines grown on TXTA. Gemmae from wild-type (Tak-1 and Tak-2) and 2 independent TXTA-resistant Mp*am16* loss-of-function lines (Mp*am16*^{GE1335} and Mp*am16*^{GE1358}) were grown on solid ½ Gamborg medium supplemented with 5 μM TXTA or 0.1 % DMSO for 12 days. Gemmalings were imaged with a Keyence VHX-7000. Scale bars represent 2 mm.

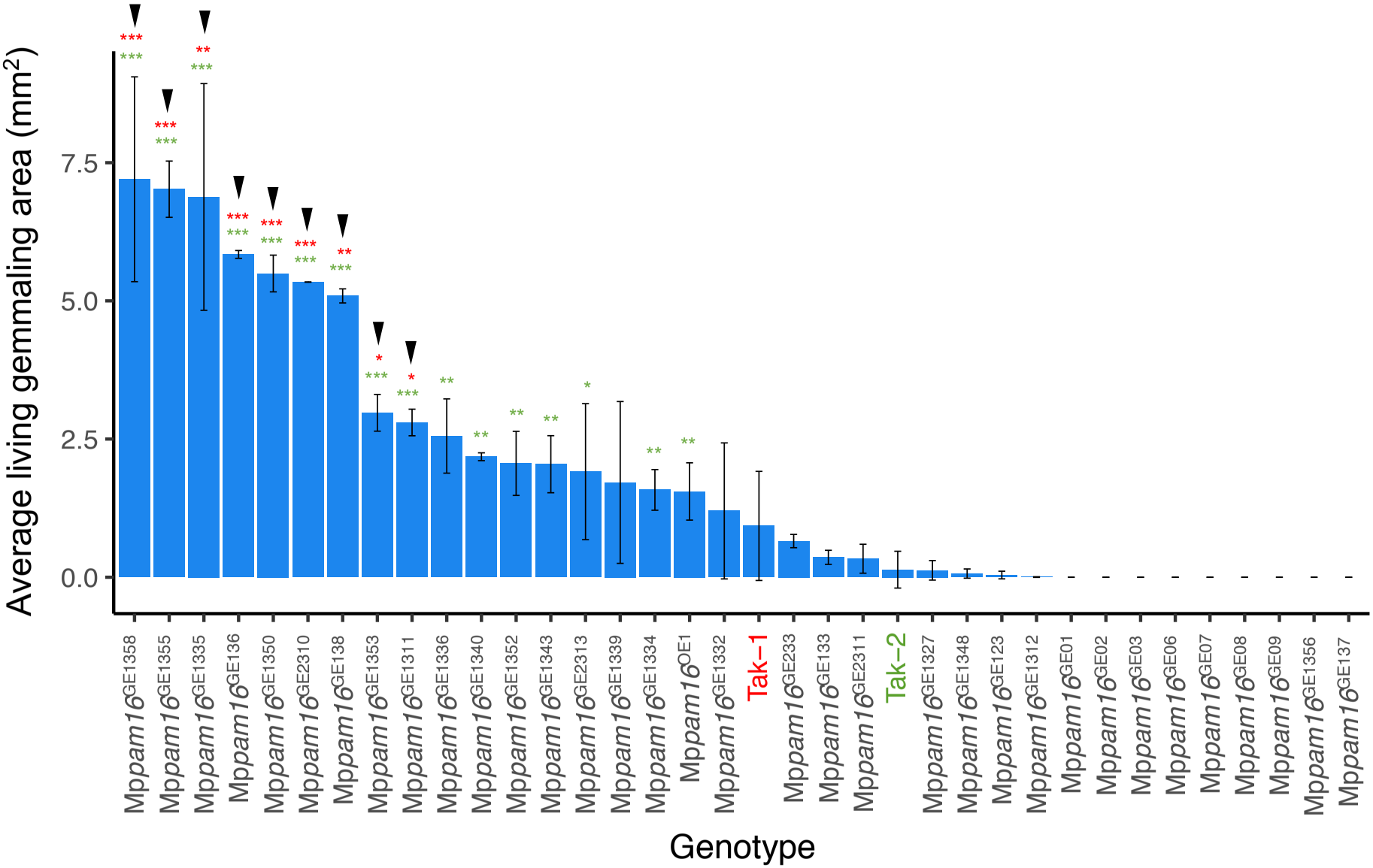

Fig. 2.9. Growth of Mp*pam16* mutant lines on 5 µM TXTA. 33 Mp*pam16* lines were generated using CRISPR-Cas9 mutagenesis to target the Mp*PAM16* gene. Gemmae from these lines were plated onto solid ½ Gamborg medium supplemented with 5µM TXTA and grown for 12 days. The lateral area of living gemmaling tissue was determined from images taken using a Berthold Nightowl II LB 983 *In Vivo* Imaging System. Black tick marks mark the Mp*pam16* lines with TXTA resistance. Stars represent the level of significance of the difference between mutant and control lines (Tak-1 in red and Tak-2 in green) as determined by Student's t-tests: * = $p < 0.05$, ** = $p < 0.01$, *** = $p < 0.001$. Error bars are ± standard deviation (n = 3-6).

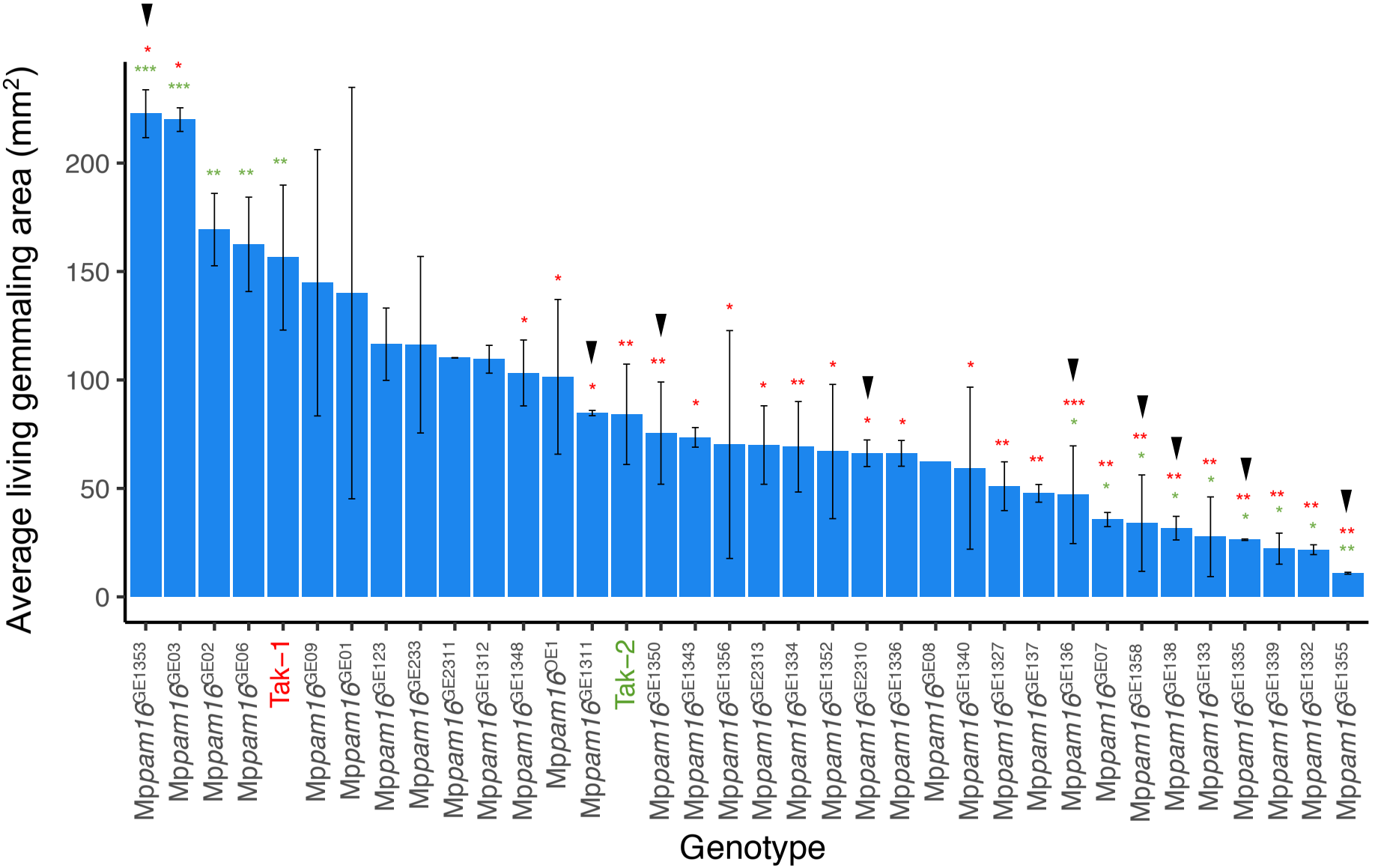

Fig. 2.10. Growth of Mp*pam16* mutant lines in control conditions. 33 Mp*pam16* lines were generated using CRISPR-Cas9 mutagenesis to target the Mp*PAM16* gene. Gemmae from these lines were plated onto solid ½ Gamborg medium supplemented with 0.1 % DMSO for 12 days. The lateral area of living gemmaling tissue was determined from images taken using a Berthold Nightowl II LB 983 *In Vivo* Imaging System. Black tick marks mark the Mp*pam16* lines with TXTA resistance. Stars represent the level of significance of the difference between mutant and control lines (Tak-1 in red and Tak-2 in green) as determined by Student's t-tests: * = $p < 0.05$, ** = $p < 0.01$, *** = $p < 0.001$. Error bars are ± standard deviation (n = 3-6).

2.4.6. Specific mutations in the Mp*PAM16* signal peptide confer TXTA resistance

The highly conserved region encoding the signal peptide (Fig. 2.1) of the MpPAM16 protein targeted by sgRNA 2 was mutated in 28 Mp*pam16* lines, including in all 9 TXTA-resistant lines (Table 2.2, Fig. 2.9). Nineteen Mp*pam16* lines in which the signal peptide was mutated were TXTA-sensitive (Table 2.2, Fig. 2.9). Consequently, not all mutations in the PAM16 protein signal peptide conferred TXTA resistance.

To determine which mutations in the region encoding the PAM16 protein signal peptide conferred TXTA resistance, I compared the predicted protein sequences of the 9 TXTA-resistant and 19 TXTA-sensitive Mp*pam16* lines with mutations in the region encoding the signal peptide.

There are no residues mutated in TXTA-resistant lines which are not also mutated in TXTA-sensitive lines. This suggests that there is no specific single residue in the MpPAM16 protein signal peptide which when mutated confers TXTA resistance.

Two independent TXTA-resistant Mp*pam16* lines with mutations in the region encoding the PAM16 protein signal peptide – Mp*pam16*^{GE2310} and Mp*pam16*^{GE136} – had the same predicted protein sequence as each other (Fig. 2.6). Three independent TXTA-sensitive Mp*pam16* lines with mutations in the region encoding the PAM16 protein signal peptide – Mp*pam16*^{GE1312}, Mp*pam16*^{GE133}, and Mp*pam16*^{GE1343} – had the same predicted protein sequence as each other (Fig. 2.6). No TXTA-resistant lines had the same predicted protein sequence as any TXTA-sensitive lines (Fig. 2.6). These results suggest that specific combinations of mutated residues in the PAM16 protein signal peptide confer TXTA resistance.

2.4.7. Putative weak loss of Mp*PAM16* function can confer TXTA resistance

In *A. thaliana*, total loss of *PAM16* function is responsible for TXTA resistance in At*pam16* lines (Scheible *et al.*, 2003). To test if total loss-of-function of *PAM16* is responsible for TXTA resistance in the 9 TXTA-resistant *M. polymorpha* Mp*pam16* lines, I referred to my classification of Mp*pam16* lines as putative strong or weak loss-of-function based on protein sequence.

Of the 4 putative strong loss-of-function lines (Mp*pam16*^{GE1352}, Mp*pam16*^{GE1356}, Mp*pam16*^{GE138}, and Mp*pam16*^{GE1340}), only 1 – Mp*pam16*^{GE138} – was resistant to TXTA (Fig. 2.9). Accordingly, of the 9 TXTA-resistant Mp*pam16* lines, only Mp*pam16*^{GE138} was a putative strong loss-of-function line; the remaining 8 lines were putative weak loss-of-function lines. This suggests that weak loss of *PAM16* function can confer resistance to TXTA in *M. polymorpha*.

2.4.8. Putative weak loss of Mp*PAM16* function can cause growth defects

At*pam16* plants with a total loss of *PAM16* function are smaller than wild-type lines (Scheible *et al.*, 2003). To test if Mp*pam16* loss-of-function mutant lines were smaller than wild type lines, I grew gemmae from each of the 33 Mp*pam16* lines (and Mp*pam16*^{OE1}) on solid ½ Gamborg medium supplemented with 0.1 % DMSO (control conditions) and quantified the area of gemmalings after 12 days (Fig. 2.10). Since only living tissue was measured, for dead gemmalings the gemmaling area is quantified as zero although the actual area is greater than zero.

Nine lines – Mp*pam16*^{GE1355}, Mp*pam16*^{GE1332}, Mp*pam16*^{GE1339}, Mp*pam16*^{GE1335}, Mp*pam16*^{GE133}, Mp*pam16*^{GE138}, Mp*pam16*^{GE1358}, Mp*pam16*^{GE07}, and Mp*pam16*^{GE136}

– were significantly smaller than Tak-1 and Tak-2 ($p < 0.05$). Mp*pam16*^{GE1353} and Mp*pam16*^{GE03} were significantly larger than Tak-1 and Tak-2 ($p < 0.05$) (Fig. 2.10).

Of the 4 putative strong loss-of-function lines (Mp*pam16*^{GE1352}, Mp*pam16*^{GE1356}, Mp*pam16*^{GE138}, and Mp*pam16*^{GE1340}), only Mp*pam16*^{GE138} was significantly smaller than both wild-type lines (Fig. 2.10). These data suggest that strong loss of *PAM16* function does not always cause growth defects in *M. polymorpha*. Accordingly, of the 9 lines which grew significantly smaller than wild-type, only Mp*pam16*^{GE138} was a putative strong loss-of-function line, and the remaining 8 lines were putative weak loss-of-function lines. These data suggest that weak loss of *PAM16* function can cause growth defects in *M. polymorpha*.

2.4.9. TXTA-resistant Mp*pam16* lines were weakly resistant to TXTA

At*pam16* lines are weakly resistant to TXTA, displaying growth inhibition on high doses of TXTA (Scheible *et al.*, 2003). To test if the 9 TXTA-resistant Mp*pam16* lines were also weakly resistant to TXTA, I compared their growth on 5 µM TXTA (the lethal dose of TXTA for wild-type lines) with their growth in control conditions (Fig. 2.11).

Eight out of the 9 TXTA-resistant lines were significantly smaller on 5 µM TXTA than they are in control conditions (Fig. 2.11) ($p < 0.05$). Mp*pam16*^{GE1358} was also smaller on 5 µM TXTA than in control conditions (Fig. 2.11), although this size difference was not significant. The growth inhibition of the TXTA-resistant Mp*pam16* lines on TXTA suggests that these lines are weakly resistant to TXTA.

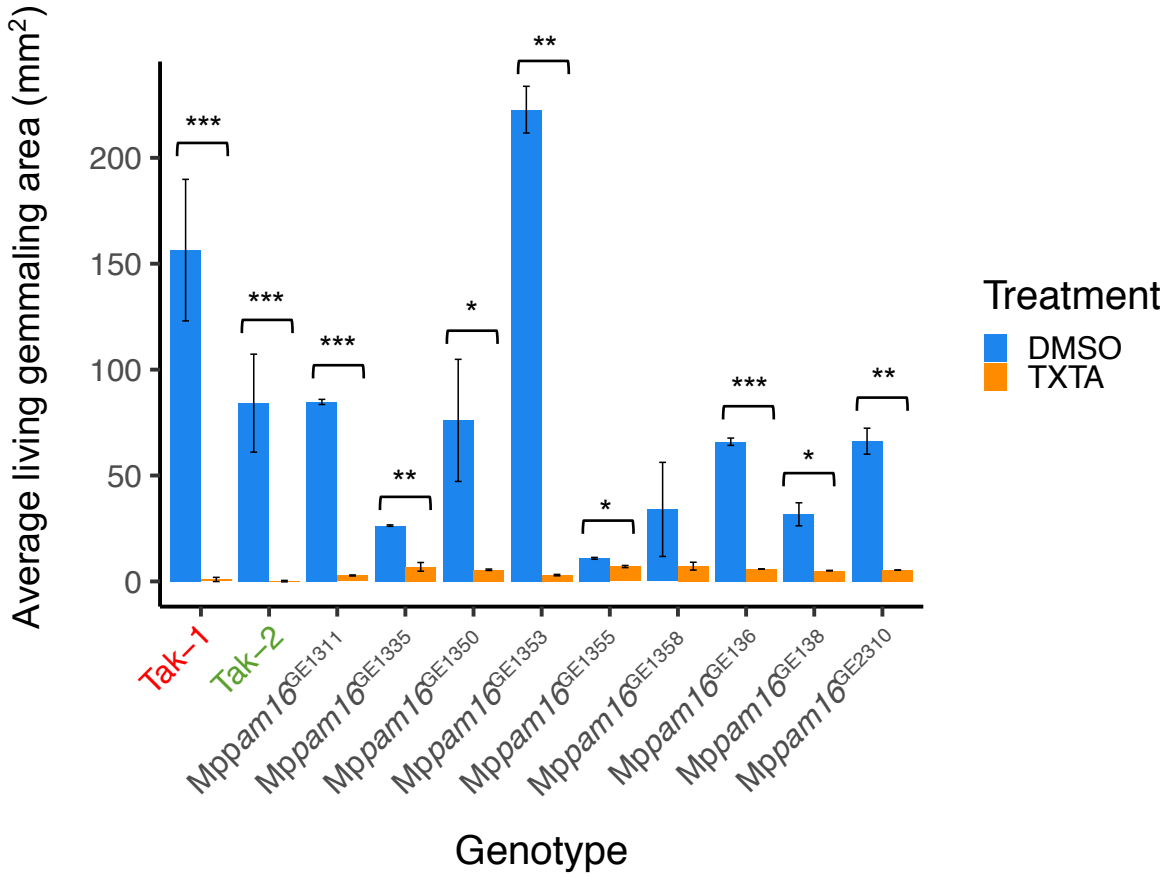

Fig. 2.11. Growth of TXTA-resistant Mp*pam16* lines in control conditions and on TXTA. Mp*pam16* lines were generated using CRISPR-Cas9 mutagenesis to target the Mp*PAM16* gene. 9 Mp*pam16* lines were resistant to TXTA. Gemmae from these 9 lines were plated onto solid ½ Gamborg medium supplemented with 0.1 % DMSO or 5 µM TXTA for 12 days. The lateral area of living gemmaling tissue was determined from images taken using a Berthold Nightowl II LB 983 *In Vivo* Imaging System. Stars represent the level of significance of the difference between plants grown on TXTA or in control conditions as determined by Student's t-tests: * = $p < 0.05$, ** = $p < 0.01$, *** = $p < 0.001$. Error bars are ± standard deviation (n = 3-6).

2.4.10. The most strongly TXTA-resistant Mp*pam16* lines were smaller than wild-type lines in control conditions

At*pam16* TXTA-resistant mutants are smaller than wild-type lines in control conditions (Scheible *et al.*, 2003). To test if TXTA-resistant Mp*pam16* lines were smaller than wild-type in control conditions, I compared the sizes of the 9 TXTA-resistant lines to the wild-type lines grown on DMSO (Fig. 2.10).

Five of the 9 TXTA-resistant Mp*pam16* lines – Mp*pam16*^{GE1358}, Mp*pam16*^{GE1355}, Mp*pam16*^{GE1335}, Mp*pam16*^{GE136}, and Mp*pam16*^{GE138} – were significantly smaller than wild-type lines in control conditions (Fig. 2.10). Of the remaining 4 TXTA-resistant lines, Mp*pam16*^{GE1311}, Mp*pam16*^{GE1350}, and Mp*pam16*^{GE2310} were significantly smaller than Tak-1 but not Tak-2, and Mp*pam16*^{GE1353} was significantly larger than Tak-1 and Tak-2. (Fig. 2.10). These data show that the size of TXTA resistant Mp*pam16* lines varies in control conditions, but most of them were smaller than wild-type lines.

Based on their size on 5 µM TXTA, the 4 lines with the strongest TXTA resistance were Mp*pam16*^{GE1358}, Mppam16^{GE1355}, Mppam16^{GE1335}, and Mppam16^{GE136} (Fig. 2.9). These 4 lines were significantly smaller than wild-type lines in control conditions (Fig 2.10). The most strongly TXTA-resistant lines were therefore smaller than wild-type lines in control conditions.

2.5. Discussion

Loss-of-function mutations in the *Arabidopsis thaliana PAM16* gene is one of the few known examples of NTSR conferred by a loss-of-function mutation. In this chapter, I demonstrated that there is a single *PAM16* gene in *M. polymorpha*, and that some putative loss-of-function mutations in Mp*PAM16* confer resistance to the herbicide TXTA. This mechanism of herbicide resistance is therefore conserved between *A. thaliana* and *M. polymorpha*.

I conducted a phylogenetic analysis of *PAM16* in land plants by searching for protein sequences similar to AtPAM16 (At3G59280). Sequence alignments of the PAM16 protein homologues showed high amino acid conservation, apart from *Picea abies* (MA_203823g0010) which lacks a signal peptide. The protein sequence of the *P. abies* PAM16 orthologue MA_203823g0010 is a “medium confidence” annotated protein and is only annotated with two exons whereas At*PAM16* has 5, two of which encode the region of the protein up until the conserved asparagine directly preceding the proposed start of the *P. abies* PAM16 protein. It is therefore likely that the protein sequence for the *P. abies* PAM16 protein is incomplete and is missing the first two exons, rather than that the protein has truly lost its signal peptide.

Of the 10 plant species I included in my phylogenetic analysis, there were 6 species with more than one *PAM16* homologue, including *A. thaliana*. The analysis identified one protein (Mp3g09390) in *M. polymorpha* that is homologous to At*PAM16*. The presence of a single copy *PAM16* gene in *M. polymorpha* means that it is possible to define *PAM16* function by mutating a single gene, simplifying the functional characterisation studies of Mp*PAM16* I undertook via loss-of-function mutant generation. However, loss of both *PAM16* paralogues in *A. thaliana* is lethal (no

At*pam16*/At*pam16L* double mutant could be generated), suggesting that the generation of a complete loss-of-function mutant of the single *PAM1*6 gene in *M. polymorpha* may be lethal (Scheible *et al.*, 2003).

The lethality of complete loss of *PAM16* function in *M. polymorpha* may explain why the majority of the 33 Mp*pam16* lines I generated were putative weak loss-of-function. Based on predicted protein sequences, 29 out of the 33 Mp*pam16* lines I generated were putative weak loss-of-function lines, with mutations affecting fewer than 15 amino acids in frame. This could be because strong loss-of-function Mp*pam16* mutant lines are less likely to survive.

Lethality of complete loss of Mp*PAM16* function could also explain why 3 out of the 5 guide RNAs I used to target the Mp*PAM16* gene did not yield any viable mutants. Furthermore, the mutation efficiency for the 2 working guide RNAS was low: between 2-5 % of transformants carrying a vector containing sgRNA1 and between 21-27 % of transformants carrying a vector containing sgRNA 2 had mutations in Mp*PAM16* (Fig. 2.4). These low mutation efficiencies could indicate that transformants with strong loss-of-function mutations were more likely to be inviable due to lethality of Mp*PAM16* total loss-of-function, and therefore mostly transformants with putative weak loss-of-function mutations survived.

Nine out of the 33 Mp*pam16* lines were significantly resistant to TXTA. Total loss-of-function of *PAM16* is the basis of TXTA resistance in At*pam16* lines: if the population of 33 Mp*pam16* lines consist mostly of weak loss-of-function lines, this could explain why only 9 of the 33 Mp*pam16* lines were resistant to TXTA. All TXTA-resistant lines were mutated in a highly conserved region encoding the signal peptide suggesting that some degree of loss-of-function of *PAM16* is required for resistance, but based

on the predicted number of amino acids affected in their protein sequences 8 out of the 9 TXTA-resistant Mp*pam16* mutant lines were putative weak loss-of-function mutants. The resistance to TXTA of these 9 lines was relatively weak; all 9 lines were smaller on 5 µM TXTA than in control conditions, so were still affected by high doses of TXTA. The weak TXTA resistance observed in the 9 TXTA-resistant lines may be due to weak rather than total loss of *PAM16* function.

These data show that putative weak loss of Mp*PAM16* function can confer weak but significant TXTA resistance in *M. polymorpha*. Furthermore, when grown in control conditions, 8 putative weak loss of *PAM16* function were significantly smaller than wild-type, suggesting that weak loss of Mp*PAM16* function can cause growth defects in *M. polymorpha*. These results are unexpected since in *A. thaliana* total rather than partial loss of *PAM16* function is responsible for TXTA resistance and growth defects. However, there is a second *PAM16* gene (*PAM16L*) in *A. thaliana*. Double *pam16/pam16l* mutants could not be isolated, suggesting that a double knockout is lethal, and that a functioning PAM16L protein therefore can at least partially complement the loss of *PAM16* function in At*pam16* mutants. TXTA-resistant At*pam16* mutants may therefore have partial rather than total loss of PAM16 protein activity, equivalent to a weak loss of *PAM16* function in *M. polymorpha* which has only one *PAM16* gene. This could explain why putative weak loss of MpPAM16 protein function in *M. polymorpha* and total loss of AtPAM16 protein function in *A. thaliana* can confer the same phenotypes (TXTA resistance and growth defects).

Although putative weak loss of Mp*PAM16* function can confer TXTA resistance and cause reduced growth, the phenotypes of putative weak loss-of-function Mp*pam16* lines were inconsistent. Of the 29 putative weak loss-of-function Mp*pam16* lines, 8

were resistant to TXTA but 21 were not, and 8 grew smaller than wild-type but 21 did not. Although Mp*pam16* mutant lines did not show consistent phenotypes, two independent TXTA-resistant lines (Mp*pam16*^{GE2310} and Mp*pam16*^{GE136}) had the same predicted protein sequence as each other, and three independent sensitive lines (Mp*pam16*^{GE1312}, Mp*pam16*^{GE133}, and Mp*pam16*^{GE1343}) had the same predicted protein sequence as each other. No TXTA-sensitive and TXTA-resistant lines had the same predicted protein sequence. These findings suggest that specific mutations in the PAM16 protein confer TXTA resistance. Studying the sequence alone does not provide enough information to determine how the mutations affect the function of the PAM16 protein: since the function of the PAM16 protein was not measured, it is possible that some Mp*pam16* mutant lines with predicted loss-of-function mutations in fact have a functional PAM16 protein, which may explain the inconsistency in the phenotypes of putative weak loss-of-function Mp*pam16* mutant lines. Future work measuring the function of the PAM16 protein in Mp*pam16* lines and modelling the effects of each mutation on the 3D structure of the protein may clarify how the mutations in each Mp*pam16* mutant line affect the function of the PAM16 protein and how this in turn affects the phenotypes of the plants.

There were 4 putative weak loss-of-function Mp*pam16* mutant lines which were both TXTA resistant and smaller than wild-type (Mp*pam16*^{GE1358}, Mp*pam16*^{GE1355}, Mp*pam16*^{GE1335}, and Mp*pam16*^{GE136}). These 4 Mp*pam16* mutant lines were also the 4 lines with the strongest resistance to TXTA based on their size on 5 µM TXTA. This suggests that growth defects are more likely in Mp*pam16* mutant lines with stronger resistance to TXTA, so the two phenotypes may be linked. Most weeds with NTSR do not display significant fitness costs when grown without herbicide (Keshtkar *et al.*, 2017, Wu *et al.*, 2018). Therefore, the mechanism of NTSR

conferred by predicted loss-of-function of *PAM16* is not a typical instance of NTSR and may not be selected for in the field. However, understanding the molecular basis behind the resistance in Mp*pam16* mutant lines can still help to understand what kinds of molecular pathways could be involved in resistance in weeds with NTSR to TXTA. It is still unclear why loss-of-function of *PAM16* confers resistance to TXTA. The phenotypes of At*pam16* mutants include slow growth, twisted leaves, and overproduction of reactive oxygen species (ROS) (Scheible *et al.*, 2003, Huang *et al.*, 2013). At*pam16* plants also accumulate less TXTA in their tissue than Col-0 plants, however it is still unclear why a mutation in *PAM16*, part of the mitochondrial inner membrane protein transport complex, causes this phenotype (Scheible *et al.*, 2003). Some Mp*pam16* lines grew smaller than wild-type lines, but the thallus of Mp*pam16* lines had no observable differences to that of wild-type lines. Measuring the concentrations of TXTA and ROS in the 9 TXTA-resistant Mp*pam16* lines could indicate whether these phenotypes are also conserved between TXTA-resistant At*pam16* lines and Mp*pam16* lines, and whether they may contribute to resistance.

In conclusion, I identified 9 Mp*pam16* lines with mutations predicted to cause some degree of loss-of-function of *PAM16* which were resistant to TXTA. This demonstrates that putative loss-of-function of *PAM16* is a mechanism of NTSR which is conserved across land plants and validates my use of *M. polymorpha* as a tool to identify novel mechanisms of NTSR. In my next chapter I will undertake a forward genetics approach to isolate herbicide-resistant *M. polymorpha* mutants which may carry novel NTSR mechanisms.

2.6. Supplementary Data

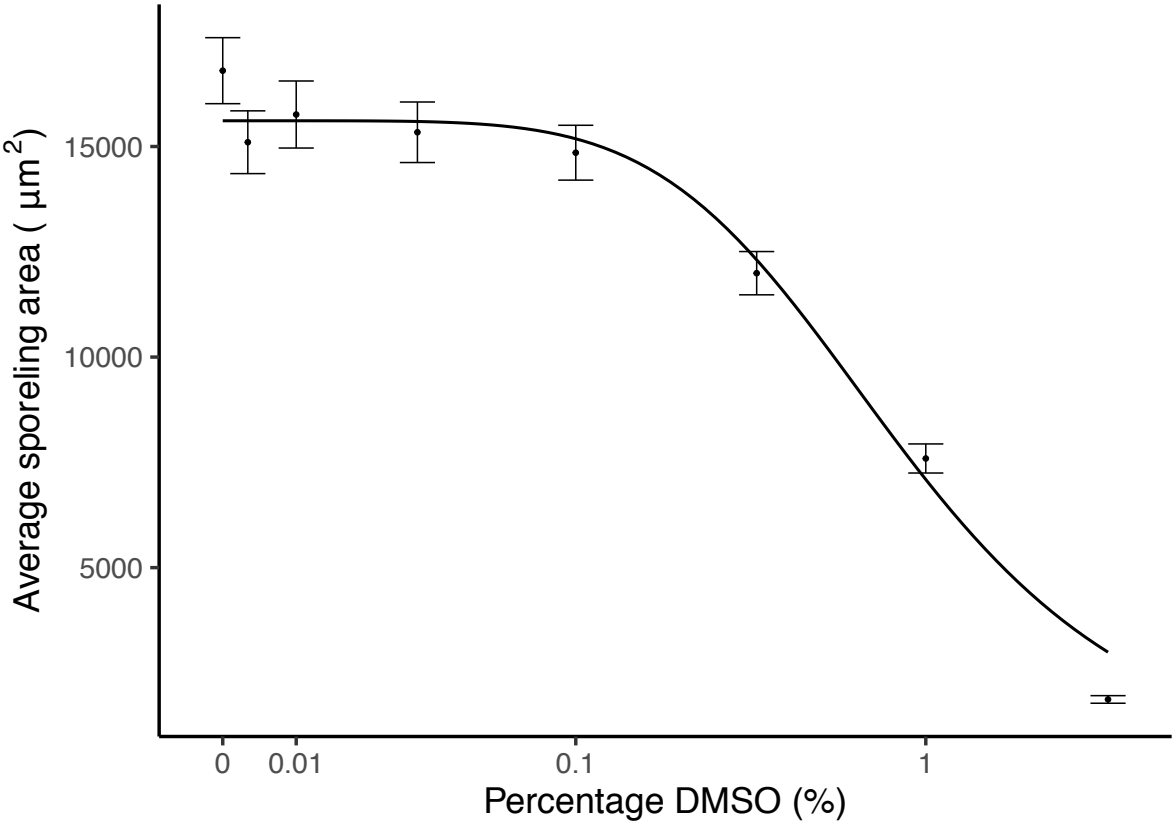

Supplementary Fig. S2.1 DMSO exerts a dose-dependent growth inhibition on *M. polymorpha* spores. Wild type spores (resulting from a cross between Tak-1 and Tak-2) were grown in liquid Johnson's medium supplemented with different % DMSO. Sporelings were imaged after 5 days of growth using an IN Cell Analyser 2500HS high content analysis imaging system (GE Healthcare). The IN Cell imaging system records chlorophyll autofluorescence (648-676 nM using the FarRed filter). The area of autofluorescing (living) sporelings was determined using the In Cell Developer Toolbox v1.6 software (GE Healthcare). No living spores were detected at 10 % or 33 % DMSO. The fitted curve was calculated using the four-parameter log-logistic equation included in the drc package in R. Error bars represent ± standard error.

Chapter 3: Generation of eighteen herbicide-resistant mutants via a forward genetic approach

3.1. Abstract

Non-target site resistance (NTSR) in weeds is a serious threat to global agriculture. It is generally more difficult to mechanistically characterise than target site resistance (TSR), and one NTSR allele can sometimes confer resistance to herbicides with different molecular targets, a phenomenon known as herbicide cross-resistance. I have developed a new approach to identify novel mechanisms of NTSR. Using large-scale forward genetics screening in the model species *M. polymorpha*, I generated herbicide-resistant mutants. To test if *M. polymorpha* could be used to screen for herbicide resistance I screened a population of 2 x 10^6 UV-B mutagenized *M. polymorpha* spores for resistance to four times the lethal dose of chlorsulfuron, an inhibitor of acetohydroxyacid synthase (AHAS). I generated 5 chlorsulfuron-resistant mutants that were resistant due to mutations in the gene encoding the chlorsulfuron target AHAS. This demonstrates that forward genetics screening in *M. polymorpha* can be used to identify herbicide-resistant mutants. To identify mutations that confer NTSR to the novel herbicide thaxtomin A (TXTA), for which no resistance has yet evolved in weeds, I screened a population of 1 x 10^7 UV-B mutagenized *M. polymorpha* spores on a lethal dose of TXTA for resistance. I isolated 13 TXTA-resistant lines; *t*haxtomin *A r*esistant (Mp*tar*) mutants. Mp*tar* mutants are weakly resistant to TXTA and some are cross-resistant to herbicides with different modes of action, suggesting that they are likely to result from mutations that cause NTSR. I hypothesize that mutations conferring resistance in Mp*tar* mutants are potential mechanisms of NTSR to TXTA that are likely to evolve in the field where TXTA is used.

3.2. Introduction

Herbicide resistance in weeds is becoming increasingly prevalent, threatening the efficacy of the herbicides upon which we rely to maintain global crop yields. There are two classes of herbicide resistance; target site resistance (TSR) and non-target site resistance (NTSR) (reviewed in (Gaines *et al.*, 2020)). TSR refers to resistance mechanisms involving changes affecting the herbicide target site, whereas NTSR encompasses any mechanism which does not involve changes at the herbicide target site but which reduces the amount of herbicide reaching the target site (decreased herbicide absorption and translocation, and increased herbicide metabolism and sequestration), or which protect the plant from the toxic effects of the herbicide downstream of its action (Gaines *et al.*, 2020). TSR is a monogenic trait usually conferring high levels of resistance. It involves mutations affecting the gene encoding the target whose identity is therefore often known beforehand. NTSR however is commonly a polygenic trait involving multiple alleles of unknown identity each conferring a low level of resistance which stack up in an individual to confer higher resistance (Delye, 2013). Therefore although resistant plants are easy to identify in the field, if they are non-target site resistant the mechanisms underlying their resistance are more difficult to characterise and by consequence less well understood (Delye *et al.*, 2011a). In addition, whereas TSR confers resistance to one herbicide or mode of action only, a single allele of NTSR can confer resistance to multiple herbicide modes of action (Burnet *et al.*, 1994). NTSR therefore arguably poses a larger potential threat to agriculture than TSR.

Several approaches have been employed to identify novel NTSR-conferring alleles. Transcriptomic analyses comparing gene expression between sensitive and resistant

weed populations have identified a number of genes encoding proteins from four large gene families involved in herbicide metabolism or sequestration – cytochrome P450s, glutathione-S-transferases, glycosyltransferases, and ABC transporters– which are over-expressed in resistant populations, leading to resistance via increased herbicide metabolism or sequestration (Yuan *et al.*, 2007, Maroli *et al.*, 2018). RNA-seq approaches can identify genes which when overexpressed confer a high level of NTSR; however, some NTSR-conferring alleles are predicted to confer low levels of resistance only, and transcriptomics also cannot identify mechanisms of NTSR which do not involve changes in gene expression. Recently, population genomics approaches comparing the genomes of glyphosate sensitive and resistant *A. tuberculatus* or *I. pupurea* populations have identified regions of the genome associated with NTSR (Kreiner *et al.*, 2019, Van Etten *et al.*, 2020, Kreiner *et al.*, 2021). Studies such as these have the potential to identify regions of the genome containing novel NTSR alleles, including NTSR conferred by loss of gene function. However, GWAS are constrained by our lack of knowledge regarding the types of genes underlying NTSR other than the four previously identified NTSR-associated gene families (Maroli *et al.*, 2018), and by the need for functional characterisation to assign causality to an identified association with NTSR.

Another approach with the potential to identify novel NTSR-conferring alleles is forward genetics, which involves mutagenizing a wild-type population and screening for herbicide resistant mutants followed by the determination of the molecular basis of resistance. A forward genetic approach in *A. thaliana* found that loss-of-function of *PAM16* confers resistance to thaxtomin A; this mechanism of resistance was confirmed to be conserved in land plants in the previous chapter. However, there has been limited success in employing mutagenesis screens to identify mechanisms of

NTSR. This is partly due to the limitations imposed by the scale of mutagenesis screens in diploid model species such as *A. thaliana*. The number of mutant individuals that can be screened when carrying out a screen with *A. thaliana* is limiting due to the need to self M_1 individuals to recover homozygous individuals to identify phenotypes caused by recessive mutations. The model species *M. polymorpha* however is uniquely suited to mutagenesis screening approaches; a single *M. polymorpha* plant produces millions of spores which can be easily mutagenized, and since it is a dominant haploid gametophyte M_1 individuals can be directly screened for a phenotype (Ishizaki *et al.*, 2016). In addition, *M. polymorpha* has low genetic redundancy and is genetically tractable, which facilitates functional characterisation of genes of interest (Sugano *et al.*, 2014, Ishizaki *et al.*, 2016). In the context of forward genetics screening *M. polymorpha* therefore overcomes the limitations of diploid angiosperm model species, and a large-scale forward genetic screen in *M. polymorpha* is a potentially powerful approach for identifying novel mechanisms of NTSR.

To use a forward genetics screen to identify novel mechanisms of NTSR, mutagenized individuals should be screened at a herbicide dose which preferentially selects for NTSR. TSR usually confers very high levels of herbicide resistance well above the lethal dose of a herbicide. Biotypes of the weed *Euphorbia heterophylla* which are target-site resistant to the AHAS inhibitor imazamox can survive more than 50 times the recommended field dose (Rojano-Delgado *et al.*, 2019). However, single alleles of NTSR usually cannot survive such high doses (Gressel, 2000). It has consequently been observed that treatment with high doses of herbicides preferentially selects for TSR, whereas treatment with lower doses (near the lethal dose) of herbicides preferentially selects for NTSR (Gardner *et al.*, 1998). For

example, *Lolium* populations sprayed with the ACCase inhibitor diclofop-methyl at three times the recommended field rate (1200 g ha^{-1}) uniquely evolved TSR. However, *Lolium* populations sprayed with the same herbicide at the recommended field rate (375 g ha^{-1}) evolved a range of resistance mechanisms some of which involve cytochrome P450s and glutathione transferases, and some populations evolved resistance to herbicides with different modes of action suggesting NTSR (Gardner *et al.*, 1998). In the context of forward genetic screens, screening at or below the lethal dose is therefore more likely to isolate mutants with NTSR, whereas screening above 3 – 10 x the lethal dose is more likely to identify mutants with TSR.

In this chapter, I tested if mutagenesis of *M. polymorpha* could be used to identify herbicide resistant mutants. I screened 2 x 10^6 UV-B mutagenized *M. polymorpha* spores for resistance to the AHAS inhibitor chlorsulfuron. Chlorsulfuron target site resistant (TSR) mutants have been previously generated via forward mutagenesis screens in *A. thaliana*, so I first screened for TSR to chlorsulfuron at four times the lethal dose of chlorsulfuron to prove that my protocol could generate herbicide-resistant mutants (Jander *et al.*, 2003). I generated 5 chlorsulfuron-resistant mutants which are TSR: all 5 lines have resistance-conferring mutations in the AHAS gene. I then screened a population of 1 x 10^7 UV-B mutagenized *M. polymorpha* spores for resistance to the lethal dose of the novel herbicide thaxtomin A (TXTA). I isolated 13 TXTA-resistant mutants. The TXTA-resistant lines are likely non-target site resistant as they were screened at the lethal dose, are weakly resistant to TXTA, and 8 out of 13 of the lines were significantly cross-resistant to herbicides with different molecular targets. Identifying the mechanisms responsible for resistance in TXTA-resistant lines could therefore lead to the discovery of novel mechanisms of NTSR.

3.3. Materials and Methods

3.3.1. Plant growth conditions

Wild-type plants consisted of *M. polymorpha* laboratory accessions Takaragaike-1 (Tak-1) and Takaragaike-2 (Tak-2) (Ishizaki *et al.*, 2008). Chlorsulfuron-resistant lines generated by UV-B mutagenesis were named Mp*chlr* (**Chl**orsulfuron **R**esistant). Chlorsulfuron-resistant mutants Mp*chlr9b* and Mp*chlr10* were previously generated using EMS mutagenesis. TXTA-resistant mutants generated by UV-B mutagenesis were named Mp*tar* (**T**haxtomin **A R**esistant).

All lines were maintained and crossed as described in Chapter 2 Section 2.3.2.

3.3.2. Fresh spore sterilisation

See Chapter 2 Section 2.3.3.

3.3.3. Chemicals and stock solution preparation

Thaxtomin A (TXTA) (SML1456), dichlobenil (45431), isoxaben (36138), chlorsulfuron (34322), 2,4-dichlorophenoxyacetic acid (2,4-D) (31518), amitrole (45324), pyributicarb (92842), and aclonifen (36792) were obtained from Sigma-Aldrich. Stock solutions were prepared by dissolving in pure dimethyl sulfoxide (DMSO) from Sigma-Aldrich.

3.3.4. Herbicide dose-response assays

3.3.4.1. Gemmaling dose-response assays

See Chapter 2 Section 2.3.5.

3.3.4.2. Spore dose-response assays

Sterilised fresh wild type spores (from a cross between Tak-1 and Tak-2) were grown on solid Johnson's medium (Chapter 2 Section 2.3.11) supplemented with different concentrations of herbicide dissolved in DMSO. Sporelings were imaged after 4 days of growth using a Leica DFC310 FX stereomicroscope (Leica microsystems). The sporeling germination ratio was determined using ImageJ.

3.3.5. Generation of herbicide-resistant *M. polymorpha* lines via UV-B mutagenesis

Sterilised fresh wild type *M. polymorpha* spores (from a cross between Tak-1 and Tak-2) were plated on solid Johnson's medium supplemented with a dose of herbicide equal to or greater than the LD_{100} (herbicide dose at which 100 % of wild-type spores are killed) (Table 3.1). The spores were exposed to UV-B irradiation (302 nm) for an exposure time corresponding to or near the LD_{50} (an exposure time of UV-B at which 50 % of spores are killed) (Fig. 3.3) using a UVP BioDoc-It™. Plates of mutagenized spores were wrapped in aluminium foil and left in the dark overnight. Plates were then unwrapped and placed in a Sanyo growth chamber at 23 °C in 24-hour light. After 14 days of growth, plates were screened for surviving sporelings. Surviving sporelings were transferred to solid Johnson's medium supplemented with fresh herbicide. Plants which survived this second transfer onto a lethal dose of herbicide were maintained. To test for inheritance of resistance through asexual reproduction, gemmae from these plants were plated onto a lethal dose of herbicide. Lines whose resistance was inherited were classified as herbicide resistant lines and maintained.

3.3.6. Sodium azide mutagenesis of *M. polymorpha* spores

Fresh wild type *M. polymorpha* spores (from a cross between Tak-1 and Tak-2) were sterilized and sporangia kept intact in sterile phosphate buffer. Sodium azide was added to a final concentration ranging from 200 µM – 1 mM and the sporangia were incubated overnight. After incubation, sporangia were rinsed with sterile water and plated on solid Johnson's medium supplemented herbicide. Mutagenized spores were wrapped in aluminium foil and left in the dark overnight. Plates were then unwrapped and placed in a Sanyo growth chamber at 23 °C in 24-hour light. After 14 days of growth, plates were screened for surviving sporelings.

3.3.7. Genotyping by Phire PCR

Mp*chlr* lines were genotyped using the Phire Plant Direct PCR Kit (Thermo Scientific™) as per the kit protocol. The primers used were designed to amplify the region of the MpAHAS gene in which target-site mutations are commonly found (Warwick *et al.*, 2008). PCR products were run on a 0.1 % agarose gel at 100 V for 15 mins, followed by gel extraction using the GeneJET gel extraction kit (Thermo Scientific™) as per the protocol. The extracted PCR products were Sanger sequenced and sequenced gene fragments were aligned with the consensus MpAHAS sequence (MpTak1v6.1) using Geneious Prime® 2019.0.3 or CLC Genomics Workbench 9 to determine the nature of any introduced mutations.

3.3.8. Primers

Primer	Sequence	Use
GCS_Fw1	CAATCGACTTTGTTGGTCCGA	Genotyping and sequencing Mp*chlr* lines
GCS_Rv1	TCTTCTAGTTCTGCCACCCA	Genotyping and sequencing Mp*chlr* lines

3.4. Results

3.4.1. The herbicides thaxtomin A, chlorsulfuron, dichlobenil, amitrole, aclonifen, and pyributicarb exert a dose-dependent toxic effect on *M. polymorpha* spores and thallus

It was necessary to determine the lethal dose (LD_{100} – the dose at which 100 % of wild-type spores are dead) of each herbicide before conducting forward genetic screens to generate herbicide-resistant mutants. Screening at high doses (3 – 10 x LD_{100}) is more likely to isolate TSR mutants, whereas screening at LD_{100} is more likely to isolate NTSR mutants. Determining LD_{100} allowed selection of a suitable dose of each herbicide against which to screen for resistance in mutagenized *M. polymorpha* spores. I used the herbicides chlorsulfuron, thaxtomin A (TXTA), dichlobenil, aclonifen, amitrole and pyributicarb. There are many characterised mechanisms of TSR and NTSR to chlorsulfuron in mutagenesis experiments and in the field, and there are several documented cases of amitrole resistant weed species (Heap, 2022), but resistance has not yet evolved in the field to the other herbicides (TXTA, dichlobenil, aclonifen, and pyributicarb).

I hypothesised that these herbicides would have a dose-dependent phytotoxic effect on the germination rate of *M. polymorpha* spores. To test this hypothesis, I plated wild-type *M. polymorpha* spores on solid Johnson's media supplemented with different concentrations of each herbicide (Fig. 3.1); after four days of growth on herbicide-supplemented media, I imaged the sporelings and used ImageJ to quantify the numbers of germinated and ungerminated spores to calculate the spore germination rate which I used as a measure of toxicity. For all herbicides, I observed that higher doses decreased spore germination rate (Fig. 3.1).

I also quantified the dose-dependent toxicity of thaxtomin A (TXTA) and chlorsulfuron on the dominant haploid gametophyte form of *M. polymorpha* by growing wild-type (Tak-2) gemmae on solid Johnson's media supplemented with different concentrations of each herbicide and quantifying the lateral area of living gemmaling tissue after two weeks of growth (Fig. 3.2). Since only living tissue was measured, for dead gemmalings the gemmaling area is quantified as zero although the actual area is greater than zero. I found that both TXTA and chlorsulfuron cause dose-dependent growth inhibition of *M. polymorpha* gemmalings. The LD_{100} for TXTA and for chlorsulfuron was the same for both spores and gemmalings (5 μM for TXTA and 33 nM for chlorsulfuron). However, for both herbicides the EC_{50} (herbicide dose at which average spore germination rate or gemmaling area is 50 % relative to untreated control) was greater for spores than gemmalings (TXTA; EC_{50} for gemmalings is 180 nM, EC_{50} for spores is 1400 nM; $p < 0.01$. chlorsulfuron; EC_{50} for gemmalings is 2.74 nM, EC_{50} for spores is 4.5 nM; $p < 0.0001$) suggesting that spores are more resistant to herbicides than gemmalings.

Herbicide	**LD_{100} (wild-type spores)**
Chlorsulfuron	33 nM
Thaxtomin A	5 μM
Dichlobenil	3.3 μM
Aclonifen	10 μM
Amitrole	333 μM
Pyributicarb	1 μM

Table 3.1. Lethal doses at which each herbicide kills 100 % of spores. Wild-type spores (resulting from a cross between Tak-1 and Tak-2) were grown on Johnson's medium supplemented with various herbicides dissolved in DMSO (to a final concentration of 0.1 % DMSO). Control conditions consisted of Johnson's medium supplemented with 0.1 % DMSO. Sporelings were imaged after 4-6 days of growth using a Leica DFC310 FX stereomicroscope. The ratio of germinated to ungerminated sporelings in each image was determined using ImageJ.

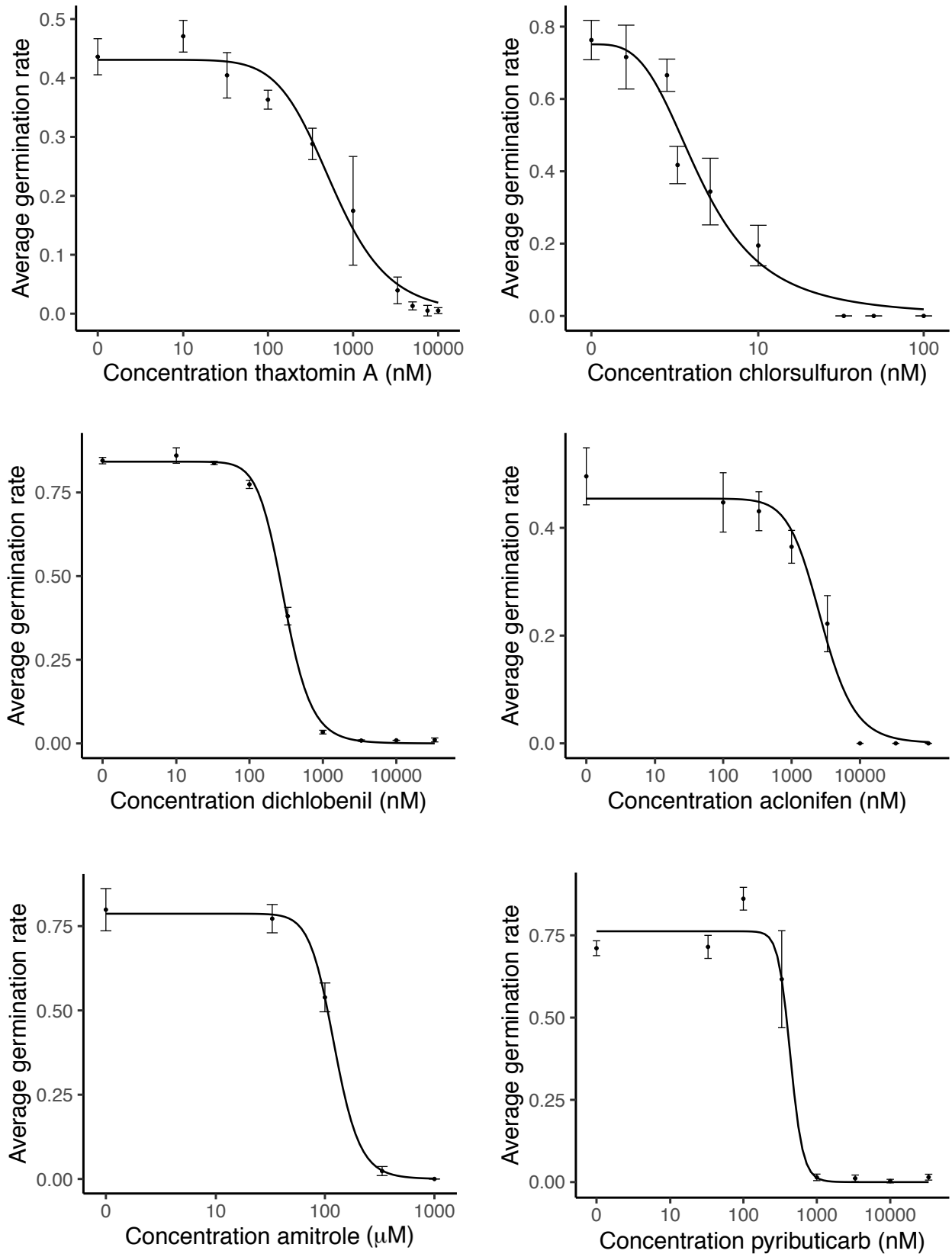

Fig. 3.1. Herbicides exert a dose-dependent growth inhibition on *M. polymorpha* spores. Wild type spores (resulting from a cross between Tak-1 and Tak-2) were grown on Johnson's medium supplemented with various herbicides dissolved in DMSO (to a final concentration of 0.1 % DMSO). Control conditions consisted of 0.1 % DMSO. Sporelings were imaged after 4 days of growth using a Leica DFC310 FX stereomicroscope. The ratio of germinated to ungerminated sporelings in each image was determined using ImageJ. The fitted curve was calculated using the four-parameter log-logistic equation included in the drc package in R. Error bars represent ± standard deviation (n = 3 images each with 100-500 spores).

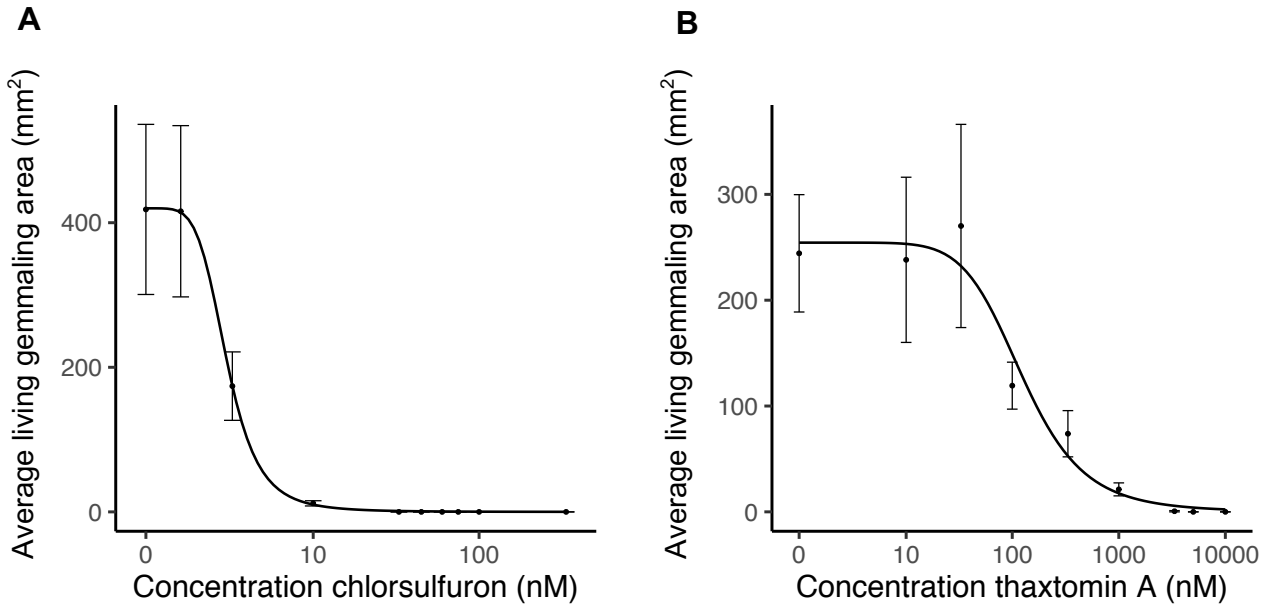

Fig. 3.2 Chlorsulfuron and thaxtomin A (TXTA) exert a dose-dependent growth inhibition on *M. polymorpha* gemmalings.
(A-B) Wild-type gemmae (Tak-2) were grown for 14 days on solid Johnson's medium supplemented with different concentrations of **(A)** chlorsulfuron or **(B)** TXTA**.** Gemmalings were imaged using a Berthold Nightowl II LB 983 *In Vivo* Imaging System which detects chlorophyll autofluorescence (560nm). The lateral area of autofluorescing (living) tissue was determined after 14 days of growth using the indiGo™ software package and plotted using the ggplot2 package in R. Since only living tissue was measured, for dead gemmalings the gemmaling area is quantified as zero although the actual area is greater than zero. The fitted curve was calculated using the four-parameter log-logistic equation included in the drc package in R. Error bars represent ± standard deviation (n = 18).

3.4.2 A UV-B exposure time of 110 s causes 50 % lethality in *M. polymorpha* spores

To use UV-B radiation to generate herbicide-resistant mutants I first determined an optimum UV-B irradiation time (Fig. 3.3). Based on studies investigating optimum doses of UV-B for inducing non-lethal mutations, I hypothesised that an exposure time of UV-B which caused a 50 % lethality (LD_{50}) would cause sufficient mutagenesis without excessive lethality (Tillich *et al.*, 2012). I found that a UV-B exposure time of 110 s caused 50 % lethality ($p < 0.001$) in wild-type *M. polymorpha* spores. During the screening process I tested higher and lower doses (90-130 s) to determine optimum parameters for mutant generation (Supplementary Table S3.1).

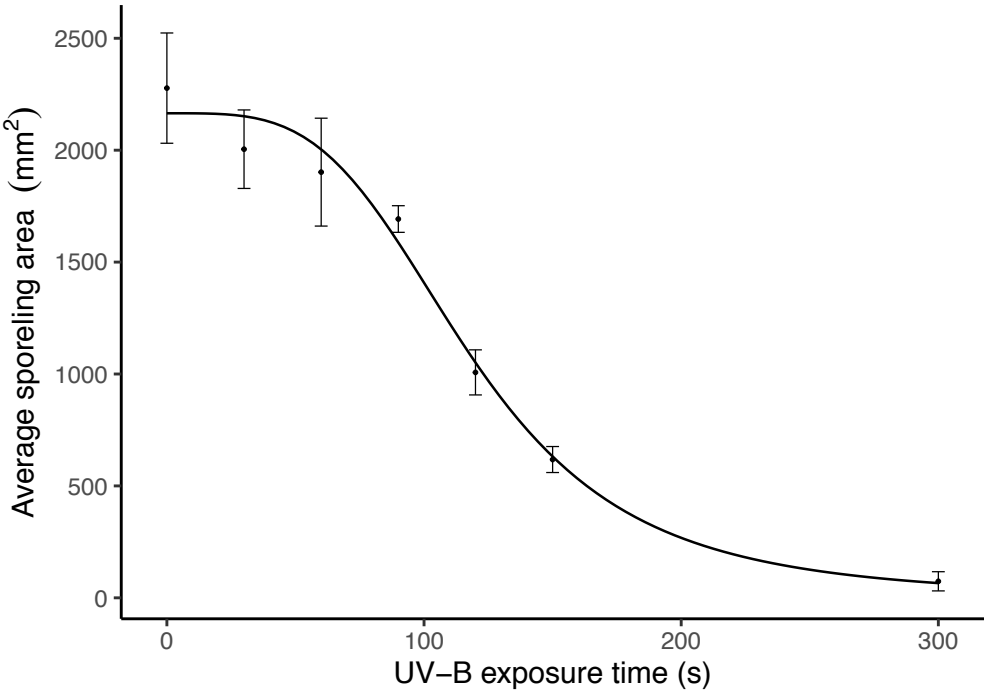

Fig. 3.3. UV-B radiation exerts a dose-dependent growth inhibition on *M. polymorpha* spores. Wild type spores (resulting from a cross between Tak-1 and Tak-2) were plated on Johnson's medium and subjected to UV-B irradiation for different lengths of time using a UVP BioDoc-It™. Sporelings were imaged after 14 days of growth using a Leica DFC310 FX stereomicroscope. The total area of sporelings on each plate was determined using ImageJ. The fitted curve was calculated using the four-parameter log-logistic equation included in the drc package in R. Error bars represent ± standard deviation.

3.4.3. Five chlorsulfuron-resistant mutants were generated by UV-B mutagenesis

To validate that UV-B mutagenesis can be used to generate herbicide-resistant mutants, I first screened a population of 2 x 10^6 mutagenized spores for resistance to the herbicide chlorsulfuron. Chlorsulfuron target site resistant (TSR) mutants have been previously generated via forward mutagenesis screens in *A. thaliana* (Jander *et al.*, 2003). I therefore used the generation of chlorsulfuron TSR mutants as proof-of-concept that UV-B mutagenesis can generate herbicide-resistant mutants in *M. polymorpha*, and to optimise the parameters of the screening protocol.

To generate chlorsulfuron-resistant mutants, I plated wild-type spores on solid Johnson's medium supplemented with chlorsulfuron and exposed them UV-B irradiation at or near a kill rate of 50 % (Supplementary Table S3.1), then screened for survivors 14 days after mutagenesis (Fig. 3.4). I used a high screening dose of 140 nM chlorsulfuron – roughly 4 x LD_{100} – to preferentially isolate TSR mutants, as these have previously been successfully generated by mutagenesis (Jander *et al.*, 2003). I transferred surviving sporelings to fresh solid Johnson's medium supplemented with 140 nM chlorsulfuron to eliminate the possibility that they survived because of factors other than genetic herbicide resistance (such as local depletion of herbicide caused by a high concentration of surrounding sporelings absorbing herbicide from the medium). I retained sporelings which survived the second round of selection, and plated gemmae from each of these lines onto fresh solid Johnson's medium supplemented with 33 nM chlorsulfuron (LD_{100}) to verify the inheritance of resistance through a generation of asexual reproduction (Fig. 3.5). Lines whose gemmae survived on 33 nM chlorsulfuron were deemed to be chlorsulfuron-resistant. Using this protocol, I generated 5 chlorsulfuron-resistant lines and named them Mp*chlr* (*chl*orsulfuron *r*esistant). This shows that the UV-B mutagenesis protocol can generate herbicide-resistant mutants.

To quantify the growth of Mp*chlr* lines on chlorsulfuron, I grew Mp*chlr* lines on 33 nM chlorsulfuron (LD_{100}) and measured the lateral area of living gemmaling tissue after 12 days of growth (Fig. 3.6). Since only living tissue was measured, for dead gemmalings the gemmaling area is quantified as zero although the actual area is greater than zero (Fig. 3.5). I also grew 2 chlorsulfuron-resistant lines previously generated in the lab by EMS mutagenesis (Mp*chlr*9b and Mp*chlr*10) to compare the growth of these lines to those I generated using UV-B mutagenesis. On

chlorsulfuron, all Mp*chlr* mutants were significantly larger than wild-type plants ($p < 0.05$) (Fig. 3.6). This confirms their resistance to chlorsulfuron. In control conditions however, all Mp*chlr* lines except Mp*chlr*9b were significantly smaller than the wild-type lines Tak-1 and Tak-2 ($p < 0.05$) (Fig. 3.6). This is likely due to background UV-B or EMS induced mutations which may cause growth defects.

No Mp*chlr* mutants were smaller on chlorsulfuron than in untreated conditions ($p < 0.05$) (Fig. 3.5, Fig. 3.6). This suggests that they are strongly resistant to chlorsulfuron, which is consistent with the hypothesis that the basis of their chlorsulfuron resistance is target site resistance (TSR).

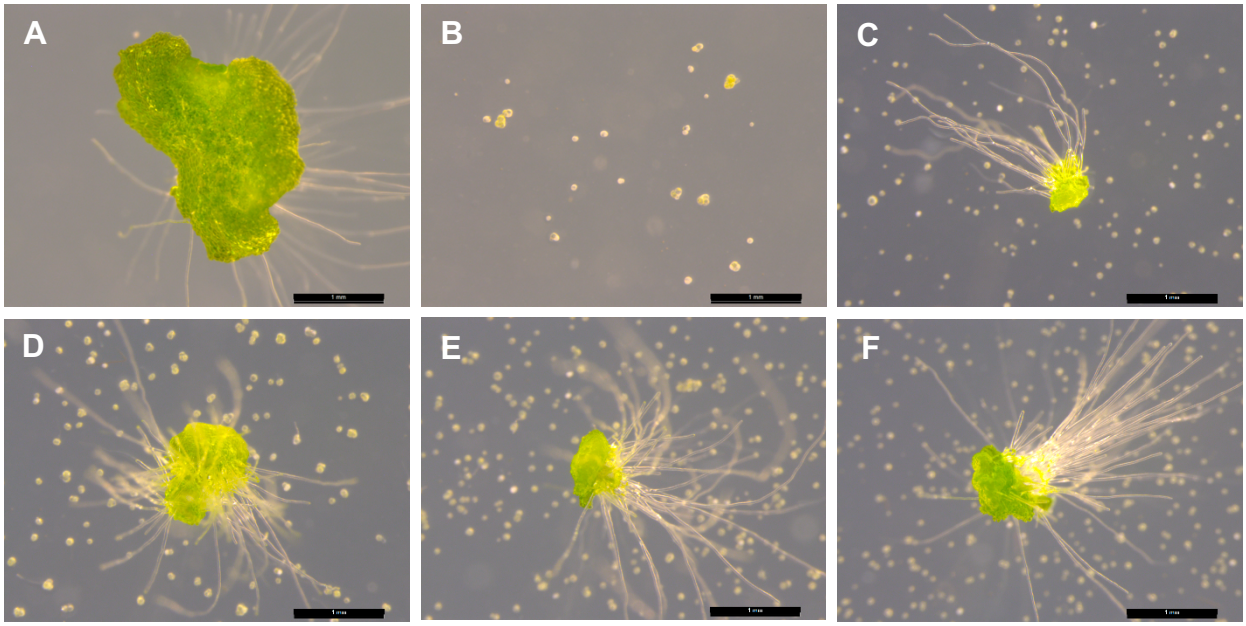

Fig. 3.4. Five chlorsulfuron-resistant were generated via UV-B mutagenesis
(A-B) Wild-type sporelings grown for 14 days on **(A)** solid Johnson's medium **(B)** solid Johnson's medium supplemented with 140 nM chlorsulfuron
(C-F) Original UV-B mutagenesis selection plates showing chlorsulfuron-resistant mutants **(C)** Mp*chlr*1, **(D)** Mp*chlr*2, **(E)** Mp*chlr*3, **(F)** Mp*chlr*4, surrounded by dead mutagenized spores which did not acquire a mutation conferring chlorsulfuron resistance. Chlorsulfuron-resistant mutants were generated by plating wild-type spores onto solid Johnson's medium supplemented with 140 nM chlorsulfuron and exposing them to UV-B radiation at 302 nm. Individuals which displayed resistance 14 days after UV-B irradiation were identified and imaged. Images were taken with a Leica DFC310 FX stereomicroscope. Scale bars represent 1 mm.

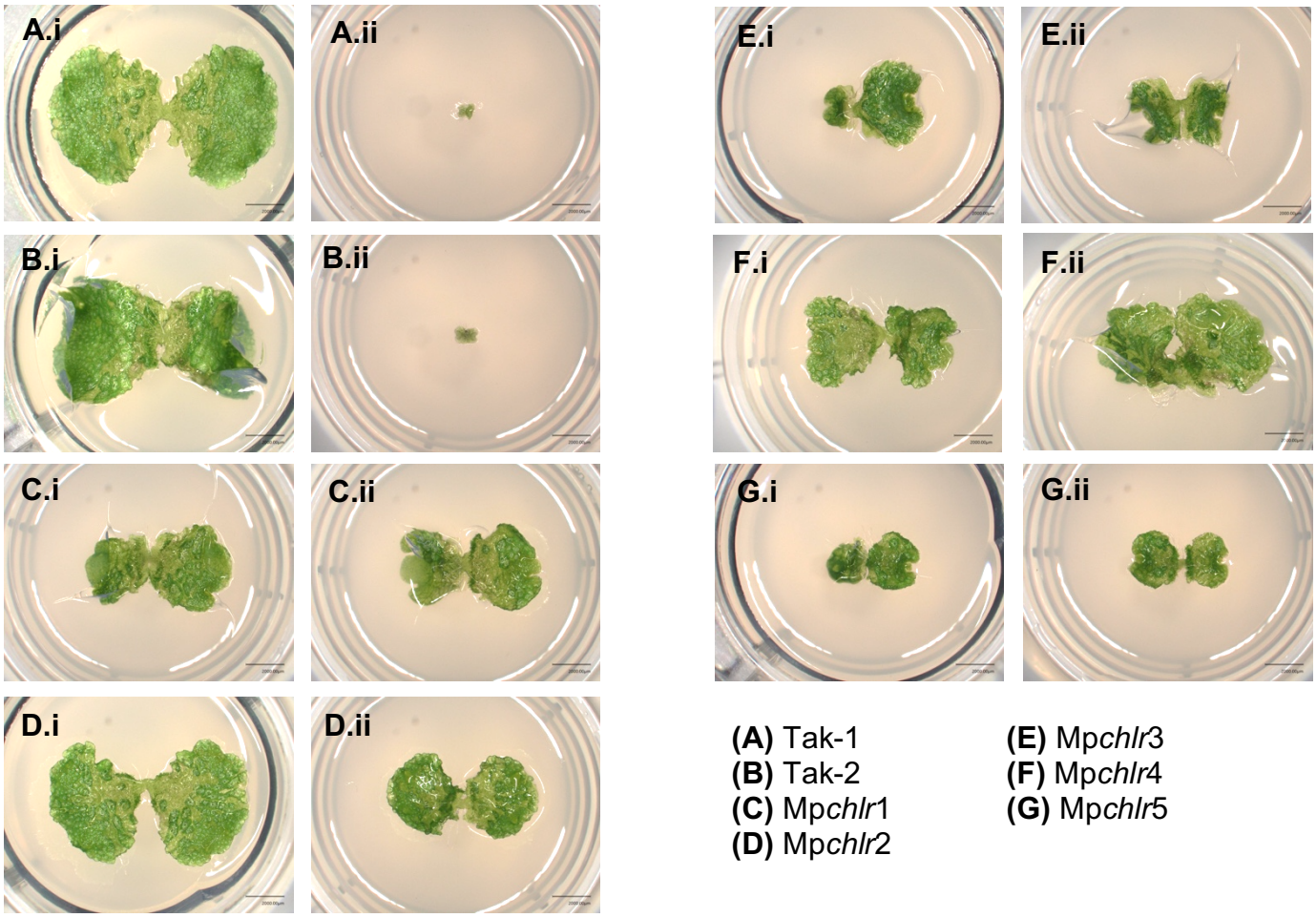

Fig. 3.5. Mp*chlr* mutants have heritable resistance to chlorsulfuron. *M. polymorpha* chlorsulfuron-resistant mutants were generated by UV-B mutagenesis. Images of gemmae grown for 10 days on **(i)** DMSO or **(ii)** 33 nM chlorsulfuron (LD_{100}) were taken with a Keyence VHX-7000. Scale bars represent 2 mm **(A-G)**.

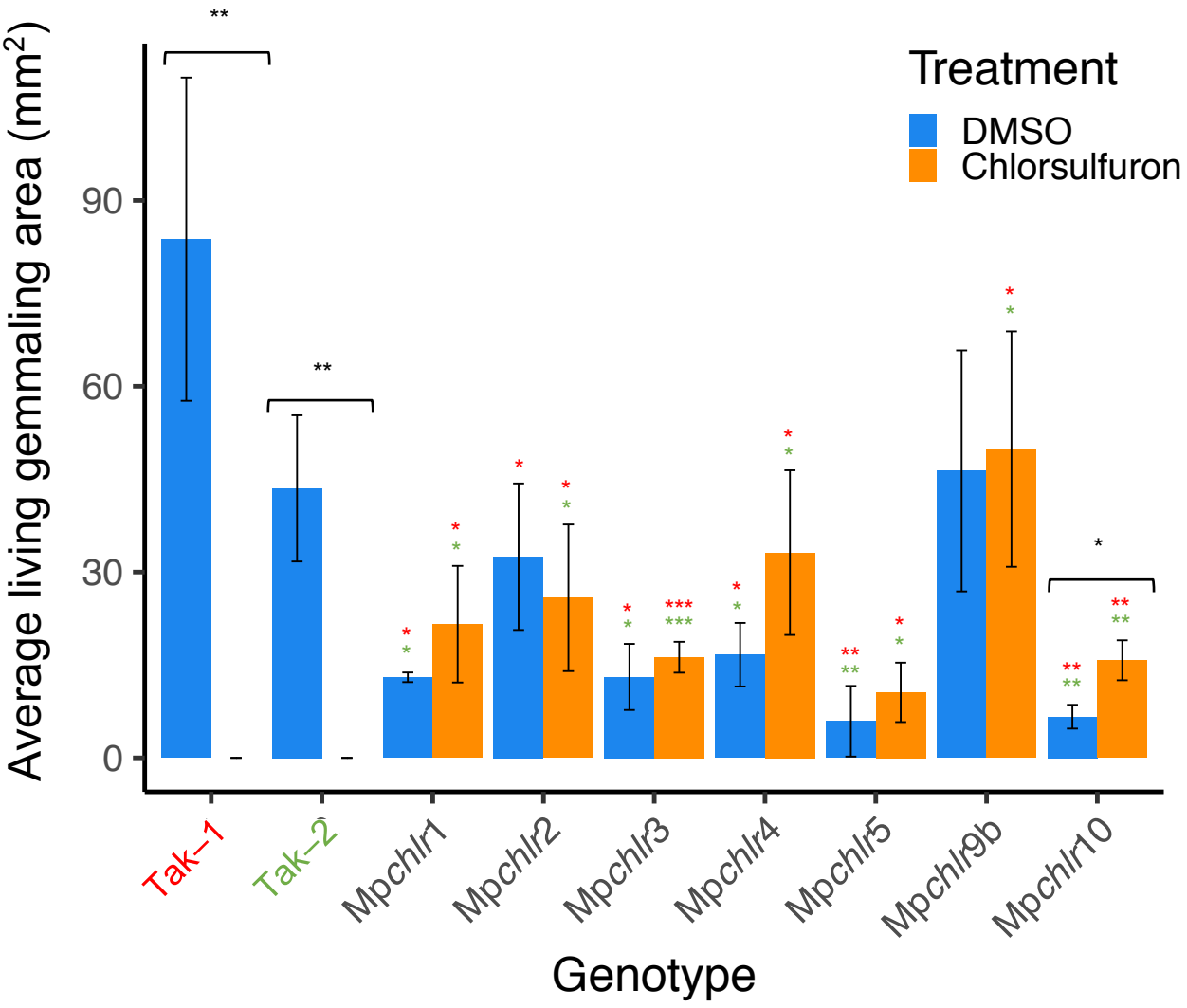

Fig. 3.6. Chlorsulfuron-resistant lines (Mp*chlr*) survive and do not show growth inhibition on a lethal dose of chlorsulfuron

M. polymorpha chlorsulfuron-resistant mutants were generated via UV-B mutagenesis (Mp*chlr*1, Mp*chlr*2, Mp*chlr*3, Mp*chlr*4, Mp*chlr*5) or previously in the lab by EMS mutagenesis (Mp*chlr*9b, Mp*chlr*10). Gemmae from these lines and from the *M. polymorpha* male and female control lines (Tak-1 and Tak-2 respectively) were plated onto solid ½ Gamborg medium supplemented with DMSO or 33 nM chlorsulfuron (LD_{100}) and grown for 12 days (n = 3). Gemmalings were imaged using a Berthold Nightowl II LB 983 *In Vivo* Imaging System. The lateral area of autofluorescing (living) tissue was determined using the indiGo™ software package and plotted using the ggplot2 package in R. Since only living tissue was measured, for dead gemmalings the gemmaling area is quantified as zero although the actual area is greater than zero. Error bars represent ± standard deviation. Stars represent the level of significance (as determined by Student's t-tests) of the difference between mutant and control lines subjected to the same treatment (comparison to Tak-1 in red and Tak-2 in green), or between individuals of the same genotype subjected to different treatments (black): * = $p < 0.05$, ** = $p < 0.01$, *** = $p < 0.001$.

3.4.4. Chlorsulfuron-resistant (Mp*chlr*) mutants are target site resistant

Herbicide resistant plants can exhibit target site resistance (TSR) or non-target site resistance (NTSR). TSR is a monogenic trait whereby a single mutation confers high levels of resistance, whereas NTSR is usually a polygenic trait where multiple alleles each conferring low levels of resistance stack to provide high levels of resistance (Delye, 2013). Screening for herbicide resistance at high doses preferentially selects for TSR, whereas screening at low doses preferentially selects for NTSR (Gardner *et al.*, 1998). I screened at a high dose of 140 nM chlorsulfuron (4 x LD_{100}) to generate the 5 chlorsulfuron-resistant (Mp*chlr*) mutants. I therefore expect that the basis of chlorsulfuron resistance in Mp*chlr* mutants is TSR.

To test if Mp*chlr* mutants are TSR, I sequenced the gene encoding the chlorsulfuron target site AHAS (acetohydroxyacid synthase) in each mutant. Chlorsulfuron TSR mutants carry a mutation in the AHAS gene which prevents the herbicide from binding the enzyme; various mutations which confer TSR to chlorsulfuron have been characterised (Jander *et al.*, 2003). I sequenced the regions in the AHAS gene (Mp7g01940.1) of Mp*chlr* mutants which are most likely to contain a TSR-conferring mutation using Sanger sequencing. All 5 Mp*chlr* mutants had mutations in their AHAS gene (Fig. 3.7). Mp*chlr2*, Mp*chlr3*, Mp*chlr4* and Mp*chlr5* had a mutation causing a Pro197Ser or Pro197Leu amino acid change which have been observed to confer chlorsulfuron resistance in plants (Kaloumenos *et al.*, 2012). Mp*chlr1* had an Asp376Asn mutation which has been observed to confer chlorsulfuron resistance in yeast but has not yet been observed in plants (Duggleby *et al.*, 2003). Mp*chlr*4 and Mp*chlr*5 had the same SNP in their AHAS gene (Fig. 3.7); this suggests that the screen was carried out to saturation as two identical alleles were recovered in

different mutants from the same screen. Since 2 x 10^6 mutagenized spores were screened, this value represents the minimum number of spores which should be screened using this protocol to reach saturation.

These findings demonstrate that the UV-B mutagenesis protocol can generate target site resistant mutants, and that a screening population of 2 x 10^6 spores is sufficient to carry out a screen to saturation at this dose of UV-B radiation.

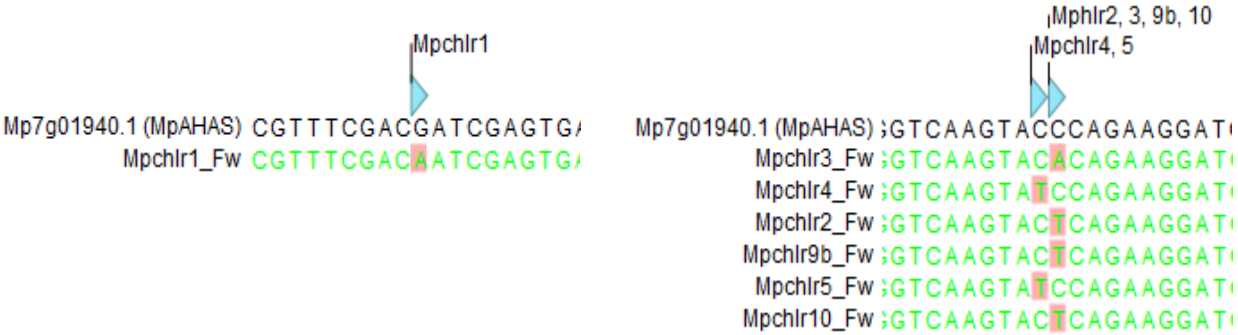

Fig. 3.7. Sanger sequencing of Mp*chlr* mutants. Regions of the AHAS gene (Mp7g01940.1) in each Mp*chlr* mutant were sequenced to identify any target-site resistance conferring mutations. The consensus sequence is shown on the top row, and results from the Sanger sequencing are shown on the subsequent rows. Mp*chlr*1, 2, 3, 4, and 5 were generated by UV-B mutagenesis in the current project; Mp*chlr*9b and Mp*chlr*10 were generated by EMS mutagenesis in a previous project.

3.4.5. Thirteen thaxtomin A-resistant mutants were generated by UV-B mutagenesis

I generated 5 TSR chlorsulfuron-resistant mutants using UV-B mutagenesis, demonstrating that this protocol can be used to produce herbicide resistant mutants. To generate herbicide resistant mutants with novel resistance mechanisms, I used the same protocol to screen mutagenized spores for resistance to the herbicides thaxtomin A (TXTA), dichlobenil, amitrole, pyributicarb, and aclonifen (Table 3.2).

No resistance has been observed in the field to TXTA, dichlobenil, aclonifen, or pyributicarb (Heap, 2022); I chose to screen for resistance to these herbicides to identify novel mechanisms of resistance. Several cases of resistance to amitrole have been reported in a variety of weed species, including in populations of *Lolium perenne* which are cross-resistant to glufosinate and glyphosate, however the molecular mechanisms underlying amitrole resistance have not been identified (Ghanizadeh *et al.*, 2015, Ghanizadeh and Harrington, 2021). I chose to screen for resistance to amitrole to identify molecular mechanisms which might underly the resistance observed in the field.

I screened 1 x 10^7 mutagenised spores for resistance to TXTA at the LD_{100} (5 µM) to preferentially select for NTSR (Table 3.2). I generated 13 TXTA-resistant lines which I named Mp*tar* (*t*haxtomin *A r*esistant) (Fig. 3.8, Fig. 3.9).

I screened for resistance to dichlobenil and amitrole at or near LD_{100} to preferentially select for NTSR mutants (Table 3.2) but was unable to generate resistant mutants.

I also screened for resistance to TXTA, dichlobenil, pyributicarb, and aclonifen at high doses (≥ 3 x LD_{100}) to preferentially select for TSR mutants (Table 3.2) but I was unable to generate resistant mutants to any of these herbicides at high doses.

The inability to produce herbicide resistant mutants to dichlobenil, pyributicarb, or aclonifen may be because there are no UV-B inducible mutations (C→T) which can confer resistance to these herbicides. I therefore used sodium azide mutagenesis – which can produce a variety of different mutations which differ from those generated with UV-B mutagenesis – to generate resistant mutants to the herbicide dichlobenil. However, I was unable to generate dichlobenil-resistant mutants from a screen of 5 x 10^5 spores mutagenized with sodium azide. I therefore carried on my analysis only with the lines I generated with resistance to TXTA (Mp*tar*).

To quantify the growth of Mp*tar* lines on TXTA, I grew Mp*tar* lines on a lethal dose of TXTA (5 µM) and measured the lateral area of living gemmaling tissue after 21 days of growth (Fig. 3.10). Since only living tissue was measured, for dead gemmalings the gemmaling area is quantified as zero although the actual area is greater than zero (Fig. 3.9 B.ii) On TXTA, all Mp*tar* mutants were significantly larger than wild-type plants ($p < 0.05$) (Fig. 3.10). In control conditions however, all Mp*tar* lines except Mptar12 and Mp*tar*13 were significantly smaller than the wild-type lines Tak-1 and Tak-2 ($p < 0.05$) (Fig. 3.10).

All Mp*tar* mutants were smaller on TXTA than in untreated conditions (Fig. 3.9, Fig. 3.10). This suggests that they are weakly resistant to TXTA, which is consistent with the hypothesis that the basis of their TXTA resistance is non-target site resistance (NTSR).

Herbicide	Screening dose (multiple of LD_{100})	Number of spores screened	Number of resistant mutants generated
Chlorsulfuron	4	2×10^6	5
TXTA	1	1×10^7	13
TXTA	9	1×10^6	0
Dichlobenil	0.3	1.5×10^5	0
Dichlobenil	1	9×10^6	0
Dichlobenil	3	1.2×10^6	0
Amitrole	1	3×10^6	0
Pyributicarb	3	3×10^6	0
Aclonifen	10	3×10^6	0

Table 3.2. Details of UV-B mutagenesis screens for each herbicide. Details include screening dose (as a multiple of the lethal dose LD_{100} for each herbicide), number of spores screened (considering lethality of UV-B radiation), and number of resistant mutants generated. For full details see Supplementary Table S3.1.

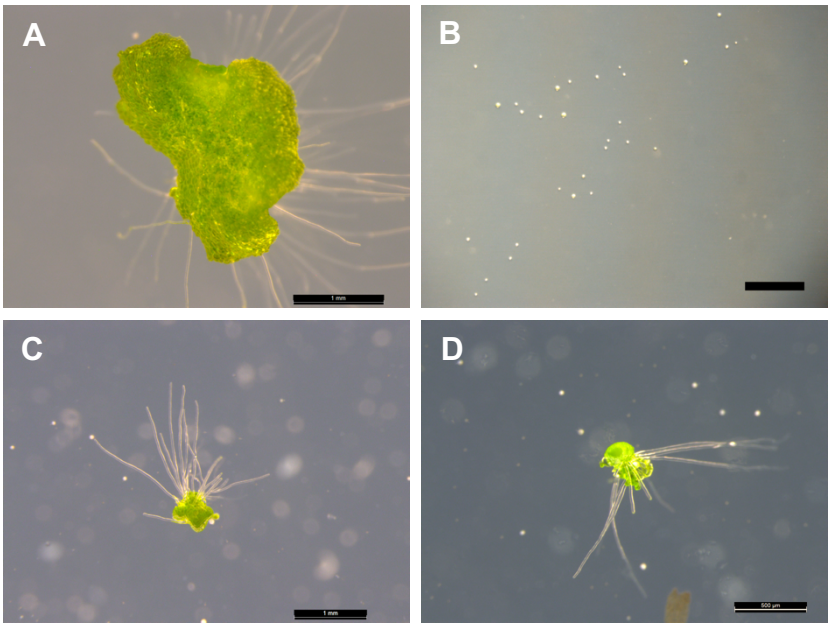

Fig. 3.8. Thirteen TXTA-resistant mutants were generated via UV-B mutagenesis
(A-B) Wild-type sporelings grown for 14 days on **(A)** solid Johnson's medium **(B)** solid Johnson's medium supplemented with 5 µM TXTA
(C-D) Original UV-B mutagenesis selection plates showing TXTA-resistant mutants **(C)** Mp*tar*1 and **(D)** Mp*tar*2 surrounded by dead mutagenized spores which did not acquire a mutation conferring TXTA resistance
TXTA-resistant mutants were generated by plating wild-type spores onto solid Johnson's medium supplemented with 5 µM TXTA and exposing them to UV-B radiation at 302 nm. Individuals which displayed resistance 14 days after UV-B irradiation were identified and imaged. Images were taken with a Leica DFC310 FX stereomicroscope. Scale bars represent 1 mm.

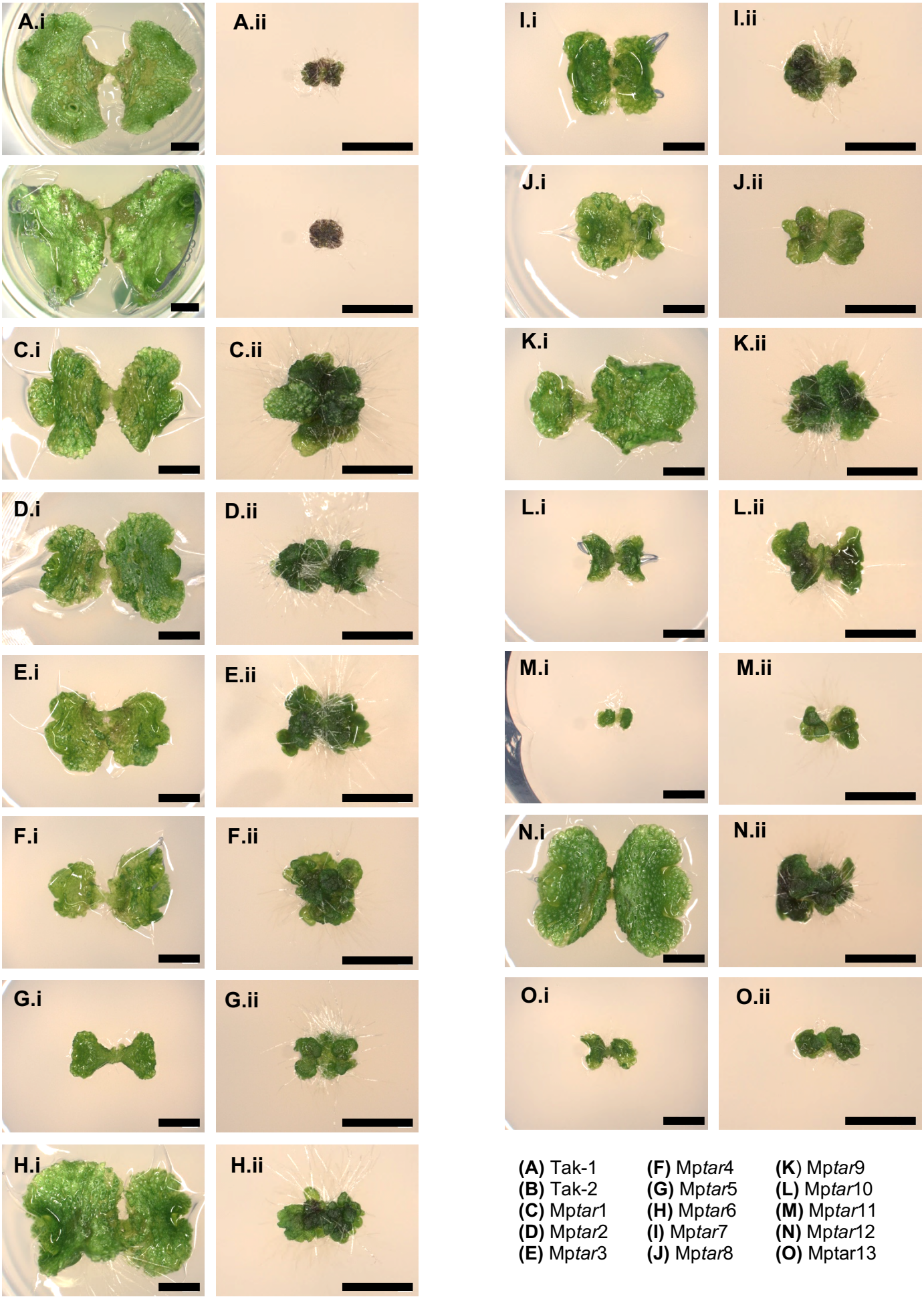

Fig. 3.9. Mp*tar* lines have heritable resistance to TXTA *M. polymorpha* TXTA-resistant lines were generated by UV-B mutagenesis. Images of gemmae grown for 14 days on **(i)** DMSO or **(ii)** 5 µM TXTA were taken with a Keyence VHX-7000. Scale bars represent 2 mm.

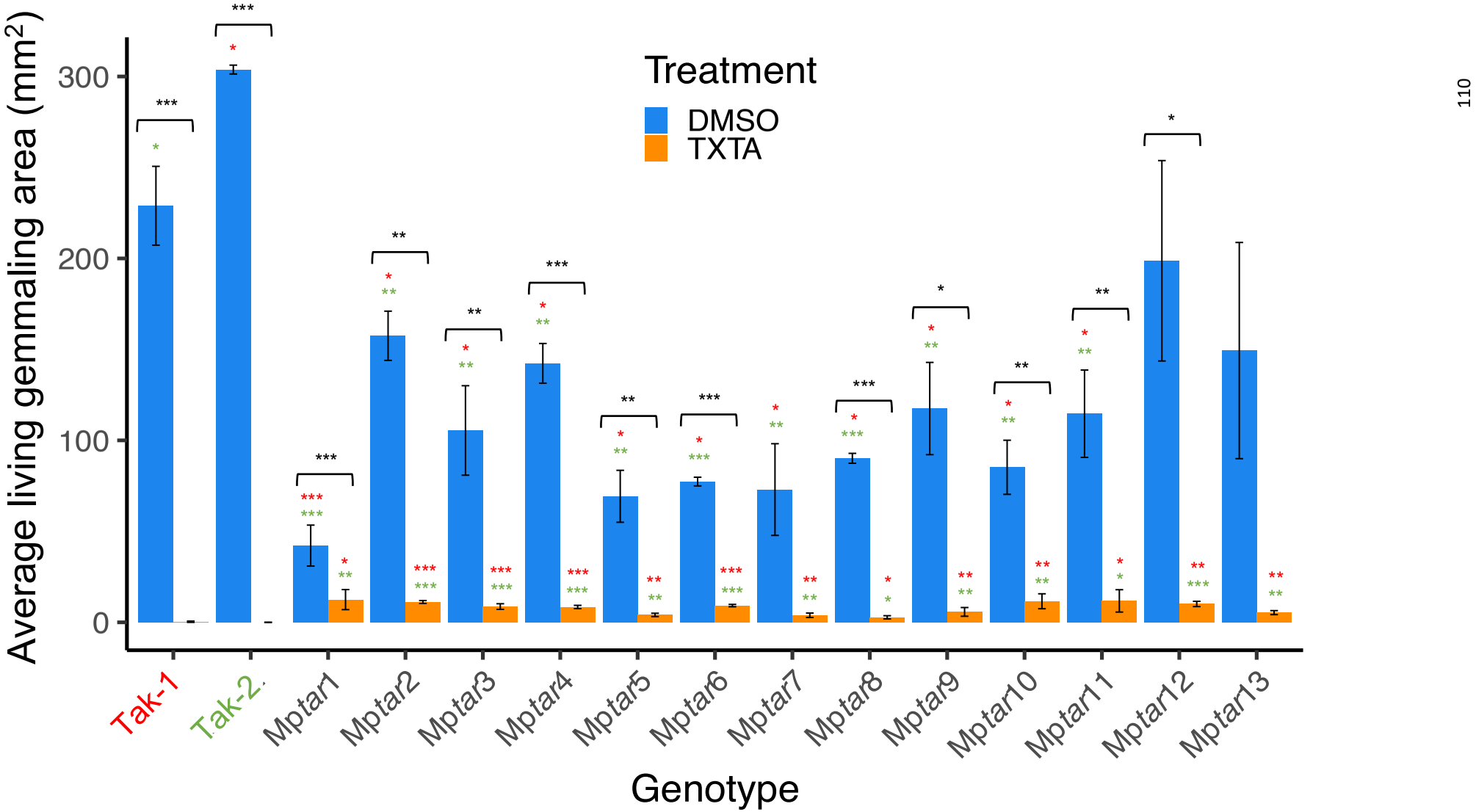

Fig. 3.10. TXTA-resistant lines (Mp*tar*) survive and show growth inhibition on a lethal dose of TXTA
M. polymorpha TXTA-resistant mutants were generated via UV-B mutagenesis. Gemmae from these lines and from wild-type lines (Tak-1 and Tak-2 respectively) were plated on solid Johnson's medium supplemented with DMSO or 5 µM TXTA and grown for 21 days (n=3-13). Gemmalings were imaged using a Berthold Nightowl II LB 983 *In Vivo* Imaging System. The lateral area of autofluorescing (living) tissue was determined using the indiGo™ software package and plotted using the ggplot2 package in R. Since only living tissue was measured, for dead gemmalings the gemmaling area is quantified as zero although the actual area is greater than zero. Error bars represent ± standard deviation. Stars represent the level of significance (as determined by Student's t-tests) of the difference between mutant and control lines subjected to the same treatment (comparison to Tak-1 in red and Tak-2 in green), or between individuals of the same genotype subjected to different treatments (black): * = $p < 0.05$, ** = $p < 0.01$, *** = $p < 0.001$.

3.4.6. TXTA-resistant mutants are likely to be non-target site resistant

Screening for herbicide resistance at high doses preferentially selects for TSR, whereas screening at low doses preferentially selects for NTSR (Gardner *et al.*, 1998). I screened at the lethal dose of TXTA to generate the 13 TXTA-resistant (Mp*tar*) mutants. I therefore expect that the basis of TXTA resistance in Mp*tar* mutants is NTSR. However, it is still possible that some of the Mp*tar* mutants are TSR: I was unable to use Sanger sequencing of the gene encoding the target of TXTA to identify potential TSR as TXTA is a herbicide with an unknown molecular target. To identify novel mechanisms of NTSR, I undertook a phenotypic analysis of Mp*tar* mutants to distinguish between TSR and NTSR.

NTSR is more likely to give rise to weaker resistance than TSR (Gardner *et al.*, 1998, Delye, 2013). I therefore hypothesised that if Mp*tar* lines are weakly resistant to TXTA, their resistance is more likely to be NTSR. Conversely, since the chlorsulfuron-resistant (Mp*chlr* lines) I generated were all TSR (Fig. 3.7), I hypothesised that these are strongly resistant to chlorsulfuron. No Mp*chlr* lines were smaller on chlorsulfuron than in untreated conditions (Fig. 3.6) whereas all Mp*tar* lines were smaller on TXTA than in untreated conditions (Fig. 3.10). Mp*chlr* mutants were therefore strongly resistant to chlorsulfuron, whereas Mp*tar* mutants were weakly resistant to TXTA. This observation suggests that the TSR-conferring mutations in Mp*chlr* mutants provide a high level of resistance, whereas the lower resistance observed in Mp*tar* mutants may be conferred by NTSR.

3.4.7. Eight out of 13 Mp*tar* mutants display herbicide cross-resistance

Mp*tar* mutants are weakly resistant to TXTA, suggesting that they are NTSR mutants to TXTA. However, weak resistance in Mp*tar* mutants could be due to TSR whereby a mutation in the target site hinders herbicide binding but does not prevent it completely, so the mutants survive on the herbicide but are still affected by it to some extent. TXTA is thought to be a cellulose biosynthesis inhibitor; TSR mutants to the cellulose biosynthesis inhibitors isoxaben and flupoxam are also smaller in treated than in untreated conditions (Shim *et al.*, 2018), so the growth inhibition of Mp*tar* mutants on TXTA is not completely inconsistent with TSR.

To further distinguish between TSR and NTSR in Mp*tar* mutants, I tested the herbicide cross-resistance of Mp*tar* mutants. TSR confers resistance to only the herbicide with that particular target whereas single alleles of NTSR can sometimes result in cross-resistance to several herbicides (Gaines *et al.*, 2020). Observation of cross-resistance in Mp*tar* mutants would therefore suggest that a mechanism of NTSR is responsible for herbicide resistance.

I first tested the cross-resistance of Mp*chlr* mutants to TXTA to confirm that TSR mutants do not display cross-resistance. No Mp*chlr* lines displayed a significantly higher TXTA resistance than Tak-1 (the more TXTA-resistant wild-type line). These findings confirm that TSR does not confer cross-resistance (Fig. 3.11).

I then tested the cross-resistance of Mp*tar* mutants to four herbicides with different molecular targets: isoxaben, dichlobenil, chlorsulfuron, and 2,4-D. TXTA and isoxaben are classed as group I cellulose biosynthesis inhibitors but have different molecular targets as TSR mutants to isoxaben are not cross-resistant to TXTA (Tegg *et al.*, 2013). Dichlobenil is a group II cellulose biosynthesis inhibitor, chlorsulfuron is

an AHAS inhibitor, and 2,4-D is an auxin mimic. Eight out of 13 Mp*tar* mutants were significantly cross-resistant to isoxaben or chlorsulfuron compared to both wild-type lines. Mp*tar*2, Mp*tar*3, Mp*tar*4, Mp*tar*5, Mp*tar*6, Mp*tar*8 and Mp*tar*13 were cross-resistant to isoxaben, and Mp*tar*6 and Mp*tar*10 were cross-resistant to chlorsulfuron (Fig. 3.12). These 8 cross-resistant mutants are therefore unlikely to display TSR to TXTA and are good candidates for studying novel mechanisms of NTSR.

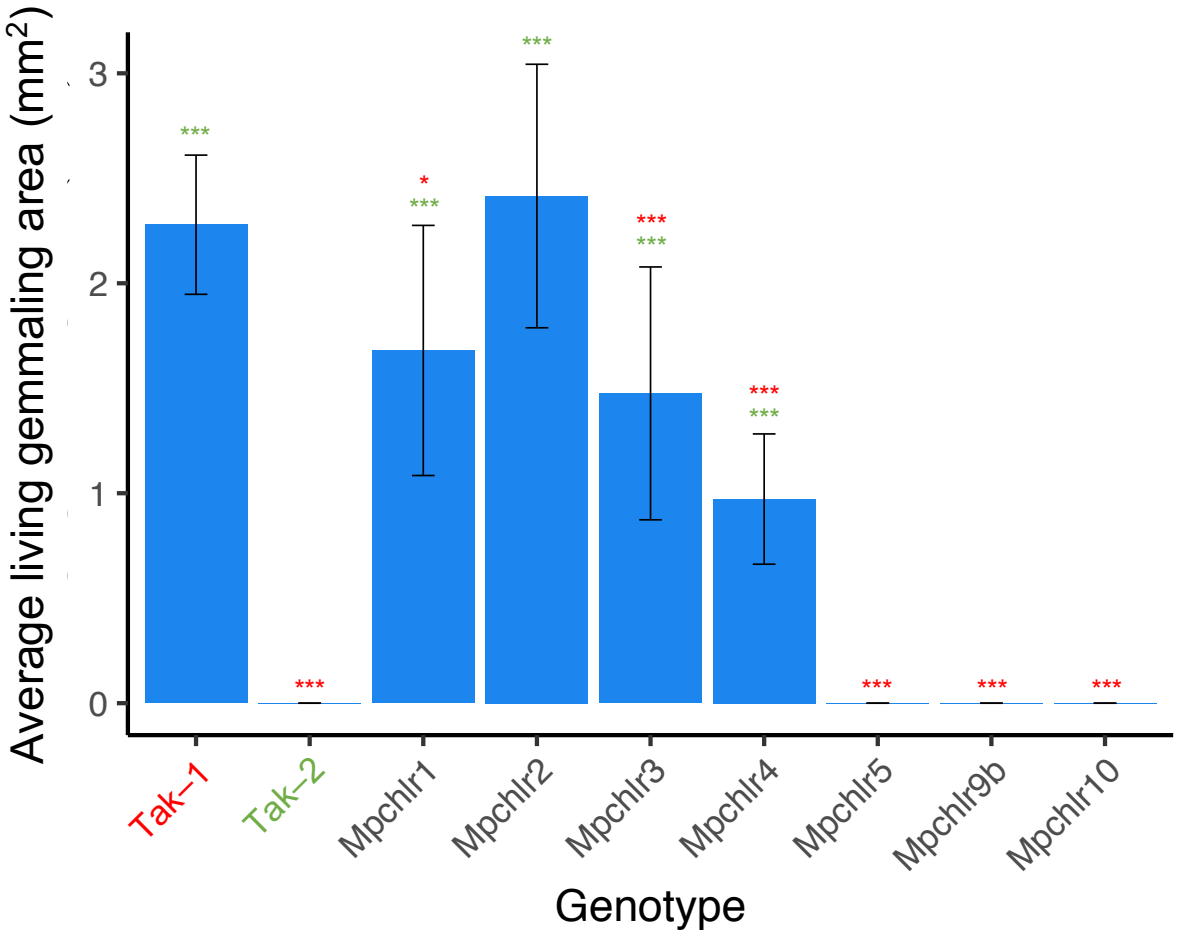

Fig. 3.11. CS-resistant lines (Mp*chlr*) are not significantly resistant to TXTA
M. polymorpha CS-resistant mutants were generated UV-B mutagenesis (Mp*chlr*1, Mp*chlr*2, Mp*chlr*3, Mp*chlr*4, Mp*chlr*5) or EMS mutagenesis (Mp*chlr*9b, Mp*chlr*10). Gemmae from these lines were plated onto solid Johnson's medium supplemented with 5 µM TXTA and grown for 21 days (n=9). Gemmalings were imaged using a Berthold Nightowl II LB 983 *In Vivo* Imaging System. The lateral area of autofluorescing (living) tissue was determined using the indiGo™ software package and plotted using the ggplot2 package in R. Since only living tissue was measured, for dead gemmalings the gemmaling area is quantified as zero although the actual area is greater than zero. Error bars represent ± standard deviation. Stars represent the level of significance of the difference between mutant and control lines (Tak-1 in red and Tak-2 in green) as determined by Student's t-tests: * = $p < 0.05$, ** = $p < 0.01$, *** = $p < 0.001$.

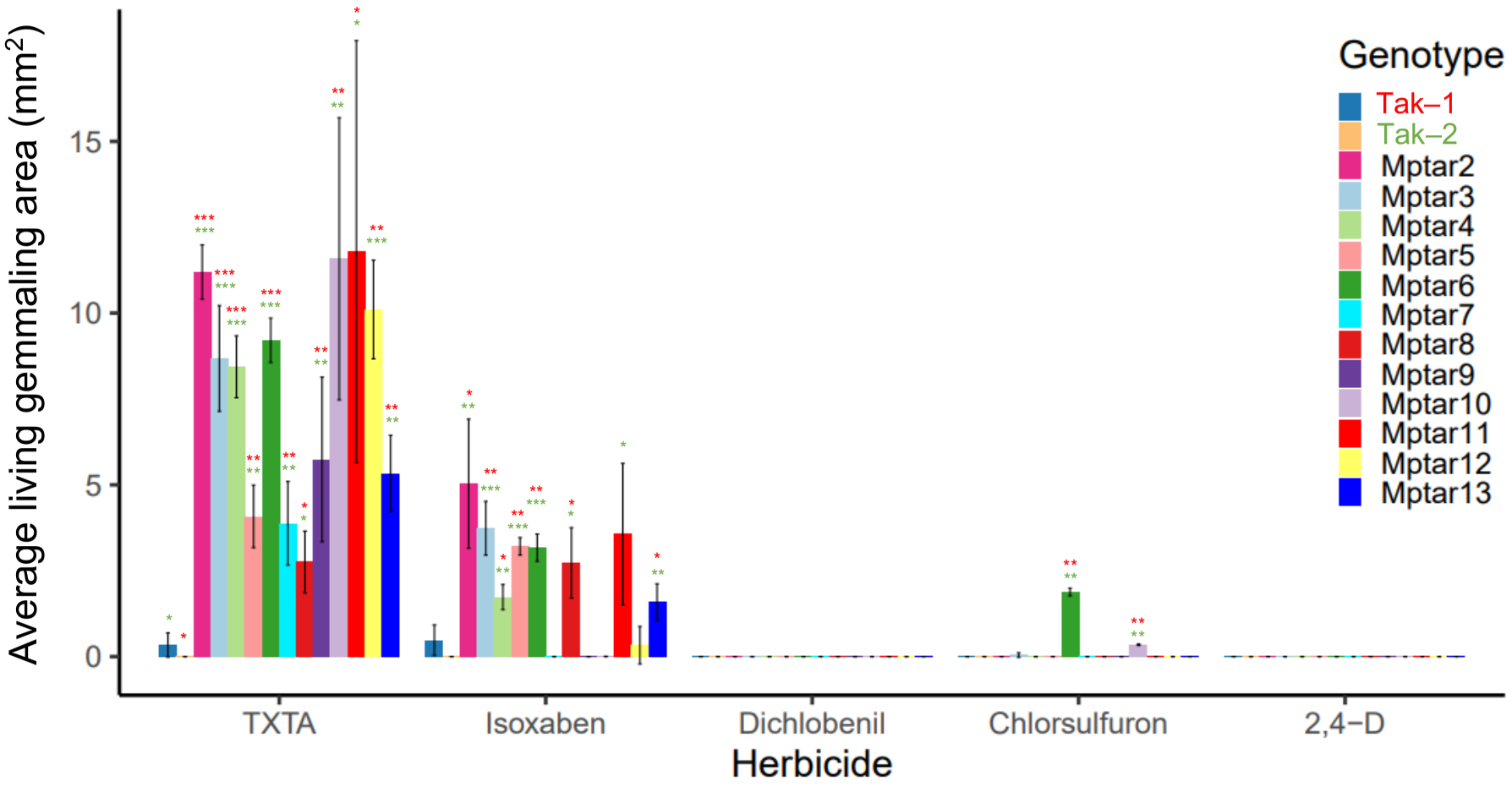

Fig. 3.12. 8 Mp*tar* lines display herbicide cross-resistance
13 *M. polymorpha* TXTA-resistant mutants (Mp*tar*) were generated via UV-B mutagenesis. Gemmae from these lines were plated onto solid Johnson's medium supplemented with lethal doses of five herbicides and grown for 21 days n (n=2-3). Gemmalings were imaged using a Berthold Nightowl II LB 983 *In Vivo* Imaging System. The lateral area of autofluorescing (living) tissue was determined using the indiGo™ software package and plotted using the ggplot2 package in R. Since only living tissue was measured, for dead gemmalings the gemmaling area is quantified as zero although the actual area is greater than zero. Error bars represent ± standard deviation. Stars represent the level of significance of the difference between mutant and control lines grown on a given herbicide (Tak-1 in red and Tak-2 in green) as determined by Student's t-tests: * = $p < 0.05$, ** = $p < 0.01$, *** = $p < 0.001$.

3.5. Discussion

In this chapter I undertook a forward genetic screen from which I generated 5 mutants resistant to chlorsulfuron (Mp*chlr*), demonstrating that it is possible to generate herbicide-resistant mutants using UV-B mutagenesis in *M. polymorpha*. I then undertook a large-scale forward genetics screen and generated 13 mutants resistant to thaxtomin A (Mp*tar*). Mp*chlr* mutants are target site resistant (TSR) to chlorsulfuron as they all have a mutation in the gene encoding the chlorsulfuron target site (Mp*AHAS*). Mp*tar* mutants are more likely to exhibit non-target site resistance (NTSR) because they were screened for resistance at the lethal dose of TXTA, they grew smaller on TXTA than in untreated conditions, and 8 out of 13 Mp*tar* lines were cross-resistant to other herbicides.

I isolated five chlorsulfuron-resistant (Mp*chlr)* mutants by screening 2 x 10^6 UV-B mutagenized spores at 4 times the lethal dose of chlorsulfuron. I used Sanger sequencing to show that all Mp*chlr* mutants carry mutations in the target-site of chlorsulfuron AHAS. Mp*chlr*4 and Mp*chlr*5 had the same SNP in their AHAS gene; this suggests that the screen was carried out to saturation as two identical alleles were identified in different mutants from the same screen, so screening at least 2 x 10^6 mutagenised spores is sufficient for saturation screening in *M. polymorpha*. Four Mp*chlr* mutants carry the Pro197Ser mutation which is found in chlorsulfuron-resistant weeds, and one carries an Asp376Asn mutation; this is the first documented case of Asp376Asn conferring chlorsulfuron resistance in plants – as of now it has only been identified in yeast (Duggleby *et al.*, 2003). I have therefore shown that this herbicide resistance mechanism is conserved across eukaryotes, and identified a mechanism of resistance which could arise (or be present but not yet

identified) in weeds. Identifying potential resistance mechanisms that have not yet been reported is important to help the identification and management of resistant weeds, as successful weed management strategies rely on knowledge of the genetic basis of resistance to assess how a resistant weed will respond to different herbicide modes of action or doses (Delye, 2013).

I screened a population of 1 x 10^7 UV-B mutagenized spores for resistance to the herbicide thaxtomin A (TXTA) at the lethal dose (LD_{100}). In this case, I expected to isolate mostly NTSR mutants, as single NTSR alleles are more likely to confer weaker herbicide resistance allowing plants to survive at the LD_{100} but not at higher doses (Gardner *et al.*, 1998). I identified 13 TXTA-resistant mutants (Mp*tar* lines).

I also screened at the LD_{100} for resistance to the herbicides dichlobenil and amitrole however was unable to generate resistant mutants. In the case of dichlobenil, this is consistent with previous unsuccessful efforts to screen for resistance (Tateno *et al.*, 2016). Since I screened more than 2 x 10^6 spores for resistance to each herbicide (Supplementary Table S3.1), I would expect these screens to be saturated and therefore to have identified any resistance mechanisms. Resistance to amitrole has been reported in multiple weed species (Ghanizadeh *et al.*, 2015, Heap, 2022), so I expected to isolate amitrole-resistant mutants from a mutagenesis screen carried out to saturation. However, most of the spores used to screen for amitrole resistance were frozen due to variability in the supply of fresh spores (Supplementary Table S3.1); frozen spores have lower germination rates than fresh spores, so the actual number of spores screened for amitrole may be lower than recorded and could drop below the limit for saturation mutagenesis. This may explain the lack of amitrole resistant mutants.

I also screened UV-B mutagenised spores for resistance to ≥ 3 x LD_{100} of TXTA, dichlobenil, pyributicarb, or aclonifen but isolated no herbicide-resistant mutants from these screens (Supplementary Table S3.1). Most mutagenized spores screened for pyributicarb resistance were frozen hence the numbers of spores screened may be overestimated, so it is possible that not enough mutants were screened to identify resistance to pyributicarb. However, the number of mutants screened is not likely to be the reason for the lack of mutants isolated for dichlobenil or aclonifen, as greater than 2 x 10^6 mutagenised spores were screened for resistance to these suggesting the screens reached saturation. I expected to isolate mainly TSR mutants screening at ≥ 3 x LD_{100} as TSR is more likely to confer higher resistance than single alleles of NTSR (Gardner *et al.*, 1998). TSR is usually associated with a fitness cost due to the mutation having a detrimental effect on the wild-type function of the enzyme (Vila-Aiub *et al.*, 2009): it is therefore possible that any mutation which affects the target protein of dichlobenil or aclonifen is lethal, preventing the isolation of TSR mutants from these screening conditions. This limitation does not apply to the generation of chlorsulfuron TSR mutants, as the most common mutations which confer TSR to chlorsulfuron do not affect the function of the AHAS protein, so there is no fitness cost associated with the resistance (Yu and Powles, 2014). It is also possible that no UV-B induced mutation (C → T) in the gene encoding the target site of these herbicides exists that can confer TSR. Furthermore, in the case of aclonifen, its molecular target has been identified as solanesyl diphosphate synthase, however it has structural similarities to known protoporphyrinogen oxidase inhibitors (Kahlau *et al.*, 2020); it is therefore possible that aclonifen has two target sites, which would make it difficult to obtain TSR mutants to aclonifen which would require mutations conferring resistance to both targets.

Thirteen TXTA-resistant (Mp*tar*) lines were isolated by screening for survival on the lethal dose of TXTA. These lines grew significantly larger than Tak-1 or Tak-2 on a lethal dose of TXTA ($p < 0.05$). It is likely that Mp*tar* lines are resistant to TXTA due to NTSR. NTSR usually confers weaker resistance than TSR; all Mp*tar* lines are weakly resistant to TXTA, growing smaller on a lethal dose of TXTA than on DMSO. Furthermore, NTSR can confer cross-resistance to herbicides with different modes of action whereas TSR cannot; 8 out of the 13 Mp*tar* lines show cross-resistance to herbicides with different modes of action. These data suggest that Mp*tar* lines are resistant due to mechanisms of NTSR. Identifying the basis of resistance in Mp*tar* lines could lead to the discovery of novel mechanisms of NTSR.

Seven out of 13 Mp*tar* mutants (Mp*tar*2, Mp*tar*3, Mp*tar*4, Mp*tar*5, Mp*tar*6, Mp*tar*8 and Mp*tar*13) were resistant to the cellulose biosynthesis inhibitor isoxaben, but none of were resistant to the cellulose biosynthesis inhibitor dichlobenil. Although the target site of TXTA is unknown, it has been classed as a cellulose biosynthesis inhibitor due to the phenotypes of TXTA-treated plants including cell swelling, incomplete cell plate formation during cell division, and inhibition of incorporation of ^{14}C into the cellulose fraction of the cell wall (Fry and Loria, 2002, Scheible *et al.*, 2003). The cellulose biosynthesis inhibitors are subdivided into groups based on their effect on the cellulose synthase enzymes at the plasma membrane (Tateno *et al.*, 2016); TXTA and isoxaben are classed into group I and dichlobenil is classed into group 2. Although classed in the same group, isoxaben and TXTA do not have the same target site; isoxaben targets subunits of the cellulose synthase enzyme, and TSR mutants to isoxaben which have mutations in the genes encoding these subunits are not resistant to TXTA (Tegg *et al.*, 2013). The 7 Mp*tar* lines which are resistant to isoxaben could therefore exhibit NTSR which confers cross-resistance to

group 1 cellulose biosynthesis inhibitors such as isoxaben and TXTA but not to group 2 such as dichlobenil. Two Mp*tar* lines (Mp*tar*6 and Mp*tar*10) were cross-resistant to chlorsulfuron; these may carry NTSR mutations which confer more general resistance to different herbicide modes of action. Three Mp*tar* lines (Mp*tar*1, Mp*tar*7, and Mp*tar*12) were only resistant to TXTA; these could therefore potentially carry TSR mutations, or NTSR mutations which confer resistance only to TXTA or confer cross-resistance to other herbicide modes of action which were not tested.

Eleven of the 13 Mp*tar* lines (all except Mp*tar*12 and Mp*tar*13) grew significantly slower than Tak-1 and Tak-2 in control conditions. The 13 Mp*tar* lines were mostly generated using a UV-B dose corresponding to a kill rate of 50-90 %, whereas the Mp*chlr* lines were generated using a UV-B dose with a kill rate of 20-50 % (Supplementary Table S3.1). Mp*tar* lines are therefore more likely to carry more background mutations than Mp*chlr* lines, which may negatively affect their growth rate and cause them to grow slower in control conditions than wild-type or Mp*chlr* lines. Since TXTA affects only growing tissue (Tegg *et al.*, 2013) it could be possible that TXTA has a weaker effect on slower-growing plants and therefore that the slow growth of the mutants is their mechanism of resistance. However, 5 Mp*chlr* mutants were also smaller than Tak-1 and Tak-2, and none of these were significantly resistant to TXTA. This suggests that not all slow-growing plants are TXTA-resistant, and that the Mp*tar* lines are resistant to TXTA due to mechanisms of resistance other than slow growth.

In conclusion, I have generated 5 TSR mutants to chlorsulfuron (Mp*chlr*), and 13 likely NTSR mutants to TXTA (Mp*tar*). Identifying the basis of resistance in the Mp*tar* mutants could lead to the discovery of novel mechanisms of NTSR.

3.6. Supplementary Data

Herbicide	Screen	Dose (μM)	Multiple of LD_{100}	N. spores mutagenized	UV-B dose (s)	Spore kill rate	N. spores screened	Total n. spores screened	N. mutants
CS	1	0.14	4	1440000	60	0.2	1152000		4
CS	2	0.14	4	1500000	110	0.5	750000	1902000	1
TXTA	0	5	1	320000	60	0.2	256000		1
TXTA	1	5	1	450000	90	0.25	337500		1
TXTA	2	5	1	230000	90	0.25	172500		0
TXTA	3	5	1	300000	90	0.25	225000		0
TXTA	4	5	1	1072000	110	0.5	536000		2
TXTA	5	5	1	1200000	110-150	0.5-0.75	480000		7
TXTA	6	5	1	5000000	110-210	0.5-0.8	1750000		0
TXTA	7	5	1	2600000	130	0.6	1040000		0
TXTA	8	5	1	3000000	110	0.5	1500000		2
TXTA	9	5	1	2200000	130	0.6	880000		0
TXTA	10	5	1	3300000	120	0.55	1485000		0
TXTA	11	5	1	1440000	60	0.2	1152000	9814000	0
TXTA	12	45	9	1827000	60	0.5	913500	913500	0
DCB	1	1	0.3	300000	110	0.5	150000		0
DCB	2	10	3	300000	110	0.5	150000		0
DCB	3	10	3	480000	110	0.5	240000		0
DCB	4	10	3	200000	110	0.5	100000		0
DCB	5	10	3	210000	110	0.5	105000		0
DCB	6	10	3	210000	110	0.5	105000		0
DCB	7	10	3	1081000	110	0.5	540500		0
DCB	8	3.3	1	1666666	110	0.5	833333		0
DCB	9	3.3	1	2500000	110	0.5	1250000		0
DCB	10	3.3	1	500000	110	0.5	250000		0
DCB	11	3.3	1	3000000	130	0.6	1200000		0
DCB	12	3.3	1	4640000	120	0.55	2088000		0
DCB	13	3.3	1	2600000	120	0.55	1170000		0
DCB	14	3.3	1	2950000	90	0.25	2212500	10394333	0
AMI	1	1000	1	900000 (frozen)	35	0.5	450000		0
AMI	2	1000	1	1100000 (frozen)	35	0.5	550000		0
AMI	3	1000	1	500000 (frozen)	45	0.5	250000		0
AMI	4	1000	1	460000	110	0.5	230000		0
AMI	5	1000	1	3100000	110	0.5	1550000	3030000	0
PYRI	1	33	3	900000 (frozen)	35	0.5	450000		0
PYRI	2	33	3	1100000 (frozen)	35	0.5	550000		0
PYRI	3	33	3	500000 (frozen)	45	0.5	250000		0
PYRI	4	33	3	460000	110	0.5	230000		0
PYRI	5	33	3	2700000	110	0.5	1350000	2830000	0
ACL	1	33	10	1650000	110	0.5	825000		0
ACL	2	33	10	1800000	110	0.5	900000		0
ACL	3	33	10	1215000	110	0.5	607500		0
ACL	4	33	10	1400000	110	0.5	700000	3032500	0

Supplementary Table S3.1. Numbers of spores mutagenized and UV doses used for forward genetics screening. Wild type spores (resulting from a cross between Tak-1 and Tak-2) were plated on Johnson's medium supplemented with herbicide and subjected to UV-B irradiation using a UVP BioDoc-It™. The table shows how many spores were mutagenized at what doses during the screening process. The number of spores screened is calculated by considering the spores which will die due to UV-B irradiation based on the graph in Fig. 3. CS; chlorsulfuron. TXTA; thaxtomin A. DCB; dichlobenil. AMI; amitrole. PYRI; pyributicarb. ACL; aclonifen.

Chapter 4: Identification of candidate SNPs conferring resistance to thaxtomin A in *Marchantia polymorpha* mutants

4.1. Abstract

Mechanisms of non-target site herbicide resistance (NTSR) are difficult to identify and as a result very few NTSR-conferring mutations have been characterised. To identify mechanisms of NTSR that will evolve in the field to a new herbicide, thaxtomin A (TXTA), I screened a population of 10^7 UV-B mutagenised *M. polymorpha* spores for TXTA resistance and isolated 13 TXTA-resistant mutants (Mp *thaxtomin A resistant* or Mp*tar*) (Chapter 3). To identify SNPs conferring NTSR in Mp*tar* mutants, I sequenced the genomic DNA from each of these mutants and used a bioinformatic analysis to identify the most likely resistance-conferring SNP in 11 of the 13 Mp*tar* mutant lines. I found 3 mutant lines (Mp*tar*2*,* Mp*tar*4*,* Mp*tar*6*)* with a mutation in Mp*RAD8*. Since three separate lines have a mutation in this gene, loss-of-function of Mp*RAD8* is likely to confer resistance to TXTA. It is hypothesised that Mp*rad8* mutants overproduce reactive oxygen species (ROS) and that this may confer resistance to TXTA; I found candidate resistance-conferring SNPs in four other genes – a peroxidase in Mp*tar*1*,* Mp*PSBP* in Mp*tar*3*,* TIM44L in Mp*tar*7, and Mp*PSAD* in Mp*tar*8 – encoding proteins that may increase cellular ROS levels when defective. I also found 4 candidate resistance-conferring SNPs in genes associated with NTSR in glyphosate-resistant *Amaranthus tuberculatus*. These data demonstrate that herbicide-resistant mutants produced via a forward genetics approach can be used to identify novel potential mechanisms of NTSR.

4.2. Introduction

In the previous chapter, I generated 18 herbicide-resistant mutant *M. polymorpha* lines using UV-B mutagenesis; 5 mutant lines resistant to chlorsulfuron (Mp*chlr*) and 13 mutant lines resistant to TXTA (Mp*tar*). Resistance in Mp*chlr* mutant lines is caused by a mutation in the gene encoding the chlorsulfuron target-site; each has a mutation in the Mp*AHAS* gene, and is resistant to high concentrations of chlorsulfuron (at least 4 x LD_{100}). By contrast, Mp*tar* mutant lines are likely to exhibit non-target site resistance (NTSR) because they are resistant but display growth inhibition at the lethal dose of TXTA, and 8 out of 13 display herbicide cross-resistance. I hypothesise that each Mp*tar* mutant line carries at least one UV-B induced SNP which confers NTSR to TXTA. In this chapter I will identify the resistance-conferring SNP in each Mp*tar* mutant line to discover the molecular basis of NTSR in these lines.

NTSR encompasses any mechanism of herbicide resistance which does not involve the herbicide target, and often results in the modification of the herbicide or its sequestration where it does not have access to its target site. The best characterised mechanisms responsible for herbicide modification are caused by increased activity of metabolising enzymes from 3 gene families – cytochrome P450s, glutathione-S-transferases, and glycosyltransferases (Kreuz *et al.*, 1996, Yuan *et al.*, 2007) – that result from mutation in resistant weeds. Other mechanisms of NTSR include increased sequestration and decreased translocation of the herbicide due to a mutation causing overexpression of ABC transporter encoding genes (Yuan *et al.*, 2007). NTSR can also be conferred by mutations mitigating the action of the herbicide; for example, overexpression of a glutathione peroxidase which reduces

herbicide-induced oxidative injury confers herbicide cross-resistance in *Alopecurus myosuroides* (Cummins *et al.*, 1999). Most mechanisms of NTSR result from overexpression of genes that confer resistance as a result of mutation or genetic rearrangement (Yuan *et al.*, 2007), and there are few examples where loss of gene function confers NTSR. One of these rare examples is the TXTA resistance caused by a loss-of-function mutation in the *PAM16* gene, which I showed to be conserved in *M. polymorpha* (Chapter 2) (Scheible *et al.*, 2003). I used UV-B mutagenesis to generate a population of mutagenised *M. polymorpha* spores which I screened for TXTA-resistant mutants to generate Mp*tar* lines (Chapter 3). UV-B radiation results in SNPs that generally lead to a decrease or complete loss of gene function as opposed to other forms of mutagenesis which can lead to increased gene expression (Jeong *et al.*, 2002, Li *et al.*, 2019). I therefore expect Mp*tar* lines to carry mutations conferring NTSR via loss-of-function; since there are few examples of loss-of-function related NTSR in the literature, there are likely to be novel mechanisms of NTSR present in Mp*tar* lines.

SNP mapping is required to distinguish between resistance-conferring and background mutations in mutant lines, and is generally carried out in bulked segregants. SNP mapping by bulk segregant analysis involves sequencing two samples of bulked genomic DNA of plants from a mapping population; one from plants with the mutant phenotype and one from plants with a wild-type phenotype. The mutant phenotype-causing SNP and closely linked SNPs are identifiable by allele frequencies of 100 % in the mutant sample (Schneeberger *et al.*, 2009). Bulk segregant analysis is facilitated in a dominant haploid model such as *M. polymorpha* as crossing to generate a homozygous line is not required. However, crossing is still required to generate the mapping population, so is impossible to carry out with

mutant lines with defects in sexual reproduction. Our laboratory has developed a protocol to identify causative SNPs in *M. polymorpha* by directly sequencing the mutant genome without crossing. This approach known as “non-allelism based SNP discovery” was successfully employed to locate the SNP in the Mp*NEK* gene responsible for a wavy rhizoid phenotype in a UV-B mutagenized mutant line (Champion *et al.*, 2021).

In this chapter, I used an adapted version of the non-allelism based SNP discovery pipeline to identify candidate resistance-conferring SNPs in 13 independent Mp*tar* mutant lines. I identified 3 Mp*tar* mutant lines with a mutation in Mp*RAD8*, strongly suggesting that a mutation in this gene is responsible for NTSR to TXTA. These mutations are expected to cause overproduction of ROS; I also identified 4 further Mp*tar* lines with candidate resistance-conferring SNPs which are also expected to cause increased cellular ROS levels. In addition, I identified strong candidate resistance-conferring mutations in 4 further Mp*tar* mutant lines by identifying mutations in genes previously associated with NTSR in other species.

4.3. Materials and Methods

4.3.1. Plant lines and growth conditions

Wild-type plants included *M. polymorpha* laboratory accessions Takaragaike-1 (Tak-1; male) and Takaragaike-2 (Tak-2; female) (Ishizaki *et al.*, 2008). Wild-type plants also included OxTak1F and OxTak2M lines generated from four backcrosses of Tak-1 or Tak-2 lines to generate female lines with Tak-1 autosomes (OxTak1F) and male lines with Tak-2 autosomes (OxTak2M). Mp*tar* lines and Mp*chlr*1, Mp*chlr*2, Mp*chlr*3, Mp*chlr*4 and Mp*chlr*5 lines were generated via UV-B mutagenesis. Mp*chlr9b* and Mp*chlr10* lines were previously generated using EMS mutagenesis.

All lines were maintained as described in Chapter 2 Section 2.3.2.

4.3.2. Kit-based genomic DNA extraction

Wild-type (Tak-1, Tak-2, OxTak1F, and OxTak2M) lines and herbicide-resistant lines (Mp*tar* and Mp*chlr*) were grown on solid ½ Gamborg medium for three weeks on in a growth chamber at 23 °C under 24-hour 10-30 µmol m^{-2} s^{-1} white light. After three weeks of growth, plant material was harvested and flash frozen in liquid nitrogen. Samples were ground in liquid nitrogen and genomic DNA was extracted using the Qiagen DNeasy Plant Maxi kit according to the kit protocol. After elution, the gDNA was cleaned up and concentrated using the Zymo Genomic DNA Clean & Concentrator kit. The gDNA was eluted in nuclease-free water.

4.3.3. Genomic DNA Quality control

The concentration of the gDNA was checked using a Nanodrop™ 1000 spectrophotometer and a Qubit® 2.0 fluorometer according to the instruction

manuals. The gDNA quality was checked by running 2 µl DNA (approximately 10 µg μl^{-1}) on a 0.7 % agarose gel at 70 V for 45 minutes and checking for degradation.

4.3.4. Whole-genome sequencing

Genomic DNA samples which had passed quality control checks were sent for sequencing to the Next Generation Sequencing Facility at Vienna BioCenter Core Facilities (VBCF), member of the Vienna BioCenter (VBC), Austria. DNA Libraries were prepared using the Westburg NGS Library Prep kit and fragment size was determined using a BioLabTech Fragment Analyzer™. The DNA was sequenced on an Illumina NovaSeq 6000 SP flowcell using 150 bp paired-end reads.

4.3.5. Non-allelism based SNP discovery

The “non-allelism based SNP discovery” pipeline from (Champion *et al.*, 2021) was used with slight adaptations to identify candidate resistance-conferring SNPs in herbicide-resistant lines. This involves a variant call analysis followed by filtering of mismatches and comparing mismatches between lines.

The raw data files used in the variant call analysis included all fasta files from the sequencing of wild-type and herbicide resistant accessions used in this project, as well as fasta files from previous sequencing projects including 2 wild-type lines, 7 chlorsulfuron-resistant lines, and 5 mutant lines with morphological defects generated via UV-B mutagenesis. Whole genome sequencing reads from a total of 38 lines were used (Table 4.1). Raw reads were trimmed to remove low-quality reads and NEB adaptors using Trimmomatic 0.38. The read coverage was then normalised using khmer 2.1.2. Reads were aligned to the *Marchantia polymorpha* reference genome (Tak-1v5.1 plus female chromosome from Tak-2v3.1; now known

as v6.1) using bowtie2. Reads were sorted by position and reads from different lanes were merged using samtools 1.10. The variant call analysis was carried out using samtools and bcftools (ploidy defined as haploid, and using the multiallelic/rare variant call option) to generate bcf files listing mismatches between the sequencing reads and the reference genome for each line. For each bcf file, only mismatches which were supported by 7 – 100 reads and where the number of reads supporting high quality alternative alleles ≥ the number of reads supporting high quality reference alleles were retained (DP4[2]+DP4[3])/sum(DP4)>0.5).

Mismatches which were not the canonical UV-B induced mismatches (C → T or G → A) and mutations were filtered out using bcftools. Lists of filtered mismatches were compared across genotypes; for each mutant with a particular phenotype (e.g. TXTA resistance), a list of mismatches present in that line but not present in any lines without that phenotype was generated using bcftools. The resulting lists were filtered to retain only mismatches present in a CDS using bash scripting, then filtered manually in Interactive Genomics Viewer v 2.10 to remove mismatches which did not induce an amino acid change and which were misaligned or poor quality.

4.3.9 Primers

Primer	Sequence	Use
GR8_3Fw	AGACACATTGAACGTTTGGAGA	Genotyping Mptar2 and Mptar4 (RAD8)
GR8_3Rv	CTCGGTCAGGTCTTAGAGTCA	Genotyping Mptar2 and Mptar 4 (RAD8)
GR8_4Fw	CAAGAGTTTCCTGGCGCTTT	Genotyping Mptar6 (RAD8)
GR8_4Rv	AAAAGATCACGAGCCTGCTG	Genotyping Mptar6 (RAD8)

4.4. Results

4.4.1. A bioinformatic analysis of whole-genome sequencing data identified putative resistance-conferring mutations in 12 out of 13 chlorsulfuron-resistant lines

The non-allelism based mutation discovery bioinformatic pipeline previously developed in the lab uses genomic sequencing data from mutants to identify candidate SNPs which could underly a phenotype (Champion *et al.*, 2021). For a SNP to be responsible for a mutant phenotype, it must be induced by the mutagen and result in an amino acid change. It must also be absent in lines without the mutant phenotype; if it is present in a line without the mutant phenotype, it cannot be responsible for the mutant phenotype. The pipeline identifies mismatches between each mutant line and the reference genome which are induced by mutagenesis and result in an amino acid change, and compares these mismatches between mutant lines to identify SNPs present in lines with the mutant phenotype and absent in lines without the mutant phenotype (Champion *et al.*, 2021). I used this pipeline to identify candidate resistance-conferring SNPs in 13 Mp*tar* mutant lines.

First, to test if the pipeline is capable of successfully identifying resistance-conferring SNPs in *M. polymorpha* herbicide-resistant mutants, I used it to identify resistance-conferring mutations in 14 chlorsulfuron-resistant lines: 5 chlorsulfuron-resistant mutants I generated via UV-B mutagenesis (Mp*chlr* lines 1-5), as well as 7 lines previously generated by UV-B mutagenesis (CSR lines 1-9) or EMS mutagenesis (Mp*chlr*9b and Mp*chlr*10) (Table 4.1). The pipeline identifies SNPs which could be responsible for a mutant phenotype by identifying SNPs present in the mutant with the phenotype of interest and absent in mutants without the phenotype of interest.

When using the pipeline to identify SNPs responsible for chlorsulfuron resistance, the SNPs identified would be those present in chlorsulfuron-resistant lines but absent in chlorsulfuron-sensitive lines. I therefore compared genomic sequencing data from 24 chlorsulfuron-sensitive lines (Table 4.1) against the 14 chlorsulfuron-resistant lines. Although Mp*tar*6 and Mp*tar*10 exhibited significant resistance to chlorsulfuron in the previous chapter, both showed signs of growth inhibition on chlorsulfuron (Fig. 3.12), as opposed to Mp*chlr* lines which show no growth inhibition on chlorsulfuron (Fig. 3.6). It is therefore unlikely that the same SNP is responsible for chlorsulfuron resistance in Mp*chlr* lines as in Mp*tar*6 or Mp*tar*10, so I classed Mp*tar*6 and Mp*tar*10 as chlorsulfuron-sensitive lines in this analysis.

I extracted high quality high molecular weight genomic DNA from the lines grown in the lab (Table 4.1) and sequenced the genomes of these lines using Illumina paired-end sequencing (150 bp reads). I also used sequencing data from previously sequenced lines (Table 4.1). Before the analysis, I evaluated the sequencing quality; all lines had sequencing of high enough quality to be used in the analysis apart from Mp*chlr*5, so this line was excluded from the analysis leaving 13 chlorsulfuron-resistant lines (Table 4.1). First, I undertook a variant call analysis to identify mismatches in the genomes of each of the lines with respect to the *M. polymorpha* reference genome (Tak-1 v5.1 + v3.1 female chromosome). I then filtered these mismatches to remove those supported by too few or too many reads to be reliable and those which were due to read misalignment. This variant call analysis identified in the region of 10^4 – 10^5 mismatches with respect to the reference genome in each line, depending on the line; Tak-1 had the least number of mismatches (1.6×10^4) and Tak-2 had the highest number of mismatches (4.3×10^5), whilst the numbers of mismatches in each of the remaining lines fell somewhere in between (Table 4.1).

Line	Phenotype	Sex	Origin	N. mismatches
Tak-1	Wild-type	Male	Lab accession	1.6×10^4
Tak-2	Wild-type	Female	Lab accession	4.3×10^5
OxTak1F	Wild-type (backcross)	Female	Lab accession	2.7×10^4
OxTak2M	Wild-type (backcross)	Male	Lab accession	4.0×10^5
CSR_wt	Wild-type	Male	Lab accession**	4.4×10^3
Morpho_Tak2	Wild-type	Female	Lab accession**	3.7×10^5
Mp*chlr*1	Chlorsulfuron-resistant	Female	UV-B	2.1×10^5
Mp*chlr*2	Chlorsulfuron-resistant	Female	UV-B	1.3×10^5
Mp*chlr*3	Chlorsulfuron-resistant	Female	UV-B	3.5×10^5
Mp*chlr*4	Chlorsulfuron-resistant	Female	UV-B	3.4×10^5
Mp*chlr*5	Chlorsulfuron-resistant	Male	UV-B	6.5×10^4
Mp*chlr*9b	Chlorsulfuron-resistant	Female	EMS*	2.2×10^5
Mp*chlr*10	Chlorsulfuron-resistant	Female	EMS*	2.4×10^5
CSR1	Chlorsulfuron-resistant	Male	UV-B**	1.4×10^5
CSR2	Chlorsulfuron-resistant	Male	UV-B**	1.6×10^5
CSR3	Chlorsulfuron-resistant	Male	UV-B**	1.7×10^5
CSR4	Chlorsulfuron-resistant	Female	UV-B**	9.6×10^4
CSR6	Chlorsulfuron-resistant	Male	UV-B**	6.6×10^4
CSR7	Chlorsulfuron-resistant	Female	UV-B**	2.1×10^5
CSR9	Chlorsulfuron-resistant	Female	UV-B**	1.7×10^5
Mp*tar*1	TXTA-resistant	Male	UV-B	2.5×10^5
Mp*tar*2	TXTA-resistant	Female	UV-B	2.5×10^5
Mp*tar*3	TXTA-resistant	Female	UV-B	1.5×10^5
Mp*tar*4	TXTA-resistant	Male	UV-B	2.4×10^5
Mp*tar*5	TXTA-resistant	Female	UV-B	4.2×10^4
Mp*tar*6	TXTA-resistant	Male	UV-B	1.9×10^5
Mp*tar*7	TXTA-resistant	Female	UV-B	2.7×10^5
Mp*tar*8	TXTA-resistant	Female	UV-B	1.4×10^5
Mp*tar*9	TXTA-resistant	Female	UV-B	3.2×10^5
Mp*tar*10	TXTA-resistant	Female	UV-B	1.7×10^5
Mp*tar*11	TXTA-resistant	Male	UV-B	1.2×10^5
Mp*tar*12	TXTA-resistant	Female	UV-B	2.2×10^5
Mp*tar*13	TXTA-resistant	Female	UV-B	1.3×10^5
morpho_14	Rhizoid defect	Female	UV-B**	1.1×10^5
morpho_536	Rhizoid defect	Male	UV-B**	1.8×10^5
morpho_63	Rhizoid defect	Male	UV-B**	1.4×10^5
morpho_nek	Rhizoid defect	Male	UV-B**	2.1×10^5
morpho_ren	Rhizoid defect	Female	UV-B**	2.6×10^5

Table 4.1. List of lines used in the bioinformatic analysis to identify candidate resistance-conferring mutations in herbicide-resistant mutants. Names of lines are included as well as their herbicide resistance phenotype, their sex, their origin (lab accession or type of mutagenesis screen they were produced from), and the number of mismatches in their sequenced genomes with regards to the reference genome (v5.1 + female chromosome from v3.1). The sequencing data from Mp*chlr*5 was of too low quality so this data was excluded from the analysis.

* lines which were generated in a previous project but whose genomic DNA was extracted for sequencing in this project

** lines whose genomic DNA was sequenced in a previous project

To identify candidate mutagenesis-induced SNPs which could confer chlorsulfuron resistance, I filtered the lists of mismatches in each line to retain only mismatches which were likely to have been induced by UV-B or EMS mutagenesis; both methods induce primarily C→T (or G→A) mutations, so only these mismatches were retained. I then compared the mismatches between lines; for each chlorsulfuron-resistant line, I generated a list containing mismatches present in that line but absent in lines without chlorsulfuron resistance. The pipeline therefore identifies SNPs unique to each chlorsulfuron-resistant line but also accounts for the possibility that the same resistance-conferring SNP is present in different chlorsulfuron-resistant lines. I then further filtered these lists to retain only SNPs which cause an amino acid change. The final lists of SNPs for each line represent mutagenesis-induced SNPs which cause an amino acid change and are unique to lines with chlorsulfuron-resistance, so are expected to contain the resistance-conferring SNP for each line.

In total, I identified 102 candidate resistance-conferring SNPs among the 13 chlorsulfuron-resistant lines. The number of candidate SNPs for each line ranged from 2 (Mp*chlr*9b) to 17 (CSR6) (Supplementary Table S4.1).

To identify the resistance phenotype-causing SNP from the list of candidate SNPs for each line, I first looked for different lines with a mutation in the same gene. If several lines with the same phenotype have a SNP in the same candidate gene, it is likely that the mutations in this gene are those which cause the phenotype. The existing bioinformatic pipeline identifies SNPs in common between lines (Champion *et al.*, 2021); I adapted the pipeline to instead identify mutated genes in common between lines. With this modification, the pipeline identified a variety of different SNPs in the Mp*AHAS* gene (Mp7g01940) in 12 out of the 13 chlorsulfuron-resistant

lines. No SNP in the Mp7g01940 gene in the Mp*chlr*3 genome was identified by the pipeline. However, I identified a SNP causing a Pro197Leu mutation by Sanger sequencing in this line (Fig. 3.7). The SNP was a non-canonical mutation (C → A), which explains why this SNP was automatically filtered out by the pipeline. The filtering of non-canonical mutations therefore represents a limitation in the pipeline but is necessary to reduce the number of candidate SNPs to a number that is feasible to work with. Having identified a mutation in Mp*AHAS* using the pipeline in 12 out of 13 cases, I concluded that the pipeline can identify resistance-conferring mutations in chlorsulfuron-resistant lines.

4.4.2. The pipeline identified 176 candidate resistance-conferring SNPs in Mp*tar* lines

Having demonstrated that the pipeline can be used to identify the resistance-conferring SNPs in chlorsulfuron-resistant mutants, I used it to identify candidate resistance-conferring SNPs in the 13 Mp*tar* lines. I ran the pipeline in exactly the same way as when screening for the SNPs conferring chlorsulfuron resistance, but this time I identified SNPs that are unique to Mp*tar* lines. In total, I identified 176 candidate resistance-conferring SNPs among the 13 Mp*tar* lines. For each line, the number of candidate SNPs varied from 6 (Mp*tar*13) to 27 (Mp*tar*11) (Supplementary Table S4.2). I hypothesise that each Mp*tar* line has one resistance-conferring SNP and that for each line this resistance-conferring SNP is present in the list of candidate SNPs.

4.4.3. There are mutations in the Mp*RAD8* gene in Mp*tar2,* Mp*tar4, and* Mp*tar6* mutant lines

To identify the strongest candidates for resistance-conferring SNP from the list of candidate SNPs in each line, I first compared the SNPs in each Mp*tar* line to determine if any single gene was mutated in more than one line. I found that there were SNPs in the Mp3g19030 gene in 3 of the 13 Mp*tar* lines (Fig. 4.1). Two of the lines (Mp*tar*2 and Mp*tar*4) carried canonical G → A mutations while one line (Mp*tar*6) carried a non-canonical T → C mutation (Supplementary Table S4.2). These three SNPs are transitions – interchanges of purines (G → A) or pyrimidines (T → C) – and therefore involve changes of bases with similar shapes, unlike transversions which involve an interchange of a purine and a pyrimidine (Guo *et al.*, 2017). Transitions are less likely than transversions to induce an amino acid change (Guo *et al.*, 2017), however all three of these SNPs induce an amino acid change in Mp3g19030 (Supplementary Table S4.2).

To verify these SNPs, the Mp3g19030 gene was amplified in each of the mutants and sequenced by Sanger sequencing. This showed that the sequences identified through whole genome sequencing were not artefacts. Since three individual Mp*tar* lines have a mutation in the Mp3g19030 gene, it is likely that a mutation in this gene confers resistance to TXTA.

Fig. 4.1. Sanger sequencing of regions of the Mp3g19030 gene in Mp*tar*2, Mp*tar*4 and Mp*tar*6 lines. Regions of Mp3g19030 in Mp*tar*2, Mp*tar*4 and Mp*tar*6 were sequenced to confirm the presence of UV-B induced mutations. The consensus sequence is shown on the top rows, and results from the Sanger sequencing are shown on the second rows. Mp*tar*2, Mp*tar*4 and Mp*tar*6 were generated by UV-B mutagenesis in the current project.

4.4.4. Eight Mp*tar* lines (Mp*tar*1, Mp*tar*2, Mp*tar*3, Mp*tar*4, Mp*tar*6, Mp*tar*7, Mp*tar*8, and Mp*tar*12) have candidate resistance-conferring SNPs which may cause increased ROS

Mp3g19030 is the *M. polymorpha* homologue of the *RAD8/RTN4IP1* gene, first identified in *C. elegans* (Hartman and Herman, 1982). RAD8 is a mitochondrial NADPH oxidoreductase with antioxidant activity; it is involved in coenzyme Q biosynthesis and therefore required for mitochondrial electron transport chain (Park *et al.*, 2021). *rad8* mutants in *C. elegans* accumulate reactive oxygen species (ROS) (Fujii *et al.*, 2011), and mouse myoblast cells with a knock-out of *RTN4IP1* accumulate higher ROS and their rates of oxidative phosphorylation are lower than wild-type (Park *et al.*, 2021). I therefore hypothesise that Mp*rad8* mutants also accumulate cellular ROS. Pre-treating *A. thaliana* cells with reactive oxygen species

(H_2O_2) confers resistance to TXTA (Awwad *et al.*, 2019); I therefore hypothesise that higher levels of cellular ROS in Mp*tar2,* Mp*tar4 and* Mp*tar6* mutants than in wild type could account for their resistance to TXTA.

If higher levels of ROS levels in Mp*tar2,* Mp*tar4 and* Mp*tar6* mutants accounts for their resistance to TXTA, then other mutations that cause an increase in ROS accumulation may also confer resistance to TXTA. To test the hypothesis that increased ROS might confer resistance to TXTA in the other ten Mp*tar* mutants, I searched for SNPs in genes that might lead to increased ROS levels when mutated. I identified SNPs in 4 genes which are annotated by GO terms that suggests that a mutation in these genes may cause defects in cellular ROS levels (Table 4.2). The genes identified include a peroxidase (Mp6g13550 in Mp*tar1*), an NAD(P)-linked alcohol dehydrogenase (Mp5g02280 in Mp*tar*4), an oxidase (Mp8g04820 in Mp*tar*4), and an oxygenase (Mp7g19170 in Mp*tar*12).

I also manually curated the list of candidate resistance-conferring SNPs to identify SNPs which I hypothesise cause a change in cellular ROS levels but which are not annotated by GO terms related to ROS. I identified 2 SNPs in genes encoding components of the photosynthetic photosystems of photosynthesis; one in Mp*PSAD* (Mp5g04200 in Mp*tar8*) and one in Mp*PSBP* (Mp8g10040 in Mp*tar3*) (Table 4.2). PSAD is required for the docking of ferredoxin to photosystem I and PSBP is an accessory protein of photosystem II (Chitnis *et al.*, 1997, Ifuku *et al.*, 2008); I predict that loss-of-function of either allele results in dysfunction of the photosynthetic electron transport chain, causing increased leakage of electrons from the chain and subsequently increased reaction of free electrons with oxygen to form ROS.

NTSR to TXTA is conferred by a loss-of-function mutation in At*PAM16* in *A. thaliana* (Scheible et al., 2003). At*pam16* mutants show overproduction of ROS in leaf tissues (Huang *et al.*, 2013); given my hypothesis that increased ROS may confer resistance to TXTA, the overproduction of ROS in At*pam16* mutants may be the basis of their TXTA resistance. I demonstrated that this mechanism of NTSR is conserved in *M. polymorpha* by showing that *Mppam16* mutants are resistant to TXTA (Chapter 2). Although I did not identify mutations in Mp*PAM16* (Mp3g09390) among the *tar* mutants, in Mp*tar7* there is a mutation leading to a premature stop codon in Mp3g01110 which encodes a gene annotated with a TIM44-like domain. Both PAM16 and TIM44 are part of the same complex; the PAM complex mediating transport across the mitochondrial inner membrane of *A. thaliana* (Frazier *et al.*, 2004). I hypothesise that loss-of-function of either *PAM16* or *TIM44* results in defective function of the PAM complex, and that this in turn leads to overproduction of ROS. The mutation in Mp3g01110 – a gene encoding a TIM44L domain containing protein – is therefore a strong candidate for conferring NTSR to TXTA in Mp*tar*7 (Table 4.2).

Gene ID	ROS-related GO term(s)	Functional annotation	Mp*tar* line(s)
Mp3g19030	GO:0016491 (oxidoreductase activity)	Mp*RAD8*	Mp*tar*2 Mp*tar*4 Mp*tar*6
Mp6g13550	GO:0006979 (response to oxidative stress) GO:0004601 (peroxidase activity) GO:0042744 (hydrogen peroxide catabolic process)	Peroxidase	Mp*tar*1
Mp5g02280	GO:0016491 (oxidoreductase activity) GO:0047834 (D-threo-aldose 1-dehydrogenase activity)	NAD(P) linked alcohol dehydrogenase	Mp*tar*4
Mp8g04820	GO:0016491 (oxidoreductase activity)	Mp*LPR11* (oxidase)	Mp*tar*4
Mp7g19170	GO:0016491 (oxidoreductase activity)	2-oxoglutarate/ Fe^{2+}-dependent oxygenase	Mp*tar*12
Mp5g04200	N/A	Mp*PSAD*	Mp*tar*8
Mp8g10040	N/A	Mp*PSBP*	Mp*tar*3
Mp3g01110	N/A	TIM44L domain	Mp*tar*7

Table 4.2. List of *M. polymorpha* genes in which a candidate resistance-conferring SNP is found which may cause changes in cellular ROS levels. ROS-related GO terms are listed as well as the Mp*tar* lines in which the candidate SNPs are found. The genes were identified by searching for ROS-related GO terms in the genes mutated in Mp*tar* lines. The three genes which are not annotated by ROS-related GO terms were identified by manual curation of the list of genes mutated in Mp*tar* lines.

4.4.5. Four Mp*tar* lines (Mp*tar*5, Mp*tar*9, Mp*tar*12, and Mp*tar*13) have SNPs in genes associated with NTSR in herbicide-resistant weeds

I identified likely resistance-conferring SNPs in 8 out of 13 Mp*tar* lines based on the identification of 3 SNPs in Mp*rad8* and a further 7 SNPs which are also predicted to cause increased ROS. To identify the most likely resistance-conferring SNP in the remaining 5 out of 13 Mp*tar* lines, I searched for SNPs in these lines in genes which have been associated with NTSR in other species. A recent genome wide association (GWA) study associated SNPs in 274 genes with NTSR in glyphosate-resistant populations of *Amaranthus tuberculatus*, although their role in resistance has not been confirmed (Kreiner *et al.*, 2019, Kreiner *et al.*, 2021). This is the first report of an association between SNPs and herbicide NTSR in the field. I hypothesised that if any candidate resistance-conferring SNPs in Mp*tar* mutant lines are found in *M. polymorpha* homologues of NTSR-associated alleles in *A. tuberculatus*, these would be strong candidates for conferring NTSR in Mp*tar* lines.

I undertook a tBLASTn search (with an E value cutoff of 1E-5) against the *A. tuberculatus* genome assembled by (Kreiner *et al.*, 2019) to identify the closest *A. tuberculatus* homologue of each of the 173 genes in Mp*tar* lines which contain a candidate resistance-conferring SNP. I identified *A. tuberculatus* homologues for 121 of the 173 genes (Supplementary Table S4.3). I then compared these 121 *A. tuberculatus* genes with the 274 NTSR-associated genes from the GWA study; I identified 4 genes in common (Table 4.3). The SNPs in these 4 genes are therefore strong candidates for conferring NTSR. The SNPs in question include one in Mp*tar*5 in Mp6g19260, a glycosyltransferase (GT); other members of this gene family have already been implicated in NTSR in other species (Yuan *et al.*, 2007). The remaining

3 SNPs are in Mp*tar*9 in Mp2g21290 (a translation initiation factor), in Mp*tar*12 in Mp8g06830 (a protein involved in the ABA response), and in Mp*tar*13 in Mp8g15020 (spermidine synthase) (Table 4.3).

***M. polymorpha* gene ID**	***A. tuberculatus* homologue**	**Functional annotation**	**Mp*tar* line**
Mp6g19260	AMATA_chromosomes_28406	*GALS2*; galactan synthase	Mp*tar*5
Mp2g21290	AMATA_chromosomes_04173	*EIF5*; translation initiation factor	Mp*tar*9
Mp8g06830	AMATA_chromosomes_28414	*ARIA*; involved in ABA response	Mp*tar*12
Mp8g15020	AMATA_chromosomes_08316	Spermidine synthase	Mp*tar*13

Table 4.3. List of *M. polymorpha* genes which carry a candidate resistance-conferring mutation in Mp*tar* lines whose *A. tuberculatus* homologues are associated with NTSR. *A. tuberculatus* homologues were determined by BLASTp search (E value cutoff < 1 E-5).

4.4.6. The strongest candidate NTSR-conferring SNP has been identified for 11 out of 13 Mp*tar* lines

I identified 176 candidate SNPs that could confer resistance to TXTA in the Mp*tar* mutant lines; I hypothesised that one mutation in each Mp*tar* line is responsible for conferring resistance to TXTA, and that for each line this resistance-conferring mutation is present in the list of 6-27 candidate resistance-conferring SNPs identified via a non-allelism based SNP calling analysis (Supplementary Table S4.2). I selected the SNP that is most likely to confer TXTA resistance in each Mp*tar* line based on 3 sets of criteria; first by looking for allelicity I found 3 SNPs in Mp*RAD8* in Mp*tar2*, Mp*tar*4, and Mp*tar*6 (Table 4.2); second by looking for SNPs predicted to cause ROS accumulation I found 6 SNPs in Mp*tar*1*,* Mp*tar*3*,* Mp*tar*4*,* Mp*tar7,* Mp*tar8*, Mp*tar*12 (Table 4.2); and finally by looking for SNPs in genes associated

with NTSR in *A. tuberculatus* I found 4 SNPs in Mp*tar*5, Mp*tar*9, Mp*tar*12, and Mp*tar*13 (Table 4.3).

The strongest candidate NTSR-conferring SNPs are the three in Mp*RAD8* (Mp3g19030) in Mp*tar*2, Mp*tar*4, and Mp*tar*6 since the same gene is mutated in more than one Mp*tar* line (Table 4.2). A mutation in Mp*RAD8* is thought to increase cellular levels of ROS, and addition of exogenous ROS confers resistance to TXTA in *A. thaliana* cells in culture (Awwad *et al.*, 2019). I therefore hypothesise that the remaining SNPs predicted to increase cellular ROS are the next strongest candidates. The remaining SNPs predicted to increase cellular ROS are those in the peroxidase (Mp6g13550) in Mp*tar*1, MpPSBP (Mp8g10040) in Mp*tar*3, MpTIM44L (Mp3g01110) in Mp*tar*7, and MpPSAD (Mp5g04200) in Mp*tar*8, and the oxygenase (Mp7g19170) in Mp*tar*12 – (Table 4.2); since Mp*tar*4 already has a SNP in Mp*RAD8*, it is unlikely that the remaining 2 SNPs found in genes predicted to increase ROS in Mp*tar*4 are responsible for resistance in Mp*tar*4. The next strongest candidates are SNPs in specific genes which have already been associated with NTSR in *A. tuberculatus*, namely MpGALS2 (Mp6g19260) in Mp*tar*5, MpEIF5 (Mp2g21290) in Mp*tar*9, MpARIA (Mp8g06830) in Mp*tar*12, and spermidine synthase (Mp8g15020) in Mp*tar*13 (Table 4.3).

Overall, these analyses identified the SNP most likely to confer resistance in 11 out of 13 Mp*tar* lines (Table 4.4). To try and identify a strong candidate SNP for conferring resistance in the remaining 2 out of 13 lines (Mp*tar*10 and Mp*tar*11), I searched for SNPs in Mp*tar*10 and Mp*tar*11 in genes from families which have been implicated in NTSR (cytochrome P450s, glutathione-S-transferases, glycosyltransferases, and ABC transporters) (Yuan *et al.*, 2007), but did not find any

(Supplementary Table S4.2). Alternatively, I hypothesised that resistance in Mp*tar*10 and Mp*tar*11 could involve SNPs which mitigate the toxic effect of TXTA by affecting the molecular pathway targeted by TXTA. Since TXTA is thought to be a cellulose biosynthesis inhibitor (Fry and Loria, 2002, Tateno *et al.*, 2016), Mp*tar*10 and Mp*tar*11 may have SNPs which modify the composition of the cell wall in a way which prevents the action of TXTA. However, the mode of action of TXTA is still uncertain; some phenotypes exerted by TXTA (binucleate cells and incomplete formation of the phragmoplast during cell division) are also consistent with microtubule inhibition (Fry and Loria, 2002). Therefore, rather than searching directly for SNPs affecting cellulose biosynthesis in Mp*tar*10 and Mp*tar*11, I undertook a GO enrichment analysis of the 176 candidate resistance-conferring SNPs across all Mp*tar* lines to identify without bias whether any particular molecular pathway is affected in multiple Mp*tar* lines (Appendix). I hypothesised that enrichment of a particular pathway would indicate that several Mp*tar* lines have defects in the same pathway, and may indicate mechanisms of NTSR affecting the unknown pathway targeted by TXTA. I found that GO:0042546 (cell wall biogenesis) was the most significantly enriched “biological process” term amongst the 176 genes containing candidate resistance-conferring SNPs in Mp*tar* lines; 4 Mp*tar* lines contain SNPs in genes annotated with this term (Mp*tar*3, Mp*tar*6, Mp*tar*7, and Mp*tar*9) (Appendix). If these SNPs are responsible for resistance in these lines, this finding supports the classification of TXTA as a cellulose biosynthesis inhibitor. However, I already identified the most likely SNP to cause resistance in these lines in this chapter, and neither Mp*tar*10 nor Mp*tar*11 had SNPs in genes involved with cell wall biogenesis. I therefore could not identify the most likely candidate for conferring resistance in Mp*tar*10 or Mp*tar*11.

Overall, I identified the most likely NTSR-conferring SNP in 11 out of 13 Mp*tar* lines (Table 4.4). I will functionally characterise loss-of-function mutants of these genes in the following results chapter.

Mp*tar* line	**Gene ID**	**Functional annotation**	**Amino acid change**	**Predicted method of NTSR**
Mp*tar*1	Mp6g13550	peroxidase	Glu → *	Increase in ROS
Mp*tar*2	Mp3g19030	Mp*RAD8*	Gly → Glu	Increase in ROS
Mp*tar*3	Mp8g10040	Mp*PSBP*	Glu → Lys	Increase in ROS
Mp*tar*4	Mp3g19030	Mp*RAD8*	Gly → Arg	Increase in ROS
Mp*tar*5	Mp6g19260	Mp*GALS2*	Ser → Phe	NTSR in *A. tuberculatus*
Mp*tar*6	Mp3g19030	Mp*RAD8*	Leu → Pro	Increase in ROS
Mp*tar*7	Mp3g01110	Mp*TIM44L*	Arg → *	Increase in ROS Associated with *PAM16*
Mp*tar*8	Mp5g04200	Mp*PSAD*	Glu → Lys	Increase in ROS
Mp*tar*9	Mp2g21290	Mp*EIF5*	Arg → Gln	NTSR in *A. tuberculatus*
Mp*tar*12	Mp8g06830	Mp*ARIA*	His → Tyr	NTSR in *A. tuberculatus*
	Mp7g19170	2-oxoglutarate/ Fe(II)-dependent oxygenase	Pro → Ser	Increase in ROS
Mp*tar*13	Mp8g15020	Spermidine synthase	Ser → Leu	NTSR in *A. tuberculatus*

Table 4.4. **List of candidates for resistance-conferring mutations in Mp*tar* lines**. Strong candidates were determined by three different approaches; SNPs in the same gene in different mutants, SNPs which would lead to an increase in ROS, or SNPs in genes which are associated with NTSR in herbicide-resistant *A. tuberculatus*.

4.5. Discussion

In this chapter, I identified 176 candidate resistance-conferring SNPs in 13 TXTA-resistant *M. polymorpha* mutant lines. I identified the most likely resistance conferring SNP in 11 out of the 13 TXTA-resistant mutant lines. I will test if these SNPs are responsible for resistance to TXTA in the next chapter.

Using the non-allelism based SNP discovery pipeline (Champion *et al.*, 2021), I identified 102 candidate resistance-conferring SNPs in chlorsulfuron-resistant mutant lines, and 176 in TXTA-resistant lines. The majority of the Mp*tar* mutant lines were generated using a UV-B dose corresponding to a kill rate of 50-90 %, whereas the Mp*chlr* mutant lines were generated using a UV-B kill rate of 20-50 % (Supplementary Table S3.1). Mp*tar* mutant lines therefore carry more mutations in their genomes than Mp*chlr* mutant lines; assuming that each Mp*tar* mutant line has a single mutation which confers NTSR, this suggests that the pipeline identifies more "false positives" (candidate resistance-conferring SNPs which do not confer resistance) the higher the mutation load in the mutants with the phenotype of interest.

All chlorsulfuron-resistant mutants are allelic, each carrying one of a variety of SNPs in the single copy Mp*AHAS* gene. However, most thaxtomin-A resistant mutants were not allelic; only 3 of the 13 mutants carried a mutation in the same gene, namely Mp*RAD8*. Therefore, a maximum of 3 Mp*tar* mutant lines could carry a target-site mutation; between 10 and 13 Mp*tar* mutant lines must carry non target site resistance (NTSR) mutations. Given the lack of knowledge surrounding mechanisms of NTSR, especially those conferred by loss-of-function mutations, the

identification of resistance-conferring mechanisms in Mp*tar* mutant lines will likely lead to the discovery of novel NTSR mechanisms.

I found that three Mp*tar* mutant lines carried a mutation in the same gene, Mp*RAD8*. Identifying allelic lines usually requires a series of crosses to define complementation groups; the 13 Mp*tar* mutant lines carry many background mutations which affect their growth and which make them recalcitrant to crossing, but I was able to bypass the need for crossing by using the non-allelism based SNP discovery pipeline. Since a mutation in Mp*RAD8* was identified in three separate Mp*tar* mutant lines, it is highly likely that loss-of-function of *RAD8* confers resistance to TXTA. RAD8 is a mitochondrial NADPH oxidoreductase required for coenzyme Q (CoQ) biosynthesis; a loss-of-function of *RAD8* causes accumulation of reactive oxygen species in *C. elegans* and in mouse myoblast cells (Fujii *et al.*, 2011, Park *et al.*, 2021). Pre-treatment of *A. thaliana* cells with ROS has previously been shown to decrease their sensitivity to TXTA, suggesting that the assumed phenotype of increased ROS in Mp*rad8* mutant lines may be the basis of their resistance to TXTA (Awwad *et al.*, 2019).

I identified 5 further SNPs in 5 other Mp*tar* mutant lines (Mp*tar*1, Mp*tar*3, Mp*tar*7, Mp*tar*8, and Mp*tar*12) lines which may also cause increased ROS, supporting the hypothesis that an increase in cellular ROS could be the basis of resistance in Mp*tar* mutant lines with a mutation in Mp*RAD8*, as well as potentially other Mp*tar* mutant lines. Two of the SNPs identified in this way are found in components of or associated with the photosynthetic electron transport chain (MpPSBP and MpPSAD). Given the role of Mp*RAD8* in the biosynthesis of CoQ, a component of the mitochondrial electron transport chain, 5 SNPs in 5 different Mp*tar* mutant lines are

predicted to disrupt an electron transport chain. This supports the hypothesis that a disruption of the electron transport chain – either in the mitochondria or in the chloroplast – leads to increased electron leakage from the chain resulting in accumulation of ROS, which could confer NTSR to TXTA. One of the other SNPs predicted to cause increased ROS is in a gene with a domain which has homology to the TIM44 subunit of the PAM complex which also includes Mp*PAM16*. Together with the mutation in the peroxidase in Mp*tar*1, this is also the only strong candidate NTSR-conferring SNP which causes an early stop codon, making it more likely to lead to loss-of-function. If this SNP confers resistance to TXTA via disruption of the PAM complex, it cross-validates the mechanism of NTSR conferred by loss-of-function of *PAM16* which presumably also causes disruption of the PAM complex.

I also identified 4 SNPs in 4 Mp*tar* lines in genes which have been associated with NTSR in glyphosate-resistant *Amaranthus tuberculatus*; *GALS2*, *EIF5*, *ARIA*, and spermidine synthase. Spermidine synthase is involved in the biosynthesis of spermidine, a polyamine with antioxidant properties which can act as a ROS scavenger (Saha *et al.*, 2015). It is therefore possible that the SNP in spermidine synthase in Mp*tar*13 leads to overaccumulation of ROS due to lack of spermidine; based on my hypothesis that increased ROS can confer resistance to TXTA, this could be the basis of resistance in Mp*tar*13. *GALS2* is a glycosyltransferase, a gene family previously associated with NTSR; the other three SNPs are in genes which had not been linked to NTSR prior to the GWA study. If these SNPs confer TXTA resistance in Mp*tar* lines, it suggests that these alleles not only constitute novel NTSR mechanisms but also novel mechanisms of cross-resistance, conferring resistance to both glyphosate and TXTA. This would be an important discovery and validates the use of my approach to cross-validate population genomics studies.

In conclusion, I identified strong candidate NTSR-conferring mutations in 11 of the 13 Mp*tar* lines purely by bioinformatic analysis without the need for crossing. Although this saved time and allowed me to identify candidate resistance-conferring SNPs in mutant lines which I was unable to cross, the ability to cross my mutants and follow the segregation of the candidate SNPs with the mutant phenotype would have allowed me to further narrow down which SNPs are responsible for resistance. Nevertheless, functional characterisation – which is now required to confirm the ability of the identified SNPs to confer NTSR – is facilitated in *M. polymorpha* by the variety of genetic tools available to perform reverse genetics, the lack of redundancy in the genome, and its dominant haploid nature. In my next chapter I will use reverse genetics to functionally characterise the effect of loss-of-function of the candidate NTSR-conferring genes I identified in this chapter in a wild-type background to determine if they play a role in NTSR in Mp*tar* lines.

4.6. Supplementary data

Line	Mutation	Amino acid change	Gene ID	Functional annotation
Mpchlr1	C->T	Ala->Thr	Mp1g02380	*NPR1*
Mpchlr1	C->T	Leu->Phe	Mp1g19350	RNA binding
Mpchlr1	G->A	Ala->Val	Mp2g00820	*ARIH1*; ariadne-1; ubiquitin ligase
Mpchlr1	C->T	Thr->Iso	Mp2g08400	Reticula related protein
Mpchlr1	C->T	Pro->Ser	Mp3g00210	
Mpchlr1	G->A	Glu->Lys	Mp5g13920	Mitochondrial elongation factor
Mpchlr1	C->T	Asp->Asn	Mp7g01940	Mp*AHAS*
Mpchlr1	G->A	Gly->Arg	Mp7g16260	ABC transporter
Mpchlr2	C->T	Leu->Phe	Mp2g10510	*DHDDS*
Mpchlr2	G->A	Pro->Ser	Mp4g08370	
Mpchlr2	G->A	Pro->Leu	Mp7g01940	Mp*AHAS*
Mpchlr3	G->T	Pro->Leu	Mp7g01940	Mp*AHAS*
Mpchlr4	C->T	Thr->Iso	Mp1g25850	Symporter
Mpchlr4	G->A	Val->Iso	Mp3g03050	Fe-S binding domain
Mpchlr4	G->A	Thr->Met	Mp3g09700	Germin related protein
Mpchlr4	C->T	Ser->Phe	Mp3g12890	Aspartyl protease
Mpchlr4	C->T	Gln->Leu	Mp3g22920	*RAD51*; DNA repair protein
Mpchlr4	C->T	Cys->Phe	Mp4g12090	Glysocysl hydrolase (chitosanase)
Mpchlr4	G->A	No start codon	Mp4g13170	RNA helicase
Mpchlr4	G->A	Pro->Ser	Mp4g19930	Phosphate symporter
Mpchlr4	C->T	Ser->Phe	Mp6g01160	
Mpchlr4	G->A	Gly->Asp	Mp6g12190	Transcriptional regulator
Mpchlr4	G->A	Pro->Ser	Mp7g01940	Mp*AHAS*
Mpchlr4	C->T	Ser->Pro	Mp7g02870	Glycosyl hydrolase
Mpchlr4	C->T	Ser->Leu	Mp8g07340	GYF domain
Mpchlr9b	G->A	Pro->Leu	Mp7g01940	Mp*AHAS*
Mpchlr9b	G->A	Glu->Lys	Mp8g00590	
Mpchlr10	G->A	Ala->Val	Mp1g02100	
Mpchlr10	C->T	Asp->Asn	Mp4g22460	*NOP9*
Mpchlr10	G->A	Glu->Lys	Mp5g16780	
Mpchlr10	G->A	Pro->Leu	Mp7g01940	Mp*AHAS*
CSR1	G->A	Ser->Phe	Mp1g00220	
CSR1	G->A	His->Tyr	Mp2g01000	Redox protein
CSR1	C->T	Thr->Iso	Mp2g01380	
CSR1	G->A	Pro->Leu	Mp7g01940	Mp*AHAS*
CSR1	G->A	Pro->Leu	MpVg00710	*MED12*; RNA pol II subunit
CSR2	G->A	Gly->Asp	Mp1g16300	Membrane protein
CSR2	G->A	Ser->Asn	Mp1g17810	Kinesin like
CSR2	C->T	Glu->Lys	Mp1g24680	
CSR2	C->T	Thr->Iso	Mp2g17140	
CSR2	C->T	Pro->Phe	Mp3g20910	Sec61
CSR2	G->A	Pro->Leu	Mp7g01940	Mp*AHAS*
CSR2	G->A	Pro->Ser	Mp8g07080	Serine protease
CSR2	C->T	Pro->Ser	Mp8g15030	RABGGTA prenyltransferase
CSR3	C->T	Ser->Asp	Mp1g14070	Kinesin line
CSR3	C->T	Gly->Glu	Mp1g17000	*CDC73* rna polii accessory factor
CSR3	C->T	Pro->*	Mp1g24100	*CLCN7* chloride channel
CSR3	G->A	Arg->Cys	Mp4g09370	
CSR3	G->A	Glu->Lys	Mp4g10260	*SYF2*; splicing factor
CSR3	G->A	Pro->Leu	Mp7g01940	Mp*AHAS*
CSR4	G->A	Pro->Leu	Mp2g09030	
CSR4	C->T	Glu->Lys	Mp2g14340	Protein kinase
CSR4	C->T	Pro->Ser	Mp3g22900	HSP70 chaperonin

CSR4	C->T	Glu->*	Mp4g12080	Glucanotransferase
CSR4	C->T	Ser->Phe	Mp5g05200	
CSR4	C->T	Glu->Lys	Mp5g20110	Pseudouridine synthase
CSR4	C->T	Glu->Lys	Mp6g01130	Redox protein
CSR4	C->T	Val->Met	Mp6g20010	Rab5 interacting protein
CSR4	G->A	Pro->Leu	Mp7g01940	Mp*AHAS*
CSR4	G->A	Arg->Lys	Mp7g16820	Splicing factor
CSR6	C->T	Asp->Asn	Mp1g21450	MpRR-MYB1
CSR6	C->T	Gln->*	Mp1g29640	Histidine kinase
CSR6	C->T	Gln->*	Mp1g29740	
CSR6	G->A	Gly->Glu	Mp3g08290	Membrane transporter
CSR6	G->A	Ser->Phe	Mp3g09840	MTIF2
CSR6	C->T	Asp->Asn	Mp3g11480	
CSR6	C->T	Glu->Lys	Mp4g02740	Ubiquitin
CSR6	G->A	Ser->Phe	Mp4g12430	Aminopeptidase
CSR6	G->A	Leu->Phe	Mp5g10130	Sentaxin
CSR6	G->A	Pro->Leu	Mp5g17290	Glutaredoxin
CSR6	C->T	Gln->*	Mp6g08750	CRN/SYF
CSR6	G->A	Glu->Lys	Mp6g13870	
CSR6	G->A	Pro->Ser	Mp7g01940	Mp*AHAS*
CSR6	G->A	Arg->STOP	Mp7g08970	
CSR6	C->T	Leu->Phe	Mp7g16360	Kinase
CSR6	C->T	Pro->Ser	Mp8g02850	
CSR6	G->A	Glu->*	Mp8g05810	Kinase
CSR7	C->T	Ala->Thr	Mp1g16360	Midasin
CSR7	C->T	Pro->Ser	Mp1g19640	Kinase
CSR7	G->A	Pro->Ser	Mp2g11520	Mp*CXC1*
CSR7	C->T	Thr->Iso	Mp3g03720	Oxidoreductase
CSR7	G->A	Pro->Ser	Mp3g17820	
CSR7	G->A	Pro->Leu	Mp5g00210	Ribosomal protein
CSR7	G->A	Ala->Val	Mp5g20470	Mitochondrial chaperonin
CSR7	G->A	Pro->Ser	Mp6g08780	Hydrolase
CSR7	C->T	Glu->*	Mp6g18490	*MOT1*
CSR7	G->A	Pro->Leu	Mp7g01940	Mp*AHAS*
CSR7	G->A	Gly->Glu	Mp7g06560	
CSR7	G->A	Gly->Asp	Mp7g09090	LRR
CSR7	G->A	Ser->Phe	Mp7g14340	
CSR7	G->A	Pro->Leu	Mp8g11930	
CSR9	C->T	Pro->Leu	Mp1g04070	Splicing factor
CSR9	G->A	Thr->Iso	Mp1g17770	CNOT6
CSR9	C->T	Ala->Val	Mp1g24360	
CSR9	C->T	Gly->Glu	Mp2g24630	Terpene cyclase
CSR9	C->T	Thr->Iso	Mp3g09810	Protease
CSR9	G->A	Arg->Cys	Mp3g10030	
CSR9	G->A	His->Tyr	Mp4g18010	Ser/Thr kinase
CSR9	G->A	Arg->Gln	Mp7g00840	Tuftelin-interacting Protein TIP39
CSR9	G->A	Pro->Leu	Mp7g01940	MpAHAS
CSR9	C->T	Pro->Ser	Mp7g02750	
CSR9	G->A	Pro->Ser	Mp7g15910	DNA gyrase

Supplementary Table S4.1. List of candidate resistance-conferring mutations found in *Mpchlr* lines. Candidate resistance-conferring SNPs were identified using an adapted version of the non-allelism based SNP discovery pipeline (Champion *et al.*, 2021).

Line	Mutation	Amino acid change	Gene ID	Functional annotation
Mptar1	C->T	Pro->Ser	Mp1g26460	Nucleoside phosphatase
Mptar1	C->T	Ser->Phe	Mp2g04330	Helicase
Mptar1	C->T	Gly->Glu	Mp3g02860	*COG7*; Golgi transport
Mptar1	C->T	Arg->Gln	Mp4g17100	LRR protein
Mptar1	G->A	Glu->*	Mp4g22890	*NAC4*
Mptar1	C->T	Glu->*	Mp6g13550	Peroxidase
Mptar1	C->T	Ala->Thr	Mp8g12790	ATP citrate lyase
Mptar1	G->A	Gly->Glu	Mp8g18770	Transcription factor
Mptar2	C->T	Ser->Phe	Mp1g17110	F box protein
Mptar2	G->A	Val->Ile	Mp2g05240	TPR; GTPase
Mptar2	G->A	Ser->Phe	Mp3g02220	Actin related protein
Mptar2	C->T	Gly->Glu	Mp3g19030	Mp*RAD8*
Mptar2	G->A	Arg->Lys	Mp4g06580	
Mptar2	G->A	Try->*	Mp4g16020	
Mptar2	G->A	Arg->Gln	Mp4g21500	
Mptar3	C->T	Pro->Ser	Mp2g12440	Xyloglucan fucosyltransferase
Mptar3	C->T	Leu->Phe	Mp2g16550	Cysteine Protease
Mptar3	C->T	Asp->Asn	Mp2g17160	Tyrosine kinase
Mptar3	C->T	Gly->Arg	Mp3g07830	Branched chain aminotransferase
Mptar3	G->A	Gly->Asp	Mp3g20420	Ran gtpase activating protein
Mptar3	G->A	Glu->Lys	Mp4g12270	
Mptar3	C->T	Glu->Lys	Mp4g02430	Dna helicase
Mptar3	C->T	Pro->Leu	Mp8g09190	Splicing factor
Mptar3	G->A	Glu->Lys	Mp8g10040	Mp*PSBP*
Mptar4	C->T	Leu->Phe	Mp1g04260	Mitochondrial RNA synthetase
Mptar4	C->T	Glu->Lys	Mp1g10330	Mp1R-MYB6
Mptar4	C->T	Pro->Ser	Mp1g18300	Adenylylsulfate kinase
Mptar4	G->A	Ala->Thr	Mp2g07440	
Mptar4	G->A	Pro->Ser	Mp2g03680	Germin-like protein
Mptar4	G->A	Leu->Phe	Mp2g20920	*BMS1*; ribosome biogenesis
Mptar4	C->T	Glu->Lys	Mp3g13070	Damage specific DNA binding complex
Mptar4	C->T	Gly->Arg	Mp3g19030	MpRAD8
Mptar4	C->T	Ser->Asn	Mp3g22320	*CBX1*; heterochromatin protein
Mptar4	C->T	Ala->Val	Mp4g15540	*RNPC3*; RNA binding protein
Mptar4	G->A	Pro->Leu	Mp5g02280	*AKR1A1* alcohol dehydrogenase
Mptar4	C->T	Val->Iso	Mp5g22100	
Mptar4	G->A	Asp->Asn	Mp5g23420	Germin-like protein
Mptar4	C->T	Ala->Val	Mp6g03430	Protein phosphatase
Mptar4	C->T	Glu->Lys	Mp7g01020	
Mptar4	C->T	thr->Iso	Mp7g11880	Elongation complex
Mptar4	G->A	Pro->Ser	Mp8g04820	Redox protein
Mptar4	G->A	Ser->Phe	Mp8g13300	*MED14*; regulator of RNA pol II transcription
Mptar4	G->A	Ser->Asn	Mp8g13400	Dehydrogenase
Mptar4	C->T	Ser->Phe	Mp8g14840	Teolmere interacting protein
Mptar5	G->A	Pro->Ser	Mp1g00100	Fucosyltransferase
Mptar5	G->A	Pro->Ser	Mp1g00330	Ubiquitin protein ligase
Mptar5	C->T	Pro->Leu	Mp1g01140	Mitochondrial elongation factor
Mptar5	G->A	Gly->Glu	Mp2g04470	*MEI2*; meiosis
Mptar5	G->A	Asp->Asn	Mp2g15090	Histidine kinase
Mptar5	G->A	Leu->Phe	Mp2g23470	*CEM1*; oxoacyl synthase
Mptar5	G->A	Pro->Leu	Mp4g07230	
Mptar5	C->T	Arg->His	Mp4g21980	Chalcone synthase
Mptar5	G->A	Pro->Leu	Mp5g05010	Ribosomal protein
Mptar5	G->A	Gln->*	Mp6g10370	DNA helicase
Mptar5	G->A	Ser->Leu	Mp6g12540	*RAY1*; beta-arabinofuranosyltransferase
Mptar5	C->T	Ser->Phe	Mp6g19260	Galactan synthase
Mptar5	C->T	Ser->Phe	Mp7g01000	RNA helicase
Mptar5	C->T	Gly->Glu	Mp8g06930	
Mptar6	C->T	Ala->Val	Mp1g20550	DNA binding protein

Mptar6	G->A	Glu->Lys	Mp2g17840	*SFR2*; galactolipid galactosyltransferase
Mptar6	G->A	Pro->Ser	Mp2g21320	*FTSZ;* cell division (microtubule)
Mptar6	G->A	Gly->Glu	Mp2g22110	MYB factor
Mptar6	G->A	Gly->Arg	Mp3g07260	
Mptar6	C->T	Glu->Lys	Mp3g13360	*ADPRHL2*; poly(ADP-ribose) glycohydrolase
Mptar6	C->T	Arg->Lys	Mp3g22120	Xylogucan endotransglucosylase
Mptar6	G->A	His->Gln	Mp4g05100	E3 ubiquitin ligase
Mptar6	G->A	Gly->Asp	Mp5g11820	
Mptar6	C->T	Ser->Phe	Mp6g12850	
Mptar6	C->T	Asp-->Asn	Mp7g01940	Mp*AHAS*
Mptar6	C->T	Ser->Phe	Mp7g06620	Mitochondrial elongation factor
Mptar6	G->A	Glu->Lys	Mp7g16560	*USP16_45*; ubiquitin carboxyl-terminal hydrolase
Mptar6	C->T	Ser->Leu	Mp8g12080	*SMG7/EST1*
Mptar6	C->T	Arg->Lys	Mp8g13160	RNA helicase
Mptar6	C->T	Pro->Ser	Mp8g14270	
Mptar6	A->G	Leu->Pro	Mp3g19030	Mp*RAD8*
Mptar7	C->T	Glu->Lys	Mp1g06710	*MSH3*; DNA mismatch repair Protein
Mptar7	C->T	Pro->Ser	Mp1g21520	Dynein assembly factor
Mptar7	C->T	Pro->Ser	Mp1g22190	*PUS1*; tRNA pseudouridine38-40 synthase
Mptar7	C->T	Asp->Asn	Mp1g24670	Cyclin
Mptar7	C->T	Gly->Ser	Mp2g01360	
Mptar7	G->A	Ser->Leu	Mp2g21800	ABC transporter
Mptar7	G->A	Asp->Asn	Mp3g16720	
Mptar7	G->A	Pro->Ser	Mp3g23610	
Mptar7	G->A	Arg->*	Mp3g01110	Mp*TIM44L*
Mptar7	C->T	Glu->Lys	Mp3g03070	
Mptar7	G->A	Ser->Leu	Mp3g03600	Lipase
Mptar7	G->A	Leu->Phe	Mp3g09230	LRR apoptotic atpase
Mptar7	G->A	Glu->Lys	Mp4g20820	
Mptar7	G->A	Arg->Lys	Mp5g02870	Protein kinase
Mptar7	C->T	Arg->Gln	Mp5g18320	Phosphoribosylglycinamide formyltransferase
Mptar7	C->T	Pro->Ser	Mp5g21570	Mur ligase
Mptar7	C->T	Gly->Arg	Mp5g22840	Pectin acetylesterase
Mptar7	G->A	Pro->Ser	Mp6g07670	Splicing factor
Mptar7	G->A	Glu->Lys	Mp7g19740	Protein deglycase
Mptar8	G->A	Gly->Glu	Mp1g25950	
Mptar8	C->T	Gly->Asp	Mp1g01470	RAN binding protein
Mptar8	G->A	Pro->Ser	Mp1g29110	Splicing factor
Mptar8	G->A	Glu->Lys	Mp2g23850	E3 ubiquitin ligase
Mptar8	G->A	Glu->Lys	Mp4g05490	ABC transporter
Mptar8	G->A	Pro->Leu	Mp4g13540	
Mptar8	G->A	Glu->Lys	Mp5g04200	Mp*PSAD*
Mptar8	C->T	Leu->Phe	Mp6g07490	PPR
Mptar8	G->A	Pro->Ser	Mp8g07660	*COPII*; vesicle coat complex
Mptar9	C->T	Glu->*	Mp1g00270	LOG
Mptar9	G->A	Ser->Leu	Mp1g02560	Chaperonin
Mptar9	G->A	Ser->Phe	Mp1g22090	
Mptar9	G->A	Ser->Leu	Mp1g25870	*SLC25A42*; mitochondrial solute transport
Mptar9	C->T	Gly->Ser	Mp2g07720	
Mptar9	G->A	Ser->Phe	Mp2g11140	HD7/KNOX
Mptar9	G->A	Arg->Gln	Mp2g21290	Mp*EIF5*
Mptar9	G->A	Gly->Ser	Mp2g24010	
Mptar9	C->T	Pro->Ser	Mp3g00360	Mp1R-MYB2
Mptar9	C->T	Gly->Glu	Mp4g19240	
Mptar9	G->A	Glu->*	Mp5g22800	*PPIL4*; peptidyl-Prolyl cis-trans Isomerase-like 4
Mptar9	C->T	Ala->Val	Mp6g05900	ABC transporter
Mptar9	C->T	Asp->Asn	Mp7g07400	Xyloglucan fucosyltransferase
Mptar9	G->A	Arg->Glu	Mp7g13480	
Mptar9	C->T	Ala->thr	Mp7g12800	GT2 TF MYB like
Mptar9	C->T	Lys->*	Mp8g08400	

Mptar9	G->A	Gly->Val	Mp8g05150	Lipase
Mptar9	C->T	Ala->Thr	Mp8g15440	
Mptar10	G->A	Glu->Lys	Mp1g26570	Hydrolase
Mptar10	G->A	His->Tyr	Mp3g02820	Voltage gated channel
Mptar10	C->T	Cys->Tyr	Mp3g11890	GDP-fucose protein O-fucosyltransferase
Mptar10	C->T	Pro->Ser	Mp3g13870	*PPCS*; phosphopantothenate-cysteine ligase
Mptar10	G->A	Glu->Lys	Mp5g09730	
Mptar10	G->A	Asp->Asn	Mp6g09000	Carbonic anhydrase
Mptar10	C->T	Arg->Glu	Mp6g14430	Cation transport atpase
Mptar10	C->T	Pro->Ser	Mp6g00060	Mp*SRC2*
Mptar10	C->T	Pro->Ser	Mp7g15140	RNA methylase
Mptar10	C->T	Gly->Ser	Mp7g19430	
Mptar11	C->T	Ser->Leu	Mp1g04850	Ribonuclease
Mptar11	G->A	Pro->Leu	Mp1g05680	Kinase
Mptar11	C->T	Glu->Lys	Mp1g08300	Transcription factor
Mptar11	G->A	Leu->Phe	Mp1g11730	Mp*PPR13*
Mptar11	G->A	His->Tyr	Mp1g22070	Ornithine decarboxylase
Mptar11	G->A	Gly->Glu	Mp2g09930	tRNA methyltransferase
Mptar11	C->T	Leu->Phe	Mp2g18500	Peptidase
Mptar11	C->T	Ser->Leu	Mp3g04910	FabZ dehydratase
Mptar11	C->T	Glu->Lys	Mp3g09570	CCD4 related
Mptar11	G->A	Pro->Ser	Mp3g10370	Karyopherin
Mptar11	G->A	Ala->Val	Mp3g15620	*TATD*; DNAse
Mptar11	G->A	His->Tyr	Mp3g23970	Mitochondrial carrier protein
Mptar11	G->A	Ser->Phe	Mp4g13120	RNA helicase
Mptar11	C->T	Glu->Lys	Mp4g15450	Methyltransferase
Mptar11	C->T	Try->*	Mp5g01910	Nucleoside transporter
Mptar11	C->T	Ser->Phe	Mp5g06320	Transcription factor
Mptar11	G->A	Arg->Lys	Mp5g20180	
Mptar11	C->T	Ser->Phe	Mp6g03190	DNA pol subunit II
Mptar11	C->T	Glu->Lys	Mp6g04100	rRNA methyltransferase
Mptar11	C->T	Pro->Ser	Mp6g06190	Munc-13 like
Mptar11	G->A	Ser->Leu	Mp6g12580	DNA repair helicase
Mptar11	C->T	Ser->Phe	Mp6g15570	Kinase/phosphatase
Mptar11	C->T	Arg->Lys	Mp6g18490	*MOT1*
Mptar11	G->A	Leu->Phe	Mp7g18010	MAP4K
Mptar11	G->A	Pro->Leu	Mp7g03220	
Mptar11	C->T	Glu->Lys	Mp8g03730	Peptidoglycan binding
Mptar11	C->T	Leu->Phe	Mp8g15560	RAS
Mptar12	C->T	Gly->Glu	Mp1g05090	Kinase
Mptar12	G->A	Pro->Ser	Mp1g22530	
Mptar12	G->A	Glu->Lys	Mp2g00260	TPR repeat protein
Mptar12	G->A	Ala->Val	Mp2g05930	Ankyrin domain
Mptar12	G->A	Arg->Gln	Mp2g13400	*DRS2*; phospholipid-transporting ATPase
Mptar12	C->T	Gly->Asn	Mp2g25720	*SUPT6H*; transcription elongation factor
Mptar12	G->A	Gly->Asp	Mp6g10360	HSP110
Mptar12	G->A	Pro->Ser	Mp7g19170	Redox protein
Mptar12	C->T	His->Tyr	Mp8g06830	Mp*ARIA*
Mptar12	G->A	Glu->Lys	Mp8g07330	HSPA9
Mptar12	G->A	Try->*	Mp8g07520	DNA helicase
Mptar12	C->T	Gly->Arg	Mp8g07680	Mp*BELL4*
Mptar13	G->A	Pro->Leu	Mp1g16360	Midasin
Mptar13	C->T	Gly->Ser	Mp3g16530	Root cap protein
Mptar13	G->A	Leu->Phe	Mp7g17660	Kinesin-like
Mptar13	G->A	Val->Iso	Mp8g08430	Adenosylmethionine synthetase
Mptar13	G->A	Ser->Leu	Mp8g15020	Spermidine synthase
Mptar13	C->T	Gly->Arg	Mp8g09860	

Supplementary Table S4.2. List of candidate resistance-conferring mutations found in Mp*tar* lines. Candidate resistance-conferring SNPs were identified using an adapted version of the non-allelism based SNP discovery pipeline (Champion *et al.*, 2021).

M. polymorpha gene ID	Evalue	A. tuberculatus gene ID	M. polymorpha gene ID	Evalue	A. tuberculatus gene ID
Mp1g00100	3E-64	AMATA_chromosomes_08764	Mp2g22110	2E-32	AMATA_chromosomes_27616
Mp1g00270	3E-18	AMATA_chromosomes_28258	Mp2g23470	2E-32	AMATA_chromosomes_27762
Mp1g00330	4E-16	AMATA_chromosomes_08194	Mp2g23850	3E-19	AMATA_chromosomes_17494
Mp1g01140	3E-43	AMATA_chromosomes_08487	Mp2g24010	9E-09	AMATA_chromosomes_12748
Mp1g01470	4E-143	AMATA_chromosomes_05941	Mp2g25720	6E-113	AMATA_chromosomes_19753
Mp1g02560	0	AMATA_chromosomes_16892	Mp3g00360	3E-06	AMATA_chromosomes_21322
Mp1g04260	6E-43	AMATA_chromosomes_02214	Mp3g01110	N/A	N/A
Mp1g04850	3E-18	AMATA_chromosomes_05874	Mp3g02220	2E-46	AMATA_chromosomes_23185
Mp1g05090	5E-69	AMATA_chromosomes_26348	Mp3g02820	N/A	N/A
Mp1g05680	3E-151	AMATA_chromosomes_28222	Mp3g02860	1E-61	AMATA_chromosomes_23090
Mp1g06710	2E-74	AMATA_chromosomes_11736	Mp3g03070	7E-20	AMATA_chromosomes_02557
Mp1g08300	N/A	N/A	Mp3g03600	N/A	N/A
Mp1g10330	8E-09	AMATA_chromosomes_11069	Mp3g04910	2E-38	AMATA_chromosomes_01138
Mp1g11730	1E-40	AMATA_chromosomes_18163	Mp3g07260	N/A	N/A
Mp1g16360	0	AMATA_chromosomes_20875	Mp3g07830	2E-10	AMATA_chromosomes_15558
Mp1g17110	6E-06	AMATA_chromosomes_05784	Mp3g09230	1E-37	AMATA_chromosomes_17399
Mp1g18300	8E-34	AMATA_chromosomes_05048	Mp3g09570	7E-13	AMATA_chromosomes_08049
Mp1g20550	N/A	N/A	Mp3g10370	4E-06	AMATA_chromosomes_03396
Mp1g21520	N/A	N/A	Mp3g11890	9E-65	AMATA_chromosomes_19847
Mp1g22070	6E-97	AMATA_chromosomes_05314	Mp3g13070	N/A	N/A
Mp1g22090	N/A	N/A	Mp3g13360	N/A	N/A
Mp1g22190	1E-50	AMATA_chromosomes_08999	Mp3g13870	9E-21	AMATA_chromosomes_08910
Mp1g22530	N/A	N/A	Mp3g15620	8E-94	AMATA_chromosomes_28085
Mp1g24670	N/A	N/A	Mp3g16530	7E-72	AMATA_chromosomes_14179
Mp1g25870	2E-59	AMATA_chromosomes_24997	Mp3g16720	N/A	N/A
Mp1g25950	N/A	N/A	Mp3g19030	9E-31	AMATA_chromosomes_14111
Mp1g26460	1E-20	AMATA_chromosomes_06311	Mp3g20420	N/A	N/A
Mp1g26570	5E-30	AMATA_chromosomes_10752	Mp3g22120	9E-70	AMATA_chromosomes_24935
Mp1g29110	4E-12	AMATA_chromosomes_06548	Mp3g22320	N/A	N/A
Mp2g00260	3E-35	AMATA_chromosomes_06284	Mp3g23610	N/A	N/A
Mp2g01360	N/A	N/A	Mp3g23970	1E-51	AMATA_chromosomes_05515
Mp2g03680	6E-20	AMATA_chromosomes_13392	Mp4g02430	0	AMATA_chromosomes_01070
Mp2g04330	7E-25	AMATA_chromosomes_13154	Mp4g05100	N/A	N/A
Mp2g04470	2E-53	AMATA_chromosomes_17598	Mp4g05490	0	AMATA_chromosomes_24939
Mp2g05240	N/A	N/A	Mp4g06580	N/A	N/A
Mp2g05930	N/A	N/A	Mp4g07230	N/A	N/A
Mp2g07440	N/A	N/A	Mp4g12270	N/A	N/A
Mp2g07720	2E-37	AMATA_chromosomes_15637	Mp4g13120	6E-35	AMATA_chromosomes_18911
Mp2g09930	4E-13	AMATA_chromosomes_13709	Mp4g13540	N/A	N/A
Mp2g11140	N/A	N/A	Mp4g15450	2E-23	AMATA_chromosomes_14527
Mp2g12440	2E-61	AMATA_chromosomes_06282	Mp4g15540	N/A	N/A
Mp2g13400	2E-174	AMATA_chromosomes_19890	Mp4g16020	N/A	N/A
Mp2g15090	2E-19	AMATA_chromosomes_06439	Mp4g17100	6E-14	AMATA_chromosomes_14461
Mp2g16550	4E-60	AMATA_chromosomes_09100	Mp4g19240	N/A	N/A
Mp2g17160	5E-25	AMATA_chromosomes_08006	Mp4g20820	N/A	N/A
Mp2g17840	6E-64	AMATA_chromosomes_19162	Mp4g21500	N/A	N/A
Mp2g18500	2E-47	AMATA_chromosomes_06232	Mp4g21980	N/A	N/A
Mp2g20920	5E-49	AMATA_chromosomes_12166	Mp4g22890	2E-46	AMATA_chromosomes_15637
Mp2g21290	**3E-101**	**AMATA_chromosomes_04173**	Mp5g01910	5E-34	AMATA_chromosomes_18027
Mp2g21320	3E-26	AMATA_chromosomes_14498	Mp5g02280	9E-38	AMATA_chromosomes_10050
Mp2g21800	0E+00	AMATA_chromosomes_24939	Mp5g02870	9E-12	AMATA_chromosomes_10437

M. polymorpha gene ID	E value	A. tuberculatus gene ID	M. polymorpha gene ID	E value	A. tuberculatus gene ID
Mp5g04200	5E-57	AMATA_chromosomes_05225	Mp7g07400	1E-47	AMATA_chromosomes_05588
Mp5g05010	2E-100	AMATA_chromosomes_12302	Mp7g11880	2E-08	AMATA_chromosomes_27315
Mp5g06320	N/A	N/A	Mp7g12800	N/A	N/A
Mp5g09730	N/A	N/A	Mp7g13480	N/A	N/A
Mp5g11820	N/A	N/A	Mp7g15140	N/A	N/A
Mp5g18320	4E-23	AMATA_chromosomes_08376	Mp7g16560	2E-46	AMATA_chromosomes_19855
Mp5g20180	3E-24	AMATA_chromosomes_19110	Mp7g17660	3E-28	AMATA_chromosomes_07395
Mp5g21570	N/A	N/A	Mp7g18010	2E-41	AMATA_chromosomes_12970
Mp5g22100	1E-20	AMATA_chromosomes_19480	Mp7g19170	8E-28	AMATA_chromosomes_08704
Mp5g22800	2E-14	AMATA_chromosomes_30348	Mp7g19430	N/A	N/A
Mp5g22840	1E-17	AMATA_chromosomes_04076	Mp7g19740	3E-23	AMATA_chromosomes_14099
Mp5g23420	2E-26	AMATA_chromosomes_26542	Mp8g03730	1E-11	AMATA_chromosomes_00181
Mp6g00060	2E-10	AMATA_chromosomes_12556	Mp8g04820	3E-38	AMATA_chromosomes_05355
Mp6g03190	1E-18	AMATA_chromosomes_06162	Mp8g05150	6E-103	AMATA_chromosomes_20463
Mp6g03430	4E-75	AMATA_chromosomes_03468	**Mp8g06830**	**3E-35**	**AMATA_chromosomes_28414**
Mp6g04100	1E-39	AMATA_chromosomes_29482	Mp8g06930	N/A	N/A
Mp6g05900	2E-79	AMATA_chromosomes_14761	Mp8g07330	0E+00	AMATA_chromosomes_06235
Mp6g06190	N/A	N/A	Mp8g07520	2E-50	AMATA_chromosomes_29898
Mp6g07490	9E-21	AMATA_chromosomes_29378	Mp8g07660	N/A	N/A
Mp6g07670	9E-167	AMATA_chromosomes_28960	Mp8g07680	N/A	N/A
Mp6g09000	1E-07	AMATA_chromosomes_20182	Mp8g08400	N/A	N/A
Mp6g10360	3E-169	AMATA_chromosomes_00483	Mp8g08430	0	AMATA_chromosomes_03472
Mp6g10370	5E-13	AMATA_chromosomes_23870	Mp8g09190	1E-52	AMATA_chromosomes_24931
Mp6g12540	4E-47	AMATA_chromosomes_06059	Mp8g09860	N/A	N/A
Mp6g12580	9E-134	AMATA_chromosomes_06509	Mp8g10040	1E-14	AMATA_chromosomes_25545
Mp6g12850	2E-11	AMATA_chromosomes_01982	Mp8g12080	6E-53	AMATA_chromosomes_12212
Mp6g13550	3E-63	AMATA_chromosomes_14868	Mp8g12790	1E-61	AMATA_chromosomes_19019
Mp6g14430	9E-09	AMATA_chromosomes_10074	Mp8g13160	1E-35	AMATA_chromosomes_06482
Mp6g15570	3E-09	AMATA_chromosomes_14081	Mp8g13300	8E-103	AMATA_chromosomes_15827
Mp6g18490	0	AMATA_chromosomes_28107	Mp8g13400	N/A	N/A
Mp6g19260	**2E-33**	**AMATA_chromosomes_28406**	Mp8g14270	N/A	N/A
Mp7g01000	0	AMATA_chromosomes_05165	Mp8g14840	4E-20	AMATA_chromosomes_05860
Mp7g01020	N/A	N/A	**Mp8g15020**	**5E-32**	**AMATA_chromosomes_08316**
Mp7g01940	0	AMATA_chromosomes_26000	Mp8g15440	N/A	N/A
Mp7g03220	N/A	N/A	Mp8g15560	1E-25	AMATA_chromosomes_14405
Mp7g06620	0	AMATA_chromosomes_04049	Mp8g18770	2E-56	AMATA_chromosomes_12448

Supplementary Table S4.3. List of genes in which there is a candidate resistance-conferring SNP in Mp*tar* lines and the corresponding *A. tuberculatus* homologue. *A. tuberculatus* homologues were identified via a tBLASTn search against the *A. tuberculatus* genome assembly by (Kreiner *et al.*, 2019). Only homologues with an E value < 1 E -5 were retained. Genes highlighted in bold are those for which the *A. tuberculatus gene* has been associated with NTSR to glyphosate (Kreiner *et al.*, 2021).

Chapter 5: Functional characterisation of a novel mechanism of non-target site resistance conferred by loss-of-function of Mp*RAD8*

5.1. Abstract

Although non-target site herbicide resistance (NTSR) in weeds is increasingly observed in the field, few of the molecular mechanisms underlying NTSR have been identified. This is partly due to our lack of knowledge of the types of genes involved in NTSR, and partly due to the difficulty of functionally characterising candidate mechanisms of NTSR in weeds. In this chapter, I used a reverse genetic approach in the model species *M. polymorpha* to demonstrate that a loss-of-function of Mp3g19030 (Mp*RAD8*) confers resistance to the herbicides thaxtomin A (TXTA) and isoxaben. I also found that Mp*rad8* loss-of-function lines overproduce reactive oxygen species (ROS), and that the actions of ROS and TXTA in the cell are antagonistic; overgeneration of ROS in Mp*rad8* lines may therefore increase their resistance to TXTA. Furthermore, I found that Mp*rad8* loss-of-function mutant lines produce less of a predicted TXTA metabolite than wild-type lines, which may contribute to their TXTA resistance. My approach combining forward and reverse genetics in *M. polymorpha* allowed me not only to identify a novel mechanism of NTSR involving loss-of-function of Mp*RAD8*, a gene not previously associated with NTSR, but also to undertake a phenotypic analysis of Mp*rad8* lines and propose several hypotheses as to how the phenotypes conferred by loss-of-function of Mp*RAD8* could lead to resistance.

5.2. Introduction

In the previous chapter, I identified SNPs most likely to confer resistance to the herbicide thaxtomin A (TXTA) in 11 *M. polymorpha* mutants (Mp*tar*). Three of these SNPs were in Mp3g19030, which is the *M. polymorpha* homologue of the *C. elegans* gene *RAD8*. It is therefore likely that a mutation in Mp3g19030 (Mp*RAD8*) confers resistance to TXTA. In this chapter, I used targeted mutagenesis in wild-type *M. polymorpha* to confirm that loss-of-function mutations in Mp*RAD8* confer resistance to TXTA, and to functionally characterise the effect of loss of Mp*RAD8* function.

The *RAD8* gene was originally identified in *Caenorhabditis elegans* as a UV-B radiation-sensitive mutant isolated from an EMS mutagenesis screen (Hartman and Herman, 1982). *C. elegans rad8* mutants are more sensitive to the oxidative stress conferred by methyl viologen, also known as paraquat, than wild-type (Ishii *et al.*, 1993). Paraquat diverts electrons from the chloroplast or mitochondria electron transport chains to O_2 forming superoxide radicals ($\cdot O_2^-$), a form of reactive oxygen species (ROS) which is toxic and can cause cell death by peroxidation of lipids in cell membranes (Fukushima *et al.*, 1993, Hawkes, 2014). The overproduction of superoxide anions in *rad8* mutants in *C. elegans* causes hypersensitivity to paraquat; mutants of the *M. musculus RAD8* homologue *RTN4IP1* also overproduce ROS (Fujii *et al.*, 2011, Park *et al.*, 2021). The human *RAD8* homologue *RTN4IP1* has been shown to be a mitochondrial NADPH oxidoreductase (Park *et al.*, 2021). Interactome profiling of *H. sapiens* cells showed that the RTN4IP1 protein interacts with components of the coenzyme Q (CoQ) biosynthetic pathway, and CoQ levels in *rtn4ip1* knockout cells are lower than wild type cells, suggesting that RTN4IP1/RAD8 is involved in CoQ biosynthesis. CoQ is an electron carrier involved in the

mitochondrial electron transport chain; the overproduction of ROS in *rad8* mutants may therefore be due to inhibition of biosynthesis of CoQ disrupting the flow of electrons through the electron transport chain, which then react with O_2 to form superoxide radicals (Park *et al.*, 2021).

Several herbicides – including paraquat, PPO inhibitors, and glufosinate – act by causing increased levels of ROS in plant cells, leading to cell death (Hawkes, 2014, Dayan *et al.*, 2019b, Takano *et al.*, 2020). It could therefore be considered unusual for a mutation such as that in *RAD8* which causes overproduction of ROS to confer herbicide resistance. However, in the specific case of TXTA, the only known mechanism of resistance in the literature – loss-of-function of *PAM16* – causes overproduction of ROS (Huang *et al.*, 2013). Furthermore, the addition of exogenous hydrogen peroxide (a form of ROS) to wild-type *A. thaliana* cells grown in culture confers significant resistance to TXTA (Awwad *et al.*, 2019). It is therefore possible that an increase in ROS at sub-lethal levels conferred by a mutation in *RAD8* could be a novel mechanism of non-target site resistance to TXTA.

In this chapter, I undertook a phylogenetic analysis of homologues of RAD-8/RTN4IP1 and found that Mp3g19030 (Mp*RAD8*) is the closest homologue of *H. sapiens, C. elegans,* and *M. musculus RTN4IP1/RAD8*, and that the residues mutated in MpRAD8 in the 3 TXTA-resistant mutants are highly conserved. I then used CRISPR-Cas9 mutagenesis to generate 19 Mp*rad8* putative loss-of-function mutants. I found that these gene edited Mp*rad8* loss-of-function mutants are significantly resistant to TXTA, as well as isoxaben, and that putative loss of Mp*RAD8* function leads to slower growth in control conditions. I found that 2 independent Mp*rad8* putative loss-of-function mutants generated by CRISPR-Cas9

mutagenesis, and at least 3 TXTA-resistant UV-B lines, produce higher levels of ROS than wild-type *M. polymorpha* lines, and that TXTA and ROS have antagonistic effects in vivo. Finally, I found that putative loss-of-function of Mp*RAD8* inhibits the production of a TXTA metabolite produced in wild-type plants. I have therefore successfully identified and functionally characterised a novel mechanism of non-target site resistance to the herbicide TXTA.

5.3. Materials and Methods

5.3.1. Phylogenetic analysis of *RAD8* homologues

Orthologues of the *H. sapiens* gene *RTN4IP1.1* were identified by protein BLASTp search against the reference proteomes of various species (Table 5.1). Only orthologues with an E value less than 1E-5 were used to construct the tree.

Orthologues were aligned via the L-INS-i strategy using MAFFT version 7 (Katoh *et al.*, 2019). The alignment was trimmed using BioEdit7.2. A maximum likelihood tree was constructed with PhyML 3.0 using an estimated gamma distribution parameter and the LG model of amino acid substitution. A non-parametric approximate likelihood ratio test based on a Shimodaira-Hasegawa-like procedure was used to calculate branch support values using PhyML 3.0 (Guindon *et al.*, 2010). The tree was rooted with the *Saccharomyces cerevisiae* Yim1p protein sequence.

5.3.2. Guide RNA design

Guide RNAs were designed which would anneal to different parts of Mp*RAD8* (Mp3g19030) for the Cas9 nuclease to introduce targeted double strand breaks. Guide RNAs were placed 5' of an "NGG" site (PAM sequence) as required by the CRISPR-Cas9 system (Sugano *et al.*, 2014). The guide RNA sequences are as follows:

sgRNA	Sequence
1	CAAATGTTTAGGTCCGTCG
2	GTGGAGAAATTTCAGCTGTG
3	CGGCCATTACCTCACTTTGC

5.3.3. Cloning of CRISPR-Cas9 vectors

See Chapter 2 Section 2.3.7.

5.3.4. Agrobacterium-mediated transformation of *M. polymorpha* spores

See Chapter 2 Section 2.3.8.

5.3.5. Genotyping potential mutants generated by CRISPR-Cas9 mutagenesis

See Chapter 2 Section 2.3.9.

5.3.6. Gemmaling dose-response assays

See Chapter 2 Section 2.3.5.

5.3.7. DAB staining

3,3'-diaminobenzidine (DAB) (D8001) in powder form was obtained from Sigma Aldrich. The DAB staining solution was prepared as in (Daudi and O'Brien, 2012). *M. polymorpha* gemmae were incubated in 3 ml solution in 24 well plates and vacuum infiltrating for 5 minutes. The plates were covered in tin foil and incubated for 1.5 hours shaking at 100 rpm. After incubation, the staining solution was replaced by bleaching solution as set out in (Daudi and O'Brien, 2012); gemmae were bleached for 2 hours. Bleached gemmae were imaged using a Keyence VHX-7000.

5.3.8. Ferric-xylenol orange (FOX) assay

A modified FOX assay was carried out as set out in (Li, 2019). The FOX working solution was prepared as follows:

500 µM ammonium ferrous sulphate

400 µM xylenol orange

200 mM sorbitol

25 mM H_2SO_4

Twelve-day old gemmalings were frozen and ground in liquid nitrogen and homogenised in 200 mM perchloric acid. Samples were centrifuged at 1000g for 5 minutes at 4 ºC. 500 µl of the supernatant were mixed with 500 µl FOX working solution. Samples were incubated at room temperature in the dark for 30 minutes followed by quantification of the absorbance at 560 nm using an Ultrospec 3100 pro spectrophotometer. The concentration of H_2O_2 in each sample was calculated using a calibration curve of known concentrations of H_2O_2 quantified using the same protocol.

5.3.9. Metabolomic analysis of pure and modified TXTA in *M. polymorpha* thallus

Gemmae were grown on autoclaved cellophane on solid ½ Gamborg medium supplemented with 0.1 % DMSO for 14 days at 23 °C in 24 h light. Gemmalings were then transferred (by transfer of the cellophane disc) onto solid ½ Gamborg medium supplemented with either 0.1 % DMSO or 5 µM TXTA and grown in these conditions for 2 days at 23 °C in 24 h light. Treated and untreated gemmalings were harvested by flash freezing in liquid nitrogen.

Frozen tissue samples were ground in liquid nitrogen and homogenised in ice-cold extraction solvent (2:1:1 methanol:acetonitrile:H_2O, v/v) for 2 min at 4 °C followed by incubation at -20 °C for one hour. Samples were centrifuged at full speed at 4 °C for

3 mins. Supernatants were collected and kept at -20 °C. Pellets were redissolved in ice cold 80 % (v/v) methanol and homogenised for 1 min at 4 °C followed by incubation at -20 °C for one hour. Samples were centrifuged at full speed at 4 °C for 3 mins. Supernatants were collected and added to the supernatants from the first extraction step. Samples were incubated at -20 °C for 2 hours. Samples were then centrifuged at full speed at 4 °C for 10 mins. Supernatants were collected and shock frozen in liquid nitrogen.

Reversed phase chromatography directly coupled to mass spectrometry (LC-MS/MS) analysis of samples was performed by the Metabolomics Facility at Vienna BioCenter Core Facilities (VBCF), member of the Vienna BioCenter (VBC), Austria. Thaxtomin A was analysed by injecting 1 µl of the metabolite extract onto a Kinetex (Phenomenex) C18 column (100 Å, 150 x 2.1 mm) connected with the respective guard column, and using a 4-minute-long linear gradient from 96 % A (1 % acetonitrile, 0.1 % formic acid in water) to 90 % B (0.1 % formic acid in acetonitrile). Detection and quantification was done by LC-MS/MS, employing the selected reaction monitoring (SRM) mode of a TSQ Altis mass spectrometer (Thermo Fisher Scientific), using the following transitions in the positive ion mode: 439.1 *m/z* to 247.1 *m/z* and 439.1 *m/z* to 219.1 *m/z*. Quantification was done by external calibration using an authentic standard. The putative Thaxtomin A metabolite was discovered by analysing the samples with precursor ion scanning for the dominant fragment ions of the Thaxtomin A standard. Here only one compound was evident with a *m/z* of 394. This metabolite was analysed in the samples using the transitions 394.1 *m/z* to 247.1 *m/z* and 394.1 *m/z* to 219.1 *m/z*. Data interpretation was performed using TraceFinder (Thermo Fisher Scientific).

5.3.10. Primers

Primer	Sequence	Use
GR8_1Fw	ACTTGTGTTCGGGTGGAGTT	Genotyping Mp*rad8* CRISPR mutants (sgRNA1)
GR8_1Rv	ACATGAGCGTCCAAGAAATCA	Genotyping Mp*rad8* CRISPR mutants (sgRNA1)
GR8_2Fw	GACTGTCGGAATTGCCCTCA	Genotyping Mp*rad8* CRISPR mutants (sgRNA2)
GR8_2Rv	CCTGCTGCGGAGTATTTGAG	Genotyping Mp*rad8* CRISPR mutants (sgRNA2)
GR8_3Fw	TCAAAGGGATGAGGTAGACATTT	Genotyping Mp*rad8* CRISPR mutants (sgRNA3)
Gr8_3Rv	CGTTCCCCGTATTGCTGTG	Genotyping Mp*rad8* CRISPR mutants (sgRNA3)

5.4. Results

5.4.1. There are SNPs in conserved residues of Mp*RAD8* in Mptar2, Mp*tar*4 and Mp*tar*6 mutants

I generated 13 TXTA-resistant *M. polymorpha* mutant lines (Mp*tar* lines) via UV-B mutagenesis (Chapter 3). I found that 3 of these lines (Mp*tar*2, Mp*tar*4, and Mp*tar*6) each have a candidate resistance-conferring SNP in Mp3g19030, a homologue of the *C. elegans RAD8* gene (Chapter 4). I therefore hypothesised that a mutation in Mp3g19030 (Mp*RAD8*) can lead to resistance to TXTA.

Mp*tar*2, Mp*tar*4, and Mp*tar*6 each have only one SNP in Mp*RAD8*. If these SNPs cause changes in conserved amino acids that are important for MpRAD8 function, they are likely to impair the function of the protein. Amino acids which are important to the function of a protein are more likely to be conserved across species. I therefore hypothesised that if the residues mutated in the MpRAD8 protein in Mp*tar*2, Mp*tar*4 and Mp*tar*6 are highly conserved amongst *RAD8* homologues, then the SNPs in Mp*tar*2, Mp*tar*4 and Mp*tar*6 are likely to cause strong loss-of-function of Mp*RAD8* in these lines.

To determine whether the residues mutated in Mp*tar*2, Mp*tar*4, and Mp*tar*6 are conserved, I compared the protein sequence of MpRAD8 and its homologues in a variety of species. I collected protein sequences similar to the human homologue of *RAD8* (*RTN4IP1*) from 9 species using the BlastP algorithm to search their proteomes (Table 5.1). These species included *Homo sapiens*, *Saccharomyces cerevisiae*, *Mus musculus*, *Caenorhabditis elegans*, *Marchantia polymorpha*, *Arabidopsis thaliana*, *Selaginella moellendorffii*, *Azolla filiculoides*, and *Picea abies*. The *RTN4IP1* homologue (*Yim1p*) from the yeast *Saccharomyces cerevisiae* was

used to root the tree. I aligned the protein sequences via the L-INS-i strategy in MAFFT.

Mp*tar*2 has a glycine → glutamic acid amino acid change at position 396 (G396E); Mp*tar*4 has a glycine → arginine amino acid change at position 402 (G402R); and Mp*tar*6 has a leucine → proline amino acid change at position 708 (L708P). Based on the alignment of RAD8 protein homologues, the glycine residues at positions 396 and 402 mutated in Mp*tar*2 and Mp*tar*4 respectively are highly conserved (Fig. 5.1). The residue at position 708 mutated in Mp*tar*6 is less highly conserved, however the equivalent residue in each homologue broadly has the same chemical properties: most of the homologues have leucine, methionine, valine, isoleucine, or phenylalanine at this position, which all have a hydrophobic side chain (Fig. 5.1). In Mp*tar*6 the leucine residue is mutated to a proline which is nonpolar and is the only cyclic amino acid, so this mutation likely causes a change in the 3D structure of the peptide. These data demonstrate that the SNPs in Mp*tar*2, Mp*tar*4 and Mp*tar*6 are found in residues which are highly conserved across homologues of Mp*RAD8*, and are therefore likely to lead to strong loss-of-function.

Organism	BLAST tool	Number of *RTN4IP1* homologues (E < 1E-5)
Homo sapiens	NCBI	7
Saccharomyces cerevisiae	NCBI	5
Caenorhabditis elegans	Wormbase	5
Mus musculus	NCBI	4
Marchantia polymorpha	marchantia.info	7
Arabidopsis thaliana	TAIR	7
Selaginella moellendorffii	NCBI	8
Picea abies	Congenie	6
Azolla filiculoides	Fernbase	7

Table 5.1. Species included in the phylogenetic analysis of *RTN4IP1* orthologues.
Proteins similar to RTN4IP1.1 (*H. sapiens*) were identified via BLASTp search of proteomes from these 9 species. Only homologues with an E value < 1 E-5 were included in the analysis.

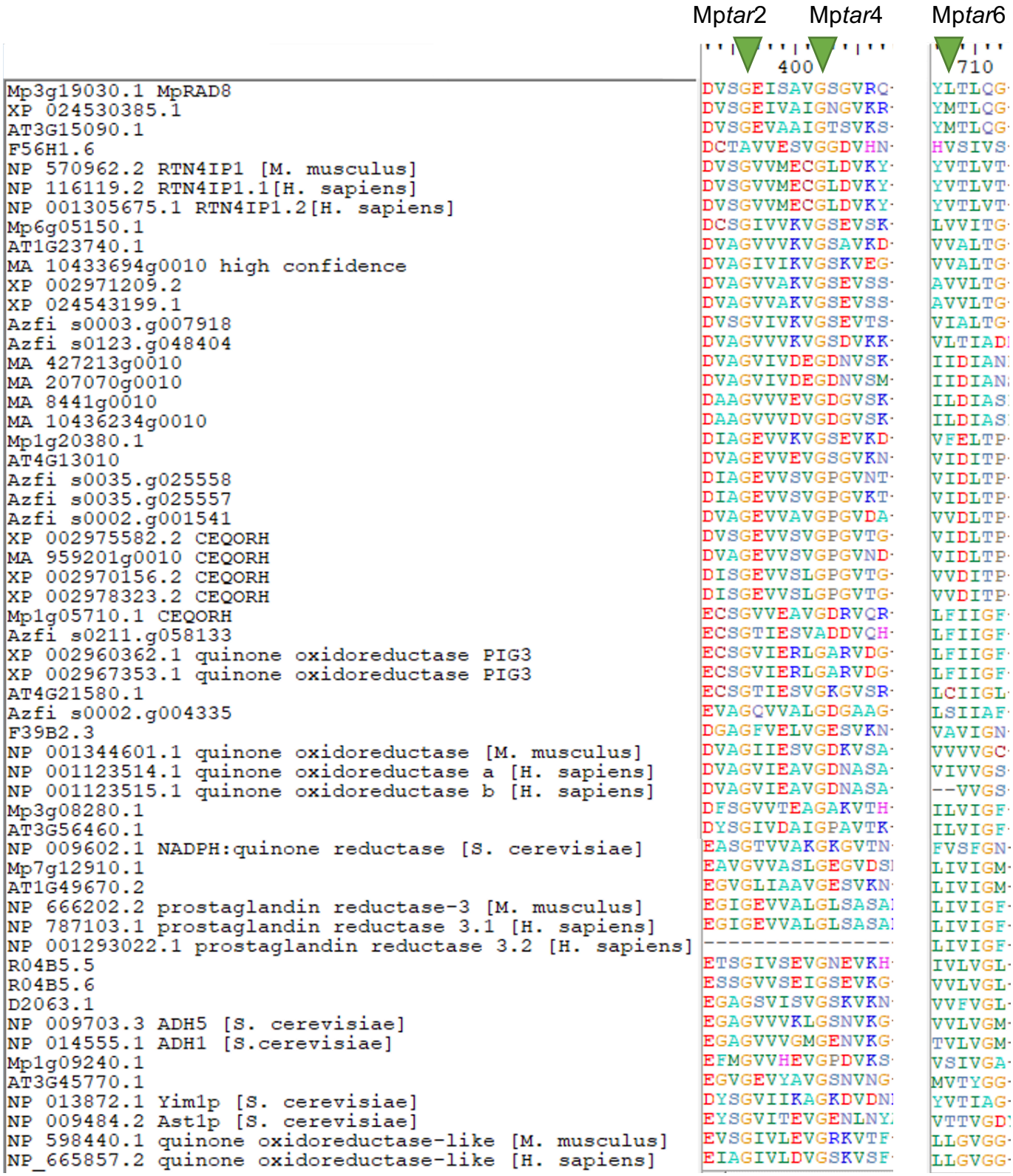

Fig. 5.1 Amino acid alignment of regions of RTN4IP1 (RAD8) homologues from a variety of species. Homologues of *RTN4IP1* from *Homo sapiens* were identified by protein BLAST search (E value < 1E-5) against the reference proteomes of various species (Table 5.1). Homologues were aligned via the L-INS-i strategy using MAFFT version 7. Green tick marks represent the amino acids mutated in Mp*tar*2, Mp*tar*4, and Mp*tar*6.

5.4.2. Mp3g19030 (Mp*RAD8*) is a member of the clade that is sister to the monophyletic group containing *H. sapiens RTN4IP1* and *C. elegans RAD8*

The most detailed functional characterisation of *RAD8/RTN4IP1* has been conducted in *C. elegans*, *H. sapiens* and *M. musculus*. The *H. sapiens*, *M. musculus* and *C. elegans* proteins with the highest sequence similarity to Mp3g019030 based on BLASTp searches of their proteomes are RTN4IP1.1 (E value 4 x 10^{-55}), RNT4IP1 (E value 1 x10^{-60}) and RAD8 (E value 2 x 10^{-21}) respectively. I therefore refer to Mp3g019030 as Mp*RAD8*. However, the evolutionary relationships between Mp3g019030 and *RAD8* homologues is unclear from sequence similarity searches. To clarify the evolutionary relationships between Mp3g19030 (Mp*RAD8*) and other *RAD8* homologues, I conducted a phylogenetic analysis. I trimmed the amino acid alignments of *RAD8* homologues (Section 5.4.1) to remove non-conserved regions and constructed a maximum likelihood tree using a non-parametric approximate likelihood ratio test based on a Shimodaira-Hasegawa-like procedure to calculate node support values in PhyML 3.0 (Guindon *et al.*, 2010) (Fig. 5.2).

I rooted the tree using the *S. cerevisiae RAD8* homologue identified by BLASTp, *Yim1p* (E value 4 x10^{-20}) (Fig. 5.2). The first branch following another yeast homologue (Ast1p) is a well-supported monophyletic group of plant-specific genes from *A. thaliana*, *A. filiculoides*, *P. abies*, *M. polymorpha*, and *S. moellendorffii* (support value 0.9999). These genes are derived from a gene in the common ancestor of land plants. Several genes in this group are annotated as 2-methylene-furan-3-one reductases. This monophyletic group also contains the *P. abies* and *A. filiculoides* homologues of *RTN4IP1* as identified by BLASTp (MA_427213g0010; E value 1.85 x 10^{-41}, and Azfi_s0123.g048404; E value 1 x 10^{-44}).

Two monophyletic groups originate at the next node. However, these groups are not well supported (support value 0.5025). One of these monophyletic groups contains Mp3g19030 (Mp*RAD8*), as well as the closest *RTN4IP1* homologues from *A. thaliana, S. moellendorffii, C. elegans, H. sapiens* and *M. musculus*. Mp3g19030 (Mp*RAD8*) and the closest *A. thaliana* and *S. moellendorffii* orthologues to *RTN4IP1* (AT3G15090.1; E value 6 x 10^{-54}, and XP_024530385.1; E value 1 x 10^{-46}) are in a well-supported sister group to a group containing the *RAD8/RTN4IP1* genes from *H. sapiens* (*RTN4IP1.1*; E value 0), *M. musculus* (*RTN4IP1*; E value 0), and *C. elegans* (*RAD8*; E value 4 x 10^{-63}) (Fig. 5.2) (support value 0.9864). I also found that the common ancestor of these groups likely underwent a plant-specific duplication to form the chloroplast envelope quinone oxidoreductase homologues (*CEQORH*); the branch containing the *CEQORH* homologues is a sister group to the monophyletic group containing the *RAD8/RTN4IP1* genes from *H. sapiens*, *M. musculus*, and *C. elegans*, although this node is not well supported (support value 0.5576) (Fig. 5.2).

The second monophyletic group from the node with a support value of 0.5025 contains a well-supported branch of mammalian quinone oxidoreductase-like genes (support value 0.9223), which is a sister group to a well-supported branch containing two monophyletic groups (support value 0.9913). The first of these monophyletic groups contains a branch with a *M. polymorpha* gene and two *C. elegans* genes which is a sister group to a monophyletic group containing genes annotated as quinone oxidoreductases. The second of these monophyletic groups contains a well-supported first branch with an *A. thaliana* NADPH:quinone reductase and an unannotated *M. polymorpha* gene (support value 0.9593). This is a sister group to a poorly supported branch (support value 0.2886) containing two groups: one group contains a *S. cerevisiae* NADH:quinone reductase and an *A. thaliana* gene, and the

other group contains a branch with two *S. cerevisiae* alcohol dehydrogenases and a *C. elegans* gene (support value 0.7753), and a branch with a *M. polymorpha* and an *A. thaliana* gene sister to mammalian prostaglandin reductases (support value 0.9999). I conclude that this clade, which is sister to the *RAD8/CEQORH* clade, contains a number of genes encoding enzymes which have similar protein sequences and activities to *RTN4IP1* such as quinone oxidoreductases.

This analysis shows that a variety of *RAD8* homologues are present in different eukaryotes, with enzymatic activities similar to that of *RAD8* (oxidoreductases, and in some cases NADPH oxidoreductases). Mp3g19030 (Mp*RAD8*) is found in a sister group to a monophyletic group containing the *RAD8/RTN4IP1* genes from *C. elegans*, *H. sapiens* and *M. musculus*, so these genes had a recent common ancestor. Because Mp3g19030 is the most closely related gene to *RAD8/RTN4IP1* in the *M. polymorpha* genome and because of the topology of the *RAD8/RTN4IP1* gene tree, I shall refer to it as Mp*RAD8*.

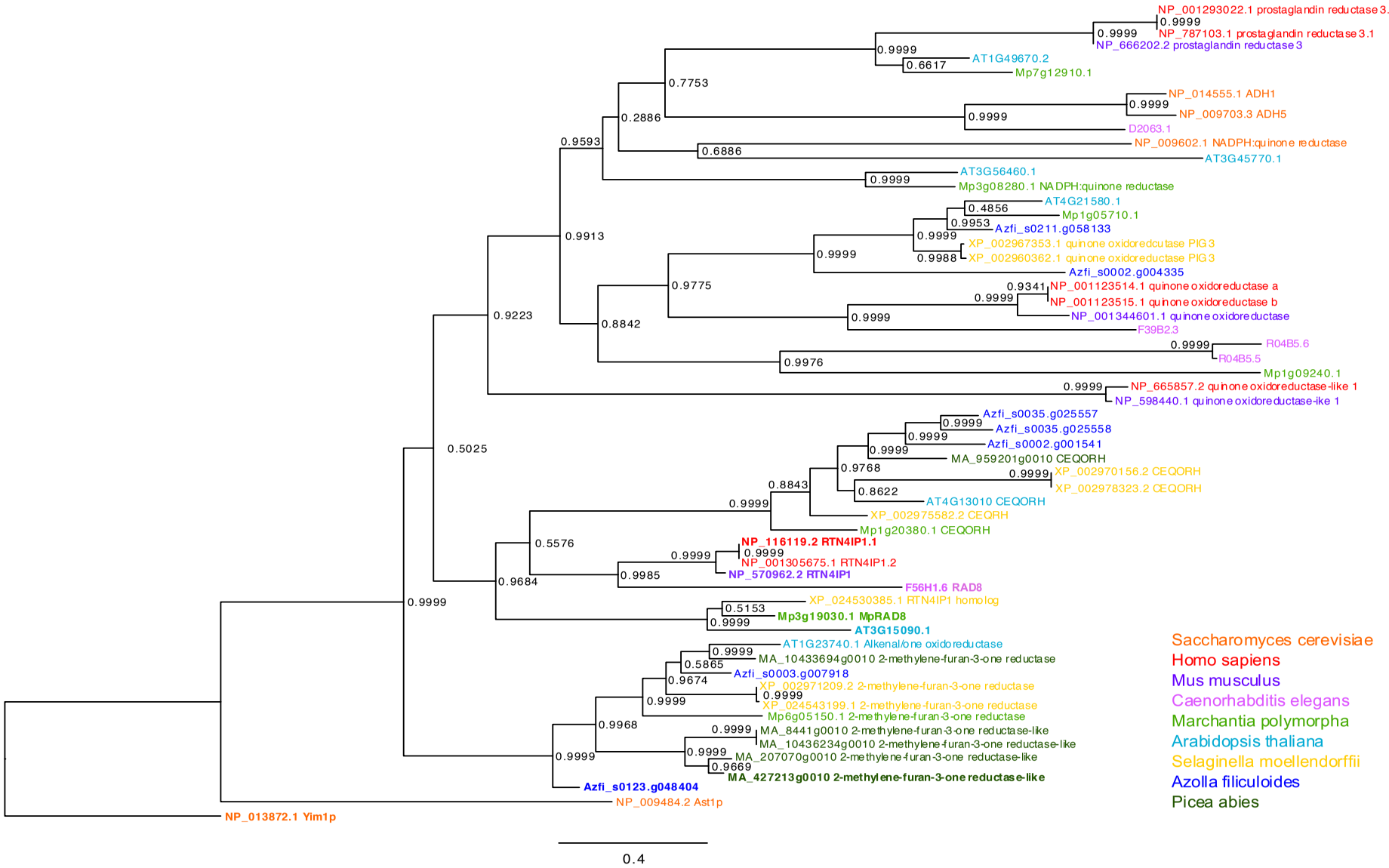

Fig. 5.2. Phylogenetic analysis of the RAD8 protein. A phylogenetic tree (rooted with *Yim1p* from *S. cerevisiae*) of a maximum likelihood analysis by PhyML 3.0 using an estimated gamma distribution parameter, the LG model of amino acid substitution and a non-parametric approximate likelihood ratio test based on a Shimodaira-Hasegawa-like procedure to calculate branch support values (Guindon *et al.*, 2010). Stars represent *H. sapiens RTN4IP1* and *M. polymorpha* Mp3g0190s0 (Mp*RAD8*). Genes in bold are those annotated as the closest homologues of *H. sapiens RTN4IP1*.

5.4.3. Nineteen Mp*rad8* putative loss-of-function mutants were generated using CRISPR-Cas9 mutagenesis

Mp*tar*2, Mp*tar*4, and Mp*tar*6 each have candidate TXTA-resistance-conferring SNPs in conserved residues in Mp*RAD8* (Fig. 5.1). These SNPs are likely to cause strong loss-of-function, so I hypothesised that loss-of-function of Mp*RAD8* would confer resistance to TXTA. To test this hypothesis, I generated Mp*rad8* mutants using CRISPR-Cas9 mutagenesis. I designed a guide RNA (sgRNA 1) at the beginning of the gene to induce frameshifts leading to strong loss-of-function (Fig. 5.3). I also designed 2 guide RNAs (sgRNA 2 and sgRNA 3) to target the regions of the gene mutated in Mp*tar*2, Mp*tar*4, and Mp*tar*6 to try and replicate the putative strong loss-of-function mutations in these lines (Fig. 5.3). The guide RNAs were cloned into vectors containing the Cas9 coding sequence and transformed into *A. tumefaciens* (Fig. 5.4). Wild-type *M. polymorpha* spores (from a cross between Tak-1 and Tak-2) were transformed with the *A. tumefaciens* strains carrying the CRISPR-Cas9 constructs, and positive transformants were selected for and genotyped. In total, 19 Mp*rad*8 mutants were generated with mutations around sgRNA 1, sgRNA 2 and sgRNA 3 (Table 5.2, Fig. 5.5). I predicted the protein sequence of Mprad8 in each Mp*rad8* mutant line based on the mutations induced by the CRISPR-Cas9 complex (Fig. 5.5). I found 5 mutants with predicted indels fewer than 15 amino acids in frame (Mp*rad8*^{GE158}, Mp*rad8*^{GE1511}, Mp*rad8*^{GE1517}, Mp*rad8*^{GE1535}, Mp*rad8*^{GE1536}), which I classed as putative weak loss-of-function. The remaining 14 mutants had predicted frameshifts or early truncations; I classed these as putative strong loss-of-function. However, since the function of the RAD8 protein was not tested in these lines, the mutations are only predicted to cause loss-of-function.

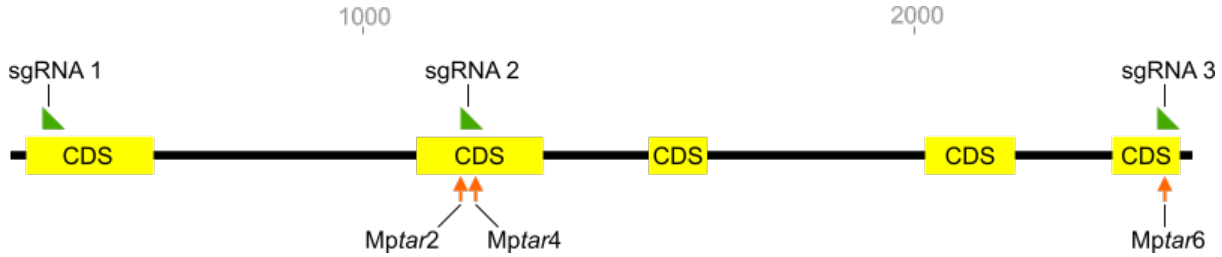

Fig. 5.3. Regions of the Mp*RAD8* gene targeted by sgRNAs. Coding sequences are annotated in yellow, sgRNA binding sites are annotated in green, and the mutations in the Mp*RAD8* gene in Mp*tar*2, Mp*tar*4 and Mp*tar*6 are annotated with orange arrows.

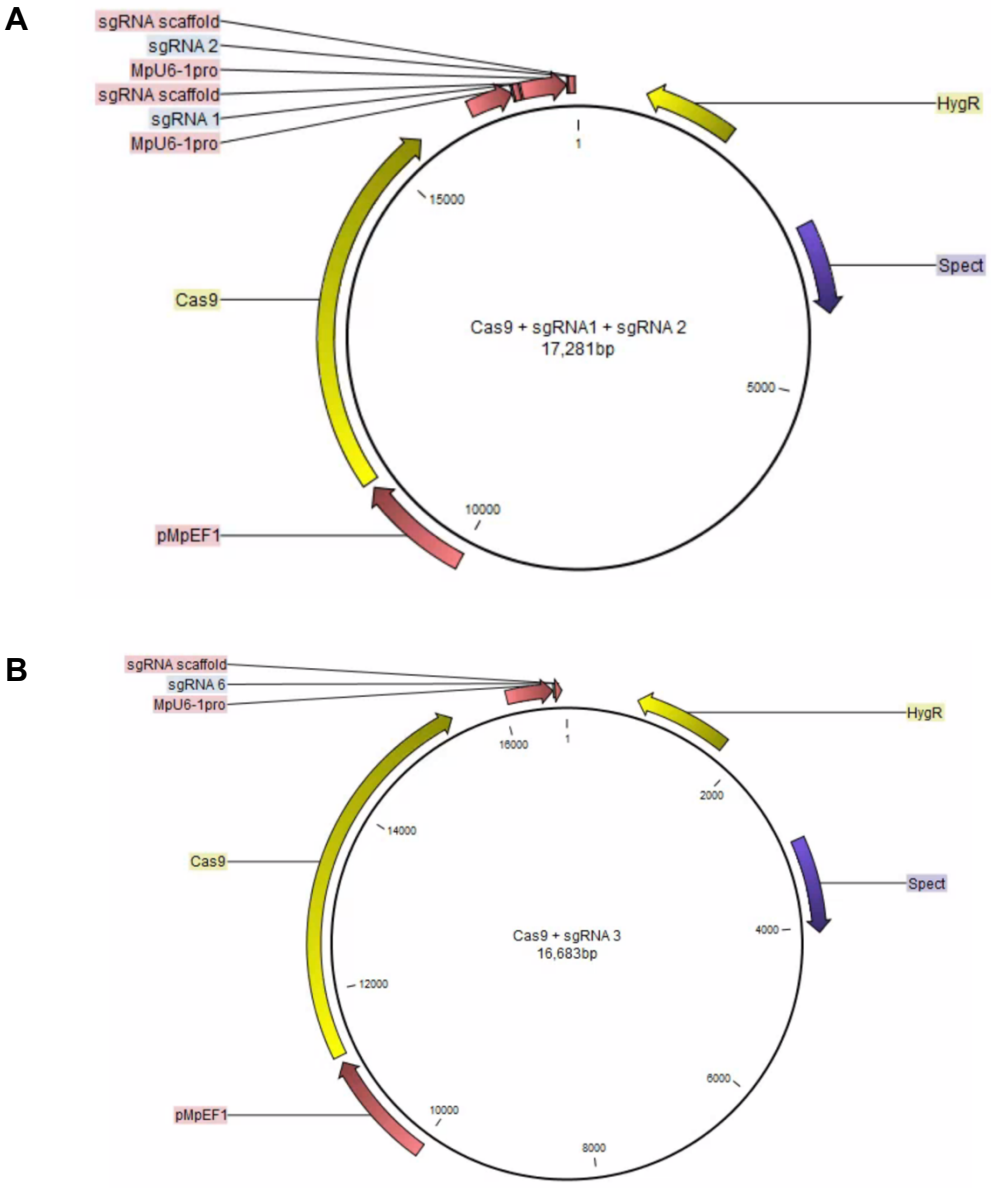

Vector	gRNA targeted	N. plants genotyped	N. mutants identified	CRISPR efficiency
A	1 and 2	43	18	41.86 %
B	3	5	1	20.00 %

Fig. 5.4. CRISPR-Cas9 vectors used to generate mutations in Mp*RAD8* and their mutation efficiencies. Vectors used to generate **(A)** Mp*rad8*^{GE152} – Mp*rad8*^{GE1554} **(B)** Mp*rad8*^{GE62}**.**

Line	gRNA	Mutation
Mp*rad8*^{GE152}	1	1 bp deletion
Mp*rad8*^{GE154}	1	4 bp deletion
Mp*rad8*^{GE158}	1	9 bp deletion
Mp*rad8*^{GE1511}	1	9 bp deletion
Mp*rad8*^{GE1512}	1	5 bp substitution
Mp*rad8*^{GE1517}	1	3 bp deletion
Mp*rad8*^{GE1518}	1	17 bp deletion
Mp*rad8*^{GE1519}	1	too large to determine
Mp*rad8*^{GE1523}	1	1 bp insertion, 4 bp substitution
Mp*rad8*^{GE1535}	1	21 bp insertion
Mp*rad8*^{GE1536}	1	11 bp insertion, 5 bp deletion
Mp*rad8*^{GE1537}	1	4 bp deletion
	2	6 bp insertion, 1bp substitution, 4 bp deletion
Mp*rad8*^{GE1538}	1	too large to determine
Mp*rad8*^{GE1539}	1	1 bp deletion
	2	3 bp deletion
Mp*rad8*^{GE1546}	1	1 bp deletion
Mp*rad8*^{GE1549}	1	8 bp deletion, 23 bp insertion
Mp*rad8*^{GE1552}	2	1 bp insertion
Mp*rad8*^{GE1554}	1	too large to determine
Mp*rad8*^{GE62}	3	2 bp deletion

Table 5.2. List of Mp*rad8* lines and the mutations present in their Mp*RAD8* gene. Mp*rad8* lines were generated using CRISPR-Cas9 mutagenesis to target the Mp*RAD8* gene. Wild-type spores (from a cross between Tak-1 and Tak-2) were transformed with *Agrobacterium tumefaciens* strains carrying the vector containing the Cas9 gene and guide RNAs to target Mp*RAD8*. Positive transformants were genotyped using Sanger sequencing to determine the mutations induced by the CRISPR-Cas9 complex.

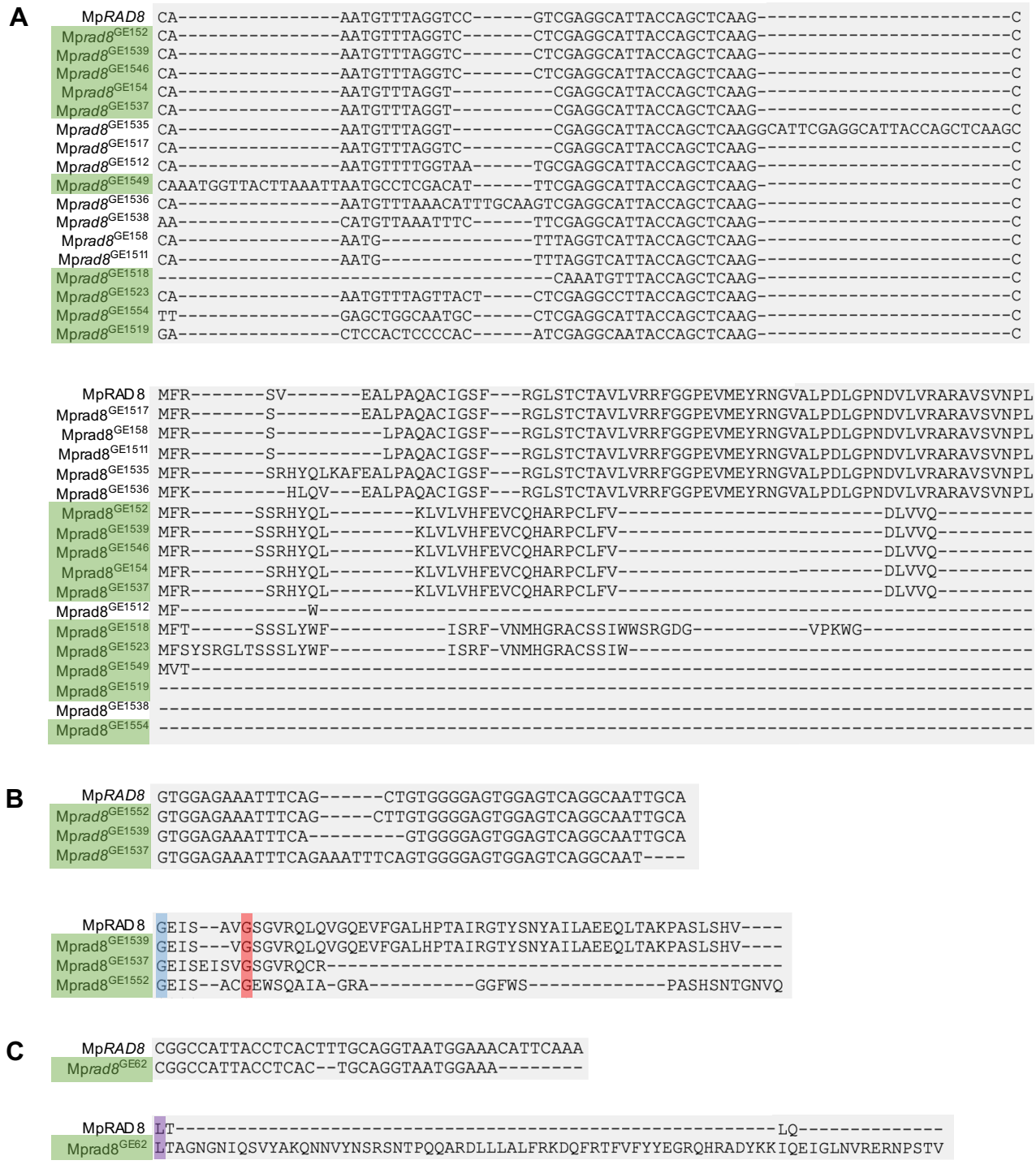

Fig. 5.5. Predicted nucleotide and protein sequences of Mp*RAD8* and MpRAD8 in Mp*rad8* loss-of-function lines. Mp*rad8* lines were generated using CRISPR-Cas9 mutagenesis to target the Mp*RAD8* gene. Wild-type spores (from a cross between Tak-1 and Tak-2) were transformed with *Agrobacterium tumefaciens* strains carrying the vector containing the Cas9 gene and **(A)** sgRNA 1 **(B)** sgRNA 2 or **(C)** sgRNA 3 targeting Mp*RAD8*. Positive transformants were genotyped using Sanger sequencing to determine the mutations induced by the CRISPR-Cas9 complex. Predicted protein sequences were determined based on the mutations in each line. Nucleotide or protein sequences were aligned via the L-INS-i strategy using MAFFT version 7. The top rows in **(A)**, **(B)** and **(C)** is the reference Mp*RAD8* nucleotide or MpRAD8 protein sequence (MpTak1v6.1). Protein sequences for Mp*rad8*^{GE1519}, Mp*rad8*^{GE1538}, and Mp*rad8*^{GE1554} could not be determined as the mutation in their nucleotide sequences were too large to align reliably to the reference genome. Lines highlighted in green are resistant to TXTA with respect to Tak-1 and Tak-2. The amino acid highlighted in blue is that mutated in Mp*tar2*; the amino acid highlighted in red is that mutated in Mp*tar*4; the amino acid highlighted in purple is that mutated in Mp*tar*6.

5.4.4. Predicted strong loss-of-function of Mp*RAD8* confers resistance to TXTA

To test if the Mp*rad8* lines are resistant to TXTA, I grew gemmae from the wild-type lines Tak-1 and Tak-2 and from the 19 Mp*rad8* lines on solid ½ Gamborg medium supplemented with 5 µM TXTA, a dose at which wild-type lines die or grow very little. I also grew on 5 µM TXTA gemmae from 4 lines which were transformed with one of the two CRISPR constructs targeting Mp*RAD8* but in which the construct had not induced a mutation in the Mp*RAD8* gene; these lines therefore have a wild-type copy of Mp*RAD8* and were included as further controls (Mp*RAD8*^{151}, Mp*RAD8*^{1553}, Mp*RAD8*^{614}, Mp*RAD8*^{618}, Mp*RAD8*^{656}). After 12 days of growth on 5 µM TXTA, I quantified the lateral area of living gemmaling tissue (Fig. 5.6). Since only living tissue was measured, for dead gemmalings the gemmaling area is quantified as zero although the actual area is greater than zero. I found that 11 out of 19 Mp*rad*8 lines grew significantly larger than Tak-1 (the more resistant wild-type line) on 5 µM TXTA (Mp*rad8*^{GE152}, Mp*rad8*^{GE154}, Mp*rad8*^{GE1518}, Mp*rad8*^{GE1519}, Mp*rad8*^{GE1523}, Mp*rad8*^{GE1537}, Mp*rad8*^{GE1539}, Mp*rad8*^{GE1546}, Mp*rad8*^{GE1549}, Mp*rad8*^{GE1552}, Mp*rad8*^{GE62}) (Fig. 5.6). Another line (Mp*rad8*^{GE1554}) grew observably larger than Tak-1, although this difference was not significant (Fig. 5.6). These data suggest that mutations in Mp*RAD8* can confer resistance to TXTA.

I used the predicted protein sequences of each Mp*rad8* line to determine whether the nature of the mutation in Mp*RAD8* affects the degree of TXTA resistance. I found that 12 of the 14 putative strong loss-of-function Mp*rad8* lines are TXTA-resistant (all except Mp*rad8*^{GE1512} and Mp*rad8*^{GE1538}), and all 5 of the putative weak loss-of-function Mp*rad*8 lines are TXTA-sensitive (Fig. 5.6). Based on these data, I conclude that loss-of-function of Mp*RAD8* confers resistance to TXTA.

To determine if loss-of-function of Mp*RAD8* affects growth rate in control conditions, I also grew gemmae from Tak-1 and Tak-2 (wild-type lines) and each of the 21 Mp*rad8* lines on solid ½ Gamborg medium supplemented with 0.1 % DMSO (the final concentration of DMSO found in TXTA-supplemented media). After 12 days of growth I quantified the lateral area of living tissue of gemmalings (Fig. 5.7). I found that wild-type lines (Tak-1 and Tak-2) and most of the putative weak loss-of-function lines grew larger than the putative strong loss-of-function lines (Fig. 5.7). These data demonstrate that loss-of-function of Mp*RAD8* is likely to cause decreased growth in control conditions.

Two of the 14 putative strong loss-of-function lines – Mp*rad8*^{GE1512} and Mp*rad8*^{GE1538} – were sensitive to TXTA (Fig. 5.6). Mp*rad8*^{GE1512} has a predicted early stop codon, and Mp*rad8*^{GE1538} has a large indel which I was unable to align with the reference genomic sequence so its predicted protein sequence is uncertain but likely significantly different to the reference sequence (Fig. 5.5). These lines therefore have two of the strongest mutations affecting their MpRAD8 protein; given my finding that loss-of-function of Mp*RAD8* confers TXTA resistance, I would have expected these lines to be strongly resistant to TXTA. However, I have also shown that loss-of-function of Mp*RAD8* is likely to cause decreased growth rate in control conditions. Accordingly, both lines grow significantly smaller than either wild-type line in control conditions (Fig. 5.7). I hypothesise Mp*rad8*^{GE1512} and Mp*rad8*^{GE1538} incur such a large fitness cost due to the very strong mutations in their Mp*RAD8* that they are unable to grow well in any condition, including on TXTA, and that this may be the reason for their apparent sensitivity to TXTA at this dose.

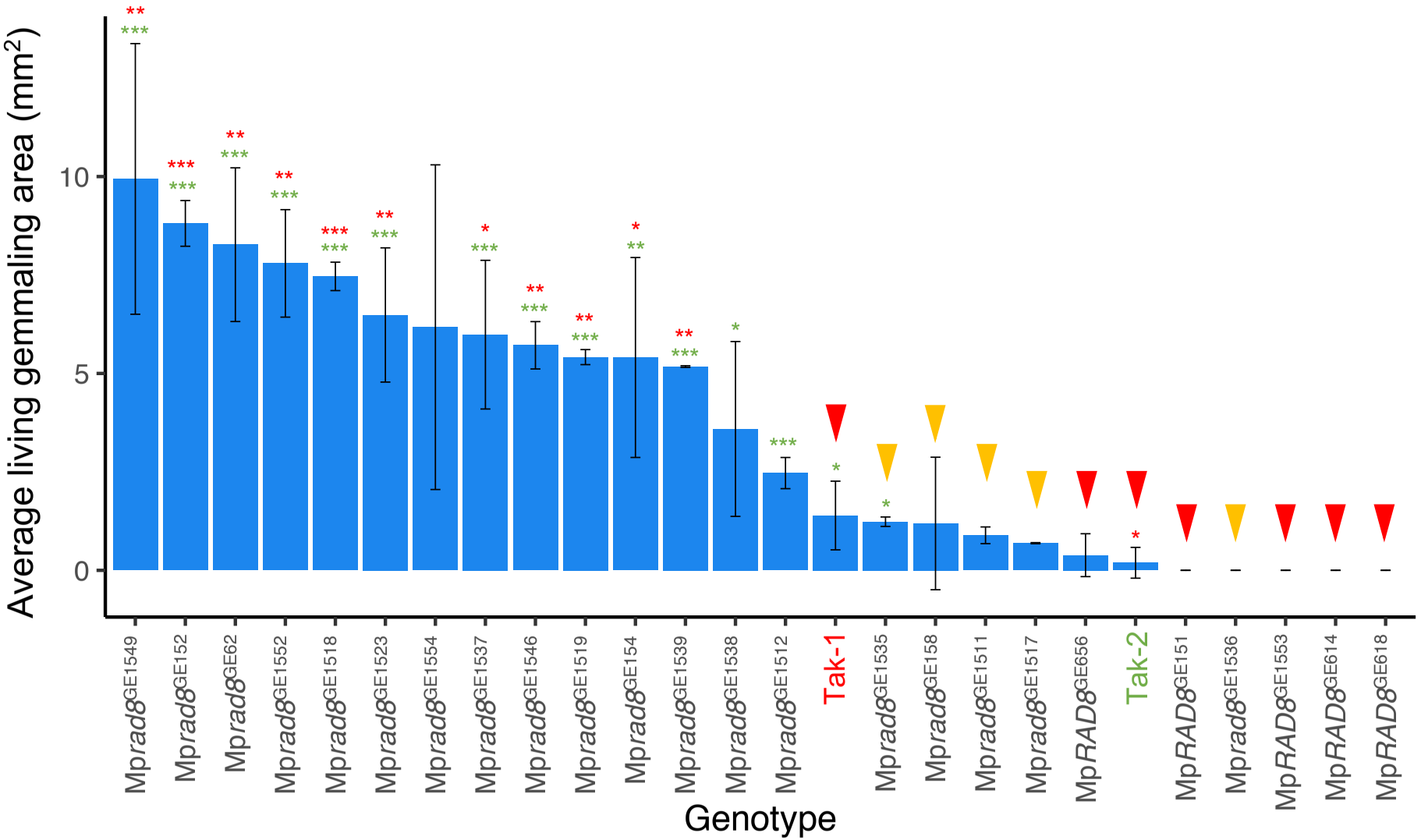

Fig. 5.6. Growth of Mp*rad8* mutant lines on TXTA. 19 Mp*rad8* lines were generated using CRISPR-Cas9 mutagenesis to target the Mp*RAD8* gene. Gemmae from these lines were plated onto solid ½ Gamborg medium supplemented with 5μM TXTA, and grown for 12 days (n=1-3). The lateral area of living gemmaling tissue was determined using a Berthold Nightowl II LB 983 *In Vivo* Imaging System. Since only living tissue was measured, for dead gemmalings the gemmaling area is quantified as zero although the actual area is greater than zero. Red tick marks mark lines with a wild-type copy of Mp*RAD8*, orange tick marks represent putative weak loss-of-function lines (in frame mutations affecting fewer than 15 amino acids). Stars represent the level of significance of the difference between mutant and control lines (Tak-1 in red and Tak-2 in green) as determined by Student's t-tests: * = $p < 0.05$, ** = $p < 0.01$, *** = $p < 0.001$. Error bars are ± standard deviation.

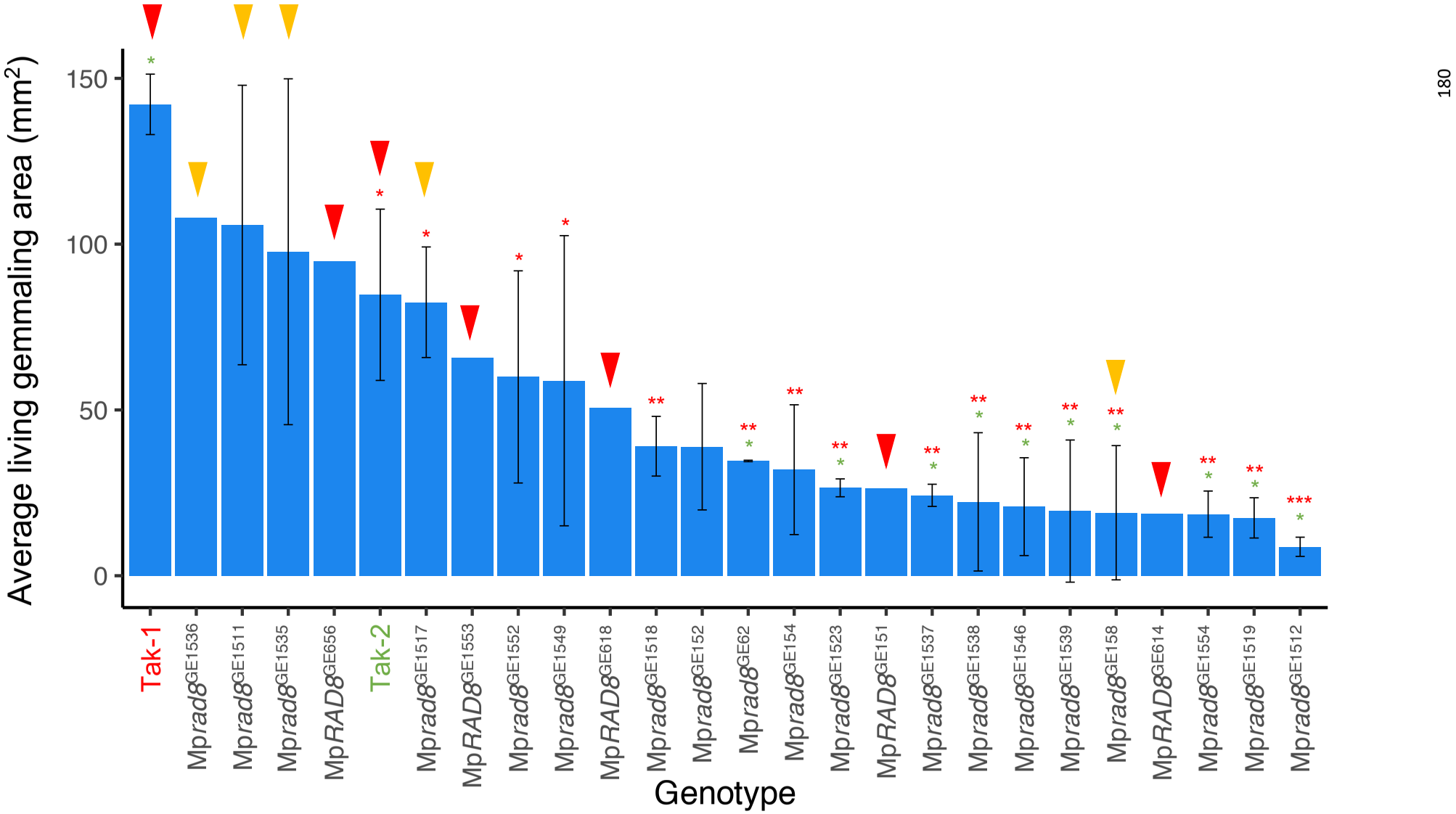

Fig. 5.7. Growth of Mp*rad8* mutant lines in control conditions. 19 Mp*rad8* lines were generated using CRISPR-Cas9 mutagenesis to target the Mp*RAD8* gene. Gemmae from these lines were plated onto solid ½ Gamborg medium supplemented with 0.1 % DMSO, and grown for 12 days (n=1-3). The lateral area of living gemmaling tissue was determined using a Berthold Nightowl II LB 983 *In Vivo* Imaging System. Red tick marks mark lines with a wild-type copy of Mp*RAD8*, orange tick marks represent putative weak loss-of-function lines (in frame mutations affecting fewer than 15 amino acids). Stars represent the level of significance of the difference between mutant and control lines (Tak-1 in red and Tak-2 in green) as determined by Student's t-tests: * = $p < 0.05$, ** = $p < 0.01$, *** = $p < 0.001$. Error bars are ± standard deviation.

5.4.5. Mp*rad*8 mutant lines are up to 9 times more resistant to TXTA than Tak-2

To quantify the dose-dependent TXTA resistance of Mp*rad8* lines, I grew gemmae from Tak-1 and Tak-2 (wild-type lines) and two independent TXTA-resistant Mp*rad8* mutant lines (Mp*rad8*^{GE1518} and Mp*rad8*^{GE1549}) on solid ½ Gamborg medium supplemented with different doses of TXTA. After 12 days of growth, I quantified the lateral area of living gemmaling tissue (Fig. 5.8, Fig. 5.9). Since only living tissue was measured, for dead gemmalings the gemmaling area is quantified as zero although the actual area is greater than zero (Fig. 5.8). I used three parameters to quantify the resistance of Mp*rad8* lines; IC_{50} (the concentration of TXTA at which the lateral area of gemmalings is reduced by 50 %), LD_{100} (lethal dose; dose of TXTA at which there is no surviving gemmaling tissue), and RI (resistance index; comparison of wild-type and mutant IC_{50}). I found that the IC_{50} and LD_{100} of both Mp*rad8* mutant lines was significantly higher than either wild-type line (Table 5.3). The ratio between the IC_{50} values of mutant and wild-type gives the Resistance Index (RI); I used the IC_{50} of Tak-2 to calculate the most conservative estimate of RI of each Mp*rad8* line. I found that Mp*rad8*^{GE1518} and Mp*rad8*^{GE1549} are at least 9 times and 4 times more resistant to TXTA than wild-type respectively (Table 5.3).

Genotype	IC_{50} (nM)	LD_{100} (µM)	RI
Tak-1	186 ± 33	5	-
Tak-2	304 ± 39	5	-
Mp*rad8*^{GE1518}	2760 ± 824	>10	9.1
Mp*rad8*^{GE1549}	1241 ± 676	>10	4.1

Table 5.3. Quantification of TXTA resistance of two independent Mp*rad8* lines. Gemmae from Tak-1, Tak-2, Mp*rad8*^{GE1518}, and Mp*rad8*^{GE1549} were grown on solid ½ Gamborg medium supplemented with different doses of TXTA. After 12 days of growth the lateral area of living gemmaling tissue was quantified using a Berthold Nightowl II LB 983 *In Vivo* Imaging System. IC_{50} was calculated by fitting a four-parameter log-logistic dose-response curve to the data using the drc package in R. LD_{100} is the lowest concentration at which living gemmaling area of all replicates was 0. RI was calculated as the ratio between Mp*rad8* and Tak-2 IC_{50}.

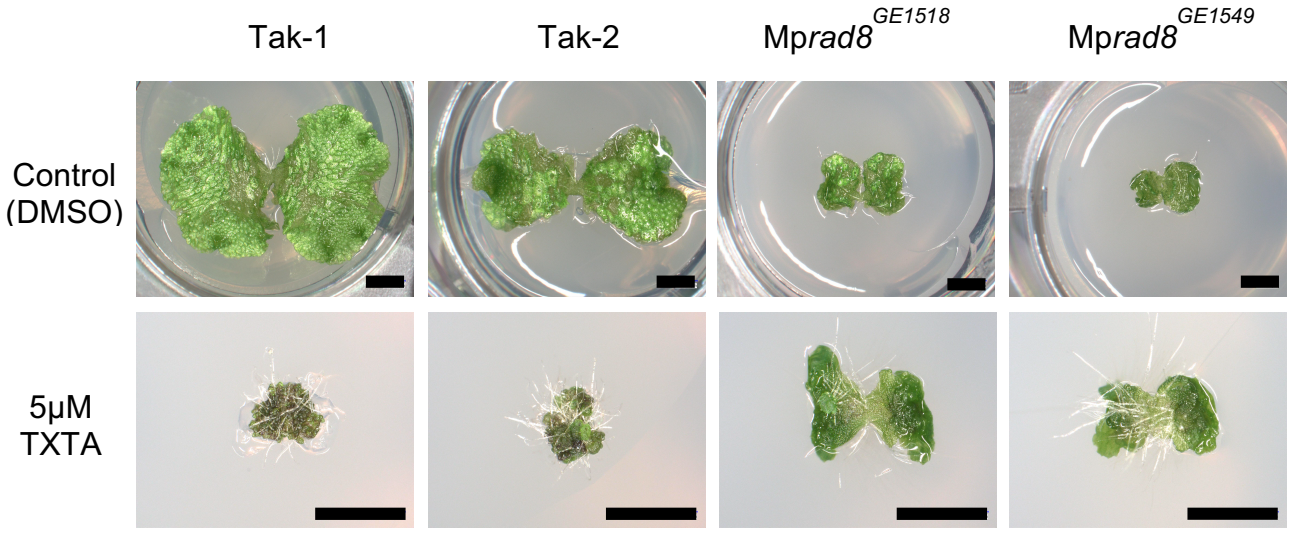

Fig. 5.8. Gemmalings from wild-type and Mp*rad8* mutant lines grown on TXTA. Gemmae from wild-type (Tak-1 and Tak-2) and 2 independent Mp*rad8* predicted loss-of-function lines (Mp*rad8*^{GE1518} and Mp*rad8*^{GE1549}) were grown on solid ½ Gamborg medium supplemented with 5 µM TXTA or 0.1 % DMSO for 12 days. Gemmalings were imaged with a Keyence VHX-7000. Scale bars represent 2 mm.

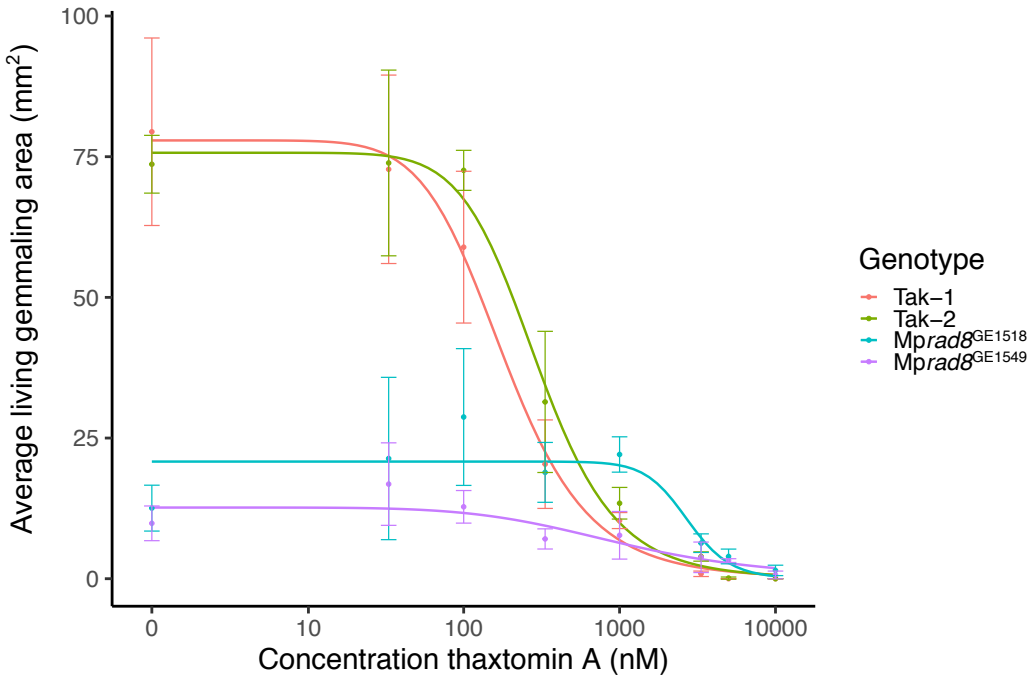

Fig. 5.9. Dose-response curve of wild-type and Mp*rad8* mutant lines on TXTA. Gemmae from wild-type (Tak-1 and Tak-2) and 2 independent Mp*rad8* predicted loss-of-function lines (Mp*rad8*^{GE1518} and Mp*rad8*^{GE1549}) were grown on solid ½ Gamborg medium supplemented with different concentrations of TXTA for 12 days. Gemmalings were imaged using a Berthold Nightowl II LB 983 *In Vivo* Imaging System which detects chlorophyll autofluorescence (560nm). The lateral area of autofluorescing (living) tissue was determined after 14 days of growth using the indiGo™ software package and plotted using the ggplot2 package in R. Since only living tissue was measured, for dead gemmalings the gemmaling area is quantified as zero although the actual area is greater than zero. The fitted curve was calculated using the four-parameter log-logistic equation included in the drc package in R. Error bars represent ± standard deviation (n = 3).

5.4.6. Mp*rad8* mutant lines are cross-resistant to the herbicides isoxaben and chlorsulfuron

I found that predicted loss-of-function mutations in Mp*RAD8* confer NTSR to the herbicide TXTA. Mechanisms of NTSR can lead to herbicide cross-resistance. To determine if loss-of-function of Mp*RAD8* confers herbicide cross-resistance, I assayed the resistance of Mp*rad8* mutant lines to the herbicides isoxaben, dichlobenil, chlorsulfuron, and 2,4-D. TXTA and isoxaben are classed as group 1 cellulose biosynthesis inhibitors, dichlobenil is a group II cellulose biosynthesis inhibitor, chlorsulfuron is an AHAS inhibitor, and 2,4-D is an auxin mimic.

To quantify the dose-dependent effect of these herbicides on wild-type and Mp*rad8* mutant lines, I grew gemmae from the wild-type lines Tak-1 and Tak-2 and from 2 independent Mp*rad8* predicted loss-of-function lines (Mp*rad8*^{GE1518} and Mp*rad8*^{GE1549}) on solid ½ Gamborg medium supplemented with different doses of the herbicides. After 10 days of growth, I measured the lateral area of living gemmaling tissue (Fig. 5.10). Since only living tissue was measured, for dead gemmalings the gemmaling area is quantified as zero although the actual area is greater than zero. I calculated IC_{50}, LD_{100}, and RI for wild-type and Mp*rad8* mutant lines from the resulting dose-response curves (Fig. 5.10).

I found that Mp*rad8* mutant lines are significantly resistant to isoxaben (Fig. 5.10A). Mp*rad8*^{GE1518} has an RI of 4.22 and Mp*rad8*^{GE1549} has an RI of 3.94 on isoxaben. The error margins of the IC_{50} values are too high for these values alone to be reliable, but both Mp*rad8* mutant lines also have a significantly higher LD_{100} than wild-type, surviving at a concentration of 20 µM isoxaben which is lethal to Tak-1 and

Tak-2. Taken together, these data demonstrate that predicted loss-of-function of Mp*RAD8* confers resistance to isoxaben.

I also found that Mp*rad8* mutant lines are slightly resistant to chlorsulfuron (Fig. 5.10C). Mp*rad8*^{GE1518} has an RI of 1.88 and Mp*rad8*^{GE1549} has an RI of 1.51 on chlorsulfuron; the error margins of the IC_{50} values do not overlap between mutant and wild-type lines, so although these RI values are low they are significant. Furthermore, Mp*rad8*^{GE1518} survives on 33 nM chlorsulfuron, which is lethal to wild-type lines. Predicted loss-of-function of Mp*RAD8* therefore confers a slight but significant resistance to chlorsulfuron.

Mp*rad8* mutant lines are not resistant to dichlobenil (Fig. 5.10B). Although the RI values for Mp*rad8*^{GE1518} and Mp*rad8*^{GE1549} on dichlobenil are 2.41 and 1.64 respectively, the error margins of the IC_{50} values are too large for these values to be significant, and neither line has a higher LD_{100} than Tak-1; both Mp*rad8*^{GE1518} and Mp*rad8*^{GE1549} are therefore not significantly resistant to dichlobenil (Fig. 5.10B).

Mp*rad8* mutant lines are also not significantly resistant to 2,4-D (Fig. 5.10D); the RI values for Mp*rad8*^{GE1518} and Mp*rad8*^{GE1549} on 2,4-D are 0.326 and 0.558 respectively, suggesting that the lines are sensitive to 2,4-D, however the error margins of the IC_{50} values are too high for the RI values to be significant. Neither Mp*rad8* loss-of-function line has a higher LD_{100} than wild-type lines on 2,4-D; Mp*rad8*^{GE1518} has a significantly lower LD_{100} as it cannot survive on 10 µM 2,4-D whereas both Tak-1 and Tak-2 survive at this dose (Fig. 5.10D).

Overall, these data show that predicted loss-of-function of Mp*rad8* confers cross-resistance to isoxaben and chlorsulfuron, but not to dichlobenil or 2,4-D (Fig. 5.10).

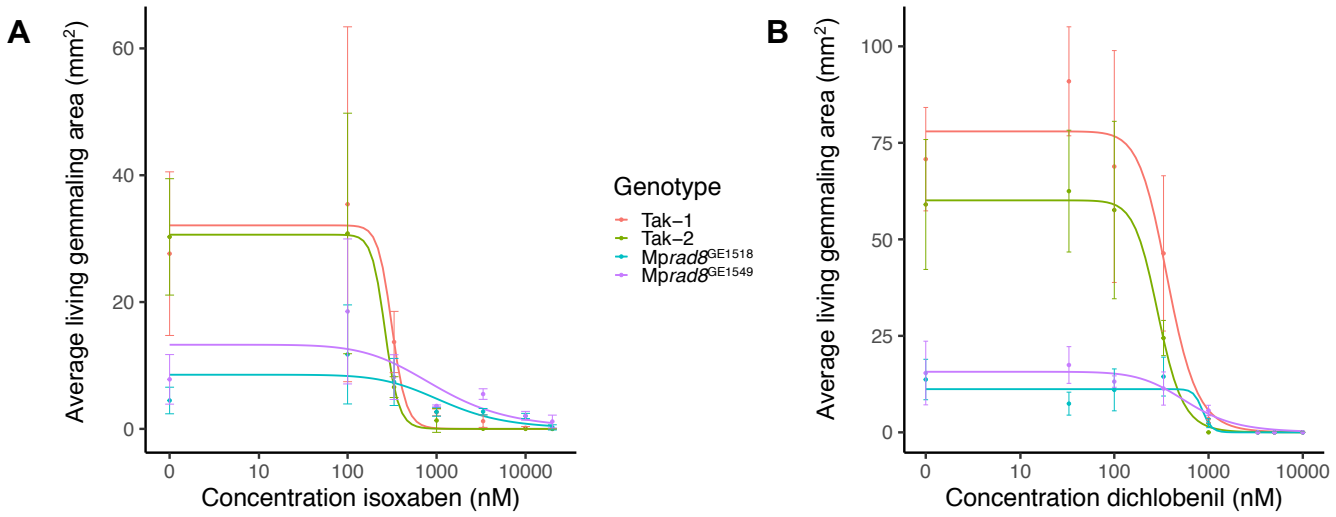

Isoxaben				Dichlobenil			
Genotype	**IC_{50} (nM)**	**LD_{100} (µM)**	**RI**	**Genotype**	**IC_{50} (nM)**	**LD_{100} (µM)**	**RI**
Tak-1	324 ± 136	20	-	Tak-1	367 ± 41	3.3	-
Tak-2	292 ± 848	10	-	Tak-2	293 ± 43	1	-
Mp*rad8*^{GE1518}	1370 ± 2850	>20	4.22	Mp*rad8*^{GE1518}	886 ± 1480	3.3	2.41
Mp*rad8*^{GE1549}	1275 ± 1870	>20	3.94	Mp*rad8*^{GE1549}	603 ± 490	3.3	1.64

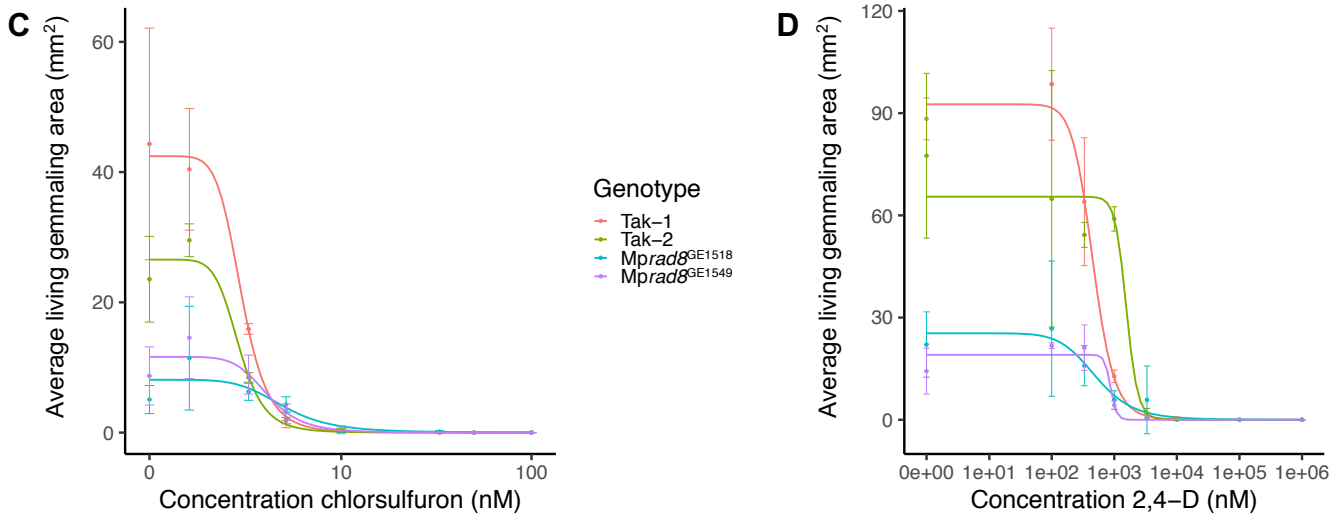

Chlorsulfuron				2,4-D			
Genotype	**IC_{50} (nM)**	**LD_{100} (nM)**	**RI**	**Genotype**	**IC_{50} (nM)**	**LD_{100} (µM)**	**RI**
Tak-1	2.51 ± 0.42	33	-	Tak-1	467 ± 52	100	-
Tak-2	2.63 ± 0.29	33	-	Tak-2	1600 ± 406	100	-
Mp*rad8*^{GE1518}	4.96 ± 1.72	50	1.88	Mp*rad8*^{GE1518}	523 ± 293	10	0.326
Mp*rad8*^{GE1549}	3.97 ± 0.78	33	1.51	Mp*rad8*^{GE1549}	892 ± 1340	100	0.558

Fig. 5.10. Quantification of cross-resistance of Mp*rad8*^{GE1518} and Mp*rad*8^{GE1549}. Wild-type (Tak-1 and Tak-2) and 2 independent Mp*rad8* loss-of-function lines (Mp*rad8*^{GE1518} and Mp*rad8*^{GE1549}) were grown on solid ½ Gamborg medium supplemented with different concentrations of the herbicides **(A)** isoxaben, **(B)** dichlobenil, **(C)** chlorsulfuron, or **(D)** 2,4-D for 10 days. Gemmalings were imaged using a Berthold Nightowl II LB 983 *In Vivo* Imaging System which detects chlorophyll autofluorescence (560 nm). The lateral area of autofluorescing (living) tissue was determined after 10 days of growth using the indiGo™ software package and plotted using the ggplot2 package in R. Since only living tissue was measured, for dead gemmalings the gemmaling area is quantified as zero although the actual area is greater than zero The fitted curves and IC_{50} were calculated using the four-parameter log-logistic equation included in the drc package in R. Error bars represent ± standard deviation (n = 3). LD_{100} is the lowest concentration at which living gemmaling area of all replicates was 0. RI was calculated as the ratio between Mp*rad8* and the wild-type line with the highest IC_{50} on that herbicide.

5.4.7. Mp*tar*2 and Mp*tar*4 are cross-resistant to isoxaben but not chlorsulfuron

To confirm the finding that loss-of-function of Mp*RAD8* confers cross-resistance to isoxaben and chlorsulfuron, I quantified the resistance to chlorsulfuron and isoxaben of the three TXTA-resistant UV-B lines with a mutation in Mp*RAD8* (Mp*tar*2, Mp*tar*4 and Mp*tar*6). In Chapter 3, based on their LD_{100}, I found that Mp*tar*2, Mp*tar*4 and Mp*tar*6 are significantly resistant to isoxaben, but that Mp*tar*2 and Mp*tar*4 are sensitive to chlorsulfuron (Fig. 3.12). Mp*tar*6 is resistant to chlorsulfuron: the sequencing of the Mp*tar*6 genome revealed that there is a mutation in Mp*tar*6 in the gene encoding the target site of chlorsulfuron (Mp*AHAS*) (Table S4.2). This may be conferring a degree of target site resistance. Quantifying resistance by LD_{100} alone may not have been sufficient to identify cross-resistance: for example, the LD_{100} of Mp*rad8*^{GE1549} on chlorsulfuron is the same as that of Tak-1 and Tak-2, but its IC_{50} and RI are significantly higher (Fig. 5.10). To assay the cross-resistance of Mp*tar*2, Mp*tar*4 and Mp*tar*6 more comprehensively, I grew gemmae from these lines on solid ½ Gamborg medium supplemented with different doses of isoxaben or chlorsulfuron. After 10 days of growth, I measured the lateral area of living gemmaling tissue (Fig. 5.11). Since only living tissue was measured, for dead gemmalings the gemmaling area is quantified as zero although the actual area is greater than zero. I calculated IC_{50}, LD_{100}, and RI for wild-type and Mp*tar* lines from the resulting dose-response curves (Fig. 5.11).

I found that Mp*tar*2, Mp*tar*4 and Mp*tar*6 are significantly resistant to isoxaben, with RIs of 5.64, 3.53, and 3.17 respectively, and a LD_{100} greater than those of either Tak-1 or Tak-2 (Fig. 5.11). This corroborates my findings that Mp*rad8* loss-of-function lines generated by CRISPR-Cas9 mutagenesis are resistant to isoxaben.

However, I found that Mp*tar*2 and Mp*tar*4 are sensitive to chlorsulfuron; the RI of Mp*tar*2 is 1.11 and that of Mp*tar*4 is 0.89, but the IC_{50} value error margins overlap with those of wild-type lines, so these RI values are not significantly different than those of wild-type lines (Fig. 5.11). The LD_{100} of both Mp*tar*2 and Mp*tar*4 is the same as wild-type lines (33 nM) (Fig. 5.11). Mp*tar*6 is significantly resistant to chlorsulfuron, with an RI of 2.04 and an LD_{100} of 100 nM (Fig. 5.11). However, this is likely due to its mutation in Mp*AHAS* rather than its mutation in Mp*RAD8*. Mp*tar*6 therefore cannot be used to make inferences about the effect of a mutation in Mp*RAD8* on resistance to chlorsulfuron. These data show that in Mp*tar*2 and Mp*tar*4, a mutation in Mp*RAD8* which leads to TXTA resistance does not confer cross-resistance to chlorsulfuron.

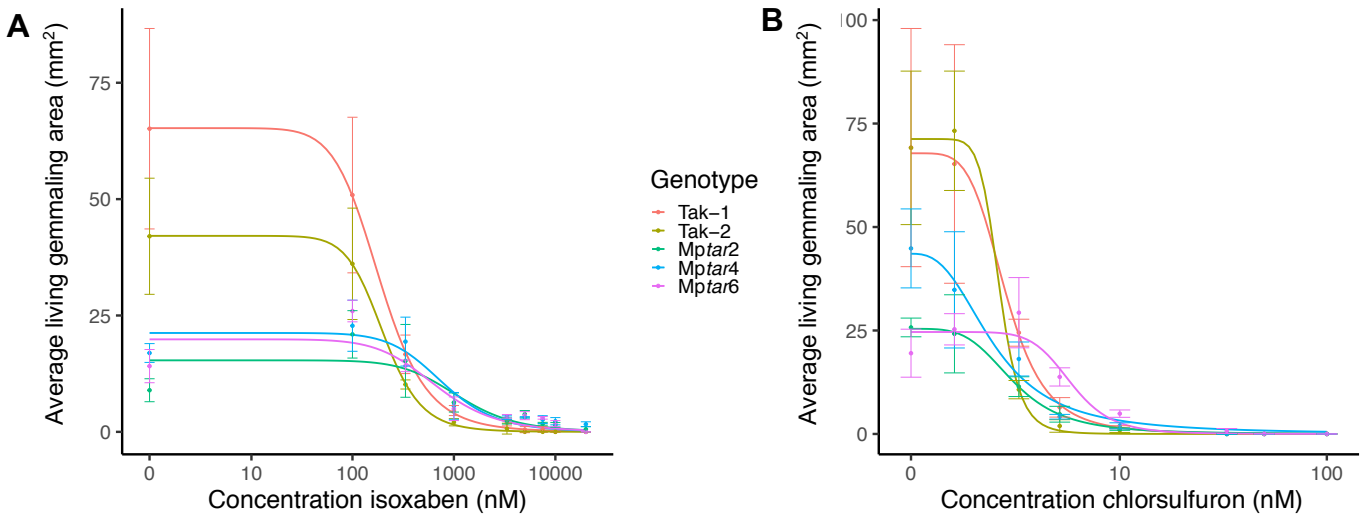

	Isoxaben				Chlorsulfuron		
Genotype	**IC_{50} (nM)**	**LD_{100} (µM)**	**RI**	**Genotype**	**IC_{50} (nM)**	**LD_{100} (nM)**	**RI**
Tak-1	193 ± 22	10	-	Tak-1	2.47 ± 0.3	33	-
Tak-2	208 ± 35	5	-	Tak-2	2.39 ± 0.74	33	-
Mp*tar*2	1173 ± 592	>20	5.64	Mp*tar*2	2.75 ± 0.78	33	1.11
Mp*tar*4	735 ± 189	>20	3.53	Mp*tar*4	2.17 ± 0.50	33	0.89
Mp*tar*6	660 ± 288	10	3.17	Mp*tar*6	5.05 ± 0.90	100	2.04

Fig. 5.11. Quantification of cross-resistance of Mp*tar*2, Mp*tar*4 and Mp*tar*6. Gemmae from wild-type (Tak-1 and Tak-2) and Mp*tar* lines (Mp*tar*2, Mp*tar*4, and Mp*tar*6) were grown on solid ½ Gamborg medium supplemented with different concentrations of **(A)** isoxaben or **(B)** chlorsulfuron for 10 days. Gemmalings were imaged using a Berthold Nightowl II LB 983 *In Vivo* Imaging System which detects chlorophyll autofluorescence (560 nm). The lateral area of autofluorescing (living) tissue was determined after 10 days of growth using the indiGo™ software package and plotted using the ggplot2 package in R. Since only living tissue was measured, for dead gemmalings the gemmaling area is quantified as zero although the actual area is greater than zero. The fitted curves and IC_{50} were calculated using the four-parameter log-logistic equation included in the drc package in R. Error bars represent ± standard deviation (n = 3). LD_{100} is the lowest concentration at which living gemmaling area of all replicates was 0. RI was calculated as the ratio between Mp*rad8* and the wild-type line with the highest IC_{50} on that herbicide.

5.4.8. Loss-of-function of Mp*RAD8* results in an increased concentration of reactive oxygen species (ROS) in thallus tissue

Since *rad8* mutants in *C. elegans* and mouse myoblast cells overproduce ROS (Fujii *et al.*, 2011, Park *et al.*, 2021), I hypothesised that Mp*rad8* lines also produce more ROS than wild-type. To measure the concentration of ROS in wild-type (Tak-1 and Tak-2) and 2 independent Mp*rad8* predicted loss-of-function lines (Mp*rad8*^{GE1518} and Mp*rad8*^{GE1549}), I stained 12-day old gemmalings with 3,3'-diaminobenzidine (DAB), which forms a brown precipitate upon reaction with hydrogen peroxide (H_2O_2), one form of ROS. I bleached the stained samples to remove chlorophyll (Fig. 5.12). The amount of brown precipitate is proportional to the concentration of H_2O_2 in each sample. Both Mp*rad8* mutant lines are visibly darker than the two wild-type lines, indicating a higher concentration of H_2O_2 in their thalli (Fig. 5.12).

To quantify tissue levels of ROS, I used a modified ferric-xylenol orange (FOX) assay (Li, 2019). This assay measures various forms of ROS, including H_2O_2 and lipid hydroperoxides (Gay *et al.*, 1999). In acid conditions, Fe^{2+} is oxidised to Fe^{3+} by ROS; upon the addition of xylenol orange (XO), a purple Fe^{3+}-XO complex forms which absorbs at 560nm (Wolff, 1994). The more ROS in the initial sample, the higher the concentration of Fe^{3+}-XO and the greater the absorbance. Using this assay, I measured the concentration of ROS in 12 day old wild-type gemmalings (Tak-1 and Tak-2) and two independent Mp*rad8* mutant lines (Mp*rad8*^{GE1518} and Mp*rad8*^{GE1549}). Both Mp*rad8* lines had significantly higher concentrations of ROS than wild-type (Fig. 5.13). Given that adding exogenous H_2O_2 confers TXTA resistance to *A. thaliana* cells in culture (Awwad *et al.*, 2019), the increased concentration of ROS in Mp*rad8* lines may be the basis of their TXTA resistance.

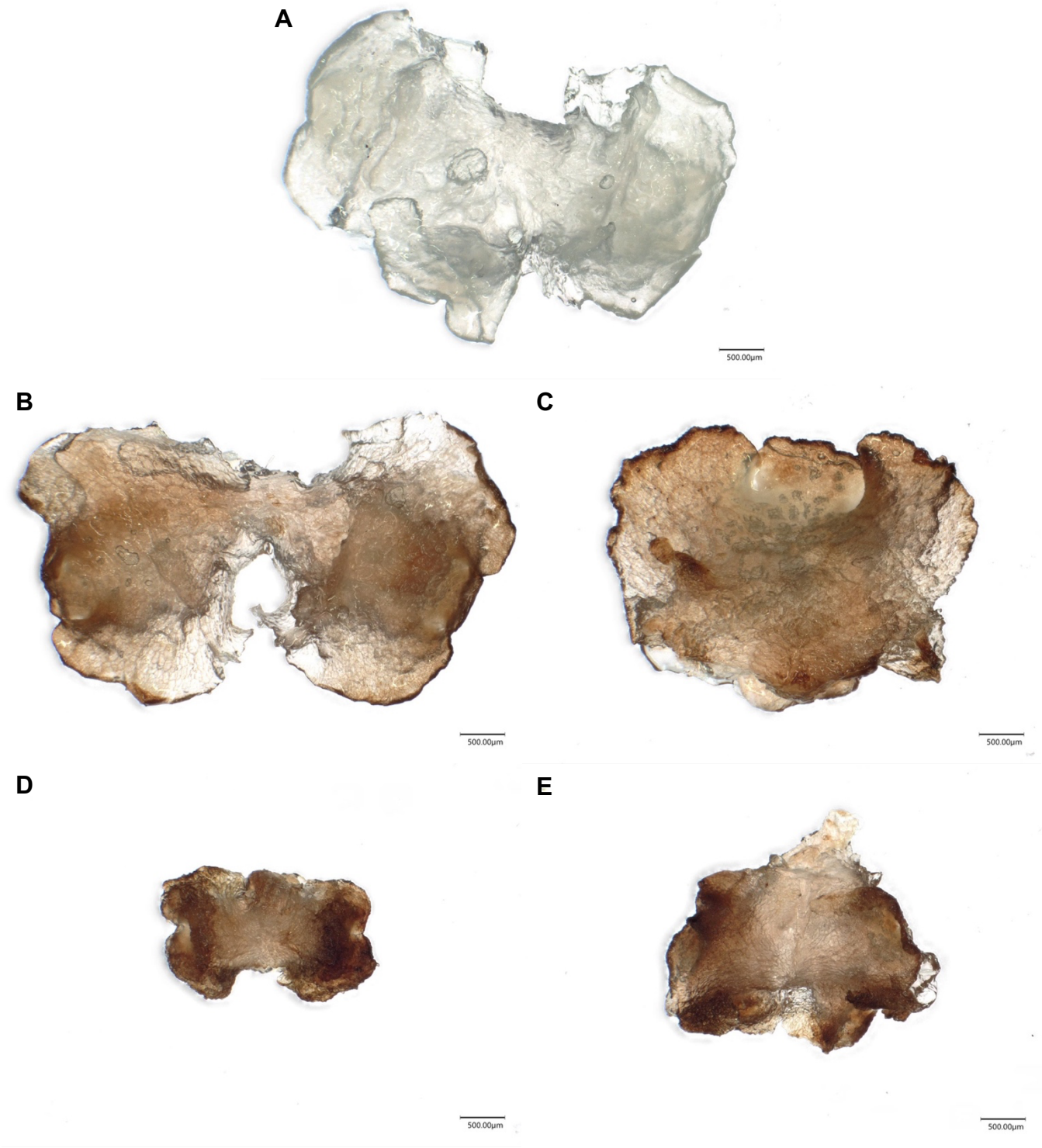

Fig. 5.12. DAB staining of wild-type lines (Tak-1 and Tak-2) and Mp*rad8* mutant lines (Mp*rad8*^{GE1518} and Mp*rad8*^{GE1549}). 12-day old gemmalings were stained with 3,3'-diaminobenzidine (DAB), which forms a brown precipitate upon reaction with hydrogen peroxide (H_2O_2), a form of ROS. Stained plants were bleached to remove chlorophyll from their tissues and imaged with a Keyence VHX-7000. Scale bars represent 500 µm.
(A) Tak-1 (no DAB) **(B)** Tak-1 **(C)** Tak-2 **(D)** Mp*rad8*^{GE1518} **(E)** Mp*rad8*^{GE1549}

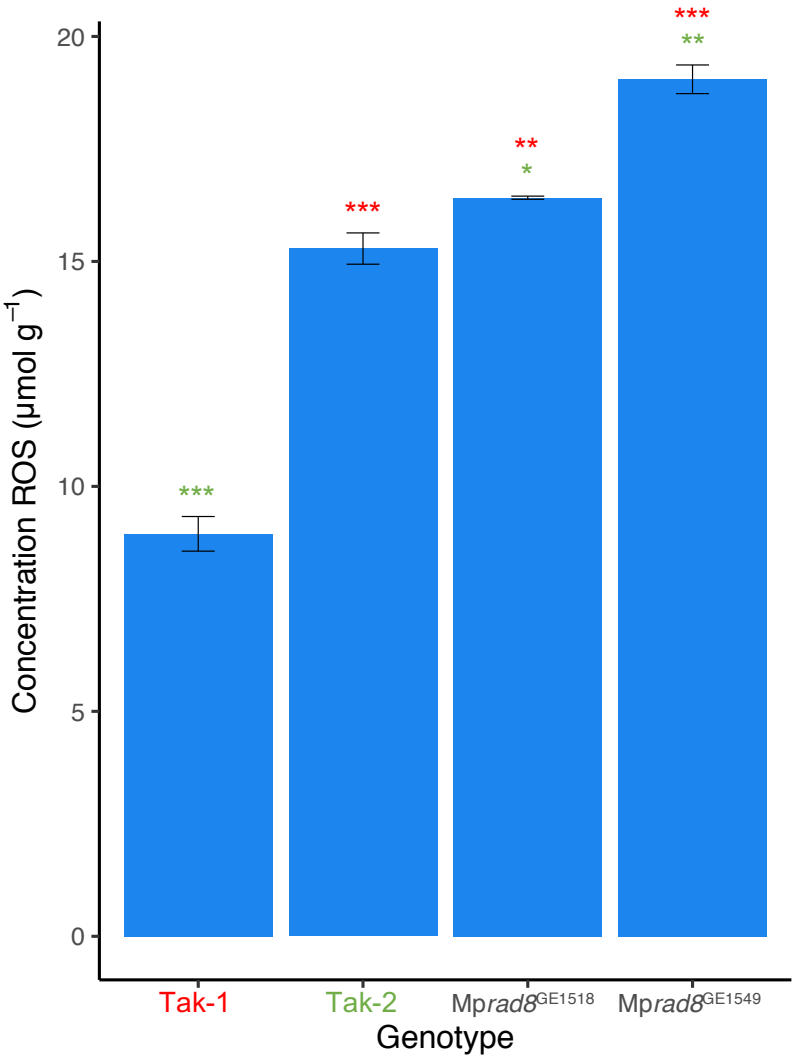

Fig. 5.13. Concentration of ROS as determined by FOX assay in wild-type and Mp*rad8* mutant lines. The concentration of ROS in 12-day old gemmalings from wild-type lines (Tak-1 and Tak-2) as well as Mp*rad8*^{GE1518} and Mp*rad8*^{GE1549} was determined by homogenising frozen samples in perchloric acid, followed by incubation with ferric xylenol-orange (FOX) and measurement of absorbance at 560 nm using an Ultrospec 3100 pro spectrophotometer. The absorbance readings were converted to concentration of ROS using a calibration curve. Stars represent the level of significance of the difference between mutant and control lines (Tak-1 in red and Tak-2 in green) as determined by Student's t-tests: * = $p < 0.05$, ** = $p < 0.01$, *** = $p < 0.001$. Error bars represent ± standard deviation (n=3).

5.4.9. Mp*tar*1, Mp*tar*3, and Mp*tar*8 mutant lines – which have mutations in a peroxidase, Mp*PSBP*, and Mp*PSAD* respectively – accumulate higher cellular ROS levels than wild-type

The 3 Mp*tar* lines with mutations in Mp*RAD8* (Mp*tar*2, Mp*tar*4, and Mp*tar*6) and 4 other Mp*tar* lines have candidate resistance-conferring SNPs in genes which when dysfunctional are predicted to cause increased ROS (Chapter 4). Mp*tar*1 has a mutation in a peroxidase (Mp6g13550), Mp*tar*3 has a mutation in Mp*PSBP* (Mp8g10040), Mp*tar*7 has a mutation in a gene containing a TIM44-like domain (Mp3g01110), and Mp*tar*8 has a mutation in Mp*PSAD* (Mp5g04200).

To determine whether these lines exhibit a change in cellular ROS levels, I carried out a FOX assay and calculated the concentration of ROS in 12-day old thallus tissue from wild-type lines (Tak-1 and Tak-2), Mp*tar*1, Mp*tar*3, and Mp*tar*8. I found increased concentration of ROS in the tissues of the Mp*tar* lines with respect to wild-type lines (Fig. 5.14). ROS levels are therefore higher in Mp*tar*1, Mp*tar*3, and Mp*tar*8 than in wild-type lines. These data support the hypothesis that increased ROS may be the basis of TXTA resistance not only in Mp*rad8* lines (Mp*tar*2, Mp*tar*4, and Mp*tar*6) but also in several other Mp*tar* lines (Mp*tar*1, Mp*tar*3, and Mp*tar*8).

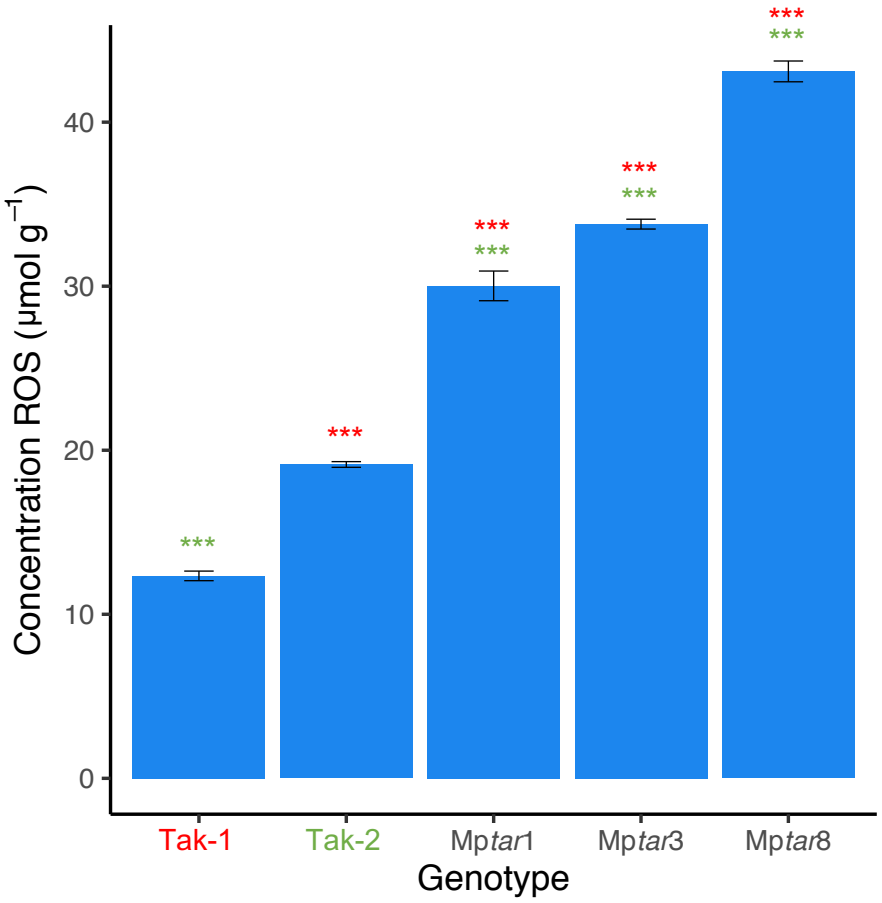

Fig. 5.14. Concentration of ROS as determined by FOX assay in wild-type and Mp*tar* mutant lines. The concentration of ROS in 12 day old gemmalings from wild-type lines (Tak-1 and Tak-2) as well as Mp*tar*1, Mp*tar*3 and Mp*tar*8 was determined by homogenising frozen samples in perchloric acid, followed by incubation with ferric xylenol-orange (FOX) and measurement of absorbance at 560 nm using an Ultrospec 3100 pro spectrophotometer. The absorbance readings were converted to concentration of ROS using a calibration curve. Stars represent the level of significance of the difference between mutant and control lines (Tak-1 in red and Tak-2 in green) as determined by Student's t-tests: * = $p < 0.05$, ** = $p < 0.01$, *** = $p < 0.001$. Error bars represent ± standard deviation (n=3).

5.4.10. Mp*rad8* predicted loss-of-function lines are sensitive to ROS

Mp*rad8* mutant lines with predicted loss-of-function mutations in Mp*RAD8* overproduce ROS (Fig. 5.13). ROS are involved in cellular signalling at low concentrations but are toxic at high concentrations (Auten and Davis, 2009, Dietz *et al.*, 2016). I hypothesised that Mp*rad8* mutant lines would be more sensitive than wild-type plants to toxic levels of ROS because of their higher baseline ROS levels.

To determine the dose-dependent toxic effect of ROS on wild-type and Mp*rad8* mutant lines, I grew gemmae from wild-type lines (Tak-1 and Tak-2) and Mp*rad8* mutant lines (Mp*rad8*^{GE1518} and Mp*rad8*^{GE1549}) on solid ½ Gamborg medium supplemented with different concentrations of H_2O_2. After 10 days of growth, I quantified the lateral area of living gemmaling tissue (Fig. 5.15). Since only living tissue was measured, for dead gemmalings the gemmaling area is quantified as zero although the actual area is greater than zero. I calculated the IC_{50}, LD_{100} and RI of each line (Fig. 5.15); I used the IC_{50} of Tak-1 to calculate the most conservative estimate of RI as Tak-1 is more sensitive to H_2O_2 than Tak-2.

I found that Mp*rad8* mutant lines are more sensitive to H_2O_2 than wild-type lines. The RI values of Mp*rad8*^{GE1518} and Mp*rad8*^{GE1549} were 0.64 and 0.88 respectively, demonstrating that these lines are more sensitive to H_2O_2 than Tak-1, the more sensitive wild-type line (Fig. 5.15). The RI value of Mp*rad8*^{GE1518} is significant, therefore Mp*rad8*^{GE1518} is more sensitive to H_2O_2 than wild-type. The error margins are too large for the RI value of Mp*rad8*^{GE1549} to be significant: however, the LD_{100} of Mp*rad8*^{GE1549} is lower than either wild-type line (Fig. 5.15). Together, these data demonstrate that Mp*rad8* predicted loss-of-function lines are more sensitive to H_2O_2 than wild-type lines.

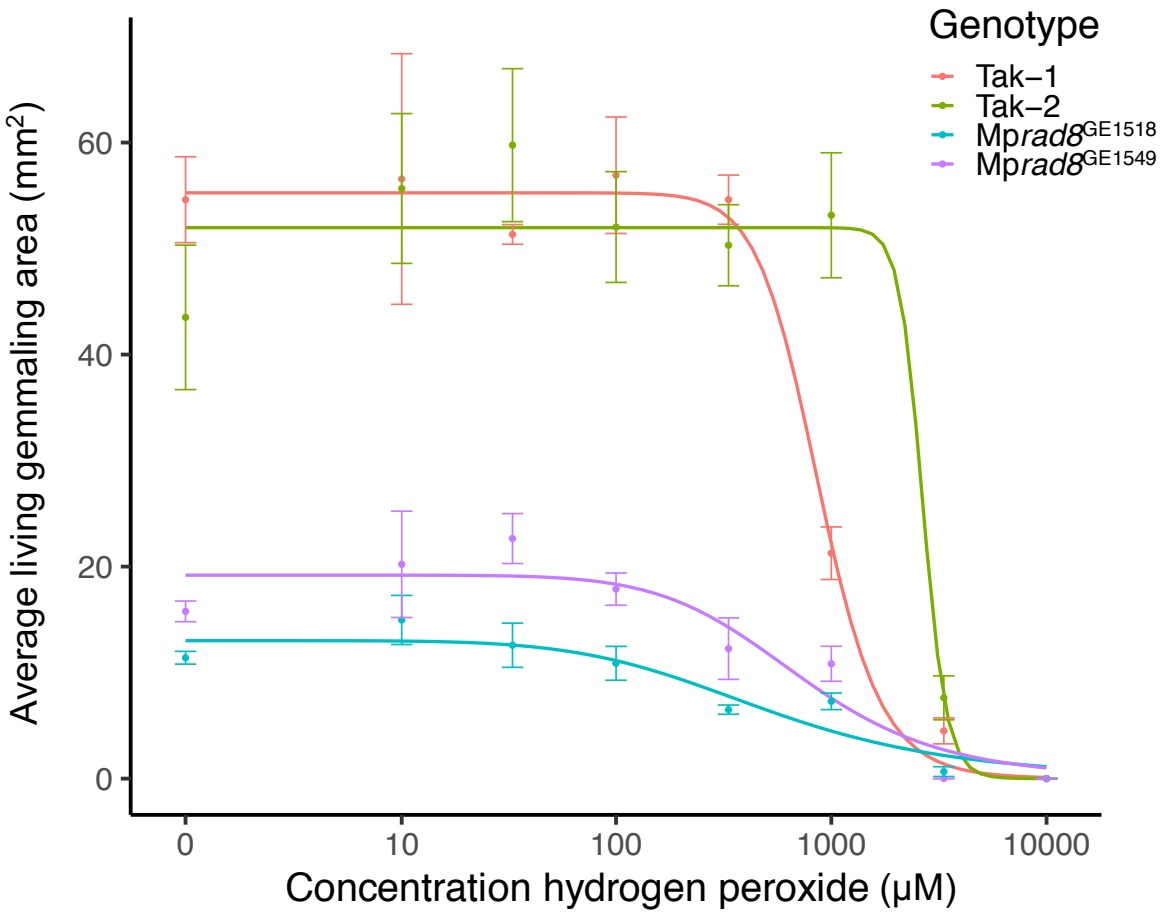

Genotype	IC_{50} (µM)	LD_{100} (mM)	RI
Tak-1	883 ± 101	10	-
Tak-2	2708 ± 2499	10	-
Mp*rad8*^{GE1518}	567 ± 223	10	0.64
Mp*rad8*^{GE1549}	777 ± 297	3.3	0.88

Fig. 5.15. Quantification of dose-dependent toxicity of H_2O_2 on wild-type and Mp*rad8* loss-of-function lines. Gemmae from wild-type (Tak-1 and Tak-2) and 2 independent Mp*rad8* loss-of-function lines (Mp*rad8*^{GE1518} and Mp*rad8*^{GE1549}) were grown on solid ½ Gamborg medium supplemented with different concentrations of H_2O_2 for 10 days. Gemmalings were imaged using a Berthold Nightowl II LB 983 *In Vivo* Imaging System which detects chlorophyll autofluorescence (560 nm). The lateral area of autofluorescing (living) tissue was determined after 14 days of growth using the indiGo™ software package and plotted using the ggplot2 package in R. Since only living tissue was measured, for dead gemmalings the gemmaling area is quantified as zero although the actual area is greater than zero. The fitted curves and IC_{50} were calculated using the four-parameter log-logistic equation included in the drc package in R. Error bars represent ± standard deviation (n = 3). LD_{100} is the lowest concentration at which living gemmaling area of all replicates was 0. RI was calculated as the ratio between Mp*rad8* lines and Tak-1 IC_{50}.

5.4.11. ROS and TXTA have antagonistic effects in vivo

Mp*rad8* predicted loss-of-function lines and at least three TXTA-resistant UV-B mutagenesis lines (Mp*tar*1, Mp*tar*3, and Mp*tar*8) over-accumulate ROS compared to wild-type lines (Fig. 5.13, Fig. 5.14). In *A. thaliana*, adding exogenous H_2O_2 to cells in culture increases their resistance to TXTA (Awwad *et al.*, 2019). I therefore hypothesised that the increased ROS in Mp*rad8* lines and in Mp*tar*1, Mp*tar*3, and Mp*tar*8 may be the basis of their TXTA resistance.

To determine whether increased ROS can confer resistance to TXTA in *M. polymorpha*, I pre-treated wild-type (Tak-1) *M. polymorpha* gemmae with different concentrations of H_2O_2 for 3 hours. I grew H_2O_2-pretreated and untreated gemmae on solid ½ Gamborg medium supplemented with 0.1 % DMSO only or 100 nM TXTA as well as the concentration of H_2O_2 applied during pretreatment for 12 days. After 12 days of growth, I quantified the lateral area of living gemmaling tissue (Fig. 5.16). Since only living tissue was measured, for dead gemmalings the gemmaling area is quantified as zero although the actual area is greater than zero.

The doses of H_2O_2 pretreatment I chose spanned the entire range of the dose-dependent effect H_2O_2 exerts on *M. polymorpha* (Fig. 5.15). Gemmalings grown without TXTA (blue boxes) show no significant decrease in growth when pretreated with 100 nM H_2O_2, but are significantly smaller when pretreated with 1000 nM H_2O_2, and die at 3333 nM H_2O_2.

Without H_2O_2 pretreatment, gemmalings grown on 100 nM TXTA are significantly smaller than those grown in control conditions (Fig. 5.16). Similarly, with a H_2O_2 pretreatment of 100 nM, gemmalings grown on 100 nM TXTA are significantly smaller than those grown on DMSO (Fig. 5.16). However, with a H_2O_2 pretreatment

of 1000 nM, plants grown on TXTA grow significantly larger than plants grown without TXTA (Fig. 5.16). This suggests that TXTA confers resistance to H_2O_2 at this concentration.

Overall, I could not conclude that ROS conferred resistance to TXTA, as no plants pre-treated with H_2O_2 and grown on 100 nM TXTA grew significantly larger than plants grown on 100 nM TXTA without H_2O_2 pretreatment (Fig. 5.16). However, the finding that 100 nM TXTA can confer resistance to 1000 nM H_2O_2 suggests that TXTA and H_2O_2 have antagonistic effects in the plant.

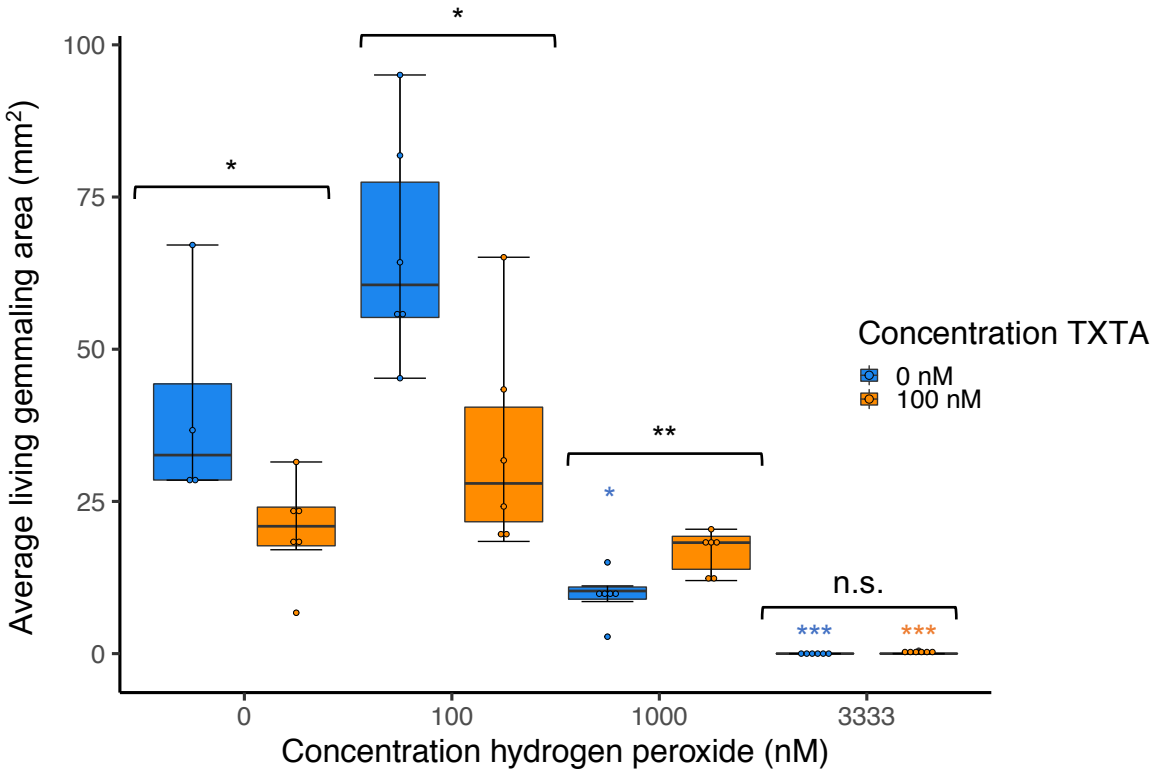

Fig. 5.16. Box and whisker plots to show growth of H_2O_2-treated and untreated Tak-1 grown on DMSO or on TXTA. Tak-1 (wild-type) gemmae were pre-treated with different concentrations of H_2O_2 for 3 hours, then grown for 12 days on solid ½ Gamborg medium supplemented with 0.1 % DMSO (0 nM TXTA – blue boxes) or 5 µM TXTA (orange boxes) (n = 6). The line intersecting the boxes represents the median; the limits of the boxes represent the lower and upper quartiles. Whiskers represent the largest and smallest values within 1.5 x interquartile range from the upper and lower quartiles respectively. Stars represent the level of significance of the difference between H_2O_2 treated and untreated plants (0 nM TXTA in blue, 100 nM TXTA in orange), and between TXTA-treated and untreated plants within each H_2O_2 pretreatment concentration (black) as determined by Student's t-tests: * = $p < 0.05$, ** = $p < 0.01$, *** = $p < 0.001$.

5.4.12. Mp*rad8* predicted loss-of-function mutants produce less of the same putative TXTA metabolite than wild-type

Mp*rad8* predicted loss-of-function lines are resistant to TXTA and accumulate higher ROS levels than wild-type lines. Herbicides can be detoxified to less toxic metabolites; Phase I of herbicide detoxification involves oxidation of the herbicide (Edwards *et al.*, 2011). I hypothesised that the increased ROS levels in Mp*rad8* mutant lines may lead to increased oxidation of TXTA to a less toxic form and that this may underlie their resistance to TXTA.

To test this hypothesis, I undertook a metabolomic analysis to determine the concentration of TXTA and chemically modified TXTA in the thallus tissue of the wild-type line Tak-1 and the Mp*rad8* mutant line Mp*rad8*^{GE1549} grown in the presence of TXTA. I grew gemmae from Tak-1 and Mp*rad8*^{GE1549} for 14 days on solid ½ Gamborg medium supplemented with 0.1 % DMSO. I then transferred plants from each line to solid ½ Gamborg medium supplemented with either 0.1 % DMSO (control) or 5 µM TXTA and grew the plants in these conditions for 2 days. I harvested TXTA-treated and untreated plants and extracted the TXTA-containing fraction. The concentration of pure and modified TXTA in each sample was quantified via LC-MS/MS (Fig. 5.17).

I found that both Tak-1 and Mp*rad8*^{GE1549} have peaks with a retention time of 8.96 minutes; this peak corresponds to pure TXTA (Fig. 5.17). The intensity of the peak of pure TXTA is high in both samples; the concentration of pure TXTA is not significantly different between TXTA treated Tak-1 and TXTA treated Mp*rad8*^{GE1549} samples ($p > 0.05$) (Fig. 5.18 A).

I also found that TXTA treated Tak-1 has a peak with a high relative intensity corresponding to a compound with a retention time of 9.24 minutes (Fig 5.17). This peak is present in TXTA treated Mp*rad8*^{GE1549} but at a significantly lower intensity corresponding to a significantly lower concentration in TXTA treated Mp*rad8*^{GE1549} than in TXTA treated Tak-1 plants (Fig. 5.18 B). The compound corresponding to this peak has a molecular mass of 45 less than that of pure TXTA, so is likely to be a metabolite of TXTA missing the nitro (NO_2) group (Fig. 5.18 C). This compound is not present in the TXTA stock used for the experiments nor is it present in DMSO-treated samples of Tak-1 or Mp*rad8*^{GE1549} (Fig. 5.18 B). I therefore conclude that Tak-1 and Mp*rad8*^{GE1549} generate the same metabolite of TXTA, but that this metabolite is produced to a lesser extent in Mp*rad8*^{GE1549} than in Tak-1. The difference in concentration of this compound between Mp*rad8*^{GE1549} and Tak-1 may therefore contribute to the basis of resistance in Mp*rad8*^{GE1549}.

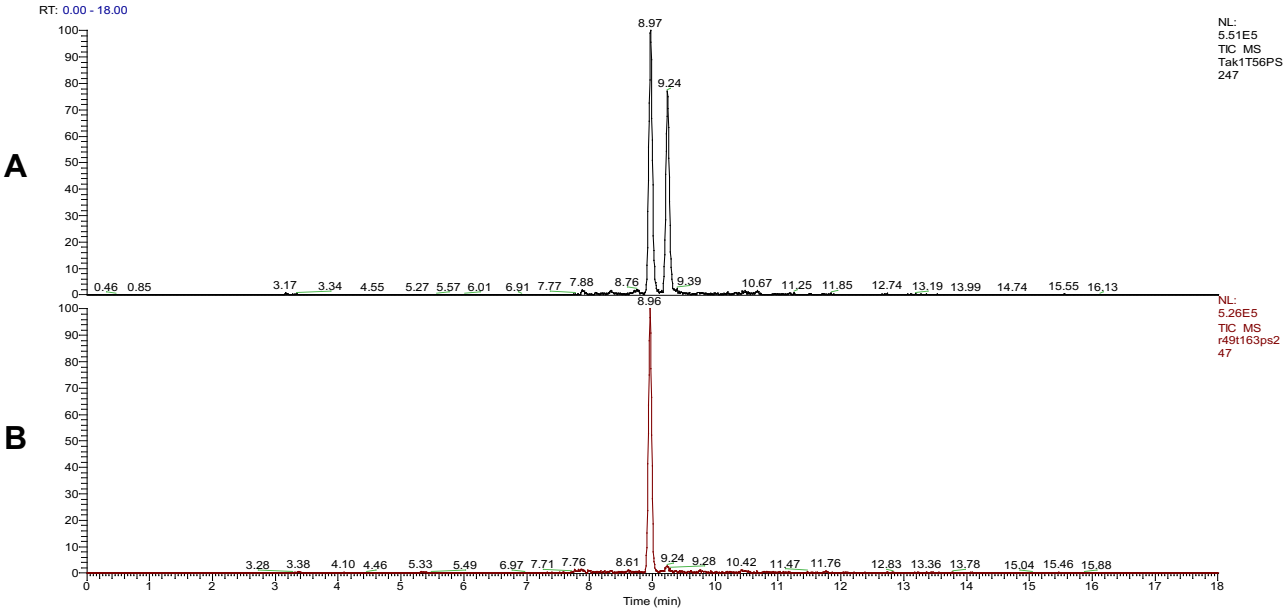

Fig. 5.17. Chromatograms of TXTA and its metabolite in Tak-1 and Mp*rad8*^{GE1549} extracts. Gemmalings from each line were grown on solid ½ Gamborg medium supplemented with 0.1 % DMSO for 14 days, then transferred to solid ½ Gamborg medium supplemented with 5 µM TXTA and grown for 2 days. Cellular fractions were extracted from TXTA-treated **(A)** Tak-1 and **(B)** Mp*rad8*^{GE1549} (n = 6) and analysed via LC-MS/MS.

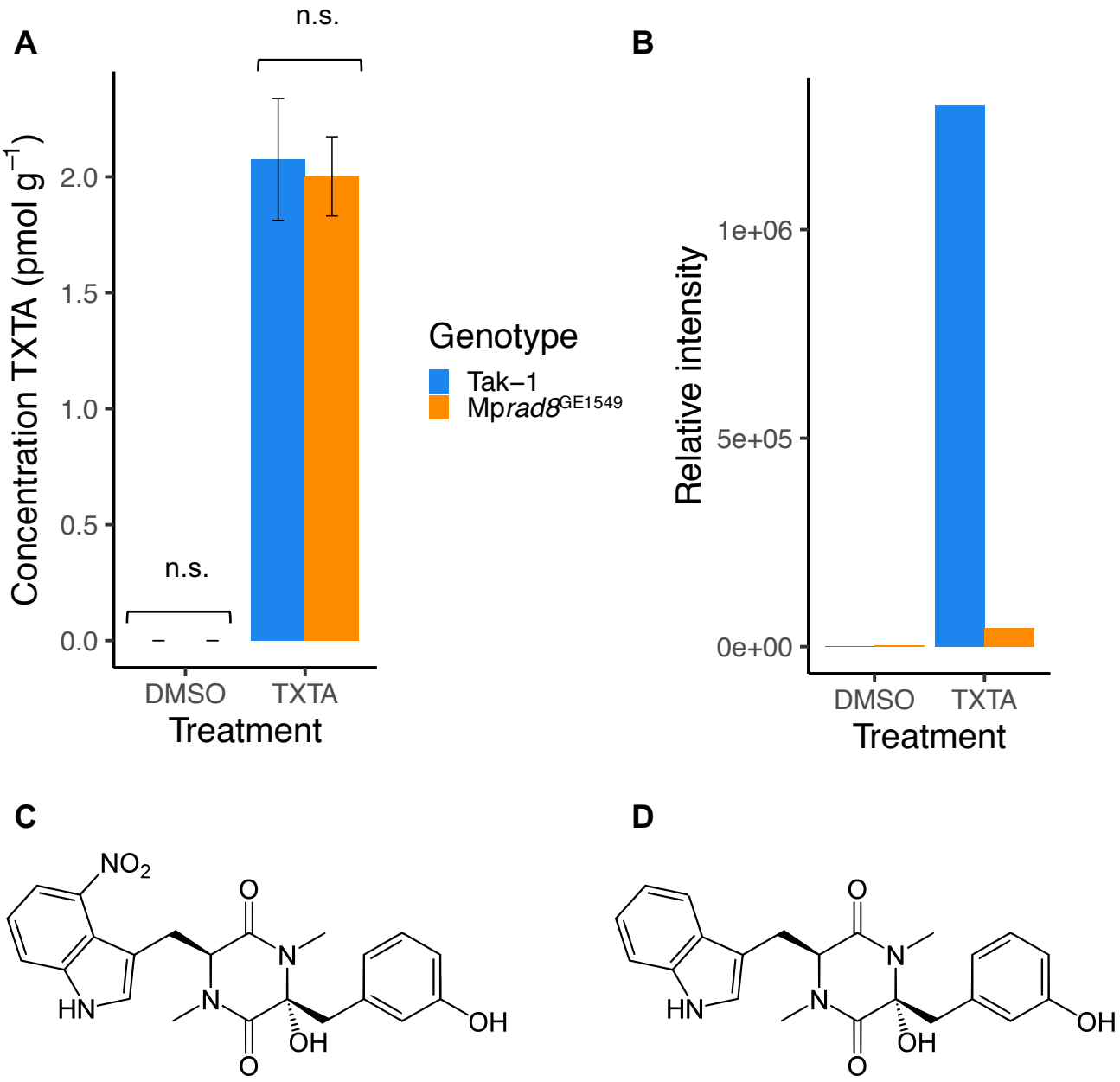

Fig. 5.18. Concentration of pure TXTA and of a predicted TXTA metabolite in Tak-1 and Mp*rad8*^{GE1549} plants. Gemmalings from each line were grown on solid ½ Gamborg medium supplemented with 0.1 % DMSO for 14 days, then transferred to solid ½ Gamborg medium supplemented with either 0.1 % DMSO or 5 µM TXTA and grown for 2 days. Cellular fractions were extracted from each sample and the concentration of pure TXTA and potential TXTA metabolites in each sample was determined by LC-MS/MS. Error bars represent ± standard deviation (n = 6). The level of significance between wild-type and mutant plants was determined by Student's t-tests.
(A) concentration of pure thaxtomin A
(B) concentration of predicted thaxtomin A metabolite with a retention time of 9.24 min
(C) chemical structure of thaxtomin A
(D) chemical structure of predicted thaxtomin A metabolite with a retention time of 9.24 min

5.5. Discussion

In this chapter, I identified a novel mechanism of non-target site resistance to the herbicide thaxtomin A involving loss-of-function of RAD8. I generated predicted loss-of-function mutants of *RAD8* in *M. polymorpha* and used these mutants to confirm my hypothesis that loss-of-function of Mp*RAD8* confers resistance to TXTA as well as to functionally characterise this mechanism of resistance.

I hypothesised that loss-of-function of Mp*RAD8* (Mp3g19030) conferred resistance to TXTA based on my finding that 3 independent TXTA-resistant UV-B lines (Mp*tar2*, Mp*tar*4, and Mp*tar*6) had a candidate resistance conferring SNP in Mp*RAD8* (Chapter 4). In the current chapter, I found that the residues mutated in Mp*tar2*, Mp*tar*4, and Mp*tar*6 are highly conserved across eukaryotes.

I also found that Mp3g19030 (Mp*RAD8*) is in a well-supported sister group to a monophyletic group containing the *RAD8/RTN4IP1* genes from *H. sapiens, M. musculus,* and *C. elegans*, the three species in which *RAD8* and its homologues have been most studied. I therefore used the phenotypic analyses of *rad8* mutants from these species to inform the phenotypes I expected in Mp*rad8* mutants (such as increased ROS) and conducted my functional characterisation of Mp*rad8* mutants accordingly.

Using CRISPR-Cas9 mutagenesis, I generated 19 Mp*rad8* predicted loss-of-function mutants. None of the mutants I generated had mutations in the residues mutated in Mp*tar2*, Mp*tar*4, or Mp*tar*6, so I was not able to confirm my hypothesis that the SNPs at these specific sites lead to strong loss-of-function of Mp*rad8*. I generated 5 putative weak loss-of-function mutants (with mutations affecting fewer than 15 amino acids in frame) and 14 putative strong loss-of-function mutants (with mutations

affecting greater than 15 amino acids in frame, frameshifts, or truncations). Although I did not measure the function of the MpRAD8 protein in these mutant lines, I found that 12 of the 14 putative strong loss-of-function Mp*rad8* lines were resistant to TXTA, and that all the putative weak loss-of-function Mp*rad8* lines were sensitive to TXTA. I therefore concluded that predicted strong loss-of-function of Mp*rad8* confers resistance to TXTA. This finding validates my novel approach of using forward genetics in *M. polymorpha* to identify – and reverse genetics in *M. polymorpha* to confirm – novel mechanisms of resistance.

Both putative strong loss-of-function Mp*rad8* lines which were sensitive to TXTA (Mp*rad8*^{GE1512} and Mp*rad8*^{GE1538}) had very strong mutations in their Mp*RAD8* genes (an early truncation and a mutation too large to identify respectively). I therefore reasoned that such strong mutations would induce a very high fitness cost, which may explain their sensitivity to TXTA. I measured the resistance of Mp*rad8* lines with respect to wild-type lines by growing them on a dose of TXTA with is lethal to Tak-2 and near-lethal to Tak-1 (5 µM), and classing Mp*rad8* lines which grew significantly larger than both wild-type lines on this dose as resistant. However, in the case of Mp*rad8*^{GE1512} and Mp*rad8*^{GE1538}, it may be more informative to conduct a dose-response curve on TXTA and calculate RI compared to Tak-1 and Tak-2, as this parameter of resistance takes into account differences in the growth of each line in control conditions.

I tested the cross-resistance of two independent Mp*rad8* mutant lines – Mp*rad8*^{GE1518} and Mp*rad8*^{GE1549} – and found that both were weakly resistant to the AHAS inhibitor chlorsulfuron. However, the TXTA-resistant UV-B lines with mutations in Mp*rad8* – Mp*tar*2 and Mp*tar*4 – are sensitive to chlorsulfuron. (Fig. 3.12). Mp*tar*6 is significantly

resistant to chlorsulfuron, but has a mutation in the gene encoding the chlorsulfuron target site (Mp*AHAS*) which may confer a degree of target-site resistance (Supplementary Table S4.2). Given that the resistance to chlorsulfuron of Mp*rad8*^{GE1518} and Mp*rad8*^{GE1549} is weak (with RI values of 1.51 and 1.88 respectively), I cannot conclude with certainty that loss-of-function of Mp*RAD8* confers cross-resistance to chlorsulfuron.

I found that Mp*rad8*^{GE1518} and Mp*rad8*^{GE1549} as well as Mp*tar*2, Mp*tar*4 and Mp*tar*6 are significantly resistant to isoxaben. Predicted loss-of-function of Mp*RAD8* therefore confers cross-resistance to isoxaben. TXTA and isoxaben are both classed as a group I cellulose biosynthesis inhibitors based on the effects they exert on cellulose synthase subunits at the plasma membrane (Tateno *et al.*, 2016). Since Mp*rad8* lines are resistant to TXTA and isoxaben but not dichlobenil, a group II cellulose biosynthesis inhibitor, it is possible that loss-of-function of Mp*RAD8* affects the cell in a way which prevents the action of group I but not group II cellulose biosynthesis inhibitors.

Most of the putative weak loss-of-function lines grew larger than the putative strong loss-of-function lines, suggesting that loss-of-function of Mp*RAD8* confers a fitness cost. Most weeds with NTSR do not exhibit a fitness cost when grown without a herbicide (Keshtkar *et al.*, 2017, Wu *et al.*, 2018): NTSR involving strong loss-of-function of *RAD8* could therefore be absent in the field. However, studying the phenotypes of Mp*rad8* mutant lines is informative to understand what cellular processes can be disrupted to confer resistance to TXTA.

I found that Mp*rad8* lines overproduce reactive oxygen species (ROS), as do at least 3 TXTA-resistant lines with mutations in other genes (MpPSBP, MpPSAD, and a

peroxidase). This is consistent with observation from metazoans where ROS levels were higher in *rad8* mutants in *C. elegans* and *M. musculus*. I also found that Mp*rad8* lines are sensitive to ROS in the form of H_2O_2, suggesting that the increase in cellular levels of ROS in Mp*rad8* lines is substantial enough to cause significant susceptibility to toxic levels of ROS.

A study in *A. thaliana* found that pretreatment with exogenous H_2O_2 at 1 mM for 3 hours increased the resistance of cells to TXTA (Awwad *et al.*, 2019), so I hypothesised that the significant increase in ROS observed in Mp*rad8* lines could underly their resistance to TXTA. The same study found that TXTA decreased levels of ROS in cells, and that TXTA-treated cells exhibited decreases in cell wall stiffness as determined by atomic force microscopy. Treating cells with H_2O_2 increased cell wall stiffness, and cells pre-treated with H_2O_2 prior to TXTA treatment retained the increase in cell wall stiffness conferred by H_2O_2 (Awwad *et al.*, 2019). The effect of H_2O_2 on cell wall rigidity was suggested to be due to changes in activity of peroxidase-mediated cross linking of cell wall components due to a change in concentration of H_2O_2 (Awwad *et al.*, 2019). If the cell walls of *M. polymorpha* cells are affected in a similar way to those in *A. thaliana*, this effect could explain not only the TXTA resistance of Mp*rad8* lines but also their cross-resistance to isoxaben; both herbicides are classed as group 1 cellulose biosynthesis inhibitors, so may be similarly hindered by a resistance mechanism involving increased cell wall rigidity.

When I repeated the experiment from (Awwad *et al.*, 2019) in *M. polymorpha*, I was unable to demonstrate that pre-treatment with H_2O_2 at 1 mM for 3 hours conferred resistance to TXTA. In *A. thaliana*, only a particular concentration of ROS with a particular time of pre-treatment was able to confer TXTA resistance (Awwad *et al.*,

2019); it is therefore possible that I did not find the specific concentration of ROS which confers TXTA resistance in *M. polymorpha*. It is also possible that the types of ROS species generated by *M. polymorpha* due to loss-of-function of Mp*RAD8* are different to those generated in *A. thaliana*, and that H_2O_2 alone is unable to confer resistance to TXTA in *M. polymorpha*. I did find that growing gemmae on 100 nM TXTA confers resistance to 1 mM H_2O_2. This finding suggests TXTA and H_2O_2 have antagonistic effects in the cell, which is consistent with the antagonistic effects of TXTA and H_2O_2 on cell wall rigidity in *A. thaliana*, but this result does not definitely prove that ROS is the basis of TXTA resistance in Mp*rad8* lines.

Finally, I undertook a metabolomic analysis to identify differences in the modification of TXTA between Mp*rad8* predicted loss-of-function lines and wild-type lines, and found that Mp*rad8*^{GE1549} produces significantly less of an unknown compound than Tak-1. The compound in question is thought to be a TXTA metabolite without the nitro group. One possible hypothesis as to why a decreased concentration of this metabolite in Mp*rad8* lines leads to TXTA resistance is that unmodified TXTA is inactive (a protoxin) but becomes modified in wild-type lines to form this compound which is the bioactive (toxic) form of TXTA. TXTA is a natural product produced by *Streptomyces* species; *Streptomyces* can produce protoxins to prevent autotoxicity if they also require the target site of the toxin to function, such as in the case of bialaphos which is produced as a protoxin but bioactivated in planta to form the toxic chemical L-phosphinothricin which inhibits glutamine synthetase (Nandula *et al.*, 2019). If the TXTA metabolite missing the nitro group is the bioactive form of TXTA, its decreased production in Mp*rad8* mutant lines could underly their resistance. However, early experiments found that synthetic analogues of TXTA without the nitro group are inactive (King *et al.*, 1989). The nitro group in TXTA is part of a

nitroaromatic group; these are known to be highly toxic and mutagenic, and *Streptomyces* species can produce a range of these compounds, including the antibiotic chloramphenicol (Ju and Parales, 2010, Kovacic and Somanathan, 2014). I therefore do not think it likely that a TXTA metabolite missing the nitro group is the bioactive form of TXTA. Instead, I hypothesise that the reaction to form this TXTA metabolite could lead to the generation of toxic by-products; it has been reported that the most common reaction of a nitro group as part of an aromatic compound is reduction to an amine, and that the reactions involved in this conversion generate highly reactive intermediate nitroso radicals which can react with biomolecules to cause toxic effects (Spain, 1995). It is possible that removal of the nitro group from the tryptophan moiety of TXTA involves reduction, and therefore that toxic nitrogen containing radicals could be generated from the reaction to generate the TXTA metabolite. Since Mp*rad8* predicted loss-of-function lines produce less of this metabolite, fewer toxic by-products would be formed, which could underly the resistance of these lines to TXTA. It is possible that the MpRAD8 protein directly catalyses this reaction, or that the increased cellular ROS levels in Mp*rad8* lines prevent this reaction from occurring.

In conclusion, I confirmed my hypothesis that loss-of-function of Mp*RAD8* confers resistance to TXTA. This finding validates the ability of my approach in *M. polymorpha* to not only identify candidate resistance-conferring SNPs via forward genetics, but also to confirm their ability to confer resistance using reverse genetics. *RAD8* is not part of any gene family which has previously been implicated in non-target site resistance; my approach can therefore identify completely novel mechanisms of NTSR without any prior knowledge of the genes involved. I also functionally characterised the phenotypes of Mp*rad8* mutant lines, leading to the

discovery that predicted loss-of-function of Mp*rad8* confers cross-resistance to isoxaben and allowing me to form hypotheses regarding the basis of resistance in these lines. My approach can therefore be used not only to identify but also to functionally characterise novel mechanisms of NTSR, and offers significant potential for the discovery and understanding of the genetic and molecular basis of NTSR in weeds.

Chapter 6: General Discussion

The extensive use of herbicides for decades in agriculture has exerted a huge selection pressure for herbicide resistance to evolve in weeds (Gaines *et al.*, 2020). Non-target site resistance (NTSR) is particularly problematic because it can cause herbicide cross-resistance, and its complex polygenic basis makes it more difficult to identify molecular mechanisms of NTSR (Delye, 2013). Those which have been identified in weeds mostly involve genes from four gene families – P450s, GSTs, GTs, and ABC transporters – and all involve gain of function mutations (Yuan *et al.*, 2007). Very few mechanisms of NTSR involving loss of gene function have been reported: two were discovered using forward genetic screening in the model species *A. thaliana* and involve loss-of-function of the genes *PAM16* or *CUL1* which confer resistance to thaxtomin A (TXTA) and indaziflam respectively (Scheible *et al.*, 2003, Huang *et al.*, 2013, Reavell-Roy, 2019). In Chapter 2, I show that the mechanism of NTSR to TXTA conferred by loss-of-function of *PAM16* is conserved in *M. polymorpha*, validating its use as a species with which to study NTSR. I generated 33 Mp*pam16* loss-of-function mutants of which 9 were weakly resistant to TXTA. Not all loss-of-function mutations in Mp*PAM16* therefore conferred NTSR; future work using homology modelling to show how each mutation affects the structure of the PAM16 protein could elucidate why only certain mutations lead to NTSR.

In *A. thaliana*, total loss-of-function mutations in the *PAM16* gene confer NTSR to TXTA (Scheible *et al.*, 2003); in *M. polymorpha*, weak loss-of-function of *PAM16* is sufficient to confer NTSR to TXTA. I hypothesise that this is due to the second *PAM16* gene in the *A. thaliana* genome (*PAM16L*) conferring genetic redundancy, whereas there is only a single copy of *PAM16* in *M. polymorpha*. These results suggest that although this mechanism of NTSR may be conserved across land plants and therefore potentially present in weeds, the level of genetic redundancy in

the species in which it occurs affects the type of mutation required in *PAM16* to confer NTSR.

The 4 Mp*pam16* lines with the strongest TXTA resistance grew smaller than wild-type plants in control conditions suggesting that growth defects are likely in Mp*pam16* mutants with stronger resistance, which is consistent with the phenotypes of *A. thaliana pam16* mutants. I conclude that this mechanism of NTSR carries a fitness cost and is therefore likely to evolve in the field only under herbicide selection or if weeds carry additional compensatory mutations. Most weeds with NTSR do not carry fitness costs (Keshtkar *et al.*, 2017, Wu *et al.*, 2018), so loss-of-function of *PAM16* may not be selected for as a mechanism of NTSR in the field. However, determining the molecular basis of resistance in Mp*pam16* loss-of-function lines can identify molecular processes which when disrupted confer resistance to TXTA, and may therefore help with the identification of further mechanisms of NTSR which do not carry fitness costs. If loss-of-function of *PAM16* is identified as a mechanism of NTSR in the field and is associated with a fitness cost, weed management practices could be designed accordingly, for example by including herbicide “off” years or fallow years, when weeds with a loss-of-function mutation in *PAM16* would be outcompeted by fitter herbicide-sensitive weeds which can then be controlled by a herbicide the following year (Neve *et al.*, 2009, Vila-Aiub *et al.*, 2009). This example illustrates how knowledge of a molecular mechanism of NTSR and its resulting phenotypes can be used to design more effective weed management strategies.

Although few mechanisms of NTSR involving loss of gene function have been identified, it is likely that these mechanisms exist in weeds but cannot be discovered by methods that have been used to identify mechanisms of NTSR such as

transcriptomics. A forward genetic approach can uncover novel mechanisms of NTSR conferred by loss of gene function (Scheible *et al.*, 2003, Reavell-Roy, 2019), however genetic screens in diploid organisms such as *A. thaliana* are limited by the number of mutants which can be screened (Jander *et al.*, 2003). *M. polymorpha* is well suited for forward genetics as one plant can produce millions of spores which can be easily mutagenized, and it is a dominant haploid so mutants can be screened in the first generation (Kohchi *et al.*, 2021). In Chapter 3, I undertook a large-scale forward genetic screen in *M. polymorpha*, and isolated 13 mutants resistant to the proposed cellulose biosynthesis inhibitor TXTA (Mp*tar*). Mp*tar* mutants are likely NTSR as they were screened at the lethal dose of TXTA, grew smaller on TXTA than in untreated conditions indicating weak TXTA resistance, and 8 out of the 13 Mp*tar* lines were cross-resistant to other herbicides. A previous forward genetic screen in *A. thaliana* was only able to isolate one TXTA-resistant mutant (Scheible *et al.*, 2003); here, the isolation of 13 Mp*tar* mutants shows that large-scale forward genetic screens in *M. polymorpha* can yield a greater number of likely NTSR mutants, so offer greater potential of identifying novel NTSR mechanisms.

In Chapter 4, using an adapted version of a “non-allelism based” mapping-by-sequencing approach (Champion *et al.*, 2021), I identified candidate NTSR conferring SNPs for 11 of the 13 Mp*tar* mutants. Three of the 13 Mp*tar* mutants had a SNP in Mp*RAD8*. In Chapter 5, I used CRISPR-Cas9 targeted mutagenesis to generate 19 Mp*rad8* loss-of-function mutants: 12 Mp*rad8* lines with predicted strong loss-of-function mutations were significantly resistant to TXTA, proving that loss-of-function of Mp*RAD8* is a novel mechanism of NTSR to TXTA. With this result I demonstrate that a forward genetic approach in *M. polymorpha* can identify novel

mechanisms of NTSR conferred by loss of gene function without the need for crossing and classical complementation analysis.

In Chapter 4, I also show that 4 Mp*tar* mutants have candidate resistance-conferring SNPs in *M. polymorpha* homologues of 4 genes associated with NTSR in *A. tuberculatus* (Kreiner et al., 2019, Kreiner et al., 2021). This result proves that a forward genetic approach in *M. polymorpha* can not only identify novel mechanisms of NTSR such as that conferred by predicted loss-of-function of Mp*RAD8*, but can also corroborate other hypothesized NTSR mechanisms that have been proposed from the association of genetic polymorphisms with NTSR in wild weed populations, further validating the use of *M. polymorpha* as a model species for studying NTSR. The four NTSR associated genes identified in common between this study and the GWAS in *A. tuberculatus* are strong candidates for conferring NTSR; whether or not this is the case will be confirmed by targeted mutagenesis to induce SNPs in these genes in a wild-type background, in the same way that reverse genetics was used to demonstrate that NTSR is conferred by mutations in Mp*RAD8*. Targeted mutagenesis in *M. polymorpha* therefore provides a straightforward method to supplement GWAS studies by confirming that a candidate mutation confers NTSR.

Reverse genetics in *M. polymorpha* can be used to confirm mechanisms of NTSR identified by forward genetics; it can also be used to functionally characterise NTSR mutants. In Chapter 5 I show that Mp*rad8* predicted loss-of-function mutants overproduce ROS. At least 3 further Mp*tar* mutants also overproduced ROS. ROS has been shown to confer resistance to TXTA in *A. thaliana* (Awwad *et al.*, 2019), and in Chapter 5 I show that TXTA and ROS have antagonistic effects in *M. polymorpha*. Based on these results I propose that the mechanism of NTSR to TXTA

in Mp*rad8* loss-of-function mutants – and potentially in the 3 further Mp*tar* lines with increased ROS levels – may be linked to their overproduction of ROS. I propose that this could be due to ROS increasing the rigidity of the cell wall (Awwad *et al.*, 2019), which may hinder the action of both TXTA and isoxaben on the cell wall, explaining the resistance of Mp*rad8* mutants to these two herbicides.

Alternatively, the decrease in putative TXTA metabolite levels in Mp*rad8* mutants compared to wild-type lines may underly their resistance. An unknown compound with a molecular mass consistent with that of thaxtomin A without the nitro group of the 4-nitro-tryptophan moiety was present at lower levels in Mp*rad8* mutant lines with respect to wild-type, suggesting that Mp*rad8* mutants metabolise TXTA to a lesser extent. The significant difference in the concentration of this compound between the sensitive wild type and resistant Mp*rad8* mutants is likely to be linked to TXTA resistance in Mp*rad8* mutants. One hypothesis to explain the resistance of Mp*rad8* mutants is that this putative TXTA metabolite which is present at a lower concentration in Mp*rad8* mutants is the bioactive form of TXTA. However, it has been shown that the nitro group of TXTA is required for its phytotoxic activity (King *et al.*, 1989), and nitroaromatic compounds are well known for their toxicity (Ju and Parales, 2010, Kovacic and Somanathan, 2014), suggesting that the unmodified form of TXTA is the bioactive form and that the putative TXTA metabolite is less active. Instead, I propose that the reaction to form the putative TXTA metabolite results in the formation of toxic by-products. The reduction of nitro groups in nitroaromatic compounds leads to the formation of toxic nitrogen containing radicals (Spain, 1995), so if the removal of the nitro group involves its reduction this could result in the formation of toxic by-products. The decreased incidence of this reaction in Mp*rad8* mutants would therefore lead to decreased levels of toxic by-products

upon TXTA treatment, hence NTSR to TXTA. I propose that Mp*RAD8* may directly catalyse the reaction generating the putative TXTA metabolite, or that the increased levels of ROS in Mp*rad8* mutants may prevent the reaction from occurring.

Further experiments elucidating the effect of ROS on the properties of the *M. polymorpha* cell wall and studying the reaction to generate the putative TXTA metabolite and its possible by-products are necessary to determine whether either of these hypotheses regarding the basis of resistance in Mp*rad8* mutants is correct. Although I am still unable to definitively explain why Mp*rad8* mutants are resistant to TXTA, the ability to functionally characterise this mechanism of NTSR and to make hypotheses regarding the basis of resistance demonstrates the potential of my approach to not only identify novel mutations conferring resistance but also to understand the mechanism behind the resistance. The growth defects of Mp*rad8* putative loss-of-function mutant lines suggests that loss of *RAD8* function incurs a fitness cost, therefore this mechanism of resistance may be less likely to evolve in the field (Keshtkar *et al.*, 2017, Wu *et al.*, 2018). However, understanding the mechanisms underlying resistance in Mp*rad8* mutant lines can indicate molecular processes which when disrupted could confer resistance to TXTA, helping to identify potential NTSR mechanisms which are more likely to be present in the field. Furthermore, if loss-of-function of *RAD8* is identified in the field, a better understanding of the basis of this resistance can inform weed management practices: based on the results in Chapter 5, weeds with NTSR due to a loss-of-function of *RAD8* are likely to overproduce ROS so are theoretically more sensitive to herbicides acting via ROS overproduction such as paraquat or glufosinate (Fukushima *et al.*, 1993, Hawkes, 2014, Takano *et al.*, 2019), cannot be controlled by isoxaben to which they are cross-resistant, and carry a fitness cost so could be

managed by exploiting their likelihood to be outcompeted by weeds with a wild-type copy of *RAD8* in non-herbicide conditions.

In conclusion, in this thesis I confirmed the conservation in *M. polymorpha* of the NTSR mechanism identified in *A. thaliana* conferred by loss-of-function of the gene *PAM16* – one of only two known NTSR mechanisms conferred by loss of gene function – and subsequently used *M. polymorpha* as a tool to identify novel mechanisms of NTSR. Using a forward genetic approach coupled with mapping-by-sequencing, I identified strong candidate NTSR-conferring SNPs in 11 TXTA-resistant Mp*tar* mutants, 4 of which were in genes associated with NTSR by a GWAS in the glyphosate-resistant weed *A. tuberculatus*, and another 3 of which were in the Mp*RAD8* gene. By generating Mp*rad8* loss-of-function mutants using targeted mutagenesis, I identified a novel mechanism of NTSR to TXTA involving loss-of-function of the *RAD8* gene and undertook a detailed phenotypic characterisation of Mp*rad8* mutants allowing me to propose hypotheses regarding the molecular basis of their NTSR. The ability to not only identify but also functionally characterise novel mechanisms of NTSR using the approach taken in this thesis presents a novel and timely framework with which to broaden our understanding of the genes and mechanisms involved in non-target site herbicide resistance in weeds.

Appendix: GO enrichment analysis of candidate resistance-conferring SNPs in Mp*tar* lines

In Chapter 4, I hypothesised that some Mp*tar* mutant lines including Mp*tar*10 and Mp*tar*11 may have SNPs which mitigate the toxic effect of TXTA by affecting the cellular pathway targeted by TXTA. These SNPs would be present in genes annotated by GO terms relating to the mode of action of TXTA, which is thought to be cellulose biosynthesis inhibition but is also consistent with microtubule inhibition (Fry and Loria, 2002).

If multiple Mp*tar* mutant lines contain SNPs conferring NTSR by affecting the pathway targeted by TXTA, I hypothesise that GO terms related to the mode of action of TXTA are enriched in the genes containing candidate resistance-conferring mutations in Mp*tar* lines. To identify enriched GO terms assigned to the candidate resistance-conferring SNPs in Mp*tar* mutant lines, I carried out a GO enrichment analysis using the ViSEAGO package in R (Brionne *et al.*, 2019). This package identifies GO terms which are significantly overrepresented in a list of candidate genes. I found that the most significantly enriched “biological process” GO term was GO:0042546 (cell wall biogenesis) ($p = 0.00256$) (Fig. A.1). The most significantly enriched “molecular function” GO term was GO:0003676 (nucleic acid binding) ($p = 0.000279$), and there were no enriched “cellular component” GO terms.

The most significantly enriched “biological process” term in Mp*tar* lines GO:0042546 (cell wall biogenesis) is unique to candidate resistance-conferring SNPs in Mp*tar* lines, whereas the most significantly enriched “molecular function” term GO:0003676 (nucleic acid binding) is common to both Mp*tar* and Mp*chlr* lines (Table A.2). Since the resistance-conferring mutations in Mp*chlr* lines are in Mp*AHAS*, all other mutations in these lines are background UV-B induced mutations. In Mp*chlr* lines, the GO term GO:0003676 (nucleic acid binding) therefore annotates one or more genes containing

background mutations which do not confer resistance to TXTA since Mp*chlr* lines are not cross-resistant to TXTA. I therefore conclude that in Mp*tar* lines also the GO term GO:0003676 (nucleic acid binding) is more likely to annotate background mutations than NTSR-conferring mutations.

I conclude that the mutations in the genes upon which the enrichment of GO:0042546 (cell wall biogenesis) is based are strong candidates for NTSR-conferring mutations in Mp*tar* lines related to the mode of action of TXTA (Table A.3). These include SNPs in xyloglucan fucosyltransferases in Mp*tar*3 and Mp*tar*9, a SNP in xyloglucan endotransglycolase in Mp*tar*6, and a SNP in mur ligase in Mp*tar*7. However, the most likely resistance-conferring SNP was already identified for these lines. The SNPs identified in Mp*tar*3, Mp*tar*6, Mp*tar*7 and Mp*tar*9 by the GO enrichment analysis will be investigated further if the SNPs identified by previous analyses in Chapter 4 are found not to confer resistance in these lines.

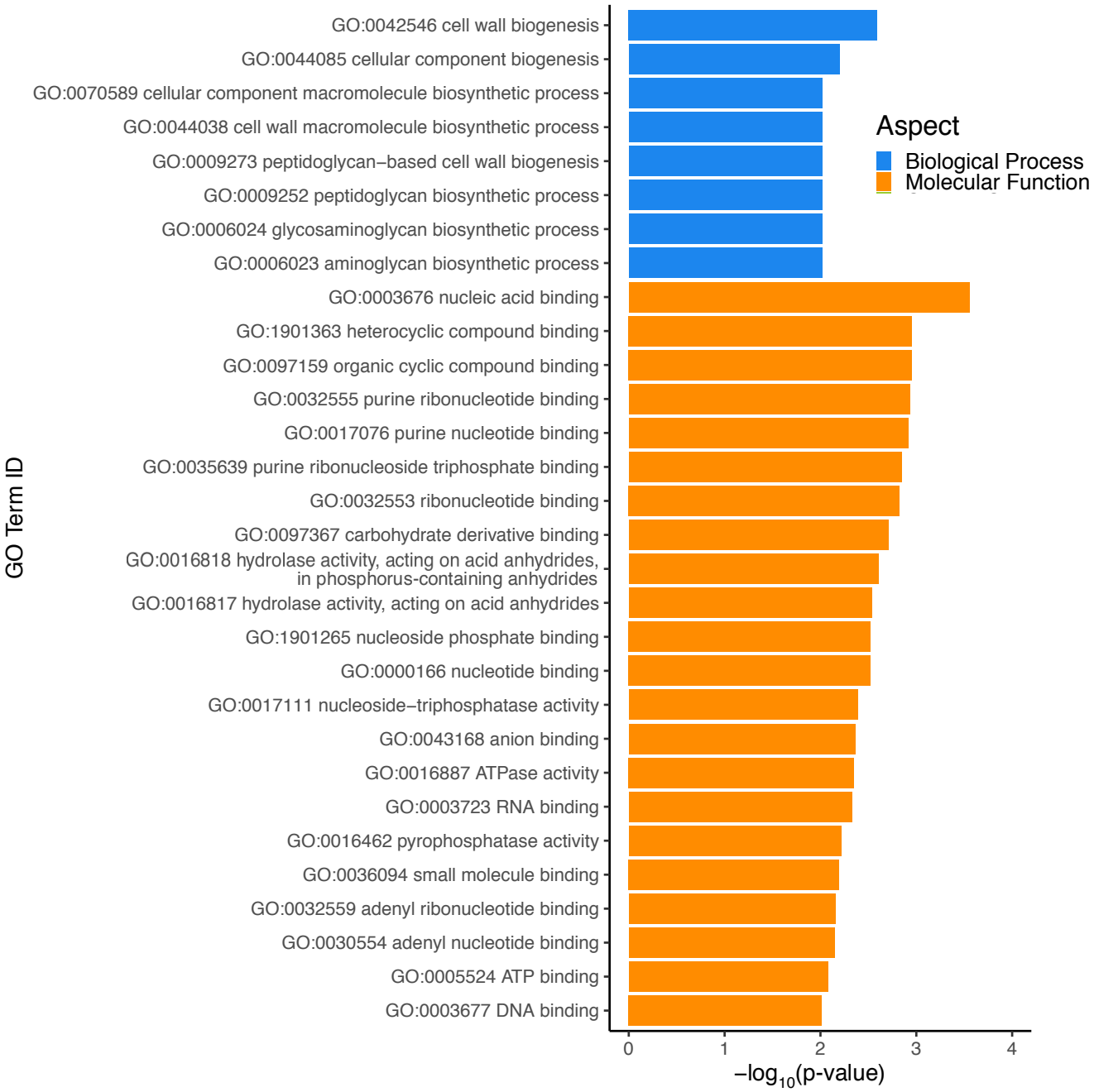

Fig. A.1. GO enrichment analysis of candidate resistance-conferring genes in thaxtomin-resistant lines. Thaxtomin-resistant lines were generated by UV-B mutagenesis. The genomes of each line were sequenced using next-generation sequencing, and candidate resistance-conferring SNPs were identified in a SNP-calling analysis. A GO enrichment analysis was carried out on the list of genes in which candidate resistance-conferring SNPs are found using the ViSEAGO package in R. A custom *M. polymorpha* GO database was built using the functional annotation of the reference *M. poymorpha* v5.1 genome, and the lists of genes of interest (those mutated in either chlorsulfuron-resistant or thaxtomin A-resistant lines) were annotated according to this database. The enrichment anlysis was performed using Fisher's exact test using the classic algorithm for GO terms of all three aspects (biological process, molecular function, and cellular component). Enriched GO terms from each GO aspect are ordered by significance as determined by -$\log_{10}$(p-value).

Thaxtomin A only			Both		Chlorsulfuron only	
GO:0000049	GO:0006511	GO:0017119	GO:0000027	GO:0009982	GO:0000150	GO:0042026
GO:0000103	GO:0006556	GO:0019898	GO:0000155	GO:0016020	GO:0000724	GO:0070006
GO:0000151	GO:0006596	GO:0020037	GO:0000160	GO:0016021	GO:0003690	GO:0071918
GO:0000398	GO:0006597	GO:0030983	GO:0000166	GO:0016310	GO:0003697	GO:0090228
GO:0000413	GO:0006606	GO:0031011	GO:0000287	GO:0016491	GO:0003700	GO:1990426
GO:0001510	GO:0006629	GO:0031119	GO:0001522	GO:0016567	GO:0004134	GO:2000022
GO:0002098	GO:0006633	GO:0031267	GO:0003676	GO:0016592	GO:0004190	GO:2000031
GO:0003678	GO:0006979	GO:0032508	GO:0003677	GO:0016772	GO:0004252	GO:2001070
GO:0003746	GO:0007017	GO:0032968	GO:0003712	GO:0016887	GO:0004674	
GO:0003755	GO:0008033	GO:0033588	GO:0003723	GO:0030145	GO:0005247	
GO:0004014	GO:0008107	GO:0035267	GO:0003735	GO:0030976	GO:0005576	
GO:0004020	GO:0008168	GO:0035658	GO:0003743	GO:0043531	GO:0005784	
GO:0004089	GO:0008233	GO:0042254	GO:0003777	GO:0047834	GO:0005968	
GO:0004222	GO:0008234	GO:0042546	GO:0003824	GO:0050660	GO:0006259	
GO:0004315	GO:0008270	GO:0042626	GO:0003924	GO:0055085	GO:0006281	
GO:0004478	GO:0008295	GO:0042744	GO:0003984	GO:0070615	GO:0006368	
GO:0004523	GO:0008757	GO:0043039	GO:0004386	GO:1990939	GO:0006415	
GO:0004553	GO:0008763	GO:0043139	GO:0004672		GO:0006817	
GO:0004601	GO:0009058	GO:0043169	GO:0004842		GO:0006821	
GO:0004644	GO:0009522	GO:0046872	GO:0005315		GO:0008094	
GO:0004722	GO:0009523	GO:0046912	GO:0005515		GO:0008097	
GO:0004812	GO:0009538	GO:0048046	GO:0005524		GO:0008236	
GO:0004818	GO:0009654	GO:0051082	GO:0005525		GO:0008318	
GO:0004843	GO:0010029	GO:0097255	GO:0005634		GO:0009055	
GO:0005337	GO:0010411	GO:0140326	GO:0005737		GO:0009408	
GO:0005507	GO:0015914	GO:1901642	GO:0005840		GO:0009416	
GO:0005509	GO:0015935	GO:1990547	GO:0005975		GO:0009862	
GO:0005618	GO:0015979		GO:0006355		GO:0010333	
GO:0005874	GO:0016192		GO:0006357		GO:0010343	
GO:0006073	GO:0016579		GO:0006396		GO:0015035	
GO:0006139	GO:0016740		GO:0006412		GO:0015204	
GO:0006189	GO:0016742		GO:0006413		GO:0016570	
GO:0006260	GO:0016746		GO:0006457		GO:0016593	
GO:0006289	GO:0016747		GO:0006468		GO:0016765	
GO:0006298	GO:0016762		GO:0006508		GO:0016798	
GO:0006325	GO:0016783		GO:0006886		GO:0016829	
GO:0006342	GO:0016787		GO:0007018		GO:0016977	
GO:0006397	GO:0016788		GO:0007165		GO:0018342	
GO:0006414	GO:0016791		GO:0008017		GO:0018344	
GO:0006418	GO:0016818		GO:0009082		GO:0019538	
GO:0006424	GO:0016836		GO:0009451		GO:0022857	
GO:0006470	GO:0016874		GO:0009507		GO:0030246	

Table A.2. List of GO terms assigned to candidate resistance-conferring SNPs in thaxtomin-A resistant lines, chlorsulfuron-resistant lines, or both. TXTA-resistant and chlorsulfuron-resistant lines were generated by UV-B or EMS mutagenesis. The genomes of each line were sequenced using next-generation sequencing, and candidate resistance-conferring SNPs were identified in a SNP-calling analysis. The GO terms in this table are those assigned to the genes containing candidate resistance-conferring SNPs.

***M. polymorpha* gene ID**	**GO terms**	**Gene annotation**	**Mp*tar* line**
Mp2g12440	GO:0042546 (cell wall biogenesis) GO:0008107 (galactoside 2-alpha-L-fucosyltransferase activity) GO:0016020 (membrane)	Xyloglucan fucosyltransferase	Mp*tar*3
Mp3g22120	GO:0042546 (cell wall biogenesis) GO:0005975 (carbohydrate metabolic process) GO:0048046 (apoplast) GO:0010411 (xyloglucan metabolic process) GO:0006073 (cellular glucan metabolic process) GO:0005618 (cell wall) GO:0016762 (xyloglucan:xyloglucosyl transferase activity) GO:0004553 (hydrolase activity, hydrolyzing O-glycosyl compounds)	Xyloglucan endotransglycolase	Mp*tar*6
Mp5g21570	GO:0009058 (biosynthetic process) GO:0005524 (ATP binding) GO:0016874 (ligase activity) GO:0009252 (peptidoglycan biosynthetic process) GO:0008763 (UDP-N-acetylmuramate-L-alanine ligase activity)	Mp*MURC*; Mur ligase	Mp*tar*7
Mp7g07400	GO:0042546 (cell wall biogenesis) GO:0008107 (galactoside 2-alpha-L-fucosyltransferase activity) GO:0016020 (membrane)	Xyloglucan fucosyltransferase	Mp*tar*9

Table A.3. List of genes containing a candidate resistance-conferring SNP upon which the enrichment of GO:0042546 (cell wall biogenesis) is based. A GO enrichment analysis was carried out on the list of genes in which candidate resistance-conferring SNPs are found in Mp*tar* lines using the ViSEAGO package in R (Fisher's exact test, classic algorithm). The most significantly enriched "biological process" GO term was GO:0042546; cell wall biogenesis ($p = 0.00255521$). The enrichment was based on the presence of the genes listed; each gene is either annotated with GO:0042546 or with a child term of GO:0042546 (e.g. GO:0009252; peptidoglycan biosynthetic process).

Bibliography

Addo-Quaye, C., Buescher, E., Best, N., Chaikam, V., Baxter, I. and Dilkes, B.P. (2017) Forward Genetics by Sequencing EMS Variation-Induced Inbred Lines. *G3-Genes Genomes Genetics*, **7**, 413-425.

Almsick, A. (2009) New HPPD-Inhibitors - A Proven Mode of Action as a New Hope to Solve Current Weed Problems. *Outlooks on Pest Management*, **20**, 27-30.

Amrhein, N., Deus, B., Gehrke, P. and Steinrucken, H.C. (1980) The Site of the Inhibition of the Shikimate Pathway by Glyphosate: II. INTERFERENCE OF GLYPHOSATE WITH CHORISMATE FORMATION IN VIVO AND IN VITRO. *Plant Physiol*, **66**, 830-834.

An, J., Shen, X.F., Ma, Q.B., Yang, C.Y., Liu, S.M. and Chen, Y. (2014) Transcriptome Profiling to Discover Putative Genes Associated with Paraquat Resistance in Goosegrass (Eleusine indica L.). *Plos One*, **9**.

Auten, R.L. and Davis, J.M. (2009) Oxygen Toxicity and Reactive Oxygen Species: The Devil Is in the Details. *Pediatric Research*, **66**, 121-127.

Awwad, F., Bertrand, G., Grandbois, M. and Beaudoin, N. (2019) Reactive Oxygen Species Alleviate Cell Death Induced by Thaxtomin A in Arabidopsis thaliana Cell Cultures. *Plants-Basel*, **8**, 13.

Bajsa, J., Pan, Z.Q., Dayan, F.E., Owens, D.K. and Duke, S.O. (2012) Validation of serine/threonine protein phosphatase as the herbicide target site of endothall. *Pesticide Biochemistry and Physiology*, **102**, 38-44.

Baker, H.G. (1974) The evolution of weeds. *Annual review of ecology and systematics*, **5**, 1-24.

Barry, G.F., Kishore, G.M., Padgette, S.R. and Stallings, W.C. (1997) Glyphosate-tolerant 5-enolpyruvylshikimate-3-phosphate synthases. United States.

Bowman, J.L., Kohchi, T., Yamato, K.T., Jenkins, J., Shu, S., Ishizaki, K., Yamaoka, S., Nishihama, R., Nakamura, Y., Berger, F., Adam, C., Aki, S.S., Althoff, F., Araki, T., Arteaga-Vazquez, M.A., Balasubrmanian, S., Barry, K., Bauer, D., Boehm, C.R., Briginshaw, L., Caballero-Perez, J., Catarino, B., Chen, F., Chiyoda, S., Chovatia, M., Davies, K.M., Delmans, M., Demura, T., Dierschke, T., Dolan, L., Dorantes-Acosta, A.E., Eklund, D.M., Florent, S.N., Flores-Sandoval, E., Fujiyama, A., Fukuzawa, H., Galik, B., Grimanelli, D., Grimwood, J., Grossniklaus, U., Hamada, T., Haseloff, J., Hetherington, A.J., Higo, A., Hirakawa, Y., Hundley, H.N., Ikeda, Y., Inoue, K., Inoue, S.-i., Ishida, S., Jia, Q., Kakita, M., Kanazawa, T., Kawai, Y., Kawashima, T., Kennedy, M., Kinose, K., Kinoshita, T., Kohara, Y., Koide, E., Komatsu, K., Kopischke, S., Kubo, M., Kyozuka, J., Lagercrantz, U., Lin, S.-S., Lindquist, E., Lipzen, A.M., Lu, C.-W., De Luna, E., Martienssen, R.A., Minamino, N., Mizutani, M., Mizutani, M., Mochizuki, N., Monte, I., Mosher, R., Nagasaki, H., Nakagami, H., Naramoto, S., Nishitani, K., Ohtani, M., Okamoto, T., Okumura, M., Phillips, J., Pollak, B., Reinders, A., Rövekamp, M., Sano, R., Sawa, S., Schmid, M.W., Shirakawa, M., Solano, R., Spunde, A., Suetsugu, N., Sugano, S., Sugiyama, A., Sun, R., Suzuki, Y., Takenaka, M., Takezawa, D., Tomogane, H., Tsuzuki, M., Ueda, T., Umeda, M., Ward, J.M., Watanabe, Y., Yazaki, K., Yokoyama, R., Yoshitake, Y., Yotsui, I., Zachgo,

S. and Schmutz, J. (2017) Insights into Land Plant Evolution Garnered from the Marchantia polymorpha Genome. *Cell*, **171**, 287-304.e215.
Bradshaw, L.D., Padgette, S.R., Kimball, S.L. and Wells, B.H. (1997) Perspectives on glyphosate resistance. *Weed Technology*, **11**, 189-198.
Brash, D.E. (2015) UV Signature Mutations. *Photochemistry and Photobiology*, **91**, 15-26.
Bridges, D.C. (1994) IMPACT OF WEEDS ON HUMAN ENDEAVORS. *Weed Technology*, **8**, 392-395.
Brionne, A., Juanchich, A. and Hennequet-Antier, C. (2019) ViSEAGO: a Bioconductor package for clustering biological functions using Gene Ontology and semantic similarity. *Biodata Mining*, **12**, 13.
Burnet, M.W.M., Hart, Q., Holtum, J.A.M. and Powles, S.B. (1994) RESISTANCE TO 9 HERBICIDE CLASSES IN A POPULATION OF RIGID RYEGRASS (LOLIUM-RIGIDUM). *Weed Science*, **42**, 369-377.
Burton, J.D., Gronwald, J.W., Somers, D.A., Connelly, J.A., Gengenbach, B.G. and Wyse, D.L. (1987) INHIBITION OF PLANT ACETYL-COENZYME A CARBOXYLASE BY THE HERBICIDES SETHOXYDIM AND HALOXYFOP. *Biochemical and Biophysical Research Communications*, **148**, 1039-1044.
Campe, R., Hollenbach, E., Kammerer, L., Hendriks, J., Hoffken, H.W., Kraus, H., Lerchl, J., Mietzner, T., Tresch, S., Witschel, M. and Hutzler, J. (2018) A new herbicidal site of action: Cinmethylin binds to acyl-ACP thioesterase and inhibits plant fatty acid biosynthesis. *Pestic Biochem Physiol*, **148**, 116-125.
Cechin, J., Piasecki, C., Benemann, D.P., Kremer, F.S., Galli, V., Maia, L.C., Agostinetto, D. and Vargas, L. (2020) Transcriptome Analysis Identifies Candidate Target Genes Involved in Glyphosate-Resistance Mechanism in Lolium multiflorum. *Plants-Basel*, **9**.
Chaleff, R.S. and Ray, T.B. (1984) HERBICIDE-RESISTANT MUTANTS FROM TOBACCO CELL-CULTURES. *Science*, **223**, 1148-1151.
Champion, C., Lamers, J., Jones, V.A.S., Morieri, G., Honkanen, S. and Dolan, L. (2021) Microtubule associated protein WAVE DAMPENED2-LIKE (WDL) controls microtubule bundling and the stability of the site of tip-growth in Marchantia polymorpha rhizoids. *Plos Genetics*, **17**, 20.
Chen, K., Peng, Y.J., Zhang, L., Wang, L., Mao, D.H., Zhao, Z.H., Bai, L.Y. and Wang, L.F. (2021a) Whole transcriptome analysis resulted in the identification of Chinese sprangletop (Leptochloa chinensis) genes involved in cyhalofop-butyl tolerance. *Bmc Genomics*, **22**.
Chen, X.J., Ghazanfar, B., Khan, A.R., Hayat, S. and Cheng, Z.H. (2013) Comparative Analysis of Putative Orthologues of Mitochondrial Import Motor Subunit: Pam18 and Pam16 in Plants. *Plos One*, **8**, 13.
Chen, Z., Wang, Z., Heng, Y.F., Li, J., Pei, J.W., Cao, Y., Deng, X.W. and Ma, L.G. (2021b) Generation of a series of mutant lines resistant to imidazolinone by screening an EMS-based mutant library in common wheat. *Crop Journal*, **9**, 1030-1038.
Chitnis, V.P., Ke, A. and Chitnis, P.R. (1997) The PsaD subunit of photosystem I - Mutations in the basic domain reduce the level of PsaD in the membranes. *Plant Physiology*, **115**, 1699-1705.
Clough, J.M., Dale, R.P., Elsdon, B., Hawkes, T.R., Hogg, B.V., Howell, A., Kloer, D.P., Lecoq, K., McLachlan, M.M.W., Milnes, P.J., O'Riordan, T.J.C., Ranasinghe, S., Shanahan, S.E., Sumner, K.D. and Tayab, S.

(2016) Synthesis and evaluation of hydroxyazolopyrimidines as herbicides; thegeneration of amitrole in planta. *Pest Management Science*, **72**, 2254-2272.

Cummins, I., Bryant, D.N. and Edwards, R. (2009) Safener responsiveness and multiple herbicide resistance in the weed black-grass (Alopecurus myosuroides). *Plant Biotechnology Journal*, **7**, 807-820.

Cummins, I., Cole, D.J. and Edwards, R. (1999) A role for glutathione transferases functioning as glutathione peroxidases in resistance to multiple herbicides in black-grass. *Plant Journal*, **18**, 285-292.

Cummins, I., Wortley, D.J., Sabbadin, F., He, Z., Coxon, C.R., Straker, H.E., Sellars, J.D., Knight, K., Edwards, L., Hughes, D., Kaundun, S.S., Hutchings, S.-J., Steel, P.G. and Edwards, R. (2013) Key role for a glutathione transferase in multiple-herbicide resistance in grass weeds. *Proceedings of the National Academy of Sciences of the United States of America*.

D'Silva, P.R., Schilke, B., Walter, W. and Craig, E.A. (2005) Role of Pam16's degenerate J domain in protein import across the mitochondrial inner membrane. *Proceedings of the National Academy of Sciences of the United States of America*, **102**, 12419-12424.

Daudi, A. and O'Brien, J.A. (2012) Detection of Hydrogen Peroxide by DAB Staining in Arabidopsis Leaves. *Bio-protocol*, **2**, e263.

Dayan, F. and Duke, S. (2014) Natural Compounds as Next-Generation Herbicides. *Plant Physiology*, **166**, 1090-1105.

Dayan, F., Haesaert, G., Thomas, V.L., Holden-Dye, L., Crossthwaite, A. and Nauen, R. (2019a) Pesticides Modes of Action and Resistance: A Perspective from the 2019 IUPAC Congress. *Outlooks on Pest Management*, **30**, 157-163.

Dayan, F.E., Barker, A., Dayan, L.C. and Ravet, K. (2019b) The Role of Antioxidants in the Protection of Plants against Inhibitors of Protoporphyrinogen Oxidase. *Reactive Oxygen Species*, **7**, 55–63.

Dayan, F.E., Owens, D.K. and Duke, S.O. (2012) Rationale for a natural products approach to herbicide discovery. *Pest Management Science*, **68**, 519-528.

Delye, C. (2013) Unravelling the genetic bases of non-target-site-based resistance (NTSR) to herbicides: a major challenge for weed science in the forthcoming decade. *Pest Management Science*, **69**, 176-187.

Delye, C., Gardin, J.A.C., Boucansaud, K., Chauvel, B. and Petit, C. (2011a) Non-target-site-based resistance should be the centre of attention for herbicide resistance research: Alopecurus myosuroides as an illustration. *Weed Research*, **51**, 433-437.

Delye, C., Jasieniuk, M. and Le Corre, V. (2013) Deciphering the evolution of herbicide resistance in weeds. *Trends in Genetics*, **29**, 649-658.

Delye, C., Michel, S., Berard, A., Chauvel, B., Brunel, D., Guillemin, J.P., Dessaint, F. and Le Corre, V. (2010) Geographical variation in resistance to acetyl-coenzyme A carboxylase-inhibiting herbicides across the range of the arable weed Alopecurus myosuroides (black-grass). *New Phytologist*, **186**, 1005-1017.

Delye, C., Pernin, F. and Michel, S. (2011b) 'Universal' PCR assays detecting mutations in acetyl-coenzyme A carboxylase or acetolactate synthase that endow herbicide resistance in grass weeds. *Weed Research*, **51**, 353-362.

Devine, M., Duke, S.O. and Fedtke, C. (1993) *Physiology of Herbicide Action*: P T R Prentice Hall.

Dietz, K.-J., Mittler, R. and Noctor, G. (2016) Recent Progress in Understanding the Role of Reactive Oxygen Species in Plant Cell Signaling. *Plant Physiology*, **171**, 1535-1539.

Dimaano, N.G., Yamaguchi, T., Fukunishi, K., Tominaga, T. and Iwakami, S. (2020) Functional characterization of cytochrome P450 CYP81A subfamily to disclose the pattern of cross-resistance in Echinochloa phyllopogon. *Plant Molecular Biology*, **102**, 403-416.

Duggleby, R.G., Pang, S.S., Yu, H.Q. and Guddat, L.W. (2003) Systematic characterization of mutations in yeast acetohydroxyacid synthase - Interpretation of herbicide-resistance data. *European Journal of Biochemistry*, **270**, 2895-2904.

Duhoux, A., Carrere, S., Gouzy, J., Bonin, L. and Delye, C. (2015) RNA-Seq analysis of rye-grass transcriptomic response to an herbicide inhibiting acetolactate-synthase identifies transcripts linked to non-target-site-based resistance. *Plant Molecular Biology*, **87**, 473-487.

Duke, S. (2012) Why have no new herbicide modes of action appeared in recent years? *Pest Management Science*, **68**, 505-512.

Duke, S.O. and Powles, S.B. (2008) Glyphosate: a once-in-a-century herbicide. *Pest Management Science*, **64**, 319-325.

Edwards, R., Dixon, D.P., Cummins, I., Brazier-Hicks, M. and Skipsey, M. (2011) New Perspectives on the Metabolism and Detoxification of Synthetic Compounds in Plants. In *Organic Xenobiotics and Plants: from Mode of Action to Ecophysiology* (Schroder, P. and Collins, C.D. eds). Dordrecht: Springer, pp. 125-148.

Edwards, R. and Onkokesung, N. (2020) Resisting resistance: new applications for molecular diagnostics in crop protection. *The Biochemist*, **42**, 6-12.

Erickson, J.M., Rahire, M., Bennoun, P., Delepelaire, P., Diner, B. and Rochaix, J.-D. (1984) Herbicide resistance in Chlamydomonas reinhardtii results from a mutation in the chloroplast gene for the 32-kilodalton protein of photosystem II. *PNAS*.

Ferhatoglu, Y. and Barrett, M. (2006) Studies of clomazone mode of action. *Pesticide Biochemistry and Physiology*, **85**, 7-14.

Frazier, A.E., Dudek, J., Guiard, B., Voos, W., Li, Y.F., Lind, M., Meisinger, C., Geissler, A., Sickmann, A., Meyer, H.E., Bilanchone, V., Cumsky, M.G., Truscott, K.N., Pfanner, N. and Rehling, P. (2004) Pam16 has an essential role in the mitochondrial protein import motor. *Nature Structural & Molecular Biology*, **11**, 226-233.

Fry, B.A. and Loria, R. (2002) Thaxtomin A: evidence for a plant cell wall target. *Physiological and Molecular Plant Pathology*, **60**, 1-8.

Fujii, M., Yasuda, K., Hartmann, P.S., Ayusawa, D. and Ishii, N. (2011) A mutation in a mitochondrial dehydrogenase/reductase gene causes an increased sensitivity to oxidative stress and mitochondrial defects in the nematode Caenorhabditis elegans. *Genes to Cells*, **16**, 1022-1034.

Fukushima, T., Yamada, K., Isobe, A., Shiwaku, K. and Yamane, Y. (1993) MECHANISM OF CYTOTOXICITY OF PARAQUAT .1. NADH OXIDATION AND PARAQUAT RADICAL FORMATION VIA COMPLEX-I. *Experimental and Toxicologic Pathology*, **45**, 345-349.

Gaines, T.A., Duke, S.O., Morran, S., Rigon, C.A.G., Tranel, P.J., Kupper, A. and Dayan, F.E. (2020) Mechanisms of evolved herbicide resistance. *Journal of Biological Chemistry*, **295**, 10307-10330.

Gaines, T.A., Lorentz, L., Figge, A., Herrmann, J., Maiwald, F., Ott, M.C., Han, H.P., Busi, R., Yu, Q., Powles, S.B. and Beffa, R. (2014) RNA-Seq transcriptome analysis to identify genes involved in metabolism-based diclofop resistance in Lolium rigidum. *Plant Journal*, **78**, 865-876.

Gardin, J.A.C., Gouzy, J., Carrere, S. and Delye, C. (2015) ALOMYbase, a resource to investigate non-target-site-based resistance to herbicides inhibiting acetolactate-synthase (ALS) in the major grass weed Alopecurus myosuroides (black-grass). *Bmc Genomics*, **16**.

Gardner, S.N., Gressel, J. and Mangel, M. (1998) A revolving dose strategy to delay the evolution of both quantitative vs major monogene resistances to pesticides and drugs. *International Journal of Pest Management*, **44**, 161-180.

Gay, C., Collins, J. and Gebicki, J.M. (1999) Hydroperoxide assay with the ferric-xylenol orange complex. *Analytical Biochemistry*, **273**, 149-155.

Ghanizadeh, H. and Harrington, K.C. (2021) Herbicide resistant weeds in New Zealand: state of knowledge. *New Zealand Journal of Agricultural Research*, **64**, 471-482.

Ghanizadeh, H., Harrington, K.C. and James, T.K. (2015) Glyphosate-resistant Lolium multiflorum and Lolium perenne populations from New Zealand are also resistant to glufosinate and amitrole. *Crop Protection*, **78**, 1-4.

Giacomini, D.A., Patterson, E.L., Kupper, A., Beffa, R., Gaines, T.A. and Tranel, P.J. (2020) Coexpression Clusters and Allele-Specific Expression in Metabolism-Based Herbicide Resistance. *Genome Biology and Evolution*, **12**, 2267-2278.

Gil, M., Vega, T., Felitti, S., Picardi, L., Balzergue, S. and Nestares, G. (2018) Characterization of Non-Target-Site Mechanisms in Imidazolinone-Resistant Sunflower by RNA-seq. *Helia*, **41**, 267-278.

Gimenez-Abian, M.I., Panzera, F., Lopez-Saez, J.F., Gimenez-Abian, J.F., De la Torre, C. and Gimenez-Martin, G. (1998) Immediate disruption of spindle poles and induction of additional microtubule-organizing centres by a phenylcarbamate, during plant mitosis. *Protoplasma*, **204**, 119-127.

Goggin, D.E., Powles, S.B. and Steadman, K.J. (2012) Understanding Lolium rigidum Seeds: The Key to Managing a Problem Weed? *Agronomy*, **2**.

Green, J.M. (2012) The benefits of herbicide-resistant crops. *Pest Management Science*, **68**, 1323-1331.

Gressel, J. (2000) Molecular biology of weed control. *Transgenic Research*, **9**, 355-382.

Gressel, J. (2009) Evolving understanding of the evolution of herbicide resistance. *Pest Management Science*, **65**, 1164-1173.

Grossmann, K. (2010) Auxin herbicides: current status of mechanism and mode of action. *Pest Management Science*, **66**, 113-120.

Gruszka, D., Szarejko, I. and Maluszynski, M. (2012) Sodium Azide as a Mutagen. In *Plant Mutation Breeding and Biotechnology* (Shu, Q.Y., Forster, B.P. and Nakagawa, H. eds). Wallingford: Cabi Publishing-C a B Int, pp. 159-166.

Guindon, S., Dufayard, J.F., Lefort, V., Anisimova, M., Hordijk, W. and Gascuel, O. (2010) New Algorithms and Methods to Estimate Maximum-Likelihood Phylogenies: Assessing the Performance of PhyML 3.0. *Systematic Biology*, **59**, 307-321.

Guo, C., McDowell, I.C., Nodzenski, M., Scholtens, D.M., Allen, A.S., Lowe, W.L. and Reddy, T.E. (2017) Transversions have larger regulatory effects than transitions. *Bmc Genomics*, **18**.

Han, H.P., Yu, Q., Beffa, R., Gonzalez, S., Maiwald, F., Wang, J. and Powles, S.B. (2021) Cytochrome P450 CYP81A10v7 in Lolium rigidum confers metabolic resistance to herbicides across at least five modes of action. *Plant Journal*, **105**, 79-92.

Hartman, P.S. and Herman, R.K. (1982) RADIATION-SENSITIVE MUTANTS OF CAENORHABDITIS-ELEGANS. *Genetics*, **102**, 159-178.

Hatzios, K.K. (1997) Regulation of enzymatic systems detoxifying xenobiotics in plants: A brief overview and directions for future research. *Regulation of Enzymatic Systems Detoxifying Xenobiotics in Plants*, **37**, 1-5.

Hawkes, T.R. (2014) Mechanisms of resistance to paraquat in plants. *Pest Management Science*, **70**, 1316-1323.

Heap, I. (2014) Global perspective of herbicide-resistant weeds. *Pest Management Science*, **70**, 1306-1315.

Heap, I. (2022) The International Survey of Herbicide Resistant Weeds.

Heim, D.R., Skomp, J.R., Tschabold, E.E. and Larrinua, I.M. (1990) Isoxaben Inhibits the Synthesis of Acid Insoluble Cell Wall Materials In Arabidopsis thaliana. *Plant Physiol*, **93**, 695-700.

Hellmann, H., Hobbie, L., Chapman, A., Dharmasiri, S., Dharmasiri, N., del Pozo, C., Reinhardt, D. and Estelle, M. (2003) Arabidopsis AXR6 encodes CUL1 implicating SCF E3 ligases in auxin regulation of embryogenesis. *Embo Journal*, **22**, 3314-3325.

Hilton, H. (1957) Herbicide tolerant strains of weeds. *Hawaiian Sugar Planters Association Annual Report*, 69-72.

Hirschberg, J., Ohad, N., Pecker, I. and Rahat, A. (1987) ISOLATION AND CHARACTERIZATION OF HERBICIDE RESISTANT MUTANTS IN THE CYANOBACTERIUM SYNECHOCOCCUS R2. *Zeitschrift Fur Naturforschung C-a Journal of Biosciences*, **42**, 758-761.

Hobbie, L., McGovern, M., Hurwitz, L.R., Pierro, A., Liu, N.Y., Bandyopadhyay, A. and Estelle, M. (2000) The axr6 mutants of Arabidopsis thaliana define a gene involved in auxin response and early development. *Development*, **127**, 23-32.

Hoss, N.E., Al-Khatib, K., Peterson, D.E. and Loughin, T.M. (2003) Efficacy of glyphosate, glufosinate, and imazethapyr on selected weed species. *Weed Science*, **51**, 110-117.

Huang, Y., Chen, X.J., Liu, Y.A., Roth, C., Copeland, C., McFarlane, H.E., Huang, S., Lipka, V., Wiermer, M. and Li, X. (2013) Mitochondrial AtPAM16 is required for plant survival and the negative regulation of plant immunity. *Nature Communications*, **4**, 13.

Ifuku, K., Ishihara, S., Shimamoto, R., Ido, K. and Sato, F. (2008) Structure, function, and evolution of the PsbP protein family in higher plants. *Photosynthesis Research*, **98**, 427-437.

Ishii, N., Suzuki, N., Hartman, P.S. and Suzuki, K. (1993) THE RADIATION-SENSITIVE MUTANT RAD-8 OF CAENORHABDITIS-ELEGANS IS HYPERSENSITIVE TO THE EFFECTS OF OXYGEN ON AGING AND DEVELOPMENT. *Mechanisms of Ageing and Development*, **68**, 1-10.

Ishizaki, K., Chiyoda, S., Yamato, K.T. and Kohchi, T. (2008) Agrobacterium-mediated transformation of the haploid liverwort Marchantia polymorpha L., an emerging model for plant biology. *Plant and Cell Physiology*, **49**, 1084-1091.

Ishizaki, K., Nishihama, R., Yamato, K. and Kohchi, T. (2016) Molecular Genetic Tools and Techniques for Marchantia polymorpha Research. *Plant and Cell Physiology*, **57**, 262-270.

Iwakami, S., Endo, M., Saika, H., Okuno, J., Nakamura, N., Yokoyama, M., Watanabe, H., Toki, S., Uchino, A. and Inamura, T. (2014a) Cytochrome P450 CYP81A12 and CYP81A21 Are Associated with Resistance to Two Acetolactate Synthase Inhibitors in Echinochloa phyllopogon. *Plant Physiology*, **165**, 618-629.

Iwakami, S., Uchino, A., Kataoka, Y., Shibaike, H., Watanabe, H. and Inamura, T. (2014b) Cytochrome P450 genes induced by bispyribac- sodium treatment in amultiple- herbicide- resistant biotype of Echinochloa phyllopogon. *Pest Management Science*, **70**, 549-558.

Jander, G., Baerson, S.R., Hudak, J.A., Gonzalez, K.A., Gruys, K.J. and Last, R.L. (2003) Ethylmethanesulfonate saturation mutagenesis in Arabidopsis to determine frequency of herbicide resistance. *Plant Physiology*, **131**, 139-146.

Jeong, D.H., An, S.Y., Kang, H.G., Moon, S., Han, J.J., Park, S., Lee, H.S., An, K.S. and An, G.H. (2002) T-DNA insertional mutagenesis for activation tagging in rice. *Plant Physiology*, **130**, 1636-1644.

Jin, M., Chen, L., Deng, X.W. and Tang, X. (2021) Development of herbicide resistance genes and their application in rice. *The Crop Journal*.

Ju, K.S. and Parales, R.E. (2010) Nitroaromatic Compounds, from Synthesis to Biodegradation. *Microbiology and Molecular Biology Reviews*, **74**, 250-+.

Kahlau, S., Schroder, F., Freigang, J., Laber, B., Lange, G., Passon, D., Kleessen, S., Lohse, M., Schulz, A., von Koskull-Doring, P., Klie, S. and Gille, S. (2020) Aclonifen targets solanesyl diphosphate synthase, representing a novel mode of action for herbicides. *Pest Management Science*, 12.

Kaloumenos, N.S., Tsioni, V.C., Daliani, E.G., Papavassileiou, S.E., Vassileiou, A.G., Laoutidou, P.N. and Eleftherohorinos, I.G. (2012) Multiple Pro-197 substitutions in the acetolactate synthase of rigid ryegrass (Lolium rigidum) and their impact on chlorsulfuron activity and plant growth. *Crop Protection*, **38**, 35-43.

Katoh, K., Rozewicki, J. and Yamada, K.D. (2019) MAFFT online service: multiple sequence alignment, interactive sequence choice and visualization. *Briefings in Bioinformatics*, **20**, 1160-1166.

Keshtkar, E., Mathiassen, S.K. and Kudsk, P. (2017) No Vegetative and Fecundity Fitness Cost Associated with Acetyl-Coenzyme A Carboxylase Non-target-site Resistance in a Black-Grass (Alopecurus myosuroides Huds) Population. *Frontiers in Plant Science*, **8**.

King, R., Lawrence, C., Clark, M. and Calhoun, L. (1989) ISOLATION AND CHARACTERIZATION OF PHYTOTOXINS ASSOCIATED WITH STREPTOMYCES SCABIES. *Journal of the Chemical Society-Chemical Communications*, 849-850.

King, R., Lawrence, C. and Gray, J. (2001) Herbicidal Properties of the thaxtomin Group of phytotoxins. *Journal of Agricultural and Food Chemistry*, **49**, 2298-2301.

Kohchi, T., Yamato, K.T., Ishizaki, K., Yamaoka, S. and Nishihama, R. (2021) Development and Molecular Genetics of Marchantia polymorpha. *Annual Review of Plant Biology, Vol 72, 2021*, **72**, 677-702.

Kovacic, P. and Somanathan, R. (2014) Nitroaromatic compounds: Environmental toxicity, carcinogenicity, mutagenicity, therapy and mechanism. *Journal of Applied Toxicology*, **34**, 810-824.

Kreiner, J.M., Giacomini, D.A., Bemm, F., Waithaka, B., Regalado, J., Lanz, C., Hildebrandt, J., Sikkema, P.H., Tranel, P.J., Weigel, D., Stinchcombe, J.R. and Wright, S.I. (2019) Multiple modes of convergent adaptation in the spread of glyphosate-resistant Amaranthus tuberculatus. *Proceedings of the National Academy of Sciences of the United States of America*, **116**, 21076-21084.

Kreiner, J.M., Tranel, P.J., Weigel, D., Stinchcombe, J.R. and Wright, S.I. (2021) The genetic architecture and population genomic signatures of glyphosate resistance in Amaranthus tuberculatus. *Molecular Ecology*, 17.

Kreuz, K., Tommasini, R. and Martinoia, E. (1996) Old enzymes for a new job - Herbicide detoxification in plants. *Plant Physiology*, **111**, 349-353.

Lamb, S.B., Lamb, D.C., Kelly, S.L. and Stuckey, D.C. (1998) Cytochrome P450 immobilisation as a route to bioremediation/biocatalysis. *Febs Letters*, **431**, 343-346.

Larossa, R.A. and Schloss, J.V. (1984) THE SULFONYLUREA HERBICIDE SULFOMETURON METHYL IS AN EXTREMELY POTENT AND SELECTIVE INHIBITOR OF ACETOLACTATE SYNTHASE IN SALMONELLA-TYPHIMURIUM. *Journal of Biological Chemistry*, **259**, 8753-8757.

Leslie, T. and Baucom, R.S. (2014) De Novo Assembly and Annotation of the Transcriptome of the Agricultural Weed Ipomoea purpurea Uncovers Gene Expression Changes Associated with Herbicide Resistance. *G3-Genes Genomes Genetics*, **4**, 2035-2047.

Li, F., Shimizu, A., Nishio, T., Tsutsumi, N. and Kato, H. (2019) Comparison and Characterization of Mutations Induced by Gamma-Ray and Carbon-Ion Irradiation in Rice (Oryza sativa L.) Using Whole-Genome Resequencing. *G3-Genes Genomes Genetics*, **9**, 3743-3751.

Li, J., Yu, H., Zhang, F.Z., Lin, C.Y., Gao, J.H., Fang, J., Ding, X.H., Shen, Z.C. and Xu, X.L. (2013) A Built-In Strategy to Mitigate Transgene Spreading from Genetically Modified Corn. *Plos One*, **8**.

Li, Z.-G. (2019) Chapter 5 - Measurement of Signaling Molecules Calcium Ion, Reactive Sulfur Species, Reactive Carbonyl Species, Reactive Nitrogen Species, and Reactive Oxygen Species in Plants. In *Plant Signaling Molecules* (Khan, M.I.R., Reddy, P.S., Ferrante, A. and Khan, N.A. eds): Woodhead Publishing, pp. 83-103.

Ligrone, R., Duckett, J.G. and Renzaglia, K.S. (2012a) Major transitions in the evolution of early land plants: a bryological perspective. In *Ann Bot*, pp. 851-871.

Ligrone, R., Duckett, J.G. and Renzaglia, K.S. (2012b) Major transitions in the evolution of early land plants: a bryological perspective. *Annals of Botany*, **109**, 851-871.

Liu, C., Liu, S.Q., Wang, F., Wang, Y.Q. and Liu, K.D. (2012) Expression of a rice CYP81A6 gene confers tolerance to bentazon and sulfonylurea herbicides in both Arabidopsis and tobacco. *Plant Cell Tissue and Organ Culture*, **109**, 419-428.

Ma, R., Kaundun, S.S., Tranel, P.J., Riggins, C.W., McGinness, D.L., Hager, A.G., Hawkes, T., McIndoe, E. and Riechers, D.E. (2013) Distinct

Detoxification Mechanisms Confer Resistance to Mesotrione and Atrazine in a Population of Waterhemp. *Plant Physiology*, **163**, 363-377.
Maroli, A.S., Gaines, T.A., Foley, M.E., Duke, S.O., Dogramaci, M., Anderson, J.V., Horvath, D.P., Chao, W.S. and Tharayil, N. (2018) Omics in Weed Science: A Perspective from Genomics, Transcriptomics, and Metabolomics Approaches. *Weed Science*, **66**, 681-695.
Martin, S.L., Parent, J.S., Laforest, M., Page, E., Kreiner, J.M. and James, T. (2019) Population Genomic Approaches for Weed Science. *Plants-Basel*, **8**.
Mascher, M., Jost, M., Kuon, J.E., Himmelbach, A., Assfalg, A., Beier, S., Scholz, U., Graner, A. and Stein, N. (2014) Mapping-by-sequencing accelerates forward genetics in barley. *Genome Biology*, **15**.
Matzrafi, M., Shaar-Moshe, L., Rubin, B. and Peleg, Z. (2017) Unraveling the Transcriptional Basis of Temperature-Dependent Pinoxaden Resistance in Brachypodium hybridum. *Frontiers in Plant Science*, **8**, 1-11.
McDougall, P. (2010) The Cost of New Agrochemical Product Discovery, Development and Registration in 1995, 2000 and 2005-8.
Mokranjac, D., Bourenkov, G., Hell, K., Neupert, W. and Groll, M. (2006) Structure and function of Tim14 and Tim16, the J and J-like components of the mitochondrial protein import motor. *Embo Journal*, **25**, 4675-4685.
Moon, J., Zhao, Y.D., Dai, X.H., Zhang, W.J., Gray, W.M., Huq, E. and Estelle, M. (2007) A new CULLIN 1 mutant has altered responses to hormones and light in Arabidopsis. *Plant Physiology*, **143**, 684-696.
Morejohn, L.C., Bureau, T.E., Molè-Bajer, J., Bajer, A.S. and Fosket, D.E. (1987) Oryzalin, a dinitroaniline herbicide, binds to plant tubulin and inhibits microtubule polymerization in vitro. *Planta*, **172**, 252-264.
Moretti, M.L., Horn, C.R., Robertson, R., Segobye, K., Weller, S.C., Young, B.G., Johnson, W.G., Sammons, R.D., Wang, D.F., Ge, X., Avignon, A., Gaines, T.A., Westra, P., Green, A.C., Jeffery, T., Lesperance, M.A., Tardif, F.J., Sikkema, P.H., Hall, J.C., McLean, M.D., Lawton, M.B. and Schulz, B. (2018) Glyphosate resistance in Ambrosia trifida: Part 2. Rapid response physiology and non-target-site resistance. *Pest Management Science*, **74**, 1079-1088.
Moss, S.R., Perryman, S.A.M. and Tatnell, L.V. (2007) Managing Herbicide-resistant Blackgrass (Alopecurus myosuroides): Theory and Practice. *Weed Technology*, **21**, 300-309.
Nandula, V.K., Riechers, D.E., Ferhatoglu, Y., Barrett, M., Duke, S.O., Dayan, F.E., Goldberg-Cavalleri, A., Tétard-Jones, C., Wortley, D.J., Onkokesung, N., Brazier-Hicks, M., Edwards, R., Gaines, T., Iwakami, S., Jugulam, M. and Ma, R. (2019) Herbicide Metabolism: Crop Selectivity, Bioactivation, Weed Resistance, and Regulation. *Weed Science*, **67**, 149-175.
Neve, P., Vila-Aiub, M. and Roux, F. (2009) Evolutionary-thinking in agricultural weed management. *New Phytologist*, **184**, 783-793.
Oerke, E. (2006) Crop losses to pests. *Journal of Agricultural Science*, **144**, 31-43.
Oettmeier, W. and Masson, K. (1980) SYNTHESIS AND THYLAKOID MEMBRANE-BINDING OF THE RADIOACTIVELY LABELED HERBICIDE DINOSEB. *Pesticide Biochemistry and Physiology*, **14**, 86-97.
Olsen, O., Wang, X.Z. and Von Wettstein, D. (1993) SODIUM-AZIDE MUTAGENESIS - PREFERENTIAL GENERATION OF A.T - G.C

TRANSITIONS IN THE BARLEY ANT18 GENE. *Proceedings of the National Academy of Sciences of the United States of America*, **90**, 8043-8047.

Ostergaard, L. and Yanofsky, M.F. (2004) Establishing gene function by mutagenesis in Arabidopsis thaliana. *Plant Journal*, **39**, 682-696.

Padgette, S.R., Kolacz, K.H., Delannay, X., Re, D.B., Lavallee, B.J., Tinius, C.N., Rhodes, W.K., Otero, Y.I., Barry, G.F., Eichholtz, D.A., Peschke, V.M., Nida, D.L., Taylor, N.B. and Kishore, G.M. (1995) DEVELOPMENT, IDENTIFICATION, AND CHARACTERIZATION OF A GLYPHOSATE-TOLERANT SOYBEAN LINE. *Crop Science*, **35**, 1451-1461.

Page, D.R. and Grossniklaus, L. (2002) The art and design of genetic screens: Arabidopsis thaliana. *Nature Reviews Genetics*, **3**, 124-136.

Pan, G., Zhang, X.Y., Liu, K.D., Zhang, J.W., Wu, X.Z., Zhu, J. and Tu, J.M. (2006) Map-based cloning of a novel rice cytochrome P450 gene CYP81A6 that confers resistance to two different classes of herbicides. *Plant Molecular Biology*, **61**, 933-943.

Pan, L., Yu, Q., Wang, J.Z., Han, H.P., Mao, L.F., Nyporko, A., Maguza, A., Fan, L.J., Bai, L.Y. and Powles, S. (2021) An ABCC-type transporter endowing glyphosate resistance in plants. *Proceedings of the National Academy of Sciences of the United States of America*, **118**.

Park, I., Kim, K.-e., Kim, J., Bae, S., Jung, M., Choi, J., Kwak, C., Kang, M.-G., Yoo, C.-M., Mun, J.Y., Liu, K.-H., Kim, J.-S., Suh, J.M. and Rhee, H.-W. (2021) In vivo mitochondrial matrix proteome profiling reveals RTN4IP1/OPA10 as an antioxidant NADPH oxidoreductase. *bioRxiv*, 2021.2010.2014.464368.

Pedroso, R.M., Al-Khatib, K., Alarcon-Reverte, R. and Fischer, A.J. (2016) A psbA mutation (Val(219) to Ile) causes resistance to propanil and increased susceptibility to bentazon in Cyperus difformis. *Pest Management Science*, **72**, 1673-1680.

Peng, Y.H., Abercrombie, L.L.G., Yuan, J.S., Riggins, C.W., Sammons, R.D., Tranel, P.J. and Stewart, C.N. (2010) Characterization of the horseweed (Conyza canadensis) transcriptome using GS-FLX 454 pyrosequencing and its application for expression analysis of candidate non-target herbicide resistance genes. *Pest Management Science*, **66**, 1053-1062.

Peters, B. and Strek, H.J. (2018) Herbicide discovery in light of rapidly spreading resistance and ever-increasing regulatory hurdles. *Pest Management Science*, **74**, 2211-2215.

Pfister, K., Steinback, K.E., Gardner, G. and Arntzen, C.J. (1981) PHOTOAFFINITY-LABELING OF AN HERBICIDE RECEPTOR PROTEIN IN CHLOROPLAST MEMBRANES. *Proceedings of the National Academy of Sciences of the United States of America-Biological Sciences*, **78**, 981-985.

Piasecki, C., Yang, Y., Benemann, D.P., Kremer, F.S., Galli, V., Millwood, R.J., Cechin, J., Agostinetto, D., Maia, L.C., Vargas, L. and Stewart, C.N. (2019) Transcriptomic Analysis Identifies New Non-Target Site Glyphosate-Resistance Genes in Conyza bonariensis. *Plants-Basel*, **8**.

Pimentel, D. (2005) Environmental and economic costs of the application of pesticides primarily in the United States. *Environ. Dev. Sustain*, **7**, 229-252.

Pires, N.D. and Dolan, L. (2012) Morphological evolution in land plants: new designs with old genes. In *Philos Trans R Soc Lond B Biol Sci*, pp. 508-518.

Powles, S., Yu, Q., Merchant, S., Briggs, W. and Ort, D. (2010) Evolution in Action: Plants Resistant to Herbicides. *Annual Review of Plant Biology, Vol 61*, **61**, 317-347.
Powles, S.B. (2008) Evolved glyphosate-resistant weeds around the world: lessons to be learnt. *Pest Management Science*, **64**, 360-365.
Powles, S.B., Lorraine-Colwill, D.F., Dellow, J.J. and Preston, C. (1998) Evolved resistance to glyphosate in rigid ryegrass (Lolium rigidum) in Australia. *Weed Science*, **46**, 604-607.
Reavell-Roy, E. (2019) Forward screening for herbicide resistance in Arabidopsis thaliana and the monocot species Triticum aestivum. University of Ontario Institute of Technology.
Ritz, C., Baty, F., Streibig, J.C. and Gerhard, D. (2015) Dose-Response Analysis Using R. *Plos One*, **10**, 13.
Rojano-Delgado, A.M., Portugal, J.M., Palma-Bautista, C., Alcantara-de la Cruz, R., Torra, J., Alcantara, E. and De Prado, R. (2019) Target site as the main mechanism of resistance to imazamox in a Euphorbia heterophylla biotype. *Scientific Reports*, **9**.
Ryan, G.F. (1970) Resistance of Common Groundsel to Simazine and Atrazine. *Weed Science*, **18**, 614-616.
Saha, J., Brauer, E.K., Sengupta, A., Popescu, S.C., Gupta, K. and Gupta, B. (2015) Polyamines as redox homeostasis regulators during salt stress in plants. *Frontiers in Environmental Science*, **3**.
Sandmann, G. and Böger, P. (1989) Inhibition of carotenoid biosynthesis by herbicides. *Target sites of herbicide action*, 25-44.
Scheible, W., Eshed, R., Richmond, T., Delmer, D. and Somerville, C. (2001) Modifications of cellulose synthase confer resistance to isoxaben and thiazolidinone herbicides in Arabidopsis Ixr1 mutants. *Proceedings of the National Academy of Sciences of the United States of America*, **98**, 10079-10084.
Scheible, W., Fry, B., Kochevenko, A., Schindelasch, D., Zimmerli, L., Somerville, S., Loria, R. and Somerville, C. (2003) An Arabidopsis mutant resistant to thaxtomin A, a cellulose synthesis inhibitor from Streptomyces species. *Plant Cell*, **15**, 1781-1794.
Schierenbeck, L., Ries, D., Rogge, K., Grewe, S., Weisshaar, B. and Kruse, O. (2015) Fast forward genetics to identify mutations causing a high light tolerant phenotype in Chlamydomonas reinhardtii by whole-genome-sequencing. *Bmc Genomics*, **16**.
Schneeberger, K. (2014) Using next-generation sequencing to isolate mutant genes from forward genetic screens. *Nature Reviews Genetics*, **15**, 662-676.
Schneeberger, K., Ossowski, S., Lanz, C., Juul, T., Petersen, A.H., Nielsen, K.L., Jorgensen, J.E., Weigel, D. and Andersen, S.U. (2009) SHOREmap: simultaneous mapping and mutation identification by deep sequencing. *Nature Methods*, **6**, 550-551.
Schreiber, M.M. (1992) Influence of Tillage, Crop Rotation, and Weed Management on Giant Foxtail (Setaria faberi) Population Dynamics and Corn Yield. *Weed Science*, **40**, 645-653.
Shaner, D.L. (2014) Lessons Learned From the History of Herbicide Resistance. *Weed Science*, **62**, 427-431.
Shim, I., Law, R., Kileeg, Z., Stronghill, P., Northey, J.G.B., Strap, J.L. and Bonetta, D.T. (2018) Alleles Causing Resistance to Isoxaben and Flupoxam

Highlight the Significance of Transmembrane Domains for CESA Protein Function. *Frontiers in Plant Science*, **9**, 14.

Shimamura, M. (2015) Marchantia polymorpha : Taxonomy, Phylogeny and Morphology of a Model System. *Plant and Cell Physiology*, **57**, 230-256.

Shino, M., Hamada, T., Shigematsu, Y., Hirase, K., Banba, S., Tsukamoto, Y. and Kadotani, J. (2021) Chapter 30 - Discovery and mode of action of cyclopyrimorate: A new paddy rice herbicide. In *Recent Highlights in the Discovery and Optimization of Crop Protection Products* (Maienfisch, P. and Mangelinckx, S. eds): Academic Press, pp. 451-457.

Smith, D.R., Quinlan, A.R., Peckham, H.E., Makowsky, K., Tao, W., Woolf, B., Shen, L., Donahue, W.F., Tusneem, N., Stromberg, M.P., Stewart, D.A., Zhang, L., Ranade, S.S., Warner, J.B., Lee, C.C., Coleman, B.E., Zhang, Z., McLaughlin, S.F., Malek, J.A., Sorenson, J.M., Blanchard, A.P., Chapman, J., Hillman, D., Chen, F., Rokhsar, D.S., McKernan, K.J., Jeffries, T.W., Marth, G.T. and Richardson, P.M. (2008) Rapid whole-genome mutational profiling using next-generation sequencing technologies. *Genome Research*, **18**, 1638-1642.

Spain, J.C. (1995) BIODEGRADATION OF NITROAROMATIC COMPOUNDS. *Annual Review of Microbiology*, **49**, 523-555.

Steinback, K.E., McIntosh, L., Bogorad, L. and Arntzen, C.J. (1981) Identification of the triazine receptor protein as a chloroplast gene product. *Proc Natl Acad Sci U S A*, **78**, 7463-7467.

Subramanian, M.V., Brunn, S.A., Bernasconi, P., Patel, B.C. and Reagan, J.D. (1997) Revisiting auxin transport inhibition as a mode of action for herbicides. *Weed Science*, **45**, 621-627.

Sugano, S.S., Shirakawa, M., Takagi, J., Matsuda, Y., Shimada, T., Hara-Nishimura, I. and Kohchi, T. (2014) CRISPR/Cas9-Mediated Targeted Mutagenesis in the Liverwort Marchantia polymorpha L. *Plant and Cell Physiology*, **55**, 475-481.

Takano, H.K., Beffa, R., Preston, C., Westra, P. and Dayan, F.E. (2019) Reactive oxygen species trigger the fast action of glufosinate. *Planta*, **249**, 1837-1849.

Takano, H.K., Beffa, R., Preston, C., Westra, P. and Dayan, F.E. (2020) A novel insight into the mode of action of glufosinate: how reactive oxygen species are formed. *Photosynthesis Research*, **144**, 361-372.

Tanetani, Y., Kaku, K., Ikeda, M. and Shimizu, T. (2013) Action mechanism of a herbicide, thiobencarb. *Journal of Pesticide Science*, **38**, 39-43.

Tateno, M., Brabham, C. and DeBolt, S. (2016) Cellulose biosynthesis inhibitors - a multifunctional toolbox. *Journal of Experimental Botany*, **67**, 533-542.

Tegg, R.S., Shabala, S.N., Cuin, T.A., Davies, N.W. and Wilson, C.R. (2013) Enhanced resistance to the cellulose biosynthetic inhibitors, thaxtomin A and isoxaben in Arabidopsis thaliana mutants, also provides specific co-resistance to the auxin transport inhibitor, 1-NPA. *Bmc Plant Biology*, **13**, 10.

Thyssen, G.N., Naoumkina, M., McCarty, J.C., Jenkins, J.N., Florane, C., Li, P. and Fang, D.D. (2018) The P450 gene CYP749A16 is required for tolerance to the sulfonylurea herbicide trifloxysulfuron sodium in cotton (Gossypium hirsutum L.). *Bmc Plant Biology*, **18**.

Tillich, U.M., Lehmann, S., Schulze, K., Duhring, U. and Frohme, M. (2012) The Optimal Mutagen Dosage to Induce Point-Mutations in Synechocystis sp PCC6803 and Its Application to Promote Temperature Tolerance. *Plos One*, **7**, 8.

Torra, J., Osuna, M.D., Merotto, A. and Vila-Aiub, M. (2021) Editorial: Multiple Herbicide-Resistant Weeds and Non-target Site Resistance Mechanisms: A Global Challenge for Food Production. *Frontiers in Plant Science*, **12**.

Tresch, S., Schmotz, J. and Grossmann, K. (2011) Probing mode of action in plant cell cycle by the herbicide endothall, a protein phosphatase inhibitor. *Pesticide Biochemistry and Physiology*, **99**, 86-95.

USDA (2004) Agricultural Chemical Use Database: National Agricultural Statistics Service (USDA - ARS).

Van Etten, M., Lee, K.M., Chang, S.M. and Baucom, R.S. (2020) Parallel and nonparallel genomic responses contribute to herbicide resistance in Ipomoea purpurea, a common agricultural weed. *Plos Genetics*, **16**.

Van Horn, C.R., Moretti, M.L., Robertson, R.R., Segobye, K., Weller, S.C., Young, B.G., Johnson, W.G., Schulz, B., Green, A.C., Jeffery, T., Lesperance, M.A., Tardif, F.J., Sikkema, P.H., Hall, J.C., McLean, M.D., Lawton, M.B., Sammons, R.D., Wang, D.F., Westra, P. and Gaines, T.A. (2018) Glyphosate resistance in Ambrosia trifida: Part 1. Novel rapid cell death response to glyphosate. *Pest Management Science*, **74**, 1071-1078.

Vila-Aiub, M.M., Neve, P. and Powles, S.B. (2009) Fitness costs associated with evolved herbicide resistance alleles in plants. *New Phytologist*, **184**, 751-767.

Wang, J.J., Chen, J.C., Li, X.J. and Cui, H.L. (2021) RNA-Seq transcriptome analysis to identify candidate genes involved in non -target site-based mesosulfuron-methyl resistance in Beckmannia syzigachne. *Pesticide Biochemistry and Physiology*, **171**.

Ward, S.M., Webster, T.M. and Steckel, L.E. (2013) Palmer Amaranth (Amaranthus palmeri): A Review. *Weed Technology*, **27**, 12-27.

Warwick, S.I., Xu, R.L., Sauder, C. and Beckie, H.J. (2008) Acetolactate Synthase Target-Site Mutations and Single Nucleotide Polymorphism Genotyping in ALS-Resistant Kochia (Kochia scoparia). *Weed Science*, **56**, 797-806.

Wickham, H. (2009) ggplot2 Elegant Graphics for Data Analysis Introduction. In *Ggplot2: Elegant Graphics for Data Analysis*. New York: Springer, pp. 1-+.

Wolff, S.P. (1994) FERROUS ION OXIDATION IN PRESENCE OF FERRIC ION INDICATOR XYLENOL ORANGE FOR MEASUREMENT OF HYDROPEROXIDES. *Oxygen Radicals in Biological Systems, Pt C*, **233**, 182-189.

WSSA (2016) WSSA glossary, https://wssa.net/wssa/wssa-glossary/.

Wu, C.X., Davis, A.S. and Tranel, P.J. (2018) Limited fitness costs of herbicide-resistance traits in Amaranthus tuberculatus facilitate resistance evolution. *Pest Management Science*, **74**, 293-301.

Yu, Q., Abdallah, I., Han, H.P., Owen, M. and Powles, S. (2009) Distinct non-target site mechanisms endow resistance to glyphosate, ACCase and ALS-inhibiting herbicides in multiple herbicide-resistant Lolium rigidum. *Planta*, **230**, 713-723.

Yu, Q., Cairns, A. and Powles, S. (2007) Glyphosate, paraquat and ACCase multiple herbicide resistance evolved in a Lolium rigidum biotype. *Planta*, **225**, 499-513.

Yu, Q., Jalaludin, A., Han, H.P., Chen, M., Sammons, R.D. and Powles, S.B. (2015) Evolution of a Double Amino Acid Substitution in the 5-Enolpyruvylshikimate-3-Phosphate Synthase in Eleusine indica Conferring High-Level Glyphosate Resistance. *Plant Physiology*, **167**, 1440-U1514.

Yu, Q. and Powles, S.B. (2014) Resistance to AHAS inhibitor herbicides: current understanding. *Pest Management Science*, **70**, 1340-1350.
Yuan, J.S., Tranel, P.J. and Stewart, C.N. (2007) Non-target-site herbicide resistance: a family business. *Trends in Plant Science*, **12**, 6-13.
Zhao, N., Li, W., Bai, S., Guo, W.L., Yuan, G.H., Wang, F., Liu, W.T. and Wang, J.X. (2017) Transcriptome Profiling to Identify Genes Involved in Mesosulfuron-Methyl Resistance in Alopecurus aequalis. *Frontiers in Plant Science*, **8**.